NASA CR-72791
AI-70-46

N71-17703

VOLTAMMETRIC SCREENING OF ELECTRODES IN FUSED SALT ELECTROLYTES

By

Leo E. Topol, William A. McCollum, Jr.
and Samuel J. Yosim

NORTH AMERICAN ROCKWELL CORPORATION
ATOMICS INTERNATIONAL DIVISION

Prepared for

NATIONAL AERONAUTICS AND SPACE ADMINISTRATION

NASA LEWIS RESEARCH CENTER
CONTRACT NAS 3-12970
Dr. Betty S. Del Duca, Project Manager

NOTICE

This report was prepared as an account of Government-sponsored work. Neither the United States, nor the National Aeronautics and Space Administration (NASA), nor any person acting on behalf of NASA:

A) Makes any warranty or representation, expressed or implied, with respect to the accuracy, completeness, or usefulness of the information contained in this report, or that the use of any information, apparatus, method, or process disclosed in this report may not infringe privately owned rights; or

B) Assumes any liabilities with respect to the use of, or for damages resulting from the use of, any information, apparatus, method or process disclosed in this report.

As used above, "person acting on behalf of NASA" includes any employee or contractor of NASA, or employee of such contractor to the extent that such employee or contractor of NASA or employee of such contractor prepares, disseminates, or provides access to any information pursuant to his employment or contract with NASA, or his employment with such contractor.

Requests for copies of this report should be referred to:

National Aeronautics and Space Administration
Scientific and Technical Information Facility
P.O. Box 33
College Park, Md. 20740

NASA CR-72791
AI-70-46

FINAL REPORT

VOLTAMMETRIC SCREENING OF ELECTRODES IN FUSED SALT ELECTROLYTES

by

Leo E. Topol, William A. McCollum, Jr. and
Samuel J. Yosim

North American Rockwell Corporation
Atomics International Division
8900 DeSoto Avenue
Canoga Park, California 91304

Prepared for

National Aeronautics and Space Administration
December 31, 1970
Contract NAS3-12970

NASA Lewis Research Center
Cleveland, Ohio 44135

Dr. Betty S. Del Duca, Project Manager

FOREWARD

The work described herein, which was conducted by Atomics International, a Division of North American Rockwell Corporation, was performed under NASA Contract NAS3-12970. The Project Manager for NASA was Dr. Betty S. Del Duca, NASA Lewis Research Center, Cleveland, Ohio.

TABLE OF CONTENTS

		Page
Abstract		ix
Recommendations		x
I.	Introduction	1
	A. General Requirements for a High-Performance Fused Salt Battery	2
	B. Rationale for a Screening Test Study	5
	C. Choice of Cell Electrolyte Solvent	5
	D. Selection of Cell Reactants	6
	E. Purification of Salts	8
	F. Screening Program	8
II.	Voltammetric Screening Techniques	9
	A. Linear Sweep Voltammetry	9
	B. Current-Step Voltammetry	13
III.	Experimental	21
	A. Preparation of Materials	21
	B. Apparatus	44
	C. Procedure	54
IV.	Results and Discussion	60
	A. Compatibility Experiments	60
	B. Electrical Conductivity Tests	62
	C. Freezing Point Measurements	66
	D. Voltammetry Tests	67
	E. Evaluation of Couples for Battery Application	194
V.	Summary	214
VI.	Conclusions	217
VII.	References	218

Page

Appendix I A-1

Characterization of the $AlCl_3$ (66%)-NaCl (20%)-KCl (14%) Mixture A-1

Appendix II A-2

Theoretical Considerations of Synthetic Circuits A-2

A. Theoretical Equation Taking Into Consideration the Rise Time of the Pulse Generator A-2

B. Determination of τ and the Rise Time A-3

C. The Effect of R_s on the Apparent Capacitance A-4

D. Theoretical E vs t Curves for Different Exchange Currents and Rise Times A-6

Appendix III A-11

Analysis of Oscilloscope Traces A-11

A. Short Pulse Traces. A-11

B. Long Pulse Traces - Redox Systems A-12

C. Long Pulse Traces - Metal/Metal Ion Systems A-15

Appendix IV A-17

Cyclic Voltammograms in Molten NaOH-KOH Systems A-17

A. Ag/Ag_2O A-17

B. Cu/Cu_2O A-20

C. Cu/CuO A-22

D. Cd/CdO A-25

E. Be/BeO A-25

F. Mg/MgO A-28

G. Zn/ZnO A-28

H. Al/Al_2O_3 . . . . . A-31

LIST OF FIGURES

		Page
1.	Current-Potential Curves in Linear Potential Sweep Voltammetry	10
2.	Potential-Time Curve for Current Step Technique	14
3.	Apparatus for Preparing and Purifying Salts	28
4.	Schematic Circuit for Linear-Sweep Voltammetry	45
5.	Schematic Circuit for Current Step Voltammetry	46
6.	Electrical Conductivity Cell	48
7.	Voltammetry Cell	50
8.	L.S.V. of 15 wt % Ag/AgCl in $ZnCl_2$ Solvent	70
9.	Linear Sweep Voltammetry of $ZnCl_2$-NaCl-KCl Solvent	76
10.	Voltammetry of Ag/AgCl in $ZnCl_2$ Melt	80
11.	Voltammetry of Cu/CuCl in $ZnCl_2$ Melt	88
12.	Voltammetry of Ni/$NiCl_2$ in $ZnCl_2$ Melts	94
13.	Voltammetry of Bi/$BiCl_3$ in $ZnCl_2$ Melts	100
14.	Voltammetry of Sb/$SbCl_3$ in $ZnCl_2$ Melts	105
15.	Voltammetry of Pt/$CrCl_2$, $CrCl_3$ in $ZnCl_2$ Melts	111
16.	Voltammetry of W/CuCl, $CuCl_2$ in $ZnCl_2$ Melt	116
17.	Voltammograms of W/$FeCl_2$, $FeCl_3$ in $ZnCl_2$ Melts	122
18.	Voltammetry of Zn/$ZnCl_2$ System	128
19.	Voltammetry of $AlCl_3$-NaCl Solvent	131
20.	Voltammetry of Ag/AgCl in $AlCl_3$ Melts	134
21.	Voltammetry of Cu/CuCl in $AlCl_3$ Melts	140
22.	Voltammetry of Ni/$NiCl_2$ in $AlCl_3$ Melts	145
23.	Voltammetry of Bi/$BiCl_3$ in $AlCl_3$ Melts	152
24.	Voltammetry of Sb/$SbCl_3$ in $AlCl_3$ Melts	159
25.	Voltammetry of W/$CrCl_2$, $CrCl_3$ in $AlCl_3$ Melts	162

Page

26. Voltammetry of W/CuCl, $CuCl_2$ in $AlCl_3$ Melts 165

27. Voltammetry of W/$FeCl_2$, $FeCl_3$ in $AlCl_3$ Melts 172

28. Voltammetry of Zn/$ZnCl_2$ in $AlCl_3$ Melt. 180

29. Voltammetry of Al/$AlCl_3$ System. 185

30. Voltammetry of NaOH-KOH Solvent. 189

Appendix

1A. Effect of Cell Resistance on Apparent Capacitance A-5

2A. Theoretical E vs t Plots (Rise Time = 0.30 μsec) A-7

3A. Theoretical E vs t Plots (Rise Time = 0.30 μsec) A-8

4A. Theoretical E vs t Plots (Rise Time = 1.83 μsec) A-9

5A. L.S.V. of Ag/Ag_2O + Na_2O in NaOH-KOH. A-18

6Aa L.S.V. of Cu/Cu_2O in NaOH-KOH A-21

6Ab L.S.V. of Cu/Cu_2O + Na_2O in NaOH-KOH. A-23

7A. L.S.V. of Cu/CuO + Na_2O in NaOH-KOH A-24

8A. Voltammetry of Cd/CdO + Na_2O in NaOH-KOH Melts A-26

9A. L.S.V. of Be in NaOH-KOH A-27

10A. L.S.V. of Mg in NaOH-KOH A-29

11A. L.S.V. of Zn/ZnO + Na_2O in NaOH-KOH A-30

12A. L.S.V. of Al in NaOH-KOH A-32

LIST OF TABLES

		Page
1.	Melting Points of Salt Mixtures	6
2.	Couples Screened	7
3.	Emission Spectrographic Analysis of Metals	23
4.	Analysis of High Purity Hydrogen Chloride and Chlorine Gases	25
5.	S. S. M. S. Analysis of KCl and NaCl	27
6.	S. S. M. S. Analysis of $AlCl_3$ and $ZnCl_2$	31
7.	S. S. M. S. Analysis of Chloride Solutes	33
8.	S. S. M. S. Analysis of Chloride Solutes	38
9.	Emission Spectrographic Analysis of Chlorides	40
10.	S. S. M. S. Analysis of Hydroxides and Oxides	42
11.	Emission Spectrographic Analysis of Hydroxides and Oxides.	42
12.	Electrical Conductivities and Thermal Halts of $ZnCl_2$-Containing Melts	63
13.	Electrical Conductivities and Thermal Halts of $AlCl_3$-Containing Melts	64
14.	Theoretical $E_{eq}-E_p$ or ΔE_p for Reversible Electrodes (n = 1).	68
15.	Tests with Synthetic Circuits	73
16.	Voltammetry of Ag/AgCl in $ZnCl_2$ Melt	78
17.	Voltammetry of Cu/CuCl in $ZnCl_2$ Solvent	86
18.	Voltammetry of Ni/$NiCl_2$ in $ZnCl_2$ Solvent	92
19.	Voltammetry of Bi/$BiCl_3$ in $ZnCl_2$ Solvent	98
20.	Voltammetry of Sb/$SbCl_3$ in $ZnCl_2$ Solvent	103
21.	Voltammetry of Pt/$CrCl_2$, $CrCl_3$ in $ZnCl_2$ Solvent	109
22.	Voltammetry of W/CuCl, $CuCl_2$ in $ZnCl_2$ Solvent.	114
23.	Voltammetry of W/$FeCl_2$, $FeCl_3$ in $ZnCl_2$ Solvent	120

Page

24. Voltammetry of $Zn/ZnCl_2$ in $ZnCl_2$ Solvent 126

25. Voltammetry of Ag/AgCl in $AlCl_3$ Melt 132

26. Voltammetry of Cu/CuCl in $AlCl_3$ Melt 138

27. Voltammetry of $Ni/NiCl_2$ in $AlCl_3$ Melt 143

28. Voltammetry of $Bi/BiCl_3$ in $AlCl_3$ Solvent. 150

29. Voltammetry of $Sb/SbCl_3$ in $AlCl_3$ Solvent. 157

30. Voltammetry of W/CuCl, $CuCl_2$ in $AlCl_3$ Solvent. 163

31. Voltammetry of $W/FeCl_2$, $FeCl_3$ in $AlCl_3$ Solvent 170

32. Voltammetry of $Zn/ZnCl_2$ in $AlCl_3$ Solvent 177

33. Voltammetry of $Al/AlCl_3$ in $AlCl_3$ Solvent. 184

34. Voltages of Couples (0.1 M) vs Zn in $ZnCl_2$-NaCl-KCl and vs Zn and Al in $AlCl_3$-NaCl 195

35. Exchange Current Densities of Couples in $ZnCl_2$-NaCl-KCl and in $AlCl_3$-NaCl 197, 199

36. Variation in Peak Voltage with Sweep Rate. 201

37. Theoretical Energy Densities of Cells in $ZnCl_2$-NaCl-KCl at 275°C and in $AlCl_3$-NaCl at 150°C 205

38. Evaluation of Cells with Zn Anodes 208

Appendix

1A. Six Cases for Theoretical E vs t Plots A-6

ABSTRACT

Conductivity, freezing point and voltammetric measurements were made on the three melts, $ZnCl_2$(60%)-NaCl(20%)-KCl(20%), $AlCl_3$(61%)-NaCl(39%), and NaOH(50%)-KOH(50%), containing various catholytes and anolytes. All of the metals and salts employed were of very high purity. This necessitated the synthesis of many of the salts. The measured exchange current densities and voltages, as well as the calculated energy densities for the halide systems were compared. From this comparison the best couples for battery feasibility were selected. Since none of the catholytes were soluble in the anhydrous hydroxide melts and since only one anode did not passivate, very few data could be obtained for the NaOH-KOH systems.

RECOMMENDATIONS

The systems studied which hold the most promise are summarized below. For the halides these consist of three redox cells, two cells with soluble cathodes, and one with a solid cathode. For hydroxide-based batteries there are two systems with possible feasibility.

In the chloride systems the redox cells are (In)/CuCl, $CuCl_2$ vs Al and (In)/$FeCl_2$, $FeCl_3$ vs Al, both in $AlCl_3$-NaCl, and (In)/$CrCl_2$, $CrCl_3$ vs Zn in $ZnCl_2$-NaCl-KCl; here (In) denotes an inert electrode. The problems with these cells are the relatively low solubilities of the reducible cathode salts, the volatility of $FeCl_3$ and the instability of $CuCl_2$. In contrast to the above, cells with highly soluble cathodes, Ag/AgCl vs Al and Cu/CuCl vs Al in $AlCl_3$-NaCl, should support high current drains. An important problem with this type of battery, however, is an adequate separator between the anode and cathode compartments. The last type of cell in the chloride system, Ni/$NiCl_2$ vs Zn in $ZnCl_2$-NaCl-KCl, utilizes a solid cathode since $NiCl_2$ is only slightly soluble in this melt. Thus this cell might not be able to sustain high current drains. However, the polarization arising under load could be minimized with a suitable electrode configuration. The advantage of this cell is the good coulombic efficiency together with the less stringent separator problem.

For the hydroxide systems the cells which appear interesting are Cu/Cu_2O vs Na and Cu/Cu_2O vs Zn. The first cell would utilize a solid cathode since none of the cathode oxides studied were found to have adequate solubility in the anhydrous melt. Sodium would be used as the anode although it does react with the molten hydroxides slowly. The second cell would be

composed of wet hydroxide and a soluble cathode oxide. A separator would be required and the extent of reaction of the zinc anode with the wet melt ascertained.

It is recommended that further studies be carried out on the above systems.

I. INTRODUCTION

It has been recognized for some time that many activities and functions, both in space and on the earth, are either limited in scope or rendered impossible for lack of high-energy density batteries which are capable of delivering high power. An actual battery energy density in excess of 100 w-hr/lb (1630 J/kg), capable of being delivered, for example, in 2 hours or less (i.e., over 50 w/lb [45 w/kg]), is a desirable goal. In many cases, high power density is the critical requirement. A secondary battery system would be preferable, although many applications would be met by a primary system exhibiting this level of performance.

None of the batteries currently available achieve this goal. Some metal-air or metal-oxygen cells show considerable promise, but their power outputs are limited by gas electrode kinetics. So-called "high-energy" batteries, employing organic solvent electrolytes with lithium anodes, show promise of energy densities reaching a 200 w-hr/lb (3260 J/kg) level. However, because these cells generally exhibit poor electrolyte conductivity and poor cathode reactivity, high power density will probably not be attainable in these cells in the foreseeable future.

Sustained high power density in cells requires a combination of rapid electrode kinetics, high electrolyte conductivity and high energy density. High energy density requires that the reactants be relatively low atomic (and molecular) weight materials, capable of reacting electrochemically with a large decrease in free energy (i.e., giving a cell with large open-circuit voltage). For these materials use of aqueous electrolytes, which possess high conductivity ($\sim$ 1 ohm^{-1}-cm^{-1}), are excluded, since reaction

between the anodic reactant and the water would occur. However, fused salts generally exhibit high conductivities (~ 1 ohm^{-1}-cm^{-1}), and many show high stability in the presence of active anode materials. For generation of electricity by galvanic processes, they have found application in thermal cells and have been investigated for use in high-temperature fuel cells.

The use of fused salt cells offers additional possibly desirable features beyond those of high power and energy density. The electrolytes in such cells are normally frozen at temperatures encountered on earth; thus, the cells are capable of indefinite shelf life. Also, as they would operate only when the electrolytes are molten, they could easily be heat-sterilized for space applications while the system is solid.

A. General Requirements for a High-Performance Fused Salt Battery

Requirements for a suitable high performance fused salt battery system include:

1) High electrolytic conductivity
2) Adequate solubility of the cathode reactant (and anode product for secondary cells)
3) Low electrolyte melting point
4) Chemical compatibility of components
5) Rapid electrode kinetics
6) A high theoretical energy density of the cell's reactants.

In molten form, most uni-univalent salts formed from very electropositive and electronegative elements (e.g., NaCl, KCl, etc.) and mixtures of these show high conductivity; however, they have high melting points. In forming lower-melting mixtures, salts with multivalent ions (e.g., $AlCl_3$)

are often added to the alkali halide, forming ternary, quaternary, and more complex mixtures. These added components usually form complex ions (e.g., $AlCl_4^-$) and can decrease the conductivity of the melt. Further addition to the electrolyte of a cathodic reactant (e.g., AgCl, CuCl, etc.) can further affect the electrolyte, generally resulting in still lower specific conductance. While the conductivities of molten salts are generally high enough that some reduction may be tolerated, the requirement for high power density places a lower limit on useful conductivities for different applications.

The active cathodic material (oxide, chloride, etc.) in a cell may be present as a solid or dissolved in the electrolyte. A cell may function in either case, but the specific requirements on the active material are different in the two cases. A solid reactant must be, and remain, in contact with the current collector and possess adequate electronic conductivity, so that it can utilize the electric charge it receives from the current collector. For secondary cells the reverse process must occur on recharge, and the oxidized galvanic cell anode material must behave in similar fashion to the cathode reactant on discharge. Dissolved reactants should, in general, show rapid electrode kinetics; but they require that separators be used, presenting an additional materials problem and increasing the internal resistance of the cell. The concentration and diffusion coefficient of the reactant species in solution, together with its rate of solution, will determine the limiting current density at the cathode; thus, the solubility should be adequately high. For secondary cells, too low a solubility may lead to rapid formation of the insoluble oxidized form over the electrode, resulting in a limited current (and power) density. In complete cells, however, problems in preventing the dissolved cathode reactant from penetrating to, and reacting directly with,

the anode must be dealt with. Any measures designed for this purpose (e.g., separators) will not be fully effective and will increase cell resistance and limit current (and power) density, in direct relation to their effectiveness in preventing transport to the anode. All these factors must be evaluated for each specific system in selecting promising cathodic materials.

Low melting point for the salt electrolyte offers many advantages for battery application. To achieve this, low-melting multicomponent eutectic salt mixtures are usually required. However, addition of a large amount of the active cathodic material can cause a rise in the melting point. Thus, if the cathode reactant is relatively soluble in the melt, significant changes in electrolyte melting point will occur during cell discharge (and charge for secondary cells) if the product is insoluble. This factor must be evaluated for each system being considered.

Chemical compatibility of the system: electrolyte, cathode (or anode) active material, current collector, and container is required for satisfactory cell operation. Therefore, compatibility must be established prior to electrochemical characterization of anode and cathode systems.

A principal requirement for high performance is rapid electrode kinetics. Relative to similar processes at ambient temperature with aqueous electrolytes, electrode kinetics in the case of fused salts in general may be expected to be more rapid. In many cases, for example, the anodic process at an active metal would not be impeded by oxide film formation that would occur in aqueous systems. However, this process may be limited by formation of an insoluble salt, as noted previously. In general, an electrochemical investigation is required to define electrode kinetics.

In addition to being able to deliver high current density with low total polarization, high power density delivered for extended periods will depend on the system having relatively high energy density. For this reason a high energy density is of considerable value.

B. Rationale for a Screening Test Study

With the large number of potential candidates for the anodes and cathodes of high performance fused salt cells, most rapid progress in a research and development effort is made by a properly designed set of screening tests. Such tests include measurement of the conductivity and melting point of the electrolytes with (1) the cathodic reactant, or (2) the products of the anodic reactant dissolved in them. They also include characterization of the electrochemical behavior of the cathodic or anodic reactant. Initially, this characterization uses tests involving passage of few coulombs; further characterization will, of necessity, involve discharge (and charge, in the case of secondary systems) of significant quantities of reactants, as is required in actual cell operation. The program described below was designed for the selection of promising anodic and cathodic systems by their characterization in initial screening tests.

C. Choice of Cell Electrolyte Solvent

A very important consideration in selection of a fused salt cell system for practical use is low melting point of the electrolyte solvent. Three solvents, which have melting points low enough to be of interest, and which are not easily oxidized or reduced, were selected for this program. These are a $ZnCl_2$-based, an $AlCl_3$-based, and a hydroxide-

containing solvent. The molar compositions and melting points of these solvents are listed in Table 1.*

TABLE 1

MELTING POINTS OF SALT MIXTURES

Salt Composition (mole %)	Melting Point[a] (°C)
$ZnCl_2$(60)-NaCl(20)-KCl(20)	203
$AlCl_3$(61)-NaCl(39)	108
NaOH(50)-KOH(50)	170

[a] G. J. Janz, Molten Salts Handbook,[11] Academic Press, New York, N.Y. 1967

D. Selection of Cell Reactants

With a given electrolyte, the most important parameter in a fused electrolyte battery is high, sustained, power-delivery capability. This requires a high exchange current density for both anodic and cathodic reactions, as well as freedom from buildup of films or deposits as the discharge (and charge, for secondary systems) proceeds. Also, the reactant and product materials must be capable of being accommodated in a practical

* Originally, the composition $AlCl_3$(66)-NaCl(20)-KCl(14) was selected for investigation because this melt allegedly had a melting point of only 70°C. However, as described in Appendix I, this melting point is incorrect and solids actually form with temperatures as high as 135°C.

cell, so as to minimize the effects of concentration polarization. Generally, with the relatively high temperature involved, electrode reactions involving condensed phases with fused salt electrolytes are expected to exhibit relatively high exchange current densities.

A list of the electrochemical couples investigated in this program is given in Table 2. These were selected because they showed promise of high power density or high energy density when investigated in other media. While the use of these anodes and cathodes might not yield energy densities higher than existing systems, development of suitable solid electrolytes could permit use of soluble cathodes with alkali metals, thus yielding improved energy densities. The couples listed in the first column were tested in both the $ZnCl_2$-containing and in the $AlCl_3$-containing solvents. Those in the second column were tested in the hydroxide-containing solvent.

TABLE 2

COUPLES SCREENED

Ag/AgCl	Ag/Ag_2O
Cu/CuCl	Cu/Cu_2O
Cu/$CuCl_2$	Cd/CdO
Ni/$NiCl_2$	Cu/CuO
Bi/$BiCl_3$	
Sb/$SbCl_3$	
In/CuCl, $CuCl_2$ [a]	Al/Al_2O_3
In/$CrCl_2$, $CrCl_3$	Be/BeO
In/$FeCl_2$, $FeCl_3$	Mg/MgO
	Zn/ZnO
Al/$AlCl_3$	
Be/$BeCl_2$	
Mg/$MgCl_2$	
Zn/$ZnCl_2$	

[a] In = Inert Electrode

E. Purification of Salts

One of the tasks of this program was the preparation of high purity salts, free not only of metal contaminants but also of non-metal impurities, an important one being oxygen. The goal of this purification task was to obtain salts containing less than 100 ppm (by weight) of any impurity. While a great deal of effort has been spent in determining metal impurities in fused salt studies, little attention has been paid to determining the concentration of non-metal impurities. An example of this is the fact that optical grade, clear and colorless single crystal NaCl was found in this study to contain over 1200 ppm (by weight) of oxygen. Thus, the removal of non-metal impurities in the purified salts constituted an important phase of this program.

F. Screening Program

The screening program of the electrochemical couples (listed in Table 2) dissolved in the solvents (listed in Table 1) consisted of the following tests. First, compatibility tests were carried out on those systems in which thermodynamic calculations indicated that the metal would chemically react with the corresponding salt or the solvent. If reaction took place, no further tests were done and the system was considered unsatisfactory. Linear sweep voltammetry was carried out on the remaining systems. If the results indicated that sufficient electroactive species were present, galvanostatic measurements were taken. In addition, the electrical conductivity and the freezing point of the solvent containing 15 wt % cathodically active or 5 wt % anodically active material were measured.

II. VOLTAMMETRIC SCREENING TECHNIQUES

To screen a large number of candidate electrode materials efficiently, rapid electrochemical methods were used. Two voltammetric techniques were used for this purpose. The first was linear sweep voltammetry, which employs a linear potential sweep. The second was current-step voltammetry and is based on the perturbation of a well-poised electrode by the sudden application of a constant current.

A. Linear Sweep Voltammetry

Linear potential sweep voltammetry (L. S. V.) is a direct outgrowth of classical polarography, which developed as solid electrodes were substituted for the more usual dropping mercury electrode, in order to extend the anodic potential range of the measurements. Another advantage of this method is that the speed of measurement is increased. In linear sweep voltammetry a potentiostat forces the potential difference between the working and reference electrodes to duplicate the signal supplied by the linear-sweep function generator. The current required to maintain this condition then appears in the indicator-counter electrode circuit. Several types of results obtained with this method are depicted qualitatively in Figure 1. The feature of greatest interest is the characteristic current peak that is obtained under certain conditions by scanning anodically or cathodically from a point of zero current. It is important to realize that a maximum current occurs only when the accelerating effect of increasing potential on the reaction rate is offset by the depletion of reacting material at the electrode. This depletion may be diffusion-limited, as in curves (a), (b), and (b'); by film stripping, as in curve (c); or by passivation through film formation, as in curve (d). If no

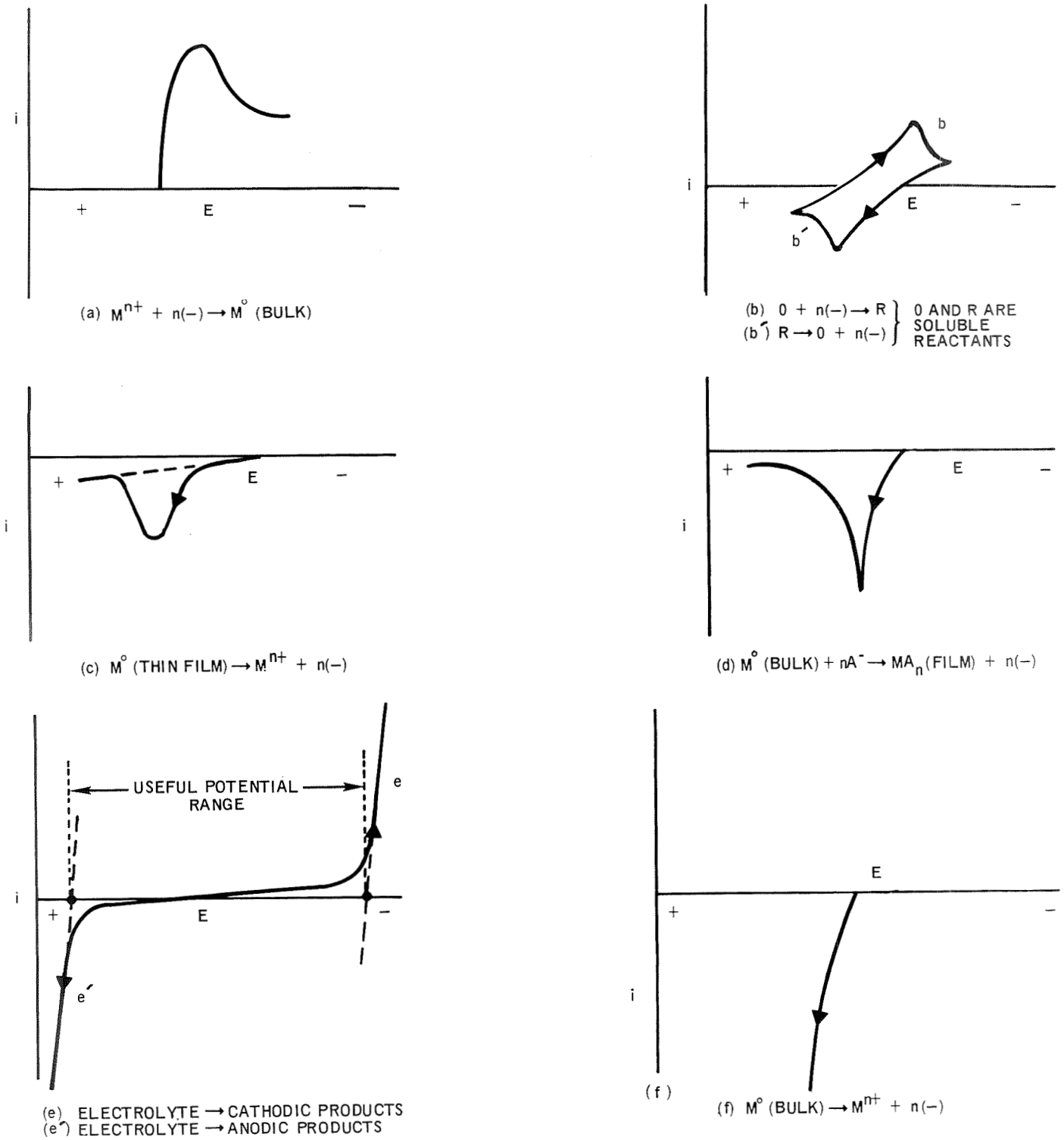

1-22-69 UNCL

00-102526A

Fig. 1. Current-Potential Curves in Linear Potential Sweep Voltammetry

depletion occurs, as in curves (e) and (f), the current continues to rise as the potential increases in that direction, and the curve loses much of its diagnostic value. Curve (f) in Figure 1 for bulk metal dissolution requires further comment. An active bulk metal phase will not be depleted during the anodic voltage sweep; hence, no peak current will appear on the anodic scan other than that occurring with the arbitrary reversal of potential. This type of behavior precludes the comparison of anodic and cathodic peak shapes and separations that are generally associated with the linear-sweep technique. The continuously increasing anodic current for bulk metal dissolution was predicted mathematically[1] by the adaptation of equations given by Berzins and Delahay for the inverse deposition method.[2]

When rapid voltage scanning is employed to minimize convection effects, the current-potential, or current-time, curves are found to exhibit peaks that depend on the sweep rate, as well as on the nature of the reactive material, its concentration, and charge-transfer kinetics. For a simple, diffusion-limited charge transfer reaction involving a reversible metal/metal-ion couple, a cathodic voltammogram will show an initially vertical rise in current and a peak given by the relation[3]

$$\begin{aligned} I_p &= 0.541\, n^{3/2} F^{3/2} A C D^{1/2} s^{1/2} / R^{1/2} T^{1/2} \\ &= 6.33 \times 10^6\, n^{3/2} A C D^{1/2} s^{1/2} / T^{1/2} \end{aligned} \qquad (1)$$

at a voltage, E_p. The difference between E_p and the open circuit voltage E_{eq} is

$$E_{eq} - E_p = 0.854\, RT/nF = 0.0737\, T/n \ \text{(mv)}. \qquad (2)$$

In the above relations I_p is the peak current in amp, A the area in cm^2, C the solute concentration in moles/cm^3, D the diffusion coefficient in cm^2/sec, s the sweep rate in volt/sec, and the other symbols have their usual significance.

Semi-infinite linear diffusion has been assumed. Thus the peak current is a linear function in $s^{1/2}$ and the peak potential is independent of sweep rate. For a non-reversible metal/metal-ion couple with a simple charge transfer reaction the slope of the initial part of the cathodic sweep is not infinite but is proportional to the exchange current density and the peak is broadened. The peak current obeys the relation[3]

$$I_p = 5.20 \times 10^6 n (\alpha n_a)^{1/2} AD^{1/2} Cs^{1/2}/T^{1/2} \quad (3)$$

and the peak potential shifts with sweep rate. In this equation α denotes the transfer coefficient and is less than unity, and n_a is the number of electrons in the rate determining step, usually less than n. Thus peak currents for irreversible processes are also proportional to $s^{1/2}$ but are generally of smaller slope and magnitude than the values expected for reversible cases. For redox couples analogous relations pertain. For simple, reversible charge transfer reactions the following relations[3] were derived assuming no reduced species present

$$I_p = 4.7 \times 10^6 n^{3/2} AD^{1/2} Cs^{1/2}/T^{1/2} \quad (4)$$

and the peak to peak voltage span, ΔE_p, which is $E_p^{cath} - E_p^{an}$,

$$\Delta E_p = 0.188\ T/n \quad (mv) \quad (5)$$

For systems where both oxidized and reduced species are present in solution the above equations should not be very different. For non-reversible couples the peak currents are smaller and the ΔE_p span greater than those given by relations 4 and 5. It should be emphasized, however, that a sizeable, uncompensated IR drop (greater than 20/n mv) in the cell will produce similar

effects[4] as irreversibility. Corrections for uncompensated IR effects on I_p and E_p or ΔE_p can be estimated[4] and applied. If none of the above equations (1-5) hold, then reactions other than simple charge transfer are occurring. Such complications can be studied and diagnosed by applying the appropriate range of voltage scans[5] but this aspect is beyond the scope of the present study. Finally, an alternate method which is independent of sweep rate can be utilized as a measure of the exchange current for couples such as a metal in equilibrium with its ions or a redox system where both oxidation states are present. The initial slope of voltammograms of such systems is determined by the total resistance of the cell (provided that the measuring instrument's response is fast enough to follow the signal). The cell resistance initially is determined by the exchange current I_o, i.e., it is given by $RT/nF\ I_o$ and the electrolyte resistance. Thus in those cases where the charge transfer resistance is much larger than the electrolyte resistance the exchange current equals $(RT/nF)(dI/dE)_{E=E_{eq}}$. For fast reactions, i.e., large exchange current densities, or in any case where the charge transfer resistance becomes smaller than the electrolyte resistance the initial slope of the voltammogram will be determined primarily by the electrolyte resistance and only a lower limit of I_o can be calculated.

B. Current-Step Voltammetry

1) Introduction

Many metal/metal-ion couples exhibit high exchange currents in molten salt electrolytes.[6,7] Perturbation techniques that operate under near-equilibrium conditions can often provide a measure of the exchange current and hence the reversibility of an electrode.

Single pulse current-step voltammetry, one of the simpler perturbation methods, was selected for the determination of the exchange current. In this method, the potential of the electrode whose kinetics is being studied is initially at its open circuit value, and a current pulse, ideally represented by a step function, is applied to the unstirred electrolytic cell. The time response of overvoltage with this technique is illustrated in Figure 2. Upon the application of a constant current, the potential of the indicator electrode shows an instantaneous vertical rise due to ohmic drop, followed by a further rise with a steep slope that accompanies the charging of the double layer. This latter process ordinarily is observed in a fraction of a microsecond or microseconds. With the onset of the faradaic reaction, the overpotential becomes proportional to $t^{1/2}$.

The procedure of Bockris and co-workers[8] was used to obtain the exchange current density i_o, the diffusion coefficient D and the double layer

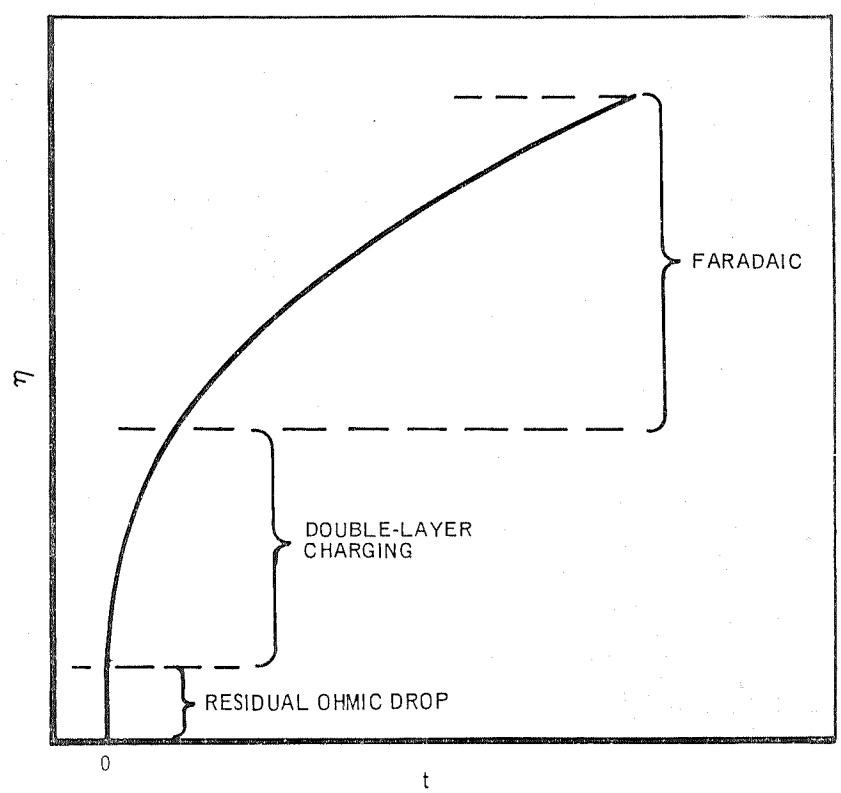

Figure 2. Potential-Time Curve for Current Step Technique

capacitance C_d. In this procedure, two separate constant pulses are applied to the cell. The first pulse is a short one, usually several microseconds in duration, with a relatively large current density, i, of about 500 ma/cm^2. The electrolyte resistance R_s, the value of which is necessary to calculate the overpotential, is obtained from the discontinuous initial increase of the potential E at time t = 0. The double layer capacitance C_d is obtained from the slope of the potential-time curve at t = 0

$$C_d = - \frac{i}{(dE/dt)_{t=0}} \tag{6}$$

A longer constant current cathodic pulse, usually about several milliseconds duration with a lower current density (usually less than 50 ma/cm^2), is then applied and the overpotential η plotted vs $t^{1/2}$. The method for obtaining the diffusion coefficient and the exchange current density is given below for a redox system and then for a metal/metal-ion system.

a) Redox Systems

The expression for the linear portion of the η vs $t^{1/2}$ curve in the case of a redox homogeneous system with an inert electrode has been shown by Berzins and Delahay[9] to be

$$\eta = - \frac{RTi}{nF} \left[\frac{2}{\pi^{1/2} nF} \left(\frac{1}{C_o D_o^{1/2}} + \frac{1}{C_r D_r^{1/2}} \right) t^{1/2} - \frac{RTC_d}{nF} \left\{ \frac{1}{nF} \left(\frac{1}{C_o D_o^{1/2}} + \frac{1}{C_r D_r^{1/2}} \right) \right\}^2 + \frac{1}{i_o} \right] \tag{7}$$

where RT/nF has its usual significance. The subscripts o and r refer to oxidized and reduced species, respectively, and C is the bulk concentration of the electroactive species.

The assumptions made in obtaining eq. (7) are:

(1) There is a large excess of supporting electrolyte

2) Conditions of semi-infinite linear diffusion prevail

3) The number of electrons involved in the rate determining step is equal to the number of electrons in the overall reaction

4) $\eta \ll RT/nF$; i.e., the departure from the equilibrium potential does not exceed a few millivolts

5) The only sources of polarization are due to charge transfer and diffusion.

The parameter containing the diffusion constant can be obtained by differentiating eq. 7 with respect to $t^{1/2}$

$$\frac{1}{C_o D_o^{1/2}} + \frac{1}{C_r D_r^{1/2}} = \frac{\pi^{1/2} n^2 F^2 \, dE/dt^{1/2}}{2RTi} \tag{8}$$

By recasting the above equation, the following expression is obtained

$$\frac{-2RTi}{\pi^{1/2} n^2 F^2 (dE/dt^{1/2})} = \frac{C_o D_o^{1/2}}{1 + \frac{C_o D_o^{1/2}}{C_r D_r^{1/2}}} = f(C_i D_i^{1/2}) \tag{9}$$

Since $f(C_i D_i^{1/2})$ makes no assumptions about the values of C and D, this parameter was determined and tabulated for all the redox systems.

If the assumption is made that $C_o = C_r$ and that $D_o = D_r$, then the following expression is obtained for D

$$D = \frac{16 R^2 T^2 i^2}{\pi n^4 F^4 C_o^2 (dE/dt^{1/2})^2} \tag{10}$$

Values of D were tabulated for all the systems.

The value of i_o can be obtained from the overpotential extrapolated to zero time, η_o. Solving eq. 7 for i_o, when t = 0, results in

$$i_o = \frac{-\frac{RTi}{nF\eta_o}}{1 - \frac{R^2T^2iC_d}{n^3F^3\eta_o}\left(\frac{1}{C_oD_o^{1/2}} + \frac{1}{C_rD_r^{1/2}}\right)^2} \tag{11}$$

The term $\frac{1}{C_oD_o^{1/2}} + \frac{1}{C_rD_r^{1/2}}$ in eq. 11 is obtained from the slope of the vs $t^{1/2}$ plot (eq. 8). In many of the runs reported in this work, the first of the two terms in the denominator of eq. 11 was negligible because of the high concentrations involved ($C = 10^{-4}$ moles/cm^3); in those cases equations 7 and 12 become, respectively,

$$\eta = \frac{-RTi}{nF}\left[\frac{2}{\pi^{1/2}nF}\left(\frac{1}{C_oD_o^{1/2}} + \frac{1}{C_rD_r^{1/2}}\right)t^{1/2} + \frac{1}{i_o}\right] \tag{12}$$

$$i_o = \frac{-RTi}{nF\eta_o} \tag{13}$$

b) Metal/Metal-Ion Systems

The linear portion of the η vs $t^{1/2}$ curve for metal/metal-ion systems has been shown by Bockris and co-workers[8] to be

$$\eta = \frac{-RTi}{nF}\left[\frac{2\,t^{1/2}}{\pi^{1/2}nFC_oD_o^{1/2}} - \frac{RTC_d}{n^2F^2C_o^2D_o} + \frac{1}{i_o}\right] \tag{14}$$

The expressions for $C_oD_o^{1/2}$ and D_o are

$$C_oD_o^{1/2} = \frac{-2\,RTi}{\pi^{1/2}n^2F^2(dE/dt^{1/2})} \tag{15}$$

$$D_o = \frac{4R^2T^2i^2}{\pi n^4F^4C_o^2(dE/dt^{1/2})^2} \tag{16}$$

When C_o is large, then

$$\eta = \frac{-RTi}{nF}\left[\frac{2t^{1/2}}{\pi^{1/2}nFC_oD_o^{1/2}} + \frac{1}{i_o}\right] \tag{17}$$

2) <u>The Effect of Finite Rise Time of Pulse Generator on the Measured Value of C_d</u>

The treatment described above for calculating R_s and C_d makes the assumption that the rise times of the instruments are negligible. While the rise time of the oscilloscope was negligibly small (50×10^{-9} sec), that of the pulse generator was about 0.3 μsec. (See p.A4 for determination of the rise time.) Thus, instead of having a discontinuous change in voltage when the current was initially applied, a continuous voltage was obtained (see for example Figure 12c). Since the current produced by the pulse generator reached its maximum in about 0.5 μsec, it was decided to determine the IR_s drop and C_d at 0.5 μsec. Therefore, it was necessary to find the conditions under which reasonably accurate values of C_d could be obtained at 0.5 μsec. These conditions were found by analyzing a synthetic circuit with a resistor (corresponding to the electrolyte resistance, R_s) in series with a parallel combination of a resistor (charge transfer resistance) and capacitor (double layer capacitance). It was assumed that the diffusion process is not important in the short time (<1 μsec) that the resistance and double layer capacity are measured. The current pulse I(t) was assumed to have the form

$$I(t) = I\left[1 - \exp\left\{-t/\tau\right\}\right] \tag{18}$$

where τ is a constant characteristic of the pulse generator and I is the current at infinite time. The details of the derivation are given in Appendix II. It is shown there (Eq. A-12) that the condition for obtaining a reliable value of the double layer capacitance from the slope of the E vs t plot is

$$\tau \ll t^* \ll R_p C \tag{19}$$

where t* here is the time that the slope is taken and in this case is 5×10^{-7} sec; R_p is the charge transfer resistance, and C is the double layer capacitance (in farads).

The charge transfer resistance R_p is given by

$$R_p = \frac{RT}{nFI_o} \tag{20}$$

where I_o is the exchange current. Substituting eq. 20 into 19 and using exchange current densities, i_o and double layer capacities C_d ($\mu F/cm^2$) instead of I and C, The condition described by eq. 19 is

$$\tau \ll t^* \ll \frac{RT\,C_d}{nFi_o} \tag{21}$$

From eq. 21 it is seen that values of C_d will be less accurate when τ becomes large, or when the ratio C_d/i_o is small.

The value of τ for the pulse generator used in this work was determined to be 0.138 μsec (see Appendix II-B, p. A4). Thus, the first condition, $1.38 \times 10^{-7} \ll 5 \times 10^{-7}$ can be considered acceptable since $\exp\left\{-t/\tau\right\}$ is 0.027. One exception to this is if R_s is unusually large (e.g. 10 Ω). Under such circumstances the measured C_d can be too low (see Appendix II-C, p. A4). For the second condition to hold, $5 \times 10^{-7} \ll \frac{RT}{nF}\,\frac{C_d}{i_o}$. In this study, RT/nF is

about 0.04 for n = 1. If C_d is about 2.5×10^{-5} F/cm^2, then the condition is $5 \times 10^{-7} \ll 1 \times 10^{-6}/i_o$. Thus in many fused salt systems where i_o is expected to be 1 amp/cm^2, the above method for obtaining C_d is not expected to be valid. Some theoretical curves of E vs t to illustrate this are given in Appendix II-D.

4) Crystallization Overpotential

The above procedure makes the assumption that charge transfer resistance and diffusion are the only sources of polarization. In that case, a plot of E vs $\sqrt{t}$ yields a straight line in times sufficiently long so that the double layer is completely charged. However, in the case of metal/metal ion electrode couples, polarization due to another source is possible — i.e., crystallization polarization.[10] During the anodic metal dissolution and the cathodic metal deposition, metal ions migrate along the surface until the metal ions are removed from the lattice or are incorporated into the crystal lattice. Such migrating ions are often referred to as adions. One indication that such a process is taking place is that the E vs $t^{1/2}$ plot is not linear at short times but would exhibit a "negative deviation" from linearity (see Fig. 11f for an example). Many cases of "negative deviation" were found in this work. However, it was beyond the scope of this study to ensure that such deviation was the result of crystallization overvoltage. In such cases, the linear portion of the E vs $t^{1/2}$ plot was extrapolated to t = 0 and the extrapolated overpotential calculated from this value was assumed to be due only to charge transfer polarization. It thus must be realized that in such cases, the calculated exchange current density will be a formal value and may not be closely related to the real value. However, it still might be of value as a screening parameter in comparing different systems. To

give some semiquantitative indication of the extent of crystallization polarization, values of η/I were calculated at 100 μsec for the linear plot and for the actual plot. (The time 100 μsec was selected because charging of the double layer should be complete by then.) The difference between these two η/I values were tabulated.

III. EXPERIMENTAL

A. Preparation of Materials

As stated earlier, one of the important tasks of this program was the preparation of high purity salts, free of non-metal contaminants as well as metal impurities. The determination of non-metal contaminants was carried out by spark source mass spectrometry (SSMS) by Bell and Howell (Pasadena, Calif.). Due to the high cost of such analyses, impurity determinations for each sample were limited to five. Examples of such impurities are C, O, H, N, F, Br, and S. All the materials were analyzed for metal impurities by emission spectroscopy by Pacific Spectrochemical Laboratory (Los Angeles, Calif.).

To obtain salts with very low levels of impurities many of the halides were synthesized from the metal and HCl or Cl_2. In those cases where syntheses were not required the materials purchased in the anhydrous form were treated as described below. After treatment or synthesis the salts were stored in jars in an inert atmosphere dry box. Unless specified, all the salts and metals used were obtained from Research Inorganic Chemical Corp. (Sun Valley, Calif.).

1. Metals

All the metals used in the salt syntheses or as electrodes were reported to be at least 99.99% pure or the highest purity available. Zinc wire, 0.25 mm diameter and 99.99+%, was purchased from Cominco-American. Magnesium wire (0.40 mm diameter, 99.99+%) and foil (0.43 mm thick, 99.99%) were kindly donated to us by the Metallurgical Laboratory of The Dow Chemical Co. Beryllium wire (0.25 mm diameter, 99.5+%) was donated to us by the Beryllium Corp. High purity distilled beryllium foil (99.99%), used in the compatibility tests, was kindly given to us by the Lawrence Radiation Laboratory of the University of California.

The emission spectrographic analyses of the metals are shown in Table 3. Only those impurities with concentrations greater than 10 ppm are included. The following metals had no impurities greater than this level and are thus not listed: Ag wire and foil, Al wire, Al lump, Bi shot, Cd wire, Cu wire and foil, Fe powder, Mg lump, Ni wire, Pt wire and foil and Sb shot. With the exception of the Be wire, no impurity exceeded 100 ppm. Due to the exorbitant cost of Be wire of higher purity, this sample was deemed acceptable for the one experiment in which the wire was used.

2. Gases

a. Hydrogen Chloride - The hydrogen chloride obtained from Precision Gas Products, Inc., was ultra high purity grade (99.995+%). The analysis reported by Precision Gas Products is presented in Table 4. The HCl was passed through $Mg(ClO_4)_2$ and a dry-ice acetone trap before use.

b. Chlorine - The chlorine was also obtained from Precision Gas Products, Inc., as their electronic grade and was 99.98+% pure. The

TABLE 3

EMISSION SPECTROGRAPHIC ANALYSIS OF METALS[a]

Impurity	Al(f)	Be(w)	Be(f)	Cd(f)	Mg(w)	Mg(f)	Ni(f)	W(w) #1	W(w) #2	Zn(w) #1	Zn(w) #2	Zn(s)
Al		840				17		<30			12	
Ca					24			40	34			
Cd											19	
Co							30					
Cr								50	60			
Cu				40			20					
Fe	20	880			37	12	50				37	25
Mg	<30						13	20				
Ni	20	30										
Si		760			70	<20		<30		15	12	
Zn				100								
C[b]		550	20									
O[b]		200	30									

(a) In ppm by weight.

(b) Analysis from supplier.

w = wire, No. 1 = 0.25 mm diam.; No. 2 = 1.5 mm diam.

f = foil

s = solid used for synthesis

reported analysis is shown in Table 4. The Cl_2 was bubbled through concentrated H_2SO_4 before contacting any salt or metals.

3. Salts

Emission spectrographic analyses of all the purified chlorides showed that the metal impurity levels did not exceed 100 ppm with the exception of $BeCl_2$. These analyses are given after the preparation and purities of all the halides (see p. 40). A similar sequence as that for the chlorides is followed for the hydroxides and oxides. As will be seen below, the following chlorides could be obtained with no impurity exceeding 100 ppm: KCl, $AlCl_3$, $ZnCl_2$, $FeCl_3$, $CuCl_2$, CuCl, AgCl, $BiCl_3$, and $NiCl_2$. The following chlorides contained up to 200 ppm contaminants: $BeCl_2$ and $SbCl_3$. The salts NaCl and $CrCl_3$ contained up to 400 ppm and only $MgCl_2$ exceeded 500 ppm.

Due to time limitations, the same intense effort on purification could not be given to the hydroxides and oxides. Consequently, the impurity levels of these compounds in general far exceeded those of the chlorides. Since preliminary experiments indicated little solubility of any of the oxides in the hydroxide melts, it was felt that it was unnecessary to extensively purify them.

a) Materials for Chloride Solvents

1) Potassium Chloride - Optical grade single crystal KCl was analyzed by spark source mass spectrometry and the results are shown in Table 5 (column 2). Since no impurity exceeded 100 ppm, no further treatment was deemed necessary.

2) Sodium Chloride - Optical grade, clear and colorless, single crystal NaCl was found to contain over 1200 ppm oxygen (see Table 5, column 3). This was rather surprising in view of the fact that NaCl is often

TABLE 4

ANALYSIS[a] OF HIGH PURITY HYDROGEN CHLORIDE AND CHLORINE GASES

Components	HCl	Cl_2
Oxygen	< 8	
Nitrogen	14	
Argon	< 10	
Carbon Dioxide	N.D. < 10	< 25
Carbon Monoxide	N.D. < 15	N.D. < 20
Methane	N.D. < 10	
Hydrogen Bromide	< 10	
Moisture	8	< 10
Air	—	27
Other Impurities	< 10[b]	< 75[c]

(a) In ppm by weight.

(b) Scanned from mass 2 through 100.

(c) Chloroform and carbon tetrachloride.

used as a primary standard. Thus, unlike KCl, NaCl could not be used untreated and had to be purified.

The method used to remove the oxygen consisted of bubbling HCl through the molten NaCl and then filtering it under vacuum. The salt was placed in a fused silica tube containing a frit at the bottom and gas inlet and outlet tubes. The inlet tube extended down to within one inch of the frit. This part of the apparatus was fitted inside another larger tube containing a large test tube to catch the molten salt as it was filtered. This

part of the assembly is also composed of fused silica. The larger outer vessel, containing the test tube, also had a stopcock to enable its evacuation and thus force the NaCl through the frit. The assembly was evacuated and heated slowly to 300°C. The system was repressurized with argon and the HCl flow started. Dry ice-acetone traps were employed on both the inlet and exit gas lines. The salt was heated above its melting point and HCl bubbled through the melt for about one hour. The HCl flow was then stopped and the outer envelope evacuated to filter the melt. After all the NaCl had come through the frit, the system was cooled under vacuum. Three batches of salt, including a separate batch obtained from Harshaw Chemical Co., were treated in the above manner. Analyses showed that the oxygen content was about 300 ppm (columns 4-6). In another treatment, solid salt was heated to 700°C under HCl before it was melted and Cl_2 bubbled through. The analysis showed the oxygen content to be 1,000 ppm (column 7) and therefore this batch was discarded. It thus appears that HCl must be bubbled through the melt to remove most of the oxygen. Bubbling both HCl and Cl_2 through the melt might have been more effective; however, time did not permit carrying out this test. Thus, to our surprise, NaCl appears to be one of the more difficult salts to obtain oxygen-free.

3) Aluminum Trichloride - Since $AlCl_3$ is an exceedingly difficult salt to prepare pure, the procedure used is described in a fairly detailed manner. The $AlCl_3$ was prepared by reacting Al metal (99.99%) with HCl at 600°C. The Al metal was cleaned in chloroform and then in a mixture of 50 cm^3 H_2SO_4, 60 cm^3 H_3PO_4 and 15 cm^3 HNO_3 for a few minutes. It was finally rinsed with distilled water and acetone and dried in air. About 100 gms of the metal was loaded into two 20 cm^3 alumina boats (Coors 99.8%)

TABLE 5

S. S. M. S. ANALYSIS[a] OF KCl AND NaCl

Impurity	KCl	NaCl				
	#1 [b]	#1 [b]	#2 [c]	#3 [d]	#4 [e]	#5 [f]
H	3	23	7	6	16	32
C	27	70	79	18	15	7
O	100	1268	280	350	350	1000
S	21					
Si		<4	10	13	8	7
Br	100		8	N.D.	N.D.	
N						3
Fe	2					

a) In ppm by weight.

b) Optical grade, clear and colorless single crystal, untreated.

c) Melted, treated with HCl for 15 min, and filtered under vacuum.

d) Melted, treated with HCl for 2 hours, and filtered under vacuum.

e) Harshaw NaCl treated in same way as (d).

f) Solid salt heated to 700°C under HCl, melted and Cl_2 bubbled through the melt.

in air and the boats positioned side by side in a fused silica tube. The alumina boats served to protect the fused silica from the hot aluminum as well as any reactive non-volatile products (e.g., AlOCl) that might be formed. The reaction apparatus, shown in Figure 3, consisted of two 50 mm tubes joined by an 18 mm tube containing a graded seal and a Pyrex frit. The frit served to minimize sudden changes in HCl flow. The reaction tube was fused silica and the distillation receptacle was Pyrex. All joints were coated with fluorinated hydrocarbon grease. The reaction vessel was connected to the vacuum system and gas manifold as shown in Figure 3. Some quartz wool was inserted

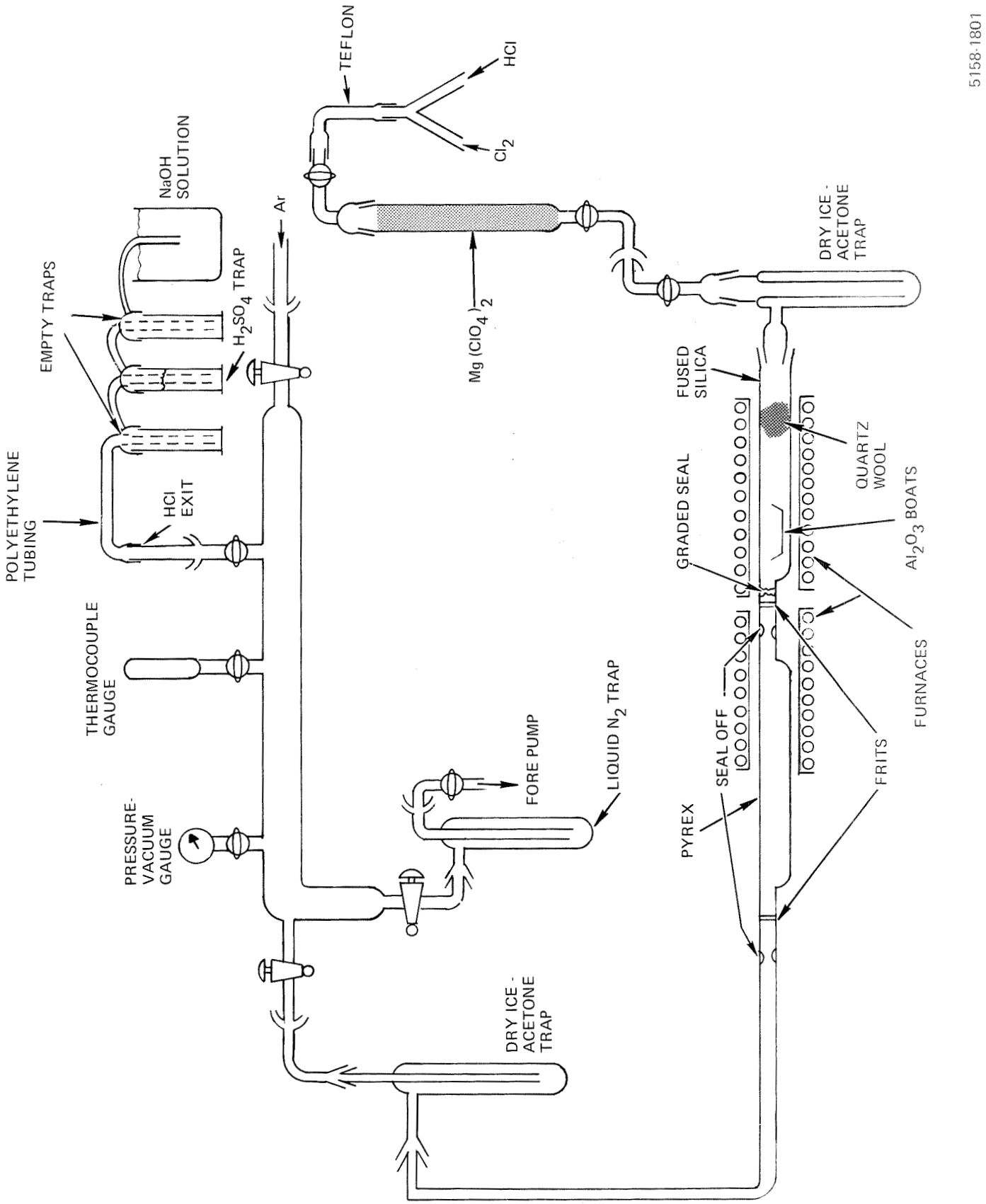

Fig. 3. Apparatus for Preparing and Purifying Salts

at the gas inlet end of the tube to prevent any volatile salt from diffusing back and plugging the inlet line. The whole assembly was placed in a vacuum hood. The system was pumped down, flamed and repressurized with argon. The HCl tank, which was joined to the system by glass and Teflon tubing, was opened and the flow rate was adjusted to about 1/2 cm^3/sec. The gas flow, which exited through a dry-ice acetone trap and a sulfuric acid bubbler, was checked for HCl from time to time with ammonia to ensure that HCl was present. An excess of HCl must be used to minimize the formation of subhalide. The furnaces, positioned as shown in the figure, were turned on and the temperatures set at 600°C for the reaction furnace and 180°C for the second one. The latter temperature was sufficient to prevent $AlCl_3$ from condensing inside and plugging the narrow connecting tube between the two chambers. An additional half-shell heater at 180°C was positioned on the top part of the second chamber after the furnace to prevent plugging in the second chamber. When about 90% of the metal was consumed, the furnaces were shut off and allowed to cool. The HCl flow was then stopped and the HCl was removed from the system by condensing it in a liquid nitrogen trap. The furnaces were moved apart and the second chamber sealed off from the first. The vacuum line was then opened to the $AlCl_3$ vessel and after the HCl was pumped out, the final seal-off was made. The $AlCl_3$ tube was removed to an argon atmosphere dry box where it was broken open and the white salt transferred into a glass jar with a Teflon liner in the screw cap. (At first, polyethylene liners were employed but these discolored in time as did the $AlCl_3$ exposed to them. The synthesis required two days. The analyses of the $AlCl_3$ preparations are given in Table 6. The first and third batch (columns 2 and 4) did not have any impurities over 100 ppm while the second batch (column 3) contained 500 ppm oxygen. The reason

for the high oxygen content in that batch, which was not used in this program, is not known. The alumina boats and fused silica chamber were cleaned in hot acids and reused after baking in air at 700°C.

4) Zinc Chloride — $ZnCl_2$ was even more difficult to prepare oxygen-free than $AlCl_3$ because the oxychloride (ZnOCl) is volatile and thus cannot be readily separated by distillation.[11] The $ZnCl_2$ was prepared by reacting Zn metal with HCl at 675°C. The Zn, 99.99%, was cleaned by melting it in a fused silica tube under vacuum and filtering it through quartz wool. The metal (about 300 gm) was then loaded into two 20 ml alumina boats (Coors 99.8%) in air and the boats positioned side by side in the reaction chamber of an assembly. This apparatus was similar to the one used in the $AlCl_3$ synthesis except that it had four chambers instead of two and was composed of fused silica throughout. The alumina boats served both to protect the fused silica from non-volatile components as well as to keep the molten zinc in the hot zone of the furnace. The frits or quartz wool in the tubes served to minimize the effects of sudden pressure changes. The system was pumped down, flamed, and brought back to atmospheric pressure with argon. After the HCl flow was started, the reaction furnace was heated to 675°C and the second furnace, which kept the distillate molten, was heated to 400°C. The HCl was flowed at a fairly rapid rate and its presence in the exit gas was checked from time to time with ammonia. (The presence of excess HCl is required to minimize ZnOCl + Zn_2Cl_2 formation.) When nearly all of the metal was consumed, the furnaces were moved down the assembly and the liquid $ZnCl_2$ distillate in the second tube was distilled at 650°C into the third tube. Care had to be taken to prevent the $ZnCl_2$ from freezing (except in the last tube) since upon remelting it could crack the tube. After most of the $ZnCl_2$ had been moved into the third chamber,

TABLE 6

S.S.M.S. ANALYSIS[a] OF $AlCl_3$ AND $ZnCl_2$

Impurity	$AlCl_3$			$ZnCl_2$			
	#1	#2	#3	#1	#2	#3	#5
H	2	7	3	14	2	2	6
C	24	12	3	59	9	27	13
O	77	500	48	1100	80-200[b]	78	120
S		33	15	15		<100	
Br		22			55	67	
Ca				115	37		

(a) In ppm by weight.

(b) Range of values found for four separate exposures (two exposures yielded 80 ppm and two yielded 200 ppm).

the first furnace and HCl flow were shut off. The liquid nitrogen trap was filled and the assembly was sealed off under partial vacuum between the second and third chambers. The molten, colorless $ZnCl_2$ was then distilled over to the last chamber at 500°C under vacuum. This tube was sealed off and removed to the dry-box where it was broken open and the salt transferred into a glass jar with a polyethylene liner. This synthesis took about four days for completion. Analyses of the $ZnCl_2$, which was white, are shown in Table 6. The last three batches, in which the HCl distillation of $ZnCl_2$ was carried out at a higher temperature (675°C), yielded a product containing only about 100 ppm oxygen. The high oxygen content in batch #1, which was discarded, is probably due to the presence of ZnOCl.

b) Chloride Solutes

1) Ferric Chloride — Anhydrous $FeCl_3$ was prepared from the elements as described in the literature.[12] About 55 gm of mossy iron

(99.99%) was loaded in an alumina boat in air. The boat was placed in a four-chamber Pyrex apparatus. The apparatus and procedure were similar to those used for the $ZnCl_2$ preparation. After the chlorine flow had commenced the two furnaces were heated slowly to 300°C. When no further color was evident in the reaction tube indicating the formation of $FeCl_3$ had ceased, the furnaces were moved down the tube to sublime the $FeCl_3$ under Cl_2 successively from the second chamber to the last. Care had to be taken to avoid plugging of the tubes. After the $FeCl_3$ was all sublimed over into the last chamber the gas flow was stopped and the last chamber sealed off under vacuum. The analyses of three different samples taken from this batch are shown in Table 7 (column 2). One sample showed about 200 ppm oxygen while the other two were well below 100 ppm. Whether this represents the precision of spark source mass spectrometry or inhomogeneity of the batch is not clear. However, it was concluded that $FeCl_3$ had acceptable impurity levels.

2) Cupric Chloride — Reagent grade, anhydrous salt from Matheson, Coleman and Bell was treated first with hydrogen chloride to dehydrate it and then with chlorine to oxidize any monovalent copper present. The $CuCl_2$ was first pumped at room temperature, then repressurized with argon. After the HCl flow had begun, the furnace was heated to 220°C. After several hours when no further evolution of water was evident, the HCl flow was shut off and the Cl_2 admitted to the system. After one hour the furnace was cooled and when the temperature reached 100°C, the Cl_2 flow was terminated. The Cl_2 in the system was condensed with liquid nitrogen and the tube containing the brown $CuCl_2$ was sealed off. Spectrographic analysis of the salt in Table 7 (column 3) indicates that the impurities are less than 100 ppm.

TABLE 7

S.S.M.S. ANALYSIS[a] OF CHLORIDE SOLUTES

Impurity	$FeCl_3$[b]	$CuCl_2$	CuCl	AgCl #1[c]	AgCl #2[d]	$BiCl_3$	$NiCl_2$
H	16 | 4 | 4	N.D.	N.D.	0.5	N.D.	0.2	–[e]
C	56 | 53 | 14	40	0.4	6	2	6	14
O	220 | 31 | 51	57	N.D.	220	2	1	9
N	– | 3 | 9			78	0.5		
S	2 | |	4	N.D.			2	
Br	7 | <7 | <7		16	280	20	9	6
Fe	| |	30					

a) In ppm by weight.

b) The three sets of values represent 3 different samples analyzed from this batch.

c) Solid salt treated with HCl.

d) Salt (#1) was repurified by passing HCl over melt and bubbling Cl_2 through melt.

e) Salt could not be analyzed for hydrogen.

3) Cuprous Chloride — Anhydrous cuprous chloride is white but is difficult to obtain in this state as is evident by the usual greenish tint due to the presence of hydrated $CuCl_2$. The salt and high purity copper metal were transferred in a dry box into a fused silica tube containing a frit near the center. The vessel was evacuated through an addition tube which was joined to it at right angles near the frit. The salt was heated at 450°C above its melting point to promote the reaction between divalent copper and the metal. The melt was slowly heated to 850°C under vacuum to distill the CuCl up the tube. The vessel was then rotated 180° and the distilled CuCl melted onto the frit. The molten salt was then filtered through the frit by opening the system to helium. The solid CuCl was white and

analyzed to be of high purity (see Table 7, column 4).

4) Silver Chloride — The salt was first purified by passing HCl over the solid. Water and a brown gas, presumably NO_2 from the nitrate present, Br_2 or both, were released. The product contained 220 ppm oxygen and 280 ppm bromine. (See Table 7, column 5.) The above-treated salt was then melted in a fused silica vessel, and HCl first and then Cl_2 was bubbled through the melt. After the dissolved Cl_2 was removed by sparging with argon, the salt was cooled and transferred to the dry-box. There it was ground up and stored in a dark bottle to protect it from light. The analysis is presented in Table 7, column 6, where it can be seen that a very pure product was obtained.

5) Bismuth Trichloride — The $BiCl_3$ was loaded in a two-chamber Pyrex vessel of similar design to that used in the $AlCl_3$ synthesis. The system was evacuated, filled with argon and then HCl. The first chamber and the inter-chamber connecting tube were heated slowly to 350°C and the second chamber to 250°C. After several hours when water evolution had ceased, chlorine was also allowed to flow through with the HCl to oxidize any reduced salt. The molten $BiCl_3$, which was dark before exposure to Cl_2, became yellow-orange after a short time. The temperature of the melt was then raised to 425°C to distill it into the second chamber under HCl. After most of the $BiCl_3$ has passed over to the second chamber, the gas flow was stopped and the HCl in the system condensed out with liquid nitrogen. The salt was sealed off under vacuum and removed to the dry-box. The $BiCl_3$ analysis shows it to be of high purity (see Table 7, column 7).

6) Nickel Chloride — Anhydrous $NiCl_2$ was prepared from Baker and Adamson, low cobalt, reagent grade $NiCl_2 \cdot 6H_2O$. The salt was

loaded into a fused silica two-chamber apparatus similar to that used for $AlCl_3$. The exit line from the apparatus led to a reservoir to collect the water evolved. The system was heated slowly over a period of four hours to 450°C in a flowing HCl atmosphere. After all of the water was driven from the chambers into the reservoir with a torch, the HCl flow was stopped and the system purged with argon. While argon was flowing, the reservoir was removed from the line and the apparatus joined directly to the vacuum manifold. The HCl flow was started again and the salt was heated slowly to 900°C in order to sublime it over to the second chamber. The furnaces were then cooled and the HCl removed from the system by condensing it with liquid nitrogen and the tube sealed off. The salt was removed from the tube in a dry-box and sublimed once more in vacuum at 820°C. The final product was yellow to brown in color and of high purity (see Table 7, column 8).

7) Chromic Chloride — The "anhydrous" salt was loaded in an inert atmosphere box in a vessel identical to that used for $NiCl_2$. The vessel was then filled with HCl and heated slowly to 700°C. After the evolution of water had ceased, the HCl flow was stopped and Cl_2 flow begun. The $CrCl_3$ was sublimed under Cl_2 at 950°C and removed in the usual manner. The violet material contained 220 ppm oxygen and 400 ppm Ni (see Table 8, column 2). Additional salt was obtained from the Oak Ridge National Laboratory. However, while the untreated salt contained only 15 ppm Ni, it contained 400 ppm carbon and 190 ppm oxygen (see Table 8, column 3). It was decided to use the purified product for the screening studies.

8) Beryllium Chloride — Anhydrous $BeCl_2$ was loaded with the aid of a plastic bag into a two-chamber, fused silica-Pyrex apparatus

similar to that used for $AlCl_3$. An argon purge was used during the loading. The system was then filled with HCl and heated slowly to 440°C, the melting point of the salt. When evolution of moisture ceased, the temperature was raised to about 520°C, the boiling point, and the salt distilled under flowing HCl. The salt was white with a slight greenish tint and contained about 200 ppm oxygen (see Table 8, column 4).

9) Antimony Trichloride — Anhydrous $SbCl_3$ purported to be 99.99% pure was submitted for analysis. The results shown in Table 8, column 5, showed that the material was not as pure as claimed. Therefore, this batch was discarded and $SbCl_3$ was synthesized by the procedure described in the literature.[13] The apparatus consisted of a two-chamber fused silica-Pyrex vessel similar to that employed for $AlCl_3$. Chlorine was passed over solid antimony in an alumina boat heated slowly to about 230°C. The product, $SbCl_5$, is a yellow liquid which boils at about 140°C. (Actually, $SbCl_5$ is colorless but when it contains dissolved chlorine it is yellow.) After the reaction was complete, the $SbCl_5$ was frozen with dry ice. The HCl was then removed by condensing it with a liquid nitrogen trap and the system sealed off. The $SbCl_5$ was then transferred slowly into a right angle Pyrex tube containing an excess of antimony metal in the argon atmosphere box. The $SbCl_5$ is a very active oxidizing agent reacting quickly with the metal at room temperature yielding $SbCl_3$. Care must be taken not to contact the rubber gloves with any of the $SbCl_5$ for a rapid reaction will ensue burning a hole in the rubber. After the reaction ceased, the tube was stoppered and removed from the dry-box. The salts in the tube were then frozen in a dry ice-acetone bath and the tube evacuated and sealed off. The tube was then heated slowly to 225°Cto ensure complete reduction of the pentachloride.

The liquid became colorless and the trichloride that distilled over was white when frozen. The analysis is shown in Table 8, column 6. While the oxygen content was virtually unchanged, the other impurities, C and F were drastically reduced.

10) Magnesium Chloride — In this preparation Mg metal was reacted with HCl and the resulting salt distilled. About 20 gms of Mg was cleaned in chloroform, dried and placed in an ATJ-type graphite boat; the boat had been outgassed in vacuum at 900°C for 24 hours. The synthesis tube was a fused silica, two-chamber vessel similar to that used for $AlCl_3$. The system was heated to 750°C under HCl in order to convert the metal to the chloride. Unfortunately, little of the salt distilled over at this temperature and the reaction chamber was full of the molten salt. To increase the distillation rate of the $MgCl_2$ the HCl flow was stopped and the system evacuated. A liquid nitrogen trap was used to remove the HCl; the salt was distilled at 800°C under vacuum. Even under these conditions it took two days to complete the distillation. The product was found to obtain 8600 ppm oxygen and 1200 ppm carbon. A small amount of magnesium was added to the salt which was then redistilled in a sealed, evacuated fused silica tube in an attempt to remove some of the impurities. The final analysis is given in the last column of Table 8 where it can be seen that substantial improvement in purity was obtained, although the oxygen content was still higher than desired. Unfortunately, lack of time did not permit further attempts to reduce the impurity level further.

11) Chromous Chloride and Ferrous Chloride — These materials were synthesized in situ by reducing the trivalent salt with an active metal. Thus, for the redox systems, $FeCl_2 + FeCl_3$ and $CrCl_2 +$

TABLE 8

S.S.M.S. ANALYSIS[a] OF CHLORIDE SOLUTES

Impurity	$CrCl_3$		$BeCl_2$	$SbCl_3$		$MgCl_2$
	#1[b]	#2[c]		#1[d]	#2[e]	
H	27	5	8	6	2	110
C	78	400	13	1700	140	100
O	220	190	200	170	160	680
S	N.D.		3	<30		27
Br						N.D.
F		24		1900	3	
Mg			120			
Na		250			7	
Ni	400	15				

(a) In ppm by weight.

(b) Salt heated to 700°C under HCl and then sublimed at 950°C.under HCl.

(c) Salt obtained from Oak Ridge National Laboratory — untreated.

(d) Untreated — purported to be 99.99% pure.

(e) Synthesized from elements.

$CrCl_3$, the mixtures were prepared in sealed tubes by equilibrating in a rocking furnace known weights of the trivalent salt and zinc or aluminum metal (depending on the solvent) with some of the solvent. Thus, for 0.10 M $CrCl_2$ and 0.10 M $CrCl_3$ (assuming complete solution in $ZnCl_2$–NaCl–KCl 0.0785 g of Zn was reacted at 350°C with 0.76 gm of $CrCl_3$ in 4.40 g $ZnCl_2$, 0.63 g NaCl and 0.81 g KCl. This sample was then added to the molten solvent consisting of 39.66 g $ZnCl_2$, 5.63 g NaCl and 7.29 g KCl in the voltammetry cell. For the $AlCl_3$ melt containing 0.1 M $FeCl_2$ and 0.1 M $FeCl_3$ 0.78 g of $FeCl_3$ was reacted at 200°C with 0.0216 g of Al in 4.50 g of $AlCl_3$ and 1.26 g NaCl. This mixture was then added to the molten solvent consisting of 27.00 g $AlCl_3$ and 7.57 g NaCl.

c) Emission Spectrographic Analyses of Chlorides

The emission spectrographic analyses of all the purified halides are given in Table 9. Just as in the metal case, only those impurities with concentrations greater than 10 ppm are given. The following salts had no impurities greater than 10 ppm and are thus not listed: AgCl, $AlCl_3$, and $BiCl_3$. No impurities over 100 ppm were found in any of the purified salts with the exception of $MgCl_2$ where 300 ppm Al and 810 ppm Si were determined.

d) Material for Hydroxide Solvent

1) Sodium Hydroxide — Baker's reagent grade NaOH, especially low in carbonate content (0.3%), was dehydrated. The hydroxide was placed in a nickel (type-270, 99.98%) cup which was contained in a Pyrex envelope. The vessel was removed from an argon atmosphere dry box and then evacuated. The NaOH was heated slowly to about 400°C and pumped on for about one hour while molten. The system was cooled under vacuum and the nickel cup removed in the dry box.

The following electrochemical procedure was carried out to further purify the melt. A nickel rod was placed in contact with the Ni cup and served as an electrical lead. After the hydroxide was remelted, a platinum wire indicator electrode was inserted into the melt and the container utilized as both the reference and counter electrodes. A cyclic voltammogram showed a very small reduction wave, presumably due to water, about 0.5 v before Na^+ reduction. Addition of a small piece of Na metal removed the wave and is presumed to have yielded anhydrous NaOH. The Ni cup was removed from the furnace and its contents poured onto a flat

TABLE 9

EMISSION SPECTROGRAPHIC ANALYSES[a] OF CHLORIDES

Impurity	$BeCl_2$	$CrCl_3$	CuCl	$CuCl_2$	$FeCl_3$	KCl	$MgCl_2$	NaCl	$NiCl_2$	$SbCl_3$	$ZnCl_2$
Ag										14	
Al	76	<70	15				300				90
Ca			30			14			41		
Co									<50		
Cu		14	X	X	36						
Fe	36		60	30	X		70				
Mg	80						X		22	13	
Mn									<20		
Ni	80	30	15				40		X		
Si			20				810	79		100	
Sn			<20								

(a) In ppm by weight.

piece of Ni foil. The melt had a slight bluish tint suggesting that not all the sodium had reacted. The hydroxide was allowed to cool, then broken up in a mortar and pestle and stored in a polyethylene bottle. The analyses are given in Tables 10 and 11. The carbon content was 1.1%, presumably due to carbonate.

2) Potassium Hydroxide — Baker's reagent grade KOH, especially low in carbonate content (0.4%), was dehydrated in a similar manner as with NaOH. Here the water content was much higher and to minimize spattering the KOH was kept at 200°C under vacuum for several hours. The temperature was then raised slowly in 20° steps until the evolution of water could no longer be observed. The KOH was then heated above its melting point and kept there for several hours under vacuum. Cyclic voltammograms showed that the KOH contained a somewhat larger quantity of water than did the NaOH after evacuation. The remaining water in the KOH was removed with Na metal. Again, a slight bluish tint was observed in the melt. Analysis of the material is presented in Tables 10 and 11. The carbon content was 0.9% — similar to that of the NaOH. The results of the spark source mass spectrometric (S.S.M.S.) method were in sharp disagreement with the emission spectrographic (E.S.) results for Al and Si. The E.S. method showed essentially none of these elements to be present, while the S.S.M.S. method showed extensive amounts (Si — 3500 ppm and Al — 3800 ppm).

e) Oxides

The oxides Al_2O_3, MgO, CdO were spectroscopic grade material obtained from Spex Industries. Both Al_2O_3 and MgO were dried by heating to

TABLE 10

S. S. M. S. ANALYSIS[a] OF HYDROXIDES AND OXIDES

Impurity	Ag_2O	CdO	CuO	Cu_2O	ZnO	KOH	NaOH
H	0.3	3	0.2	3.4	3		
C	1100	240	2	1000	320	9000	11,000
Si	55	210	280	1400	200	3500	53
Ca		540	290				
Cl	29					150	160
Al			220	270	41	3800	61
Fe					41		
V		470					
Nb	1100						

(a) In ppm by weight.

TABLE 11

EMISSION SPECTROGRAPHIC ANALYSIS[a] OF HYDROXIDES AND OXIDES

Impurity	NaOH	KOH	Ag_2O	Al_2O_3	BeO	CdO	CuO	Cu_2O	MgO	ZnO
Ag			X		78	12	100			100
Al				X				50	100	
B								300		
Bi										100
Ca	10						88	70		13
Cu						17	X	X		
Fe								10	15	
Mg						13		30	X	
Pb						45				
Si	13	<50	54		25	50	39	700	61	31
Sn							<20			

(a) In ppm by weight.

500°C in vacuum. The CdO was heated to 350°C in flowing oxygen. Single crystal BeO was kindly supplied to us by S. Austerman of the Autonetics Division of North American Rockwell Corp. It was treated as the Al_2O_3 and MgO. Zinc oxide was heated to 350°C under flowing oxygen while CuO was heated to 400°C in flowing oxygen. Spectroscopic grade Ag_2O from Johnson Matthey Chemicals Ltd. was dried at 100°C for one hour in air.

Cuprous oxide could not be obtained commercially better than 99% pure and therefore was prepared by the method of Donnan and Thomas.[14] About 40 g each of $CuSO_4 \cdot 5H_2O$ and dextrose were dissolved in a liter of water at 30°C. A concentrated KOH solution was added until the insoluble $Cu(OH)_2$ that first formed dissolved. The dark greenish-blue solution was then heated to 70°C where Cu_2O formed and precipitated. The solution was allowed to cool and the reddish-brown precipitate was filtered and washed. The Cu_2O was dried by heating to 400°C in vacuum.

Sodium oxide, which was added to the hydroxide melts in an attempt to increase the solubility of the metal oxides, was not available commercially in high purity. It was prepared[15] by reacting Na_2O_2 with Na in a nickel cup at 150°C in vacuum for 1 1/2 hours and then raising the temperature to 500°C for another 1/2 hour to distill off the excess Na.

The S.S.M.S. and E.S. analytical results of the oxides are shown in Tables 10 and 11, respectively. Samples of Al_2O_3, BeO, and MgO were not submitted for S.S.M.S. analysis due to their complete insolubilities in the melts. Again, the S.S.M.S. results indicated far more impurities than the E.S. results.

B. Apparatus

1. Dry Box

All the measurements were carried out while the cell was in an argon atmosphere dry box. The box, manufactured by Vacuum Atmospheres Corp., had an evacuable entrance port, a recirculating atmosphere line and an internal refrigeration unit (model HE-173-I). Thermocouple leads, electrical circuits and binding posts, were sealed through the box. The gas purification train removed water, oxygen and carbon dioxide and was regenerated about once a month with an H_2-Ar (5-95%) mixture. The atmosphere in the box was analyzed initially for O_2 by gas chromatography.[16] After it was found to contain less than 20 ppm oxygen, the limit of detection, a lighted 60 watt bulb with the filament exposed was utilized to monitor the oxygen content. A dish with P_2O_5 was kept in the box to serve as an additional dehydrating agent as well as a monitor for water. A positive pressure was always maintained in the box at some set value by means of an automatic pressure control (HE-63-P). The salts were weighed in the dry box on a torsion balance, style DLT-2, manufactured by The Torsion Balance Co., to $\pm$ 0.01 gram.

2. Conductivity Measurements

The A. C. conductivity measurements were made with a Leeds and Northrup Jones Bridge (Model No. 4666, accuracy 0.1%), a Hewlett Packard Audio Oscillator (Model 200CD) and a General Radio Tuned Amplifier and Null Detector, Type 1232-A, accuracy 3%.

3. Freezing Point Measurements

The temperatures and freezing point measurements were read on a Westronics recorder (Model D118/U) and a Leeds and Northrup potentiometer (Model No. 8687, accuracy 0.05%). A calibrated chromel-alumel thermocouple (accuracy $\pm$ 1°C) with an ice-bath cold junction was used throughout.

4. Linear Sweep Voltammetry

The linear sweep voltammetry studies were made with an instrument built at Atomics International and modeled after one described in the thesis of G. Lauer.[17] An analagous instrument has been discussed in the literature.[18] The basic circuits of the instrument are similar to those used by many other investigators for a three electrode system. The schematic circuit is given in Figure 4. Both the voltage between the reference and indicator electrode as well as the current are measured by operational amplifiers in the follower modes. Since commercial high-gain solid state operational amplifiers were employed throughout, the instrument is

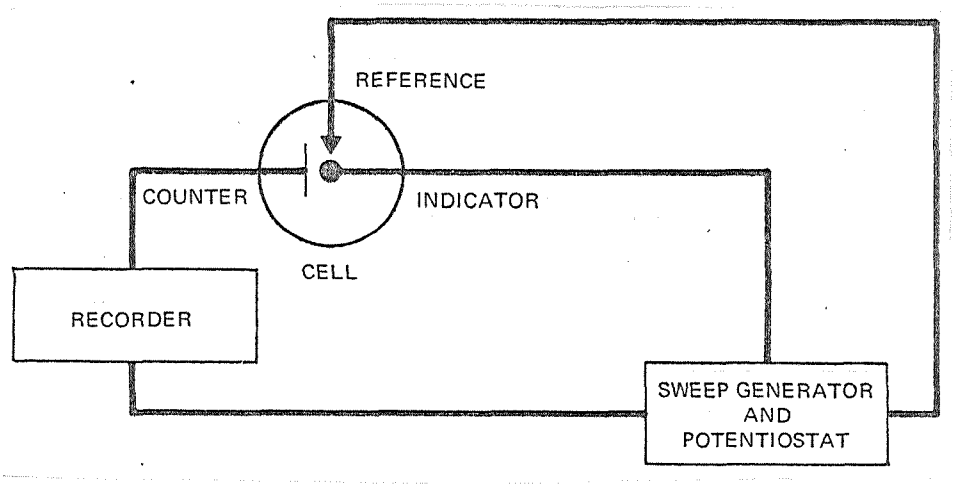

Fig. 4: Schematic Circuit for Linear-Sweep Voltammetry

limited to ± 10 volts at 200 ma. The voltammograms were recorded on a Mosely X-Y recorder, Model 2-D, accuracy = 0.2%.

5. Current-Step Voltammetry

For the galvanostatic measurements a Tektronix Type-160A Power Supply, Type-162 Waveform Generator, and Type-163 Pulse Generator combination were employed. This setup could be adjusted to produce single pulses, positive with respect to ground, of up to about 20 volts amplitude and from 1 to 10,000 microseconds duration. The rise time (the time for the pulse to go from 10% to 90% of its constant value) of the assembly was determined to be about 0.3 microsecond (see p. A-4). To convert the constant voltage pulse to one of constant current, a 1000 Ω resistor (accuracy 0.5%) was put in series with the cell. It was found that ringing was minimized by inserting the resistor at the positive cell terminal. Shielded cable (Type RG 58 C/U) was used throughout and care was taken to avoid ground loops. The leads were connected to the cell with alligator clamps. The output pulse voltages were read on the oscilloscope. The pulses were detected on a Tektronix Type-535A Oscilloscope with a Type-W plug-in unit (tolerance = 3%) and were photographed with a Polaroid camera and film (ASA 3000). The circuit is shown schematically in Figure 5.

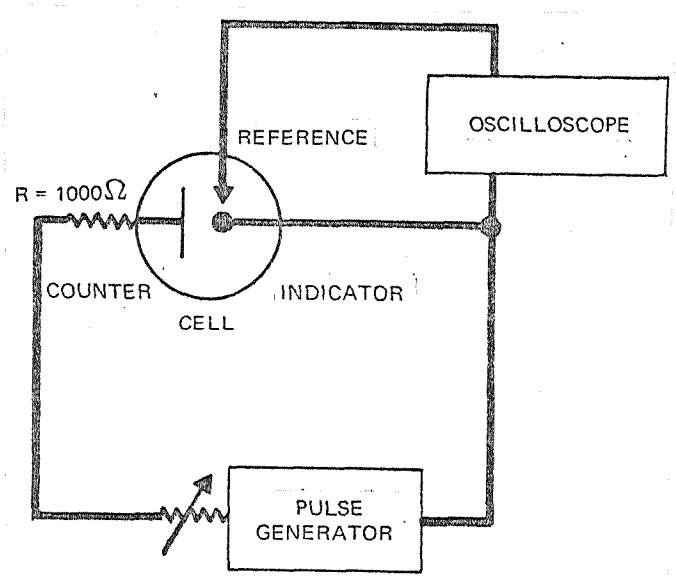

Fig. 5. Schematic Circuit for Current Step Voltammetry

6. Conductivity Cells

The conductivity cell is shown in Figure 6. The cell used for the chloride melts was fabricated of Pyrex and had tungsten electrodes. The tungsten rods (0.51 mm diam.) were sealed in Pyrex tubing with about 3 mm exposed to the melt. The electrodes were positioned just above 20 mm lengths of 1 mm I.D. capillary tubing which served to increase the cell constant. The electrode tubes were inter-connected above the melt by means of a three-way stopcock which enabled solution to be flushed in and out of the capillaries to facilitate taking repeated measurements as well as cleaning. Pressure or suction was applied to the system by means of a syringe with a ball joint connector. The electrode assembly was sealed in a standard taper 34/45 joint and was not sealed to the cell head. This allowed the electrodes to be readily inserted into and removed from the melt. A thermocouple well could also be moved in or out of the melt. The cell head made a gas-tight fit with the base by means of a ground glass flange and some vacuum grease. The melt was contained in a Pyrex cup set inside a heavy-walled aluminum cup to minimize temperature gradients.

A glass encapsulated stirring bar in the solution was rotated by means of an Alnico horseshoe magnet positioned underneath the cell. The magnet was secured to the shaft of a sealed induction motor below the furnace. An induction motor was used to avoid sparking and burn-out problems that occur with electric motors in inert dry box atmospheres.

For the hydroxide melts a similar cell was used except that Coors 99.8% alumina instead of Pyrex was allowed to contact the solution. Two 13 cm tubes, 2.3 mm O.D. x 1 mm I.D., served as the electrode compartments

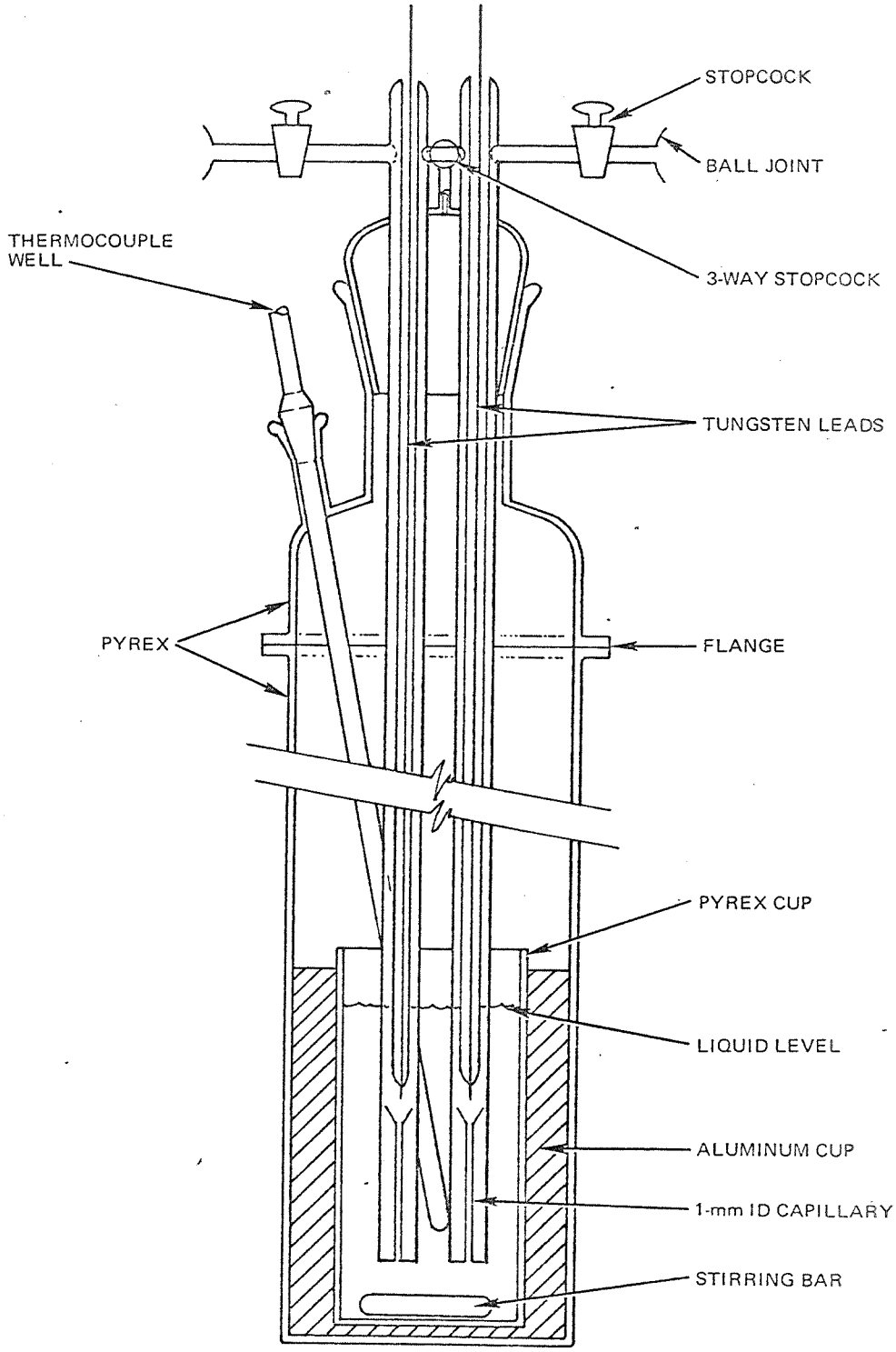

Fig. 6: Electrical Conductivity Cell

and a 13 cm tube, 6.3 mm O.D. x 3.9 mm I.D. and closed at one end, was the thermocouple well. The three tubes were sealed to Pyrex tubes of slightly larger diameter by means of graded seals. Instead of tungsten electrodes 0.50 mm diameter gold wire, which is inert in molten hydroxide, was used. Each gold wire was wrapped around a tungsten lead-through sealed in a standard taper joint. The Pyrex joints fitted their counterparts sealed on top of the electrode tubes and provided a tight seal to enable melt to be forced in and out of the tubes. Although the area of the gold electrodes immersed in the melt varied with the height of solution, the cell constant was relatively insensitive to this variable. (The small diameter alumina tubing below the electrodes provided the chief resistance in the cell.) A Coors alumina crucible (CN-50) contained the melt a nickel (type-270) stirrer was employed.

7. Voltammetry Cells

The voltammetry cell employed for the chloride melts is depicted in Figure 7. It was constructed of Pyrex and the base was interchangeable with that of the conductivity cell. As in the conductivity cell the head made a tight seal with the base by means of a ground glass flange and some vacuum grease. The head contained a thermocouple well, a standard taper joint for the counter electrode lead-through and a syringe barrel for the indicator and reference electrodes. A 20 cm^3 hypodermic syringe was used to allow these electrodes to be positioned at any depth in the melt with ease and still have a relatively tight system. Not shown in the figure is another standard taper joint in the head to accommodate a right-angle addition tube for introducing the solutes. The reference electrode compartment consisted of a tube sealed through the syringe head,

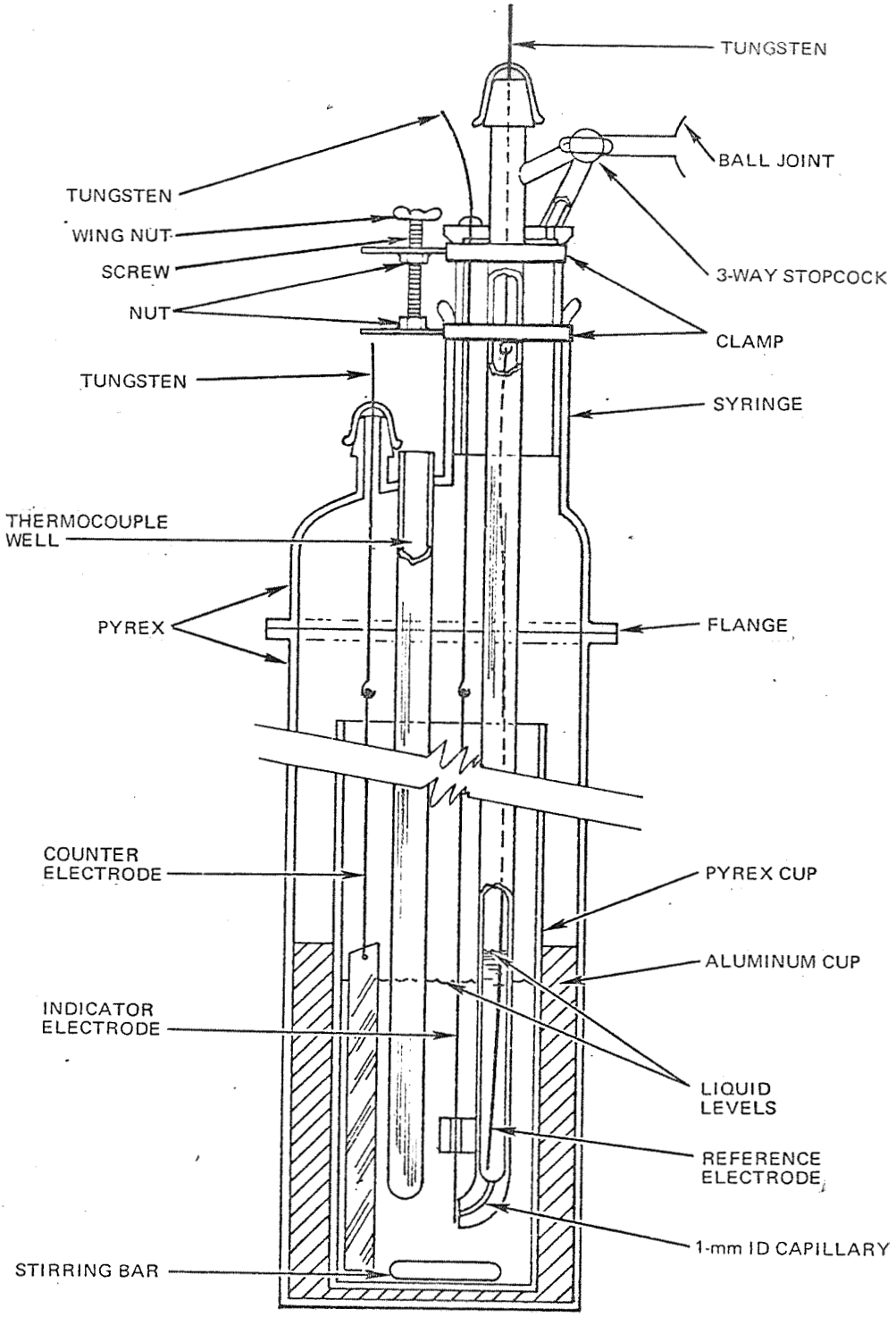

Fig. 7: Voltammetry Cell

with a 12 mm length of 1 mm I. D. capillary joined at the end and bent at a right angle. The capillary was packed with prewashed and dried quartz wool to minimize diffusion between the reference and working compartments. The reference electrode, consisting of appropriate lengths of 1.5 mm diam. Zn or 0.5 mm Al wire in the $ZnCl_2$ or $AlCl_3$ melts, respectively, was wrapped around the lead-through and inserted into the tube. The solvent was drawn into the reference tube with a syringe and a ball joint connector to a level above that in the cup and held there by closing the three-way stopcock. The higher level with its hydrostatic head minimized diffusion of solute into the reference compartment. The indicator or working electrode was usually a 0.25 mm diameter wire, wrappedtightly around the tungsten lead-through, sealed in the syringe head. The indicator electrode was positioned at the mouth of the capillary and held in place there by threading it through a piece of 1 mm capillary sealed to the reference tube about 1.3 cm above the capillary mouth. In those systems where wire electrodes were not available, e.g., Bi and Sb, the metals were melted and filtered into sealed off pieces of heavy-walled capillary of 0.25 cm I.D. The molten metal was contacted with a molybdenum wire lead. The metal was allowed to freeze and the sealed off end of the electrode was cut flush with a silicon carbide wheel yielding a planar electrode of surface area = 0.50 cm^2. Since Bi and Sb expand on freezing, a tight seal was expected in the capillary. These electrodes were secured to a different reference electrode compartment (identical to that above except without the capillary positioner) by fastening the capillary electrode alongside the reference tube with wire so that the exposed electrode face was just above the end of the tube. Care was taken not to wrap any wire near the bottom of the electrode

where the melt might contact it. In those redox systems, where tungsten electrodes sealed in glass were used, the electrodes were also secured alongside the reference tube as with the Sb and Bi capillary electrodes. The depth of immersion of the indicator electrode could be set by means of the screw arrangement shown and could be measured accurately with a micrometer.

The counter electrode, of the same metal as the indicator electrode, usually consisted of a 2.5 cm x 1.3 cm piece of 0.25 mm diam. foil joined to a wire of the same material. The wire lead was fastened through a hole or grooves at the top of the foil and was wrapped around the tungsten lead-through sealed in a standard taper joint. To ensure that the counter electrode stayed in position and did not contact the indicator electrode, especially when the stirrer was on, a heavy-walled glass capillary, or ceramic tube in the hydroxides, was put around the lead wire. Where foils were not available (e.g., Sb, Bi, Zn and W) the metals were cast into other shapes. Thus, Sb and Bi were melted into large flat lumps and contacted with 0.25 mm diameter molybdenum wire imbedded in them. For Zn, 1.5 mm diameter wire was wound into a tight flat spiral of about 18 mm diameter. The tungsten counter electrode was a 1.5 mm diameter wire folded tightly back and forth about ten times at 2.5 cm lengths while hot to yield a compact large area. The melt was contained in a high Pyrex cup positioned inside an aluminum heat ballast. The glass cup was of larger diameter than that employed in the conductivity measurements to accommodate the electrodes and was also much taller to prevent loss of solute upon addition through the head. The melt was stirred with a magnetic stirrer as in the conductivity cell.

For the hydroxide systems the above cell was modified by replacing the glass exposed to the melt with Coors 99.8% alumina. The container was a tall crucible (CN-170); the thermocouple well was a 6 mm O.D. x 3.9 mm I.D. tube closed at one end and the reference electrode compartment was another 6 mm tube with a 0.25 mm diameter hole drilled through one wall about 3 mm from the bottom. As with the conductivity cell both alumina tubes were joined with graded seals to Pyrex tubes at the top. The reference electrode, a gold wire that was anodized in the melt to yield a gold, gold oxide couple, was joined to a tungsten lead-through as before and positioned near the hole in the reference tube with the aid of a one-hole length of alumina tubing. This piece of tubing was secured to the reference tube with molybdenum wire about 2.5 cm above the hole. A bare nickel (type-270) rod served as a stirrer.

8. Heaters

The furnaces for the cells were made from Lindberg/Hevi-Duty semicylindrical heating units, 20 cm in length and 8 cm I.D., wired in parallel. The units were enclosed in an alumina tube, 9 cm I.D., and aluminum foil was wrapped around the outside to decrease heat losses. The furnaces were open at both ends and were secured in a vertical position to ring stands. The furnace temperatures were monitored by chromel-alumel thermocouples and were controlled by West S-C-R Stepless Controllers outside the dry box.

To minimize sublimation of the volatile $AlCl_3$ in the aluminum chloride tests, a Sylvania 1000 watt tungsten halogen lamp in a reflector was used to heat the top of the cell. The temperature of the lamp was controlled with a Variac external to the dry box. Aluminum foil was placed

cylindrically around the cell above the furnace as a reflector to maintain a fairly uniform hot zone.

C. Procedure

The salts were handled and weighed in the dry box. The weights of salts used were sufficient to yield volumes of melt in the voltammetry cells of about 24 cm^3. The concentrations of the solutes added were 15 wt % in the freezing point and conductivity measurements (as well as in some initial voltammetry studies in $ZnCl_2$) and 0.10 M in the voltammetry cells.

1. Compatibility Experiments

Compatibility experiments were made on various halide systems in which thermodynamic data (see p. 60) indicated that a chemical reaction between a metal and a component of the electrolyte should occur. These systems are Cu + $CuCl_2$, Al + $ZnCl_2$, Be + $ZnCl_2$, Mg + $ZnCl_2$, Be + $AlCl_3$ and Mg + $AlCl_3$. In these tests a cleaned, weighed piece of the metal and some of its halide were sealed in an evacuated Pyrex tube containing the solvent. For the copper runs in both $ZnCl_2$ and $AlCl_3$ melts, 15 wt % $CuCl_2$ was added. In all the other tests 5 wt % of the metal halide was used. The system was equilibrated in a rocking furnace for several hours at the highest temperature of measurement required in the program. In many cases, reaction between the metal and melt could be ascertained by inspecting the system during the run. In other instances, at the end of the experiment the solid salts were dissolved away from the metal, and the metal dried and weighed. Changes in weight were taken as evidence of incompatibility. In those cases where the weight change was small (with Be) the surface of the metal was analyzed for Al or Zn by X-ray fluorescence.

2. Conductivity Measurements

The solvent and solute salts were ground together in a mortar and pestle and added to the crucible in the cell by means of a Pyrex funnel inserted through the standard taper joint. The electrodes were then replaced in the cell and manipulated carefully until the standard taper joint was closed. The cell was then positioned in the furnace and heated to the maximum temperature of measurement for the $ZnCl_2$ and hydroxide systems and the melt was stirred for about one hour to ensure complete solution. The temperatures were read with a calibrated chromel-alumel thermocouple inserted in the well. A minimum of three resistance measurements at a frequency of 10 kilocycles per second were read with the leads reversed each time and fresh solution in the capillaries. The solution in the electrode compartments was replaced by flushing the melt in and out of the tubes with a hypodermic syringe and ball joint connector. After a set of reproducible readings was taken, the temperature was lowered in 50° steps and the procedure repeated.

For the $AlCl_3$ melts, the cell was heated to 150°C for the initial temperature of measurement to minimize composition changes due to volatility losses. A tungsten arc was employed to heat the upper portion of the cell and reduce sublimation. It is felt that any small composition changes due to some losses of volatile compounds that occurred would have only a minimal effect on the conductivity values. After the readings at the initial temperature were completed as described above, the temperature was then raised to 200° and the second set of data taken. The final measurements were made at the lowest temperature (about 125°C). Usually another set of measurements was made at 150°C cooling the cell from 200°C, and in most cases, these data checked the initial ones to within 2%.

The cell constants of the conductivity cells for the halides and hydroxides were determined with aqueous 1.00 M KCl at 26.5°C. The constants were 470.5 cm^{-1} for the halide cell and 398.1 cm^{-1} for the hydroxide cell.

3. Freezing Point Studies

Cooling curves were taken on all the systems after the conductivity measurements were completed. The cell was heated to 50° above the minimum temperature of measurement and a cooling curve taken. To minimize temperature gradients and supercooling, the cell was stirred throughout the cooling period. To keep the cooling rate low (about 5° per minute) in order to minimize supercooling, a small steady current was supplied to the furnace. The cooling curve was recorded and the temperatures of interest measured with a potentiometer. Before the experiment was terminated, the cell was heated up again and the thermocouple well and electrodes removed from the melt. The cell, after cooling, could then be disassembled and cleaned easily.

4. Voltammetry Studies

The electrode metals were cleaned in acetone and chloroform and then in acid solution. For most of the metals, dilute HCl or HNO_3 was employed. For aluminum, a mixture of 10 cm^3 H_2SO_4, 3 cm^3 HNO_3 and 12 cm^3 of H_3PO_4 was used. For nickel, a 20 vol % HNO_3, 2% HF solution was employed, while for beryllium the mixture consisted of 10 cm^3 HNO_3 and 1 cm^3 HF in 39 cm^3 of H_2O. Tungsten was electrolyzed with A. C. current in a dilute aqueous NaOH solution. The metals were then washed free of acid, immersed in acetone, and allowed to dry in air or under vacuum.

After the cell was assembled, it was washed again with acetone and dried overnight under vacuum.

The solvent salts were weighed, ground together and added to the crucible, set in the cell. For this addition, a glass funnel was inserted through the syringe barrel in the cell head. The reference and indicator electrodes were then replaced in the syringe barrel and the cell positioned in the furnace. Note that the electrochemically active material was not mixed with the solvent until after the cell was at temperature and the reference compartment filled. The $ZnCl_2$ and hydroxide melts were heated to the maximum temperature of measurement and the $AlCl_3$ melts were heated to about 125°C to minimize distillation. As in the conductivity runs, a heating lamp and aluminum foil reflector were employed to eliminate cold areas in the $AlCl_3$ cells. After the cell had been at temperature for 1/2 hour with stirring, some of the solvent was drawn into the reference compartment and the stopcock closed. This syringe assembly was then slowly lifted out of the melt by means of the screw. When contact with the melt was broken, as determined by the resistance, the distance between the two horizontal metal strips, moved by the screw, was measured with a micrometer. The syringe was then lowered until the indicator electrode was immersed 7.5 mm to yield an electrode area of 0.061 cm^2 for 0.25 mm wire. It was assumed that meniscus and creepage effects up the electrode were negligible. For the glass-sealed electrodes (Sb, Bi, W) the exposed metal was merely submerged completely into the melt. A cyclic voltammogram was then run from a point of zero current to determine that everything was working correctly and to check the solvent purity. The electrochemically active solute was then added by means of the addition tube or with a

funnel inserted through the addition tube joint. The melt was stirred for about one hour at temperature and the bias of the instrument adjusted to the new open circuit potential before measurements were begun. In all the $AlCl_3$ melts, as well as those $ZnCl_2$ melts containing volatile or decomposable solutes, e.g., $FeCl_3$, $SbCl_3$, and $CuCl_2$, the solute was preequilibrated with some of the solvent in an evacuated, sealed Pyrex tube in a rocking furnace. The sample was then quenched, ground up in the dry box and added to the molten solvent in the cell to hasten solution of the solute and minimize volatility losses.

Cyclic voltammograms of the electrode couple were taken at each temperature at four sweep rates: 23, 92, 207, and 368 mv/sec in ascending order. These values were chosen to yield ratios the square root of which equaled 1, 2, 3 and 4 and such that the fastest sweep could still be followed by a pen recorder. The voltammograms were always started from the open circuit potential in a cathodic direction and were usually cycled only once. Frequently after the four voltammograms were recorded, the initial one at the slowest sweep rate was repeated to check the effect of the measurements on the electrode. For the hydroxide melts after the initial voltammograms were run, some Na_2O was added and the voltammograms repeated.

After the cyclic voltammetry sequence was completed at a given temperature, the current-step measurements were made on those cells that exhibited reasonably shaped waves. This condition eliminated the latter measurements being carried out on all the hydroxide as well as the $CrCl_2$ + $CrCl_3$ in $AlCl_3$-NaCl cells. For the galvanostatic studies the cell leads used in the cyclic voltammetry were replaced with shielded cable leads.

In most of the runs, where cathodic pulses were measured, the positive current lead was connected to the counter electrode and the other lead (ground) to the indicator. The oscilloscope probe was attached to the reference and the ground side to the indicator electrode. In those experiments where anodic current pulses were applied to the indicator, the current leads to the cell were reversed since the pulse generator produces positive pulses only. Here, however, the probe leads could not be simply reversed since this would short the reference electrode to ground and send current through it. Two probes were employed in these anodic runs, one connected to the reference and the other to the indicator. The grounds of both probes were shorted to the counter electrode. The pulse was then observed on the oscilloscope by means of the differential input display. During the current-step measurements, all electrical circuits in the box including the furnace and heating lamps were turned off. The solution resistance and double layer capacitance of the cell were measured first by passing a large current (usually 20 ma) for several microseconds. The applied current was determined by measuring the voltage across a 1000 Ω resistor on the oscilloscope. The error involved in neglecting the cell resistance here (of the order of a few ohms) is negligible. For these pulses, maximum intensity and the delayed time scale on the oscilloscope were employed. Pictures were taken with a Polaroid camera set at f-1.9 and a time exposure. After one or more of these short time pulses were taken, long time pulses (up to several milliseconds) were measured at three different current settings (e.g., 1/2, 1, and 2 ma). Although the same camera exposures were used as with the short time pulses, the oscilloscope intensity was turned down and no time delay was necessary. After the long-time pulses were completed,

another short-time run was made to check the reproducibility of the system and the temperature was changed. The above procedure was repeated at each temperature. For the anode systems, Zn and Al, both anodic and cathodic current-steps were run with the cathodic step first. After the final measurement, the electrodes were pulled out of the melt to facilitate cleaning the cell.

IV. RESULTS AND DISCUSSION

The results of the compatibility tests are given first. This is followed by the electrical conductivity and freezing point results. Then the results of the electrochemical screening tests are presented.

A. Compatibility Experiments

Thermodynamic data (see below) indicated that the $Cu/CuCl_2$ couple was incompatible in both $ZnCl_2$-containing and $AlCl_3$-containing solvents. In addition, the data suggested that beryllium and magnesium were incompatible with both solvents and that aluminum would chemically react with the $ZnCl_2$-containing solvent. Equilibrations of the above systems were carried out and it was found that chemical reactions did indeed take place. This incompatibility precluded any further testing for these systems. The results and free energy data[19] at 500°K for the reactions written are given for each system below.

1) Cu-$CuCl_2$

$$Cu(s) + CuCl_2(s) \longrightarrow 2CuCl(s); \quad \Delta G^\circ = -15 \text{ kcal } (-63 \text{ kJ})$$

In both the $ZnCl_2$ and $AlCl_3$ solvents little solid metal and a brownish coppery sludge were present at the end of the experiment. Thus $Cu/CuCl_2$ electrodes cannot be used in these melts.

2) Al-$ZnCl_2$

$$2Al(s) + 3ZnCl_2(s) \rightarrow 2AlCl_3(\ell) + 3Zn(s); \Delta G^\circ = -46 \text{ kcal } (-190 \text{ kJ})$$

The aluminum foil sample, which was initially shiny, became dull grey in appearance in the clear and colorless melt. The metal, which was still intact, showed a 50% gain in weight; x-ray fluorescence corroborated that the coating was zinc.

3) Be-$ZnCl_2$

$$Be(s) + ZnCl_2(s) \rightarrow BeCl_2(s) + Zn(s); \Delta G^\circ = -15 \text{ kcal } (-63 \text{ kJ})$$

The beryllium showed a small gain in weight and x-ray fluorescence indicated that a Zn coating was present. In addition, the melt had dark particles present.

4) Mg-$ZnCl_2$

$$Mg(s) + ZnCl_2(s) \rightarrow MgCl_2(s) + Zn(s); \Delta G^\circ = -52 \text{ kcal } (-220 \text{ kJ})$$

The Mg strip acquired a heavy grey coating in the melt. When this coating was removed, the specimen showed a large weight loss. Some $MgCl_2$ had not dissolved in the melt at 300°C, indicating its solubility in the $ZnCl_2$-containing solvent to be less than 5 wt %.

5) Be-$AlCl_3$

$$3Be(s) + 2AlCl_3(\ell) \rightarrow 3BeCl_2(s) + 2Al(s); \Delta G^\circ = -1 \text{ kcal } (-4 \text{ kJ})$$

The beryllium turned black and showed a very small weight gain in this system. X-ray fluorescence corroborated that a zinc coating was present on the sample. $BeCl_2$ was found to be not very soluble in this $AlCl_3$-NaCl melt.

6) Mg-$AlCl_3$

$$3Mg(s) + 2AlCl_3(\ell) \longrightarrow 3MgCl_2(s) + 2Al(s); \Delta G^\circ = -112 \text{ kcal } (-470 \text{ kJ})$$

The Mg on removal from the melt had a grey coating. After the coat was removed, the metal showed an appreciable weight loss. Again, as in the $ZnCl_2$ melt, not all of the $MgCl_2$ had dissolved in the $AlCl_3$ solvent.

All the above tests (2-6) indicate that reaction of the electrode material and the solvent has occurred. Thus for $ZnCl_2$ melts the only compatible anode metal to be tested in this study is Zn metal; for $AlCl_3$ melts both Zn and Al can be employed as anodes.

B. Electrical Conductivity Tests

The specific electrical conductivities κ of the $ZnCl_2$ solutions are presented in Table 12 and those for the $AlCl_3$ melts in Table 13. Only two sets of data were measured for the hydroxide systems; therefore they have not been tabulated but are given in the text below.

Since no reported conductivity data for this $ZnCl_2$-NaCl-KCl melt composition were found, comparisons cannot be made with other studies. The conductivity of the melt was increased by the addition of the completely soluble monovalent AgCl and CuCl. This increase was virtually the same for both solutes and amounts to about 10%. All the other solutes decreased the conductivity of the melt. If one takes into account the small differences in temperature (e.g., 331° for the solvent and 323° for $CrCl_3$), it can be seen that the decrease is small for $CrCl_3$, $CuCl_2$, $FeCl_3$, $SbCl_3$ and the 5 wt % addition of $ZnCl_2$. The small effect of the first three salts is probably due to their relatively low solubility in this solution. Undissolved $CrCl_3$ was readily evident in the melt and although the $CuCl_2$ and $FeCl_3$ solutions were too dark

TABLE 12

ELECTRICAL CONDUCTIVITIES AND THERMAL HALTS OF $ZnCl_2$-CONTAINING MELTS*

Solute	T (°C)	κ (ohm-cm)$^{-1}$	Thermal Halts (°C)	Comments
None	233 283 331	0.0927 0.198 0.329	205	clear, colorless
AgCl (15 wt %)	225 266 323	0.109 0.202 0.364	188	clear, colorless
CuCl (15 wt %)	226 275 328	0.110 0.221 0.361	200 (small) 156 (large)	clear, colorless, viscous below 200°
$NiCl_2$ (15 wt %)	228 270 322	0.064 0.138 0.204	197	much solid even at 322°
$BiCl_3$ (15 wt %)	225 275 323	0.063 0.147 0.224	212 (small) 197 (larger) 170 (largest)	opaque
$SbCl_3$ (15 wt %)	229 274 287	0.080 0.163 0.199	199 178	heavy refluxing above 295°; clear, colorless
$CrCl_3$ (15 wt %)	225 279 323	0.072 0.175 0.275	216 (small) 201 (large)	slightly purplish color, solid present
$CuCl_2$ (15 wt %)	230 274 325	0.087 0.164 0.304	194	opaque; some solid present
$FeCl_3$ (15 wt %)	225 270 327	0.0902 0.138 0.273	244 (small) 194 (large) 177 (large)	melt is blackish with some solid present; solidified melt is yellow
$ZnCl_2$ (add'l 5 wt %)	223 270 336	0.068 0.152 0.319	208	clear, colorless

*Solvent consists of 60 mole % $ZnCl_2$, 20 mole % NaCl, and 20 mole % KCl.

TABLE 13

ELECTRICAL CONDUCTIVITIES AND THERMAL HALTS OF $AlCl_3$-CONTAINING MELTS*

Solute	T (° C)	κ (ohm-cm)$^{-1}$	Thermal Halts (°C)	Comments
None	116 150 197	0.141 0.211 0.294	112, 107	clear, colorless
AgCl (15 wt %)	132 152 199	0.232 0.275 0.384	131, 105	clear, colorless
CuCl (15 wt %)	136 150 202	0.221 0.274 0.377	135, 88	clear, light yellow
$NiCl_2$ (15 wt %)	121 153 202	0.150 0.216 0.305	121, 103	reddish-orange melt; precipitate present at 200°
$BiCl_3$ (15 wt %)	121 150 203	0.133 0.182 0.269	120, 114	solidified material was pink and homogeneous
$SbCl_3$ (15 wt %)	121 149 204	0.147 0.187 0.275	108 98	clear, colorless with some solid present
$CrCl_3$ (15 wt %)	122 151 200	0.112 0.190 0.269	110	colorless with purple solid present
$CuCl_2$ (15 wt %)	126 152 198	0.133 0.170 0.258	120, 92	clear, yellow-brown with solid present
$FeCl_3$ (15 wt %)	124 149 200	0.118 0.148 0.268	123, 104	yellow-brown melt with precipitate at 150°
$AlCl_3$ (add'l 5 wt %)	121 150 202	0.152 0.197 0.288	114	clear, colorless
$ZnCl_2$ (5 wt %)	129 154 199	0.154 0.198 0.280	124	clear, colorless

*Solvent consists of 61 mole % $AlCl_3$ and 39 mole % NaCl.

to make definitive observations, there appeared to be solid present in both systems. In the $SbCl_3$ melt it was difficult to detect the presence of solid due to excessive refluxing. These observations of low solubility have been corroborated by the voltammetry results. The low conductivities at 323°C for both $BiCl_3$ and $NiCl_2$ are interesting, especially in the latter case where the voltammetry tests indicated that the solubility was extremely low. It is possible that a change in melt composition has occurred due to a solid complex compound being formed. This is in agreement with the thermal halt found (see Table 12).

For the 61% $AlCl_3$-39% NaCl melt no reported conductivity values have been found. This system exhibited much higher conductivities than the ternary $AlCl_3$ (66%)-NaCl (20%)-KCl (14%) also measured. Values for the latter system were 0.220 and 0.134 ohm^{-1}-cm^{-1} at 201° and 136°C (just above the liquidus temperature 135°C). As in the $ZnCl_2$ system the conductivity was increased by the addition of the completely soluble monovalent AgCl and CuCl. The increase is similar for both salts and is about 30%. No change in conductivity was found with $NiCl_2$, in contrast to its behavior in $ZnCl_2$-NaCl-KCl. Although its solubility is low in this system also, the voltammetry results indicate that the $NiCl_2$ is more soluble in the $AlCl_3$ than in the $ZnCl_2$ melt. All the other solutes decreased the conductivity of the melt. The decrease was small and virtually identical for the completely soluble 5 wt % additions of $AlCl_3$ and $ZnCl_2$. A slightly greater decrease was observed with $SbCl_3$, followed by $BiCl_3$, $CuCl_2$, $CrCl_3$ and $FeCl_3$. The solubility of the last three salts is low with that for $CrCl_3$ being extremely small, according to the voltammetry results. In view of the fact that $CrCl_3$ did not alter the freezing point of the melt, the change in conductivity cannot be explained.

The conductivities of the equimolar anhydrous NaOH-KOH were found to be 0.490, 0.796 and 1.174 ohm^{-1}-cm^{-1} at 196°, 247° and 303°C. In another experiment the conductivities of the hydroxides with MgO added were found to be 0.506, 0.899 and 1.195 ohm^{-1}-cm^{-1} at 196°, 260° and 304°C. The values are in excellent agreement (within 3%) as would be expected since MgO is completely insoluble in this system. (The only conductivity value that was found in the literature[20] was $\kappa \leqq 0.642$ ohm^{-1}-cm^{-1} at 200°C for 97.0% NaOH-KOH containing 3.0% H_2O.) Since none of the other oxides added to this melt appeared to be very soluble and since the conductivity may depend strongly on the water concentration, no further measurements were made on the hydroxides.

C. Freezing Point Measurements

Cooling curves were run on all the chloride melts and the thermal halts are included in Tables 12 and 13. The data for NaOH-KOH are given below.

For $ZnCl_2$-NaCl-KCl only one halt was observed, at 205°, in good agreement with the reported value,[21] 203°C. Most of the solutes added decreased the freezing point of the solution. Note that although $ZnCl_2$-melts containing AgCl and CuCl showed identical conductivities, the freezing points were quite different. This indicates that the effect of the two salts on the phase relations may be very dissimilar in these systems. As mentioned above, $NiCl_2$, even though it has a low solubility, produced a pronounced change in the freezing point. This could be due to a change in the melt composition by the formation of a solid double salt of $NiCl_2$ with one or more of the solvent components. The solutes that produced an increase in liquidus temperature were the trivalent salts $FeCl_3$, $CrCl_3$ and $BiCl_3$. Many of the systems

exhibited several thermal halts and none of these, with the possible exception of the $CrCl_3$ melt, corresponded to the solvent eutectic temperature. Thus the addition of solute yields pronounced changes on the temperature-composition equilibria of the solid phases formed on cooling.

The eutectic temperature, 107°C, for the $AlCl_3$-NaCl composition is in excellent agreement with the literature value,[22] 108°C.

In contrast to their behavior in $ZnCl_2$, all of the solutes except for $CrCl_3$, which is insoluble, and $SbCl_3$ produced an increase in liquidus temperature. The largest increase was exhibited by CuCl with AgCl next.

The eutectic temperature for the NaOH-KOH melt was measured as 169°C. This agrees with the most recent literature value,[23] 170°C.

D. Voltammetry Tests

The linear sweep voltammetry (LSV) and current-step voltammetry (CSV) results are given below.

The important features of an electrode couple that will be dealt with are its voltage, reversibility, polarizability due to low concentration in solution, and the possible presence of side or consecutive reactions. The voltage of each couple was measured against a constant reference in the same solvent and so are directly comparable. The reversibility of the electrode is given foremost by its exchange current density. Similar, but less quantitative information can also be derived from L. S. V. from the appearance of the curves and the value as well as constancy of the peak voltage with sweep rates. The theoretical values for the peak voltage in terms of $(E_{eq} - E_p)$ for reversible metal/metal ion electrodes were calculated from eq. 2 and ΔE_p, the span between the cathodic and anodic peaks, for reversible

redox couples, were calculated from eq. 5 for the temperature of interest in this study. The results are presented in Table 14 for purposes of comparison with the experimental values. A measure of the polarizability of an electrode can be obtained from the $(\eta/iA)_{5\,msec}$ value from which the charge transfer resistance is subtracted. The parameter $(\eta/iA)_{5\,msec}$ is the total resistance at the end of the long pulse (usually about 5 msec). This parameter can also be correlated with $CD^{1/2}$ values. The non-

TABLE 14

THEORETICAL $E_{eq} - E_p$ or ΔE_p FOR REVERSIBLE ELECTRODES (n = 1)

Temp (°C)	$(E_{eq} - E_p)$ or ΔE_p (mv)	
	Metal/ion	Redox
122	29	73
150	32	77
200	35	85
225	36	91
275	40	100
325	44	110

occurrence of complex or side reactions with an electrochemical couple is shown by the linear behavior of the peak current density value i_p with $s^{1/2}$. Such i_p data are given for all systems that showed diffusion-limited voltammograms.

1. Preliminary Tests

The results of two types of tests are described in this section. The first set deals with linear sweep voltammetry measurements in which

a relatively high concentration of solute, 15 wt %, was used. The second describes current-step voltammetry experiments with synthetic circuits to test the validity of measurements of R_s and C_d at 0.5 μsec.

a) Linear Sweep Voltammetry with High Concentrations

Since high concentrations (e.g., 15 wt %) of electroactive species would be used as cathodes in any actual battery, voltammetric studies with similar concentrations would appear to be most relevant. Calculations, using eq. 1, showed that an i_p value of about 0.1 amp/cm^2 should be obtained at 250°C, if the following values are used for a 15 wt % AgCl solution, C = 2.3 x 10^{-3} moles/cm^3*, D = 10^{-6} cm^2/sec and s = 23 mv/sec. However, actual voltammograms with 15 wt % AgCl and 15 wt % $BiCl_3$ showed no peaks. Instead, resistance-limited voltammograms, i.e., virtually straight lines of slope determined by the melt resistance, Figure 8, were obtained. For the AgCl melt the slopes were independent of sweep rate whereas for the $BiCl_3$ the slopes (or resistance) increased with sweep rate. The occurrence of resistance-limited voltammograms indicate that the actual peak current density would have been much greater than 1 amp/cm^2, the saturation limit of the instrument.

Although some error is involved in the present study assuming linear diffusion with small cylindrical electrodes, this error is not large[3] (about 10% for the worst cases, at s = 23 mv/sec) and does not explain the lack of attainment of a current peak in these systems. In order to ensure the appearance of a peak, which is very important in the application of the L.S.V. technique, the solute concentrations were lowered to 0.1 M.

---

*A density of 2.50 g/cm^3 was estimated for this melt at 225°C. This was based on density measurements of KCl -$ZnCl_2$ (40-60%) melts.[24]

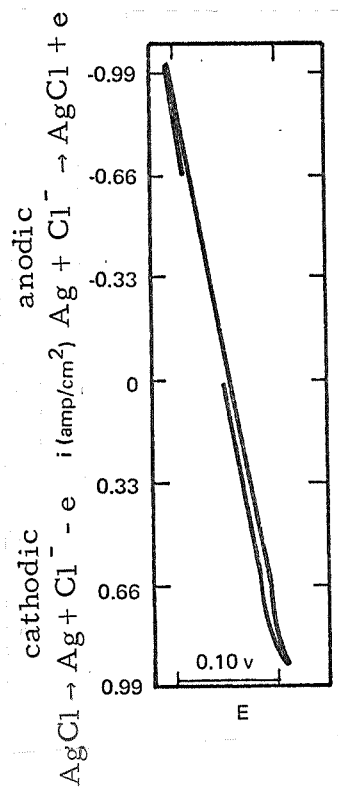

Fig. 8: L. S. V. of 15 wt % Ag/AgCl in $ZnCl_2$ Solvent. T = 320°C, s = 23 mv/sec E_{eq} = 0.600 v

For the $ZnCl_2$-NaCl-KCl solutions densities of 2.50, 2.47 and 2.44 g/cm^3 were assumed at 225, 275 and 325°C. For the $AlCl_3$-NaCl solutions densities of 1.69, 1.67 and 1.62 g/cm^3 were taken at 120, 150 and 200°C from reported data[25] for 61.8% $AlCl_3$-38.2% NaCl. For the NaOH-KOH melts densities of 2.0 g/cm^3 were assumed from a published value[23] of 1.90 g/cm^3 at 200°C for an equimolar NaOH-KOH composition containing 2.2 mole % water.

b) Current Step Voltammetry with Synthetic Circuits

Preliminary tests in which a pulse was passed through a resistor suggested that due to the rise time of the pulse generator, the IR_s drop and C_d determination should be made at 0.5 μsec (p. 18 and A-4). In order to determine whether measuring these quantities at 0.5 μsec was valid when the circuit more closely simulated the actual tests, synthetic circuits consisting

of (1) a resistor, R_s; (2) a resistor, R_s, in series with a capacitor, C; and (3) a resistor R_s in series with a parallel combination of a resistor, R_p and capacitor, C, were placed in the dry box and tested. Each set was carried out on different days. The first three sets A, B and C were done with resistors only; the remaining sets D-G included the more complex circuits.

The results are shown in Table 15. It can be seen that, in general, the agreement between the measured R_s and the actual R_s was quite good with the exception of set D. It is not clear why the agreement in that case was not satisfactory. The agreement in capacitance was not as good. Set E demonstrates that better agreement in C is gotten as R_pC becomes larger. (R_pC varies from 2.2 to 10 μsec.) Set G demonstrates the poor agreement obtained in C when R_s is large (25Ω). Fortunately, unsatisfactory agreement in C does not affect to any significant effect the accuracy of the exchange current density value, which is the primary determination of the current-step measurements.

2. Results of Voltammetry Tests

The results of the voltammetric screening measurements are given in Tables 16-33 and typical curves are shown in Figs. 8-30 and 5-A to 12-A.

a) Explanation of Tables

To clarify the tables, the following explanations are given. The first number under the general title refers to the order in which the system was studied. Thus, the system in Table 16 was the first in the program. The second number A gives the area of the indicator electrode. A roughness factor of one was assumed for all the electrodes. The last number (n) in this row gives the number of electrons assumed in the electrochemical reaction.

(It was assumed that no consecutive or side reactions are taking place.) The sign conventions used in this report are that cathodic potentials are negative and cathodic currents are positive.

(1) Linear Sweep Voltammetry

The first column gives the temperature while the second column gives the open-circuit potential, E_{eq}. The voltages are with respect to $Zn/ZnCl_2$-solvent and $Al/AlCl_3$-solvent.

The third column lists values for $CD^{1/2}$. These values were calculated from eq. 3 for metal/metal ion couples and eq. 4 for redox couples using the average i_p values in the system. In those cases where i_p/m values were not constant, the average calculated $CD^{1/2}$ values are given in parentheses. The fourth column lists the four different sweep rates that were used in this study. The values of m are 1, 2, 3 and 4; here m is $(s_j/s_1)^{1/2}$ where j is 1, 2, 3 and 4. Values of i_p/m are given in the fifth column where i_p is the peak current density. The parameter i_p/m is listed rather than i_p because the former is independent of sweep rate in ideal systems and thus the deviation from this constancy is more transparent. Note that the i_p/m value at m = 1 is i_p at 23 mv/sec. The last column gives $E_{eq} - E_p$ or ΔE_p where E_p is the voltage at which the peak current occurs and ΔE_p is the peak to peak voltage for a redox couple.

(2) Current-Step Voltammetry

For many parameters listed in the tables, two equations will be referred to. The first is from the basic equations given on pp 15-19 and the second is from the equations given in Appendix III. The latter are equations in terms of the number of divisions of the oscilloscope trace with

TABLE 15

TESTS WITH SYNTHETIC CIRCUITS

trace	I (ma)	Time Scale (μsec/div)	R_s (Ω) actual	R_s (Ω) observed	C (μF) actual	C (μF) observed	R_p (Ω)
A 1	1	500	5	4.82			
A 2	1	500	5	4.82			
A 3	20	1	5	4.66			
B 1	20	1	5	4.68			
B 2	10	1	5	4.86			
B 3	20	1	5	4.77			
C 1	20	1/2	2	1.92			
C 2	20	1/2	5	4.56			
C 3	20	1/2	10	9.50			
D 1	20	1/2	5	6.61	1	0.70	
D 2	20	1/2	5	6.70	1	0.71	
D 3	20	1/2	5	4.96	5	5.0	
D 4	20	1/2	5	5.82	1	2.0	2
D 5	20	1/2	5	5.84	1	1.7	2
E 1	20	1/2	2	1.85			
E 2	20	1/2	2	2.02	2	2.1	—
E 3	20	1/2	2	1.98	2		0
E 4	20	1/2	2	2.06	2	3.4	1.1
E 5	20	1/2	2	2.00	2	2.8	2
E 6	20	1/2	2	2.03	2	1.9	5
F 1	20	1/2	2	2.11	2	3.6	1.1
F 2	20	1/2	2	2.04	2	3.3	1.1
F 3	20	1	2	2.18	2	3.1	1.1
F 4	20	2	2	2.01	2	2.3	1.1
G 1	10	1/2	25	24.5	0.1	.037	—
G 2	10	1/2	25	21.6	—	—	—
G 3	10	1/2	25	24.0	0.1	.045	10
G 4	10	1/2	25	25.0	0.1	.050	10

appropriate conversion factors. These equations were used in this work since, instead of plotting η vs $t^{1/2}$ in terms of mv and sec, which would have necessitated computing the values of η and $t^{1/2}$ for each point on that curve, quantities directly from the oscilloscope trace were plotted in terms of divisions or cm.

(i) Short Pulse

The first column gives the temperature and the second column gives the applied current density. The third column gives the oscilloscope trace number so it can be seen in what sequence the traces were taken. The fourth and fifth columns give the values of C_d and R_s, respectively. Eq. (6 or 18A) was used to calculate C_d; however, for eq. 6, (dE/dt) was measured at 0.5 μsec rather than at t = 0. The value of R_s (eq. 16A) was also measured at 0.5 μsec. As shown in Appendix II, values for C_d cannot be calculated for a trace which exhibits resistor-like appearance and therefore in those cases a dash is placed in the C_d column.

(ii) Long Pulse

The first and second columns give the temperature and applied current, respectively. The third column gives the oscilloscope trace number, the fourth column gives the value of R_s which is an average of the R_s values listed at a given temperature in part i above. Values for the charge transfer resistance R_p were obtained from eq. 20 or 28A, and are listed in column 5. Column 6 tabulates values for the parameter $(\Delta\eta/iA)_{0.1\,msec}$ which are given by eq. 31A. The parameter $f(C_i D_i^{1/2})$ is given by eq. 9 or eq. 19A for redox systems and the results are tabulated in column 7. In the case of metal/metal ion couples, $f(C_i D_i^{1/2})$ is replaced by $C D^{1/2}$ given by eq. 15 or eq. 33A. The diffusion coefficients are tabulated in column 8. In the case of the redox couples it is assumed that $C_o = C_r = 10^{-4}$ mole/cm^3 and that $D_o = D_r$; the equation for D is then given by eq. 10 or eq. 20A. For metal/metal ion couples, it is assumed that the concentration of the electroactive species in solution is 10^{-4} moles/cm^3; D is then given by eq. 16 or 34A. In many cases D will have exceptionally low values. In such cases the low

values will probably be due to low concentrations and should therefore be regarded as formal values rather than real ones. The eighth column gives results of η_{5msec} (given by eq. 32A) which are total overpotentials at the end of the long pulse (usually about 5 msec). The next to the last column gives the "resistance" due to this total overpotential. The last column then tabulates the exchange current densities given by eqs. 11 or 24A for redox couples and 17 or 35A for metal/metal ion couples. If there is more than 10% difference between those values from the exact equations and those from the approximate equations 13 or 25A, these are marked with an asterisk, and the approximate values are given in footnotes. Exchange current densities which are negative are marked W.S. (wrong sign).

b) Explanation of Figures

For each couple there is given at least one L.S.V. curve and one set of C.S.V. curves consisting of one short pulse curve, one long pulse curve and one plot of E vs $\sqrt{t}$. As stated in Appendix III, the last plot is given in terms of divisions rather than in mv and seconds. If the actual points fall below the line extrapolated from longer times (1-5 msec), such as Figure 13, this is defined as negative deviation in spite of the fact that $(\Delta\eta/iA)_{0.1\ msec}$ values will be positive. If unusual behavior is noted in the systems, then additional curves are presented.

c) Voltammetry Results of $ZnCl_2$-containing Melts

Both linear sweep voltammetry (L.S.V.) and current step voltammetry (C.S.V.) results are given together for each system. First, the L.S.V. trace of the pure solvent with no additives is discussed. Then with

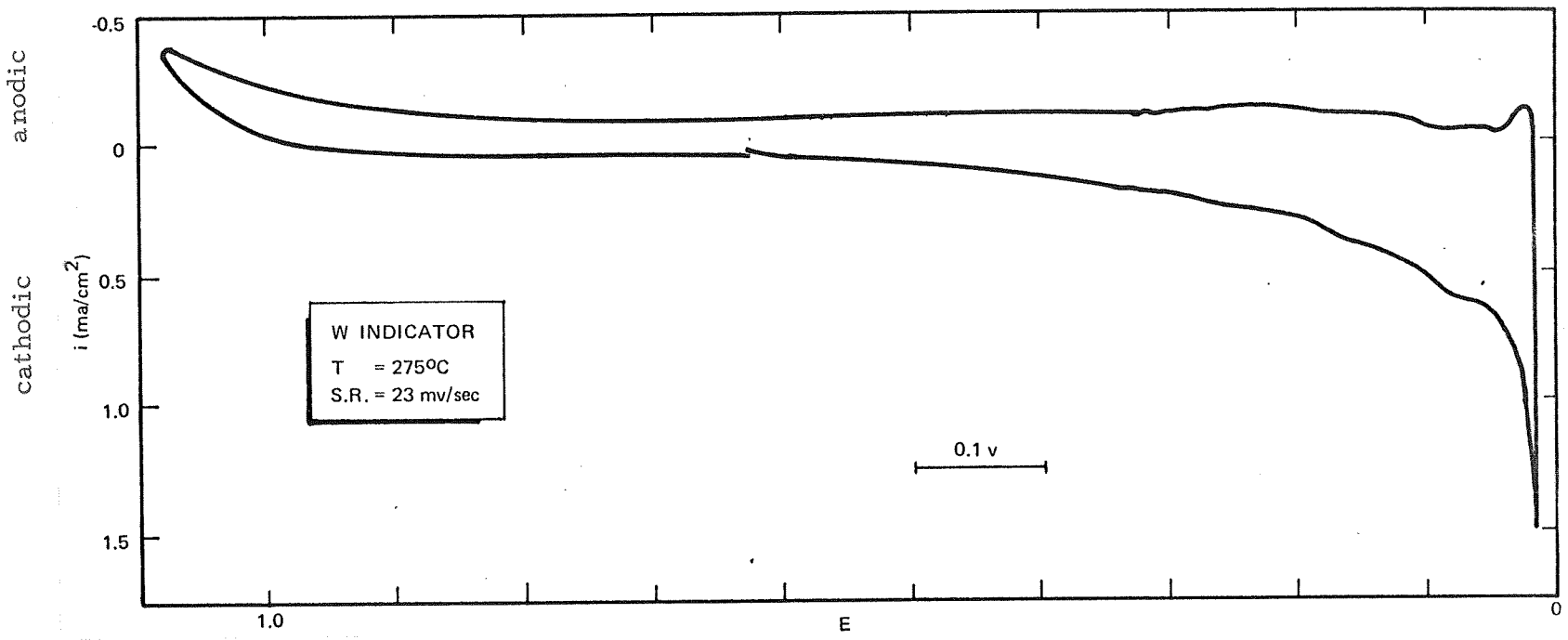

Fig. 9: Linear Sweep Voltammetry of $ZnCl_2$-NaCl-KCl Solvent

the solute present, the L.S.V. results are given first. The short pulse C.S.V. results are given next, followed by the long pulse data. The systems are discussed in the following order. First the results of electropositive systems are given and then the electronegative systems. In both of the above categories the lowest valence cations are discussed first. When the cations have the same valence, they are arranged alphabetically by symbol.

(1) $ZnCl_2$-NaCl-KCl Solvent

To check the purity of the solvent a cyclic voltammogram was run with tungsten electrodes at 275°C (Fig. 9). No peaks were observed but a background current density of less than 0.10 ma/cm^2 occurred over most of the voltage range. Since the current component due to the capacitance C_d, given by $i_c = C_d s$, is insignificant here (about 10^{-3} ma/cm^2), the observed current may be due to small amounts of impurities in solution or on the electrode.

The working voltage range for this solvent was found to be about 1.75, 1.70 and 1.65 v at 225, 275 and 325°C with tungsten electrodes and about 0.3 v less with platinum. The limiting cathodic voltage is set by the reduction of Zn(II) (at the right end of the figure) and the limiting anodic potential is determined by the oxidation of chloride to chlorine or the anodization of the electrode metal. Thus the above potentials are an upper limit to the voltages that can be derived in a battery with a $ZnCl_2$ melt.

(2) Ag/AgCl

The voltammetry results are shown in Table 16 and in Fig. 10. The open circuit potentials of this couple vs $Zn/ZnCl_2$ varied from 0.355 v at 222° to 0.450 v at 320°C.

TABLE 16

VOLTAMMETRY OF Ag/AgCl in $ZnCl_2$ MELT

(#1; A = 0.061 cm^2; n = 1)

a) LINEAR SWEEP VOLTAMMETRY

Temp (°C)	E_{eq} (v)	$CD^{1/2} \times 10^7$ $\left(\frac{moles}{cm^2 sec^{1/2}}\right)$	s (mv/sec)	i_p/m (ma/cm^2)	$E_{eq} - E_p$ (mv)
222	0.355	0.81	23	2.7	40
			92	3.9	39
			207	3.4	37
			368	3.9	81
270	0.365	0.51	23	2.4	50
			92	2.0	45
			207	1.9	45
			368	2.1	45
320	0.450	2.6	23	10.5	63
			92	10.5	65
			207	10.3	64
			368	24.1	85

b) CURRENT STEP VOLTAMMETRY-SHORT PULSE

Temp (°C)	i (ma/cm^2)	trace	C_d ($\mu F/cm^2$)	R_s (Ω)
222	330	12	3.0	7.54
270	330	1	5.2	3.60
328	330	14	—	3.22

TABLE 16 (cont'd)

VOLTAMMETRY OF Ag/AgCl in $ZnCl_2$ MELT

c) CURRENT STEP VOLTAMMETRY-LONG PULSE

Temp (°C)	i (ma/cm^2)	trace	R_s (Ω)	R_p (Ω)	$\frac{\Delta\eta_{0.1\,msec}}{iA}$ (Ω)	$CD^{1/2}$ x10^7	D x 10^6 (cm^2/sec)	$\eta_{5\,msec}$ (mv)	$\frac{\eta_{5\,msec}}{iA}$ (Ω)	i_o (A/cm^2)
226	8.3	6	7.5	-3.7	-0.2	1.25	1.6	- 4.0	-8.1	0.19
225	16.5	8	7.5	-3.3	0	1.58	2.5	- 6.7	-6.7	0.21
225	33	9	7.5	-3.5	-0.1	1.43	2.0	-14.7	-7.3	0.19
226	33	10	7.5	-4.2	-0.3	1.44	2.0	-15.9	-8.0	0.16
270	8.3	5	3.6	+0.04	-0.2	1.66	2.8	- 1.8	-3.5	WS, -0.19
270	16.5	4	3.6	-0.54	-0.1	1.60	2.6	- 4.2	-4.2	1.47
270	33	2	3.6	-1.2	-0.2	1.60	2.6	-10.0	-4.8	0.65
324	8.3	18	3.2	-0.68	0	4.00	16	- 1.1	-2.3	1.20
320	16.5	17	3.2	-0.76	0	3.35	11	- 2.7	-2.7	1.03
320	33	16	3.2	-0.64	-0.1	3.24	10	- 5.0	-2.5	1.26

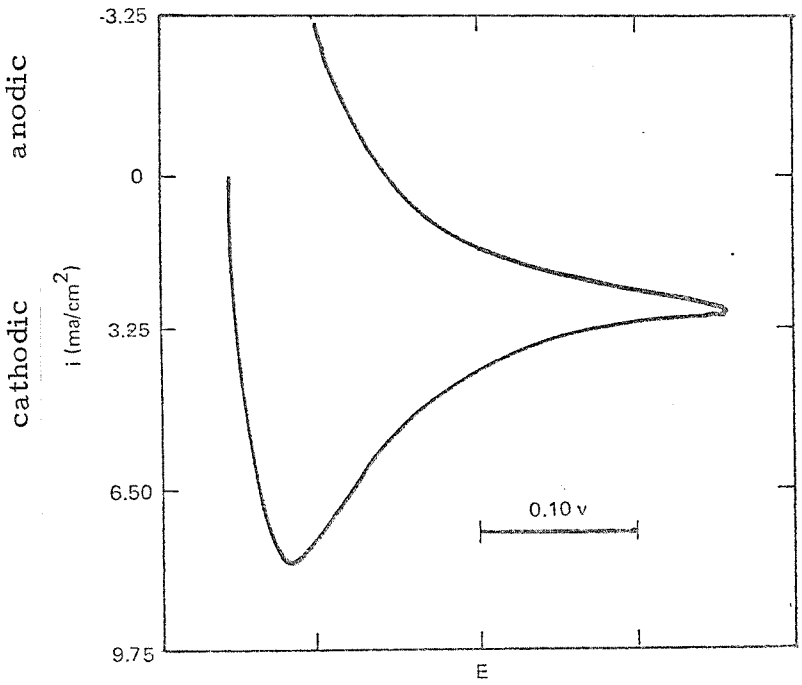

a) L.S.V. T = 222°C; s = 92 mv/sec
E_{eq} = 0.355 v

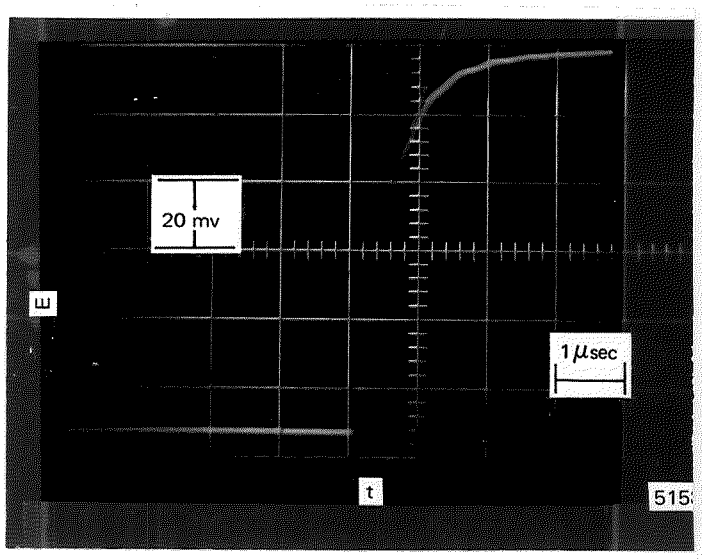

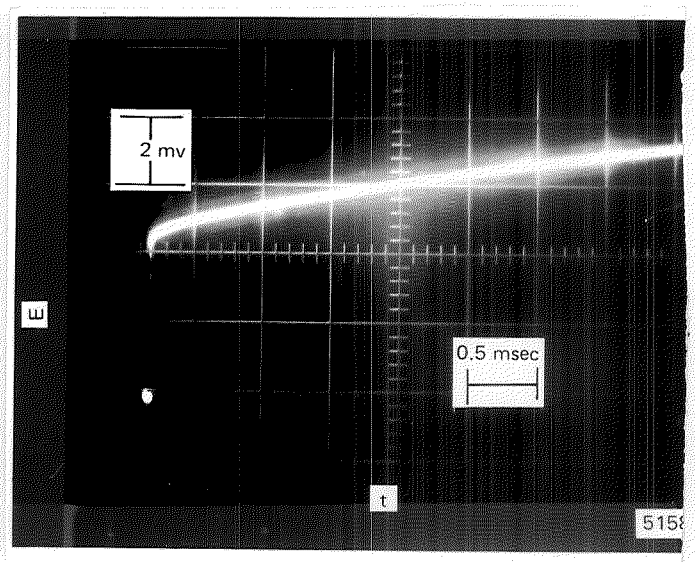

b) C.S.V. Short Pulse
T = 270°C; i = 330 ma/cm^2
Trace #1

c) C.S.V. Long Pulse
T = 270°C; i = 16 ma/cm^2
Trace #4

Fig. 10: Voltammetry of Ag/AgCl in $ZnCl_2$ Melt

80

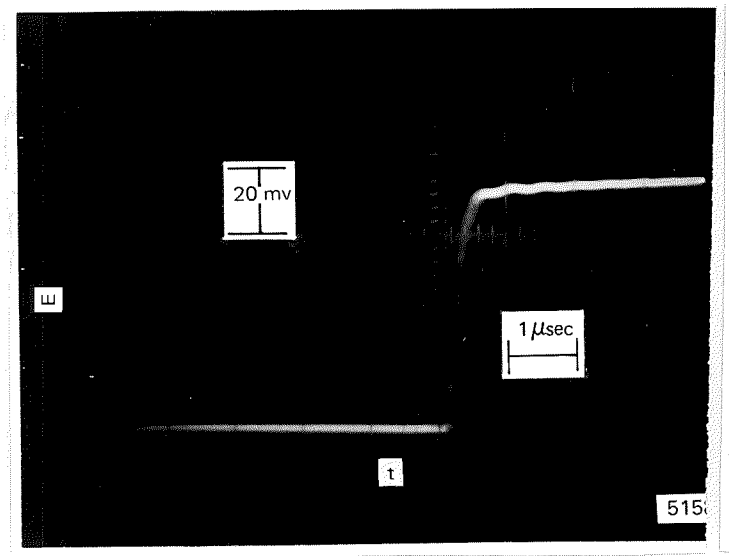

d) C.S.V. Short Pulse
T = 338°C; i = 330 ma/cm^2
Trace #14

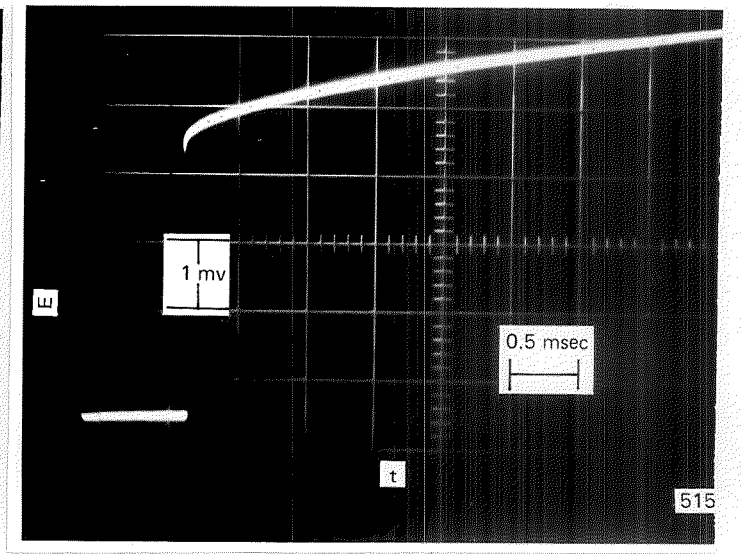

e) C.S.V. Long Pulse
T = 320°C; i = 16 ma/cm^2
Trace #17

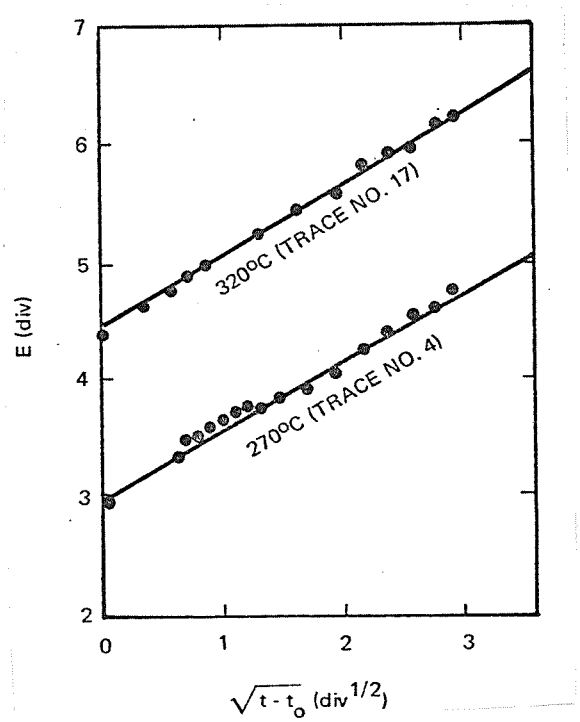

f) E vs $\sqrt{t}$ Plot

Fig. 10: Voltammetry of Ag/AgCl in $ZnCl_2$ Melt

A typical L.S.V. trace is shown in Figure 10a. Most of the L.S.V. curves appeared typical for reversible, diffusion-limited waves. The initial portion of the wave was virtually vertical and the value and constancy of the peak potential for all but the fastest sweep at 222°C and 320° indicated reversible behavior. These results are consistent with those for the 15 wt % melt where resistance-limited voltammograms with slopes independent of sweep rate were found. The change in E_p at the fastest sweep rate at 222° and 320° as well as the large, although constant, $E_{eq} - E_p$ values at 320° are puzzling. (The measured value of $E_{eq} - E_p$ at 320° was about 64 mv rather than the theoretical value of about 44 mv, shown in Table 14.) The i_p/m values were in general constant and this behavior suggests that no complicated reactions occurred. On the basis of the limited data the one high i_p/m value at 320° is open to question. The smaller peak current values at 270° (the temperature studied first) than at 222° suggest that the AgCl was not all dissolved when the measurements commenced. (In all the subsequent experiments to ensure complete solution, longer stirring times were employed before measurements were initiated.) The $CD^{1/2}$ values indicate that the AgCl is soluble in this system. At the end of the test dendrites were found on the counter electrode and in the cell but not on the indicator electrode.

Typical current-step voltammograms are shown in Figure 10b-e. Different behavior was noted in the short pulse behavior at the highest temperature (Fig. 10b) and at the lower temperature (Fig. b). At 270°C a smoothly rising curve (b) is seen while at the higher temperature the curve (d) has the same shape as that of a pulse passed across a pure resistor. This type of short pulse curve is not surprising since the time t* at which

the slope is taken (5×10^{-7} sec) is larger than R_pC. For example, if we use an average value of 4×10^{-6} F/cm^2 for C_d ($C = 0.24 \times 10^{-6}$ F), R_pC for trace 17 at 320° is $(0.7)(0.24 \times 10^{-6}) = 1.7 \times 10^{-7}$ sec and the condition $t^* \ll R_pC$ is not fulfilled. Thus, there is no linear portion of the curve at 0.5 μsec, which can give an accurate C_d; therefore C_d was not calculated at this temperature. At the lowest temperatures, where R_p is much larger ($\sim 4\Omega$), R_pC is about 10^{-6} sec. However, even then the condition $t^* \ll R_pC$ does not strictly hold. Thus the values for C_d, which are considerably lower than one might expect, should not be taken seriously here.

The deviation from linearity (which is given by $\Delta\eta_{0.1\,msec}/iA$ (6th column) is very small. See, for example, Fig. (10f) where E vs $\sqrt{t-t_o}$ is plotted. This indicates that charge transfer and diffusion are the only sources of polarization. This is in contrast to the work of T. B. Reddy[26] who carried out galvanostatic pulsing of silver electrodes in 0.1 M AgCl dissolved in LiCl-KCl melts at 450°C. His results suggested that the mechanism of electro-deposition included a step for surface diffusion of adions from the point of deposition to growth sites on the metal surface - i.e., crystallization polarization. In addition our analysis of the data of Bockris and co-workers,[27] who investigated the electrode kinetics of silver with 0.01 M $AgNO_3$ dissolved in $NaNO_3$-KNO_3 melts at 250°C, showed negative deviation at 0.1 msec; i.e., $\Delta\eta_{0.1\,msec}/iA$ was 2Ω in their Fig. 3. This negative deviation suggests that in their system crystallization polarization takes place.

The values of $CD^{1/2}$ obtained by C.S.V. are somewhat smaller than those obtained from L.S.V. data. The overpotential at 5 msec

exceeded 5 mv for about one-half the cases. However, in spite of the fact that in the derivation of eq. 7 the assumption was made that η should not exceed about 5 mv[9] the value of i_o did not seem to be affected by the high values of the overpotential at 5 msec. The resistance (column 10) due to the total overpotential (including that resulting from diffusion) did not seem excessively high, the highest values being at the lowest temperatures.

The exchange current densities were about 0.2 A/cm^2 at 225°C and about 1 A/cm^2 at the higher temperatures. Considerable scatter in i_o was obtained at the intermediate temperature; in fact, a negative value was obtained in one case (trace 5). Calculation of i_o by the simplified equation (eq. 13) yielded the same results as the more rigorous equation (eq. 17). This was found to be the case in most systems in this work.

It is not clear whether the different behavior of the Ag/AgCl couple at elevated temperatures represents a real temperature effect or whether it represents an "aging" effect. The electrode had undergone considerable multiple cycling during the L.S.V. tests after the C.S.V. tests at 270° and before the L.S.V. tests before 320°C.

The Ag/AgCl electrode appears to be quite reversible on the basis of the L.S.V. results and on the basis of the exchange currents obtained from C.S.V. measurements. The fact that dendrites are formed is a complication for battery applications. The high solubility, at least 15 wt %, indicates concentration polarization should not pose a problem.

(3) Cu/CuCl

The voltammetry results are shown in Table 17 and in Fig. 11. The open circuit potentials in this system, 0.398 v at 279° and 0.310 v at 327°C, varied with time indicating some diffusion of CuCl into the reference compartment where it reacted with the zinc electrode. The 327° value may be somewhat low and the 225° value, 0.137, appears out of line. The voltammograms at 327° appeared reasonable and the E_p was constant although $E_{eq} - E_p$ is somewhat high when compared to the values in Table 14. At the lower temperatures the initial part of the waves was not vertical (see Fig. 11a) although the E_p values at 279° are still reasonably constant. These results indicate that at the lowest temperatures this couple is not as reversible as the Ag/AgCl. The i_p vs $s^{1/2}$ behavior was again in general linear. The $C D^{1/2}$ data suggest that the CuCl is completely soluble. Dendrites were evident on the counter electrode in this cell.

Typical current-step voltammograms are shown in Fig. 11b-e. Just as in the Ag case, different behavior was noted at the highest temperature where the short-pulse curves (d) were resistor-like. Therefore, no C_d values were calculated at 327°C. The C_d values at 278°C were considerably higher (22 $\mu F/cm^2$) than at 226°C (6 $\mu F/cm^2$) and were higher than those for Ag/AgCl. The shapes of the long pulse traces for the lowest two temperatures in the Cu/CuCl case were markedly different from those of the Ag/AgCl case, the former (c) having a much longer tail. The long pulse curves exhibited a marked negative deviation from linearity at the lowest temperature (225°), as shown by the magnitude of $\Delta\eta_{0.1\ msec}/iA$. and Fig. 11f. This suggests that charge transfer and diffusion polarization are not the only significant sources of polarization. Thus any exchange

TABLE 17

VOLTAMMETRY OF Cu/CuCl in $ZnCl_2$ SOLVENT

(#2; A = 0.061 cm^2; n = 1)

a) LINEAR SWEEP VOLTAMMETRY

Temp (°C)	E_{eq} (v)	$CD^{1/2} \times 10^7$ $\left(\frac{moles}{cm^2 sec^{1/2}}\right)$	s (mv/sec)	i_p/m (ma/cm^2)	$E_{eq} - E_p$ (mv)
225	(0.137)	3.0	23	11.3	70
			92	12.9	70
			207	12.9	75
			368	19.7	105
279	0.398	3.6	23	15.3	60
			92	14.9	60
			207	14.8	60
			368	14.1	70
327	0.310	5.1	23	20.3	60
			92	20.4	60
			207	19.3	63
			368	26.8	65

b) CURRENT STEP VOLTAMMETRY-SHORT PULSE

Temp (°C)	i (ma/cm^2)	trace	C_d ($\mu F/cm^2$)	R_s (Ω)
226	330	10	4.7	4.14
226	330	16	6.0	4.20
278	330	1	22.2	2.27
278	330	2	21.6	2.31
275	330	8	21.6	2.31
327	330	17	—	1.60
327	330	24	—	1.69

TABLE 17 (cont'd)

VOLTAMMETRY OF Cu/CuCl in $ZnCl_2$ SOLVENT

c) CURRENT STEP VOLTAMMETRY-LONG PULSE

Temp (°C)	i (ma/cm^2)	trace	R_s (Ω)	R_p (Ω)	$\frac{\Delta\eta_{0.1\,msec}}{iA}$ (Ω)	$CD^{1/2}$ x 10^7	D x 10^6 (cm^2/sec)	$\eta_{5\,msec}$ (mv)	$\frac{\eta_{5\,msec}}{iA}$ (Ω)	i_o (A/cm^2)
225	4.1	15	4.2	-16.0	+11.2	.42	0.2	- 1.3	-30	0.043
225	8.3	13	4.2	-14.6	+ 8.8	1.3	1.7	- 9.4	-19	0.048
225	16.5	12	4.2	-13.0	+ 7.5	3.6	13	-15	-15	0.052
225	33	11	4.2	- 9.5	+ 3.2	5.7	32	-20	-10	0.075
276	4.1	7	2.3	- 2.3	+ 1.4	.76	0.6	- 2.5	-10	0.33
276	8.3	6	2.3	- 2.3	+ 2.0	1.5	2.3	- 3.7	-7.3	0.21
276	16.5	4	2.3	- 2.2	+ 1.5	2.3	5.3	- 5.8	-5.8	0.21
276	33	3	2.3	- 2.5	+ 1.1	3.7	14	- 2.2	-1.1	0.30
326	8.3	23	1.7	-0.25	0	4.2	18	-0.89	-1.8	3.4
326	16.5	22	1.7	-0.29	0	4.3	19	- 1.8	-1.8	2.8
326	16.5	21	1.7	-0.18	0	3.8	14	- 1.7	-1.7	4.6
326	33	18	1.7	-0.25	0	4.9	24	- 3.5	-1.7	3.3
326	33	20	1.7	-0.33	0	4.6	21	- 3.5	-1.7	2.5

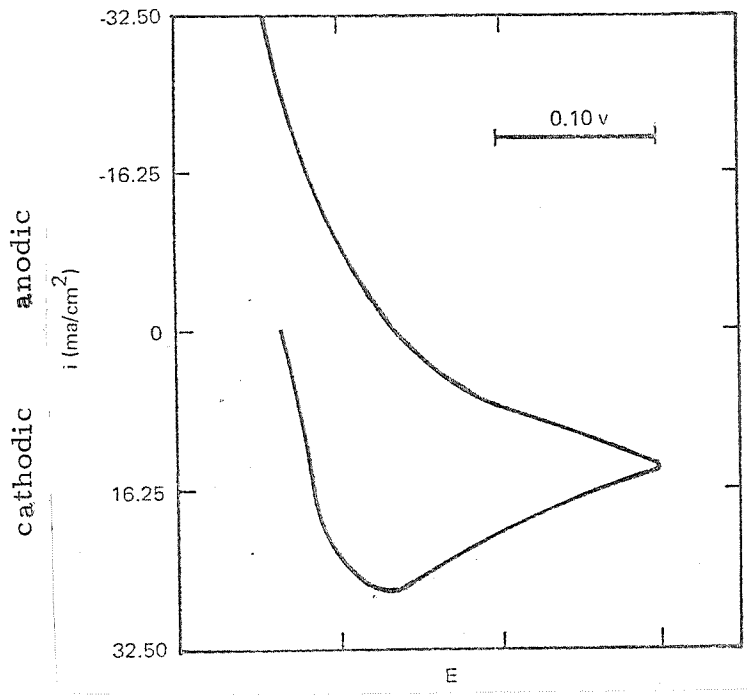

a) L.S.V.; T = 225°C; s = 92 mv/sec; E_{eq} = 0.137 v

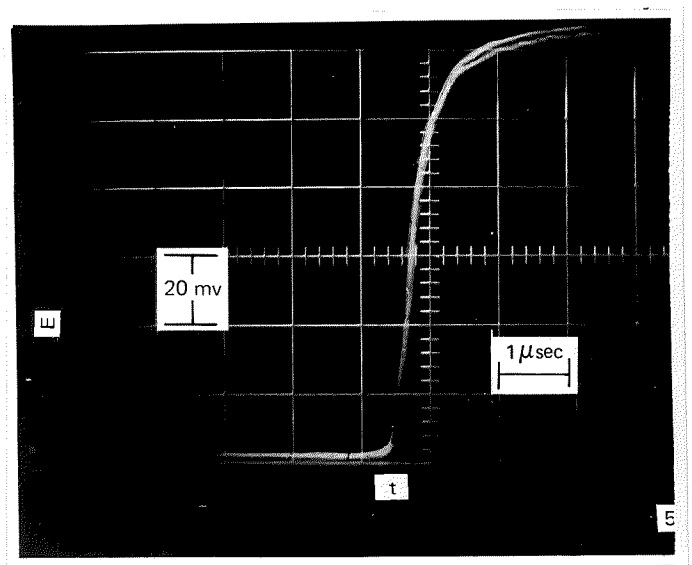

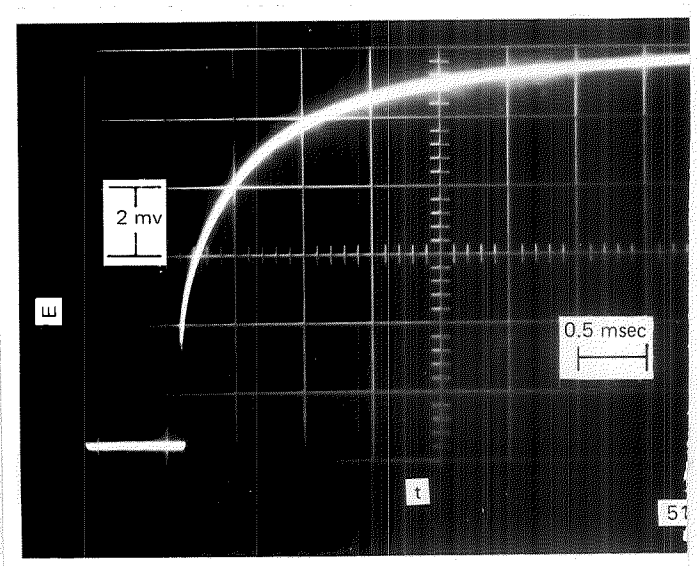

b) C.S.V.; Short Pulse
T = 226°C; i = 330 ma/cm^2
Trace #16

c) C.S.V.; Long Pulse
T = 225°C; i = 8 ma/cm^2
Trace #13

Fig. 11: Voltammetry of Cu/CuCl in $ZnCl_2$ Melt

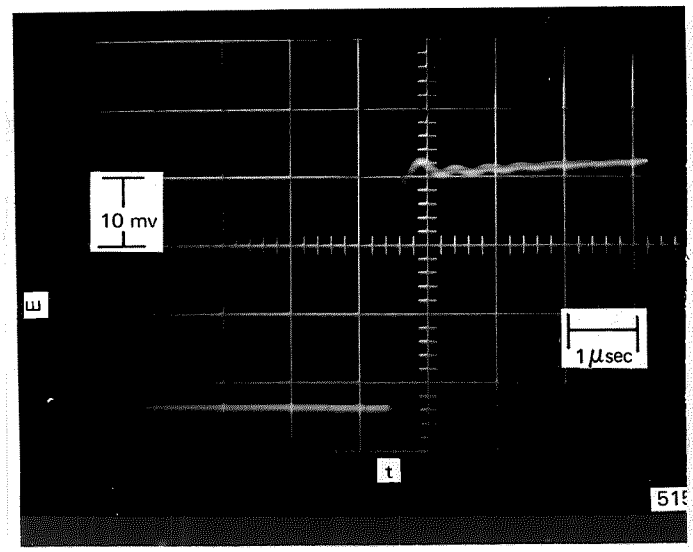

d) C.S.V.; Short Pulse
T = 327°C; i = 330 ma/cm^2
Trace #17

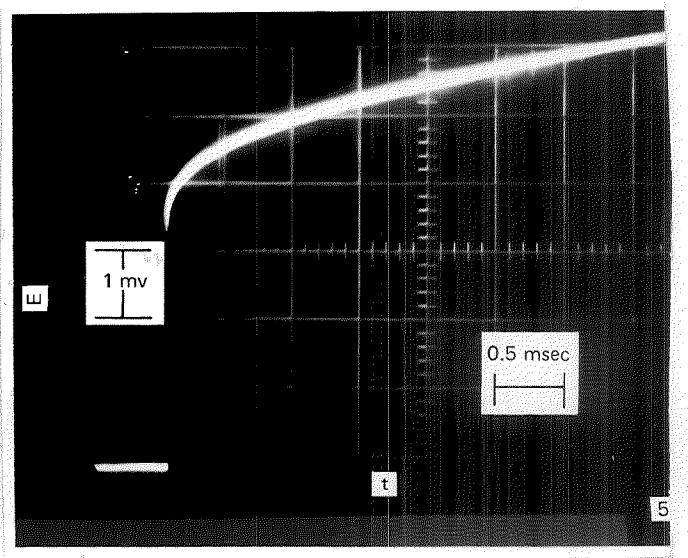

e) C.S.V.; Long Pulse
T = 326°C; i = 33 ma/cm^2
Trace #20

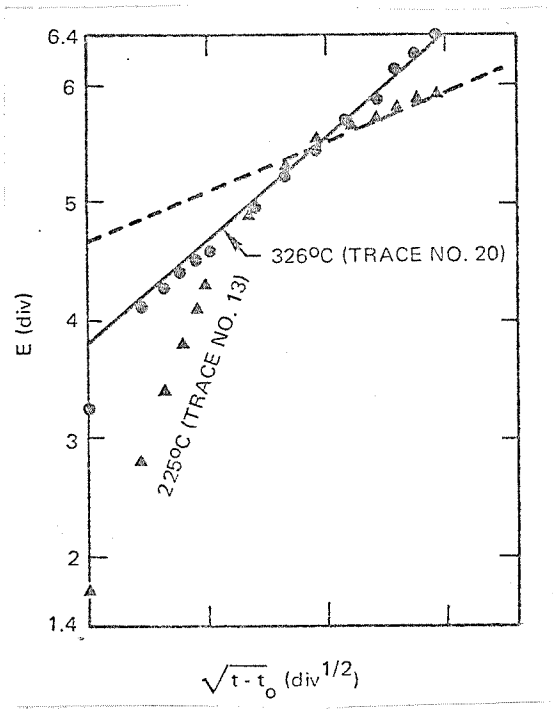

f) E vs $\sqrt{t}$ Plot

Fig. 11: Voltammetry of Cu/CuCl in $ZnCl_2$ Melt

current densities reported for the lowest temperature should be regarded as formal numbers. At the two lowest temperatures the $CD^{1/2}$ values varied markedly with the applied current density. This is the only system studied in this program that exhibited this effect. The total overpotential at 5 msec exceeded 5 mv in only four cases. However, the resistance (column 10) due to the total overpotential was moderately high at the lowest temperature. Except for trace 15, the contribution of concentration overpotential to the total was not great.

The formal exchange current at the lowest temperature is considered to be low (< 0.1 A/cm^2). However, if this value were corrected for the other source of polarization taking place, there is no doubt that the true exchange current would be higher.

At the highest temperature, all the unusual behavior disappeared. The plots of E vs $\sqrt{t-t_o}$ (see Fig. 10f) exhibited an ideal behavior with respect to deviation from linearity. Further, the $CD^{1/2}$ values were independent of current density. The exchange currents were considerably larger. Again it is not clear whether the different behavior of the Cu/CuCl couple at the highest temperature is a real temperature effect or an aging process of the electrode. However, if it were an aging process, one would have expected the largest deviations to take place at the intermediate temperature which was the first studied. Instead the most extreme behavior took place at the second temperature studied (225°C). On this basis this would appear to be a temperature effect. Clearly, this unusual behavior warrants further study.

In view of the dependency of $CD^{1/2}$ on current density, no meaningful comparison can be made with $CD^{1/2}$ from L.S.V. measurement. However, at the highest temperature, the agreement is quite good.

On the basis of the C.S.V. results, the Cu/CuCl electrode appears to be quite reversible, at least at the two highest temperatures. The L.S.V. results agree with these conclusions at the highest temperature. Just as in the Ag/AgCl case, dendrite formation is a disadvantage for battery application. Again, concentration polarization should not pose a problem due to the high solubility.

(4) Ni/$NiCl_2$–

The voltammetry results are shown in Table 18 and Fig. 12. The open circuit potentials varied from 0.573 v at 228° to 0.545 v at 330°C and probably depended on the $NiCl_2$ solubility (see below). The cathodic waves appeared to be diffusion-limited but all showed a little shoulder at the initial portion of the sweep (Fig. 12a). This shoulder suggests that the electrode kinetics slow up shortly after the flow of current begins. The E_p values were relatively independent of sweep rate except at the highest temperature but the $E_{eq} - E_p$ values are quite large compared to the theoretical values of Table 14 (taking into consideration that n = 2). The general constancy of i_p/m indicates that no complications occurred in the reduction of Ni(II) in solution. The small i_p values as well as their large change with temperature indicate that the solubility limit of $NiCl_2$ was exceeded. If a $D^{1/2}$ value of 10^{-3} cm/sec$^{1/2}$ is assumed, then the solubility of $NiCl_2$ ranges from 0.0023 M at 228° to 0.024 M at 330°. It is interesting that in this system, where the concentration of electroactive species is much lower than with AgCl or CuCl, the i_p vs $s^{1/2}$ behavior is much more constant. No dendrites were observed in this system in contrast to the Ag and Cu systems. During the anodic sweeps, current peaks indicative of film formation (presumably $NiCl_2$) were observed (Fig. 12b). On reversal a non-diffusion limited cathodic peak of

TABLE 18

VOLTAMMETRY OF $Ni/NiCl_2$ in $ZnCl_2$ SOLVENT

(#3; A = 0.061 cm^2; n = 2)

a) LINEAR SWEEP VOLTAMMETRY

Temp (°C)	E_{eq} (v)	$CD^{1/2} \times 10^7$ $\left(\frac{moles}{cm^2 sec^{1/2}}\right)$	s (mv/sec)	i_p/m (ma/cm^2)	$E_{eq} - E_p$ (mv)
228	0.573	0.023	23	0.14	38
			92	0.13	40
			207	0.14	45
			368	0.14	50
275	0.543	0.047	23	0.31	50
			92	0.28	50
			207	0.27	53
			368	0.27	55
330	0.545	0.24	23	1.4	38
			92	1.4	40
			207	1.3	45
			368	1.2	50

b) CURRENT STEP VOLTAMMETRY-SHORT PULSE

Temp (°C)	i (ma/cm^2)	trace	C_d ($\mu F/cm^2$)	R_s (Ω)
228	330	11	2.0	5.18
227	330	17	1.8	4.25
275	330	6	5.2	3.40
276	330	10	5.2	2.93
331	330	1	—	0.95
330	330	5	—	0.98

TABLE 18 (cont'd)

VOLTAMMETRY OF $Ni/NiCl_2$ in $ZnCl_2$ SOLVENT

c) CURRENT STEP VOLTAMMETRY-LONG PULSE

Temp (°C)	i (ma/cm^2)	trace	R_s (Ω)	R_p (Ω)	$\frac{\Delta\eta_{0.1\,msec}}{iA}$ (Ω)	$CD^{1/2}$ x 10^7	D x 10^6 (cm^2/sec)	$\eta_{5\,msec}$ (mv)	$\frac{\eta_{5\,msec}}{iA}$ (Ω)	i_o (A/cm^2)
228	.16	16	4.72	+44.7	-12	.004	.00002	-2.9	-290	WS-0.0051
228	.40	15	4.72	+23.9	-10	.007	.00005	-6.7	-260	WS-0.010
228	.40	19	4.72	+18.7	-19	.005	.00003	-4.6	-180	WS-0.013
228	.80	14	4.72	+24.7	0	.004	.00002	-15	-290	WS-.010
228	1.6	12	4.72	+16.1	-10	.004	.00002	-30	-300	WS-.014
228	1.6	13	4.72	+23.7	0	.005	.00003	-28	-280	WS-.010
276	.32	9	3.17	+49.1	-25	.012	.0001	-2.4	-120	WS-.0081
276	.80	7	3.17	+45.1	-26	.011	.0001	-7.0	-140	WS-.0091
276	1.6	8	3.17	+41.6	-30	.012	.0001	-11	-110	WS-.0091
330	.80	4	0.97	+37.3	-22	.014	.0002	-3.8	- 86	WS-.012
330	1.6	3	0.97	+26.0	-13	.017	.0003	-7.2	- 72	WS-.017
330	4.0	2	0.97	+11.5	-15	.020	.0004	-17.3	- 69	WS-.039

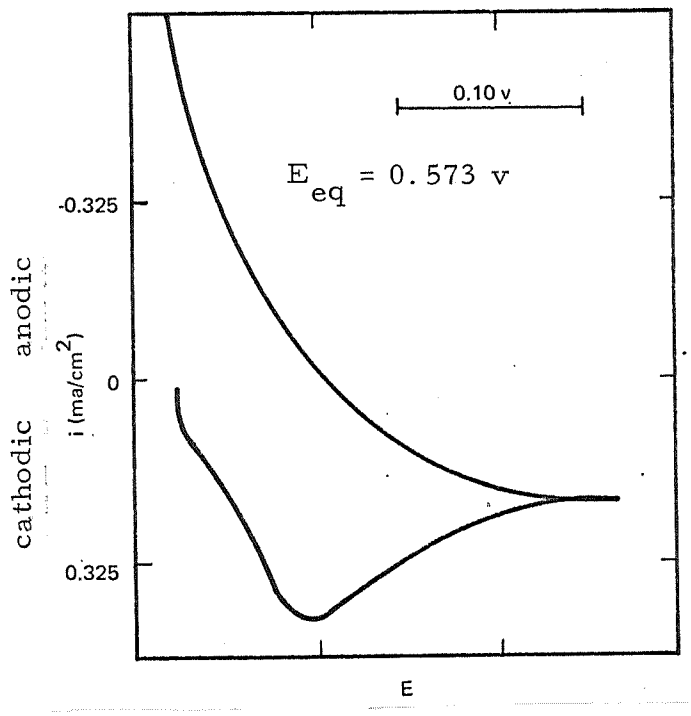

a) L.S.V.; T = 228°C; s = 207 mv/sec

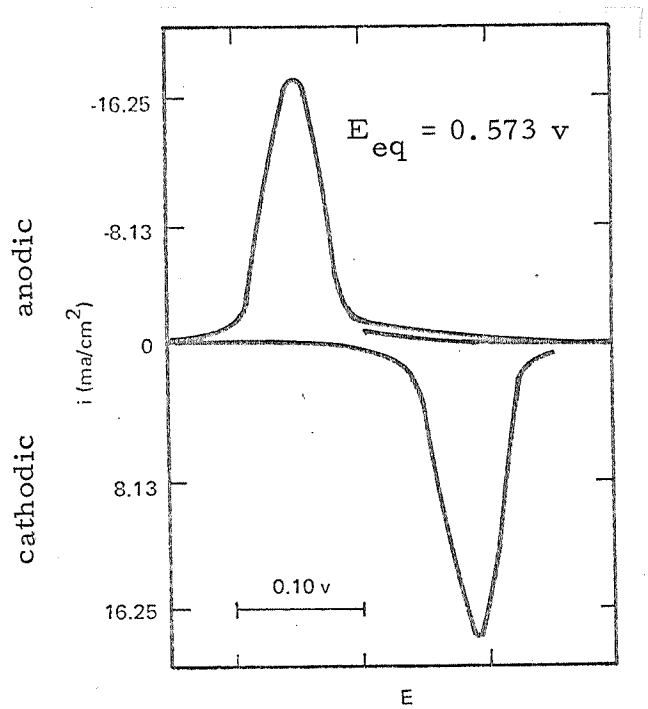

b)* L.S.V.; T = 228°C; s = 23 mv/sec

*Film formation was observed during the anodic sweep

Fig. 12. Voltammetry of $Ni/NiCl_2$ in $ZnCl_2$ Melts

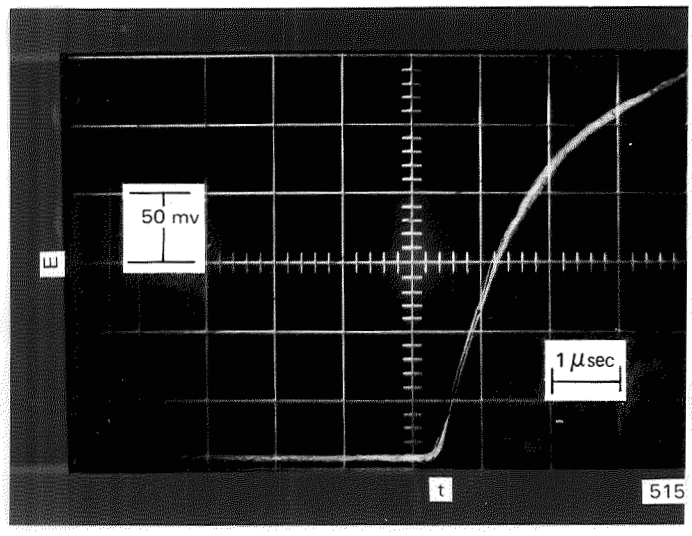

c) C.S.V.; Short Pulse
T = 228°C; i = 330 ma/cm^2
Trace #11

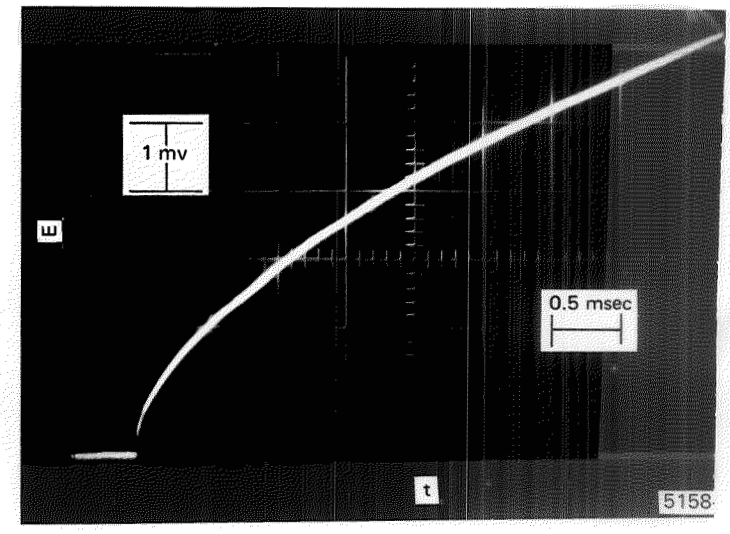

d) C.S.V.; Long Pulse
T = 228°; i = 0.41 ma/cm^2
Trace #19

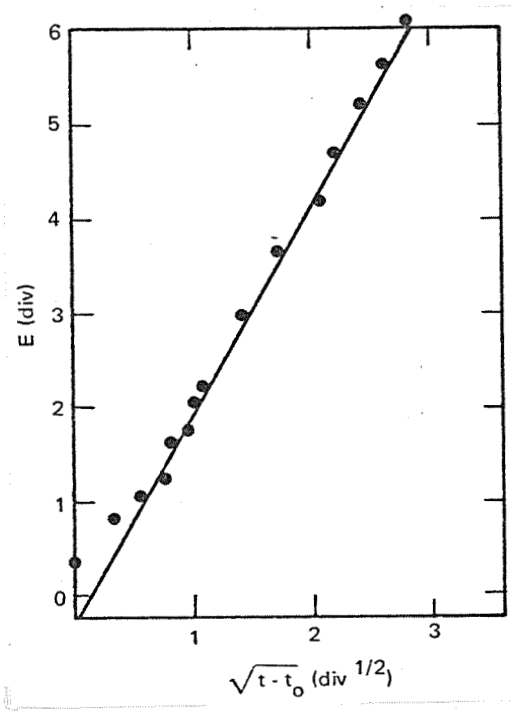

e) E vs $t^{1/2}$ Plot

Fig. 12: Voltammetry of $Ni/NiCl_2$ in $ZnCl_2$ Melts

about equal area to the anodic peak occurred. This peak, which is presumably due to the reduction of the film formed on the anodic sweep, is also shown in Fig. 12b. The peak to peak voltage separation increased from 0.14 v at s = 23 mv/sec to about 0.3 v at 368 mv/sec. Some of this voltage spread is due to IR drop.

Typical current step voltammograms are shown in Fig. 12c-d. Again the short pulse curves at the lowest two temperatures exhibited different behavior from that at the highest temperature, similarly to the Ag and Cu cases. However, there were many features about the $Ni/NiCl_2$ system which differed markedly from the other cases. In this system, the exchange currents all had the wrong sign (as was also found for the $Ni/NiCl_2$ couple in the $AlCl_3$-containing solvent). There is a good possibility that this wrong sign is due, in part, to high concentration polarization resulting from the very low solubility of $NiCl_2$ in the solvent. Thus concentration polarization could contribute to the potential even in times as short as 1/2 μsec. This would result in an electrolyte resistance which is too high and an apparent C_d which is too low. Time, unfortunately, did not permit a thorough analysis of this effect. The sign of R_p was also, of course, incorrect. Extreme positive deviation was noted (see Fig. 12e). Values of $C D^{1/2}$ were very small, and were considerably smaller than those obtained from L.S.V. data.

As a result of the low solubility of $NiCl_2$, the resistance corresponding to the total overpotential at 5 msec is very large and is indeed the largest of any couple studied in this investigation. This is no doubt a result of concentration polarization.

The above results indicate that the $Ni/NiCl_2$ couple is not a satisfactory one if a soluble catholyte is desired. However, based on the ability to reduce virtually all of the film formed during anodization, the possibility of a solid $Ni/NiCl_2(s)$ couple should not be discounted.

(5) $\underline{Bi/BiCl_3}$ –

The voltammetry results are shown in Table 19 and Fig. 13. The potentials of the Bi couple were 0.717 v at 220° and 0.673 v at 250°C. This cell was not run above 270° to prevent the metal electrodes from melting (Bi M.P. = 271°C). The voltammograms (Fig. 13a) are diffusion-limited and are initially non-vertical indicating that the couple is not as reversible as the Cu and Ag systems. Further, the E_p values, even after correction for the ohmic drop, are not independent of sweep rate at either temperature, also indicative of irreversibility. (These results are in accord with those for the 15 wt % melt which yielded resistance-limited voltammograms with slopes that increased with sweep rate.) The low values of $E_{eq} - E_p$ at the slow sweeps suggest that a 3-electron change occurs here (monovalent bismuth is shown to be present in the $AlCl_3$ melt below). The i_p/m data were not constant at 220° but except for the first value were constant at 250°C. The $CD^{1/2}$ results are in accord with complete solution of the solute at 250°. Additonal evidence for the complete solubility of $BiCl_3$ in 0.1 M solution is that much larger current densities were attained with a 15 wt % $BiCl_3$. Small pieces of bismuth were found in the cell at the end of the experiment. These probably result from anodic attack on the counter electrode.

Typical current step voltammograms are shown in Fig. 13b-c. Almost all the short pulse traces but one (#1) had a resistor-like

TABLE 19

VOLTAMMETRY OF $Bi/BiCl_3$ in $ZnCl_2$ SOLVENT

(#5; A = 0.049 cm^2; n = 3)

a) LINEAR SWEEP VOLTAMMETRY

Temp (°C)	E_{eq} (v)	$CD^{1/2} \times 10^7$ $\left(\frac{moles}{cm^2 sec^{1/2}}\right)$	s (mv/sec)	i_p/m (ma/cm^2)	$E_{eq} - E_p$ (mv)
220	0.717	(2.0)	23	11.2	32
			92	13.0	50
			207	18.0	92
			368	17.0	110
250	0.673	2.9	23	30.0	15
			92	21.3	15
			207	21.0	25
			368	22.8	50

b) CURRENT STEP VOLTAMMETRY-SHORT PULSE

Temp (°C)	i (ma/cm^2)	trace	C_d ($\mu F/cm^2$)	R_s (Ω)
220	200	6	2.2	18.65
220	200	11	2.0	17.40
243	400	5	2.6	10.60
245	400	1	3.3	8.60
246	400	14	—	11.89
254	400	19	—	11.10

TABLE 19 (cont'd)

VOLTAMMETRY OF $Bi/BiCl_3$ in $ZnCl_2$ SOLVENT

c) CURRENT STEP VOLTAMMETRY-LONG PULSE

Temp (°C)	i (ma/cm^2)	trace	R_s (Ω)	R_p (Ω)	$\frac{\Delta\eta_{0.1\,msec}}{iA}$ (Ω)	$CD^{1/2}$ x 10^7	D x 10^6 (cm^2/sec)	$\eta_{5\,msec}$ (mv)	$\frac{\eta_{5\,msec}}{iA}$ (Ω)	i_o (A/cm^2)
220	2.0	10	18.0	-3.5	+3.3	0.47	.22	-0.5	- 5.2	0.078
220	5.0	8	18.0	-2.7	+0.1	0.02	.0004	-1.5	- 6.1	0.11
220	5.0	9	18.0	-2.0	+0.3	0.02	.0004	-1.5	- 5.9	0.13
220	10.0	7	18.0	-2.0	0	0.02	.0004	-1.7	- 3.4	0.13
243	2.0	4	10.5	-4.8	+1.6	0.02	.0004	-0.9	- 8.8	0.058
243	5.0	3	10.5	-3.8	+1.0	0.03	.0009	-1.5	- 6.1	0.075
250	5.0	16	10.5	-1.2	0	0.21	.043	-3.4	-13.6	0.23
243	10.0	2	10.5	-3.8	+0.4	0.03	.0009	-3.2	- 6.3	0.073
246	10.0	15	10.5	-2.3	0	0.04	.0016	-2.1	- 4.1	0.12
252	20.0	17	10.5	-0.9	0	0.04	.0016	-2.9	- 2.9	0.32
253	20.0	18	10.5	-1.1	0	0.05	.0025	-2.6	- 2.6	0.26

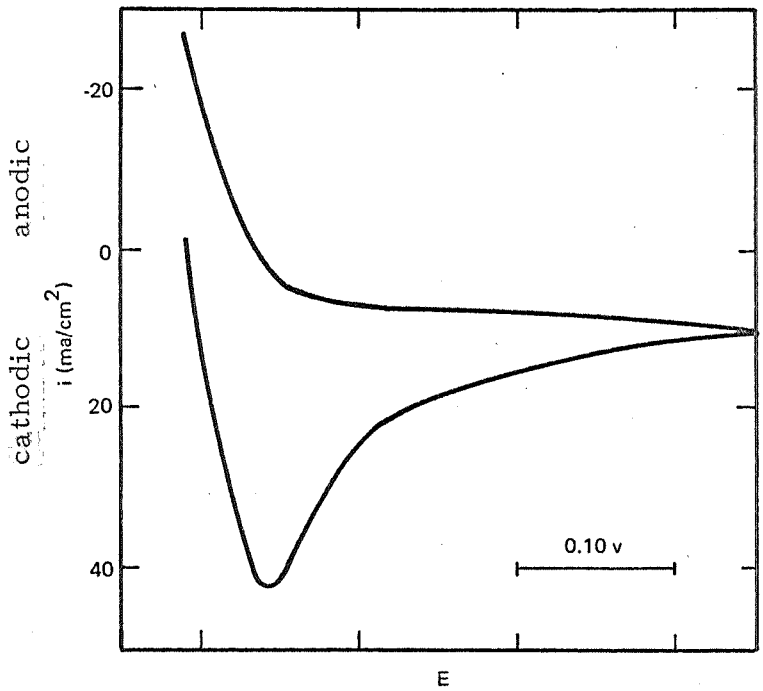

a) L.S.V.; T = 250°C; s = 92 mv/sec
E_{eq} = 0.673 v

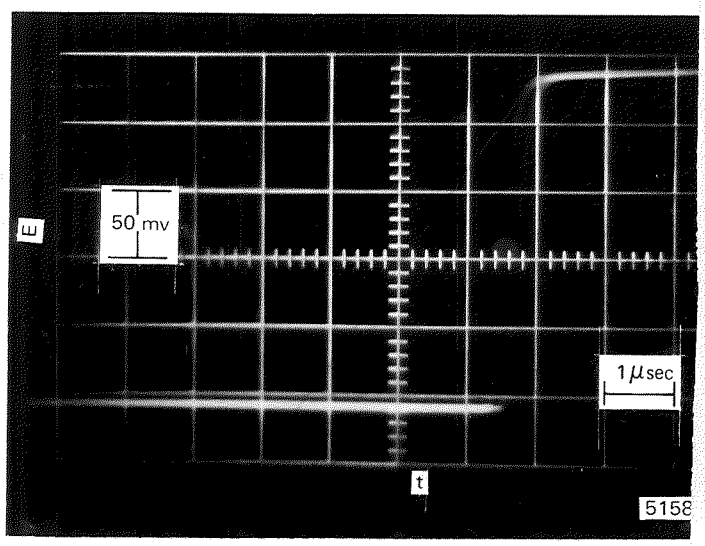

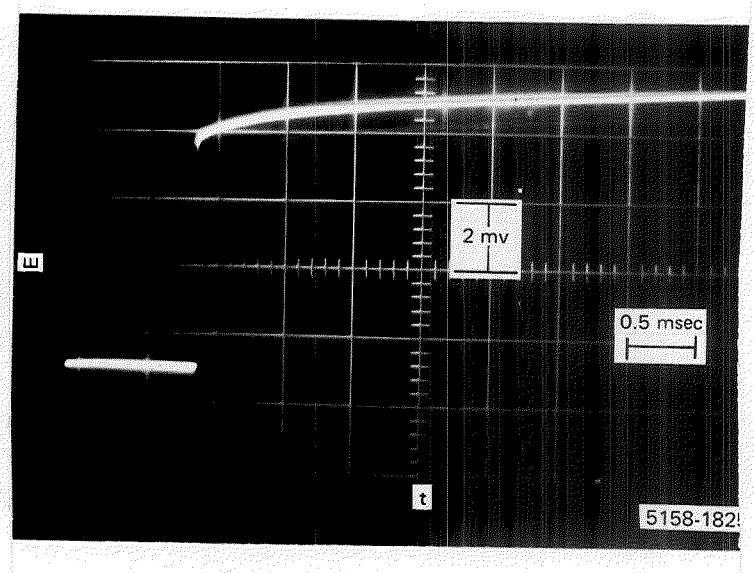

b) C.S.V.; Short Pulse
T = 246°C; i = 400 ma/cm^2
Trace #14

c) C.S.V.; Long Pulse
T = 243°C; i = 10 ma/cm^2
Trace #2

Fig. 13: Voltammetry of $Bi/BiCl_3$ in $ZnCl_2$ Melts

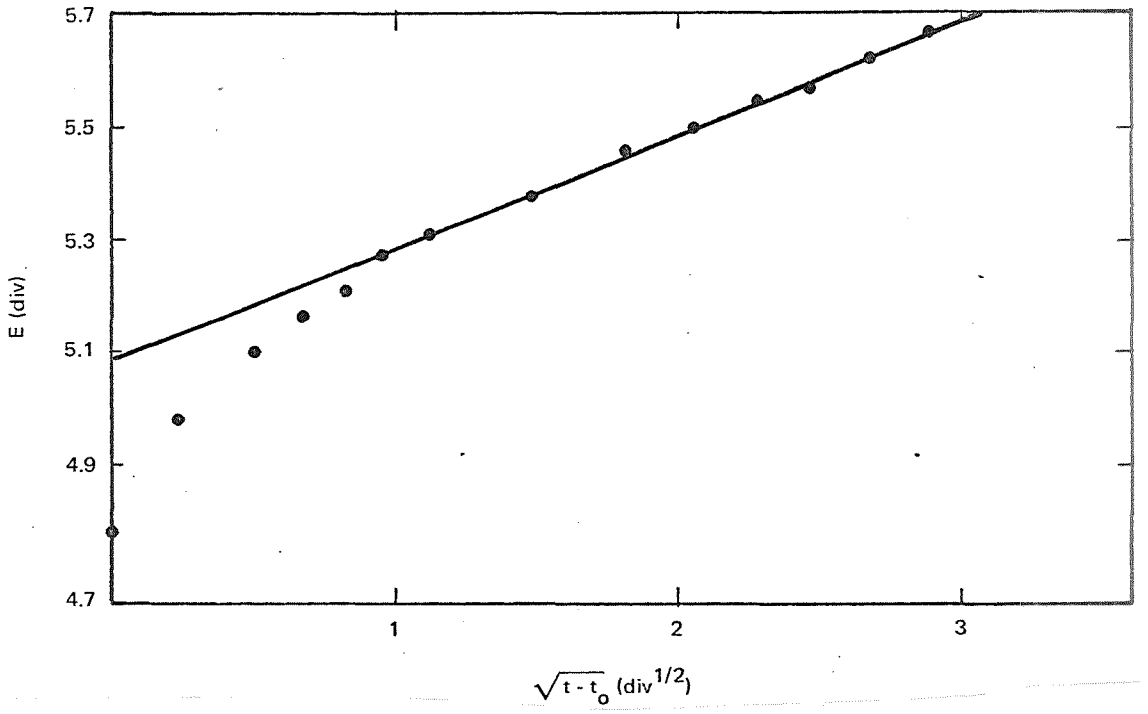

d) E vs $\sqrt{t}$ Plot

Fig. 13: Voltammetry of $Bi/BiCl_3$ in $ZnCl_2$ Melt

appearance. However, this appearance was not due to a high exchange current but probably to the high values of R_s. As shown in Appendix II-C, such high values probably contributed to the very low values of C_d. In addition, these high values of R_s resulted in considerable loss in sensitivity both in the short pulse and long pulse calculations.

In this system there appeared to be an aging effect of the electrode, since the i_o's increased in general with increasing trace number. In addition, the deviation from linearity was least in the last 4 traces. This deviation was rather small except for traces 3, 4 and 10. As in the $Ni/NiCl_2$ case the $CD^{1/2}$ values measured by C.S.V. are considerably smaller than those measured by L.S.V. The total overpotential at the end of 5 msec and the resistance corresponding to this overpotential was not very large. The exchange current densities were about 0.1 A/cm^2 at 220°C and about 0.15 A/cm^2 at 243-253°C.

Based on the C.S.V. results, the exchange current densities are satisfactory and concentration polarization should not pose a great problem. The L.S.V. results also indicate that the couple is not as reversible as the Ag or Cu ones. The low melting point of bismuth does not permit a wide temperature range of battery operation if a solid electrode is desired. Also the fact that pieces of bismuth were found in the cell is a discouraging result as far as secondary battery application is concerned.

(6) $\underline{Sb/SbCl_3}$ –

The voltammogram results are shown in Table 20 and in Fig. 14. The open circuit potentials in this system were 0.716 v at 224°C and 0.662 v at 271°. Due to excessive volatility of the $SbCl_3$, no measurements were carried out at any higher temperature.

The initial portion of the wave in the L.S.V. at 224°C (Fig. 14a) was non-vertical. In addition, the voltammograms showed a two-step consecutive reaction. The apparent peak voltage and peak current at the 23 mv/sec sweep are listed for both peaks in Table 20a. On cycling, the second peak decreased in magnitude. Further, with an increase in the sweep rate the second peak disappeared (Fig. 14b). The anodic behavior is also not typical and indicates that some species is being reduced during the anodic sweep soon after reversal. A possible explanation for this cathodic behavior is that the reduction of Sb(III) occurs in two steps, Sb(III) $\rightarrow$ Sb(I) $\rightarrow$ Sb(0). Since the first step involves a 2-electron change and the last one only 1-electron, the increase in i_p with $s^{1/2}$ for the first peak (the less cathodic) will be about 2.8 times larger than the second (see eq. 1). This plus any irreversibility in the first step, which would broaden the wave, would tend

TABLE 20

VOLTAMMETRY OF $Sb/SbCl_3$ in $ZnCl_2$ SOLVENT

(#19; A = 0.049 cm^2; n = 3)

a) LINEAR SWEEP VOLTAMMETRY

Temp (°C)	E_{eq} (v)	$CD^{1/2} \times 10^7$ $\left(\frac{moles}{cm^2 sec^{1/2}}\right)$	s (mv/sec)	i_p/m (ma/cm^2)	$E_{eq} - E_p$ (mv)
224	0.716	1.6	23	12.4, 14.0	55, 95
			92	12.3	80
			207	11.8	100
			368	11.0	125
271	0.662	(2.2)	23	17.0	—, 55
			92	16.9	58
			207	14.3	58
			368	14.3	70

b) CURRENT STEP VOLTAMMETRY-SHORT PULSE

Temp (°C)	i (ma/cm^2)	trace	C_d ($\mu F/cm^2$)	R_s (Ω)
220	300	1	1.0	9.25
220	300	2	1.0	11.1
219	300	6	0.9	11.3
273	400	7	2.2	6.25
271	400	8	1.9	6.05
271	400	9	2.4	7.46

TABLE 20 (cont'd)

VOLTAMMETRY OF $Sb/SbCl_3$ in $ZnCl_2$ SOLVENT

c) CURRENT STEP VOLTAMMETRY-LONG PULSE

Temp (°C)	i (ma/cm^2)	trace	R_s (Ω)	R_s (Ω)	$\frac{\Delta\eta_{0.1\,msec}}{iA}$ (Ω)	$CD^{1/2} \times 10^7$	$D \times 10^6$ (cm/sec)	$\eta_{5\,msec}$ (mv)	$\frac{\eta_{5\,msec}}{iA}$ (Ω)	i_o (A/cm^2)
218	2.0	5	10.6	-23.5	+2.5	0.26	0.07	-2.6	-26.4	0.012
218	5.0	4	10.6	-24.5	+1.0	0.21	0.05	-6.9	-27.6	0.011
219	10.0	3	10.6	-25.0	+1.2	0.35	0.12	-14.0	-28.0	0.011
270	5.0	10	6.6	- 5.8	+0.4	0.81	0.65	-1.7	-6.8	0.051
271	10.0	9	6.6	- 5.9	+0.3	0.75	0.55	-3.5	-7.0	0.051
271	20.0	11	6.6	- 5.7	+0.1	0.48	0.23	-7.2	-7.2	0.054

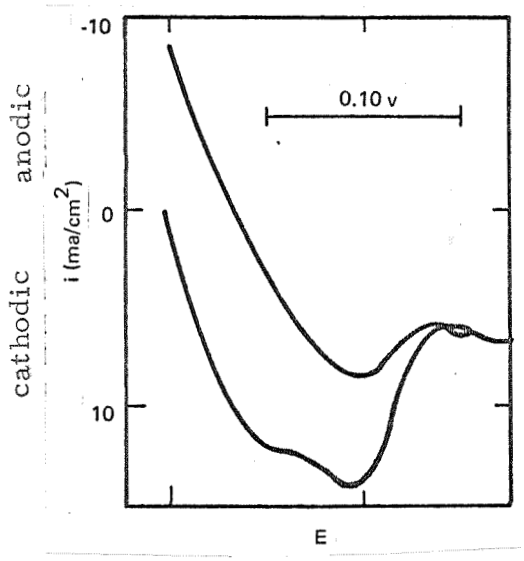

a) L.S.V.; T = 224°C; s = 23 mv/sec
E_{eq} = 0.716 v

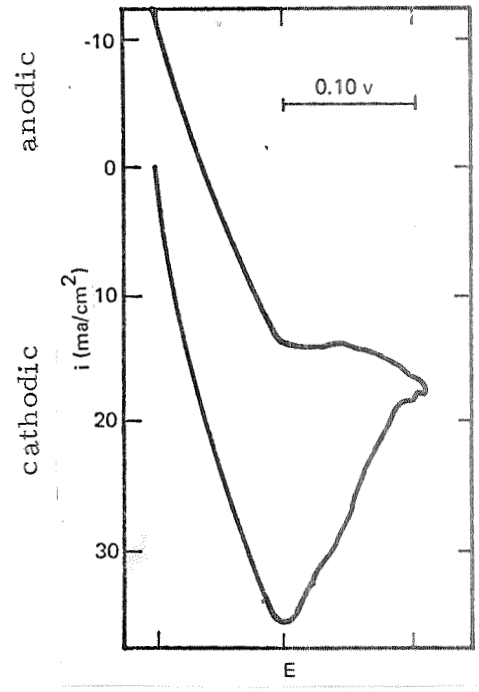

b) L.S.V.; T = 224°C; s = 207 mv/sec
E_{eq} = 0.716 v

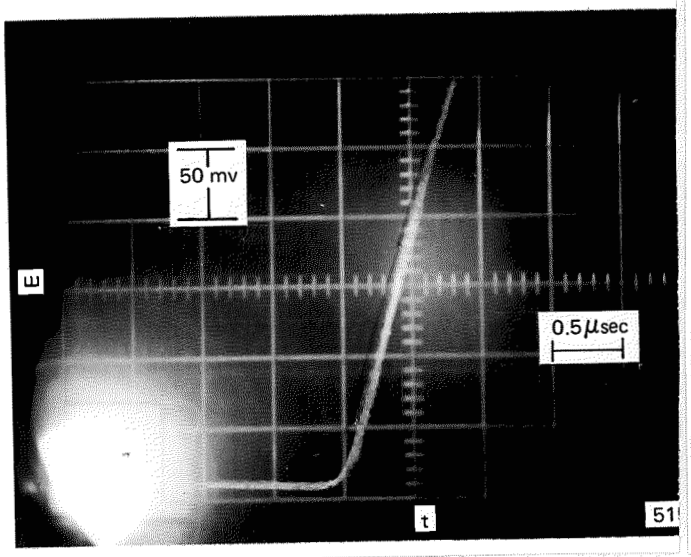

c) C.S.V.; Short Pulse
T = 219°C; i = 300 ma/cm^2
Trace #6

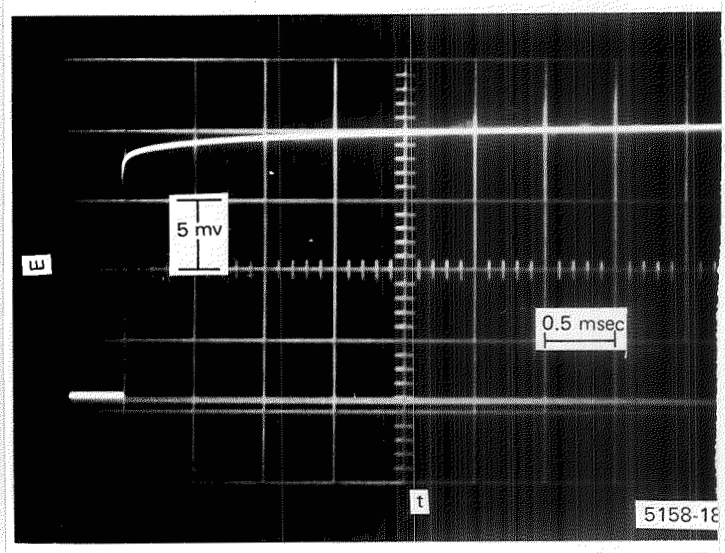

d) C.S.V.; Long Pulse
T = 219°C; i = 10 ma/cm^2
Trace #3

Fig. 14: Voltammetry of $Sb/SbCl_3$ in $ZnCl_2$ Melts

105

to mask the second peak. For the first peak the $E_{eq} - E_p$ values are large and the large shift in peak voltage with sweep rate also is in accord with a non-reversible couple. On the other hand, the i_p/m values are constant with sweep rate.

At 271° the waves commenced more steeply and appeared more normal. A second peak was still evident at the slower sweeps, but much less so than at the lower temperature. The $E_{eq} - E_p$ values at 271°C were fairly constant except for the fastest sweep and were smaller than at 224°. The i_p/m data were constant for the first two sweeps and for the last two sweeps. The difference between the two pairs may be due to a change in the electrodes. The $CD^{1/2}$ values are somewhat smaller than those for $BiCl_3$ and suggest that all the $SbCl_3$ had dissolved. No attack of the electrodes was evident.

Typical current step voltammograms are shown in Fig. 14c-d. As in the Bi case, R_s was rather large. The C_d's obtained at 200°C were the lowest obtained in this work. The exchange currents were the smallest of all the $ZnCl_2$-containing melts. Negative deviation from linearity was pronounced at 200°C (see Fig. 14e). Again $CD^{1/2}$ values were lower when measured by C.S.V. than when done by L.S.V. The resistance corresponding to the total overvoltage at 5 msec was quite large at 200°C, most of it being due to the low exchange current. At 270°C the exchange current was considerably higher, but still relatively low. Thus, the comments concerning reversibility in the L.S.V. section are consistent with the C.S.V. results. It should be cautioned that since there is more than one electrochemical step, the i_o values must be regarded as formal numbers.

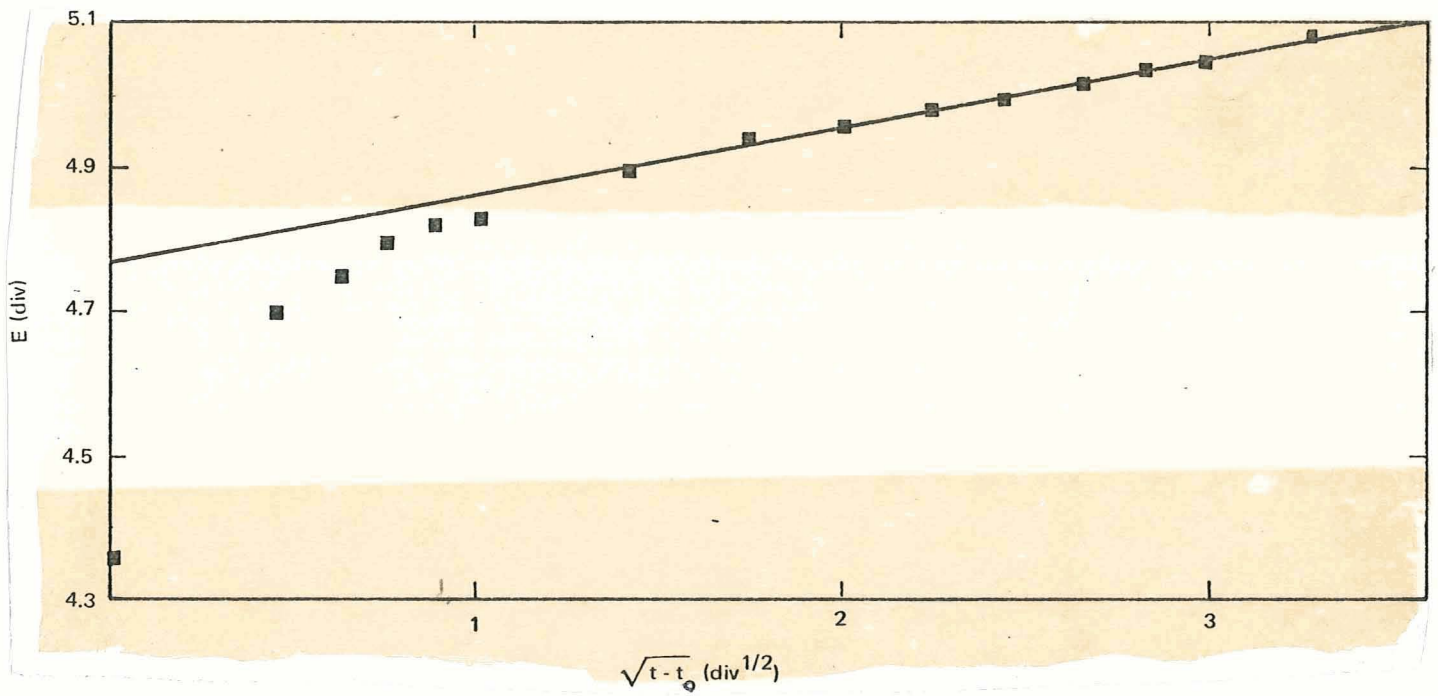

e) E vs $t^{1/2}$ Plot

Fig. 14: Voltammetry of $Sb/SbCl_3$ in $ZnCl_2$ Melts

The application of the $Sb/SbCl_3$ couple does not appear favorable for a $ZnCl_2$-based battery for two reasons. The system appears to be relatively irreversible and the $SbCl_3$ is too volatile.

(7) $\underline{Pt/CrCl_2, CrCl_3}$ –

The voltammogram results are shown in Table 21 and in Fig. 15. This system yielded open circuit voltages of 0.920, 0.945 and 0.959 v at 230, 275 and 320°C, respectively. Cr(II) reduction to the metal occurred at about 0.10 v. The cathodic waves showed an infinite slope initially and the couple appears to be reversible (Fig. 15a); the cathodic peak to anodic peak voltage span, ΔE_p, is constant at all temperatures and closely approaches the calculated value in Table 14. The cathodic i_p/m values are constant at all temperatures indicating the reduction to be a straightforward process. Although eq. 5 does not pertain exactly to the redox systems studied here since the concentration of reduced species is not zero, the $CD^{1/2}$ values calculated suggest that the solubility of $CrCl_3$ is less than 0.1 M in this melt. From the i_p values of single cathodic and anodic sweeps from the rest potential, the ratio i_p (anodic)/i_p (cathodic) = 1.3 at the three temperatures. Thus if the diffusion coefficients of Cr(II) and Cr(III) are similar, the concentration ratio of Cr(II) to Cr(III) is also about 1.3.

A typical current-step voltammogram set is shown in Fig. 15 b-d. In this redox system the C_d values were in general significantly higher than in the metal/metal ion systems. The deviations from linearity were, as with most redox systems, less at all temperatures than with most metal/metal ion couples.

TABLE 21

VOLTAMMETRY OF $Pt/CrCl_2, CrCl_3$ in $ZnCl_2$ SOLVENT

(#8; A = 0.062 cm^2; n = 1)

a) LINEAR SWEEP VOLTAMMETRY

Temp (°C)	E_{eq} (v)	$CD^{1/2} \times 10^7$ $\left(\frac{moles}{cm^2 sec^{1/2}}\right)$	s (mv/sec)	i_p/m (ma/cm^2)	$E_{eq} - E_p$ (mv)
224	0.920	0.12	23	0.37	100
			92	0.38	100
			207	0.38	100
			368	0.38	100
275	0.945	0.21	23	0.65	120
			92	0.65	120
			207	0.65	115
			368	0.64	115
320	0.959	0.26	23	0.79	135
			92	0.76	130
			207	0.74	130
			368	0.74	130

b) CURRENT STEP VOLTAMMETRY-SHORT PULSE

Temp (°C)	i (ma/cm^2)	trace	C_d ($\mu F/cm^2$)	R_s (Ω)
224	330	18	9.2	1.59
224	330	22	10.3	1.57
276	330	13	11.8	1.66
276	330	15	15.0	1.52
276	330	17	12.8	1.66
315	330	5	15.0	1.08
319	330	10	16.3	1.50

TABLE 21 (cont'd)

VOLTAMMETRY OF $Pt/CrCl_2$, $CrCl_3$ in $ZnCl_2$ SOLVENT

c) CURRENT STEP VOLTAMMETRY-LONG PULSE

Temp (°C)	i (ma/cm^2)	trace	R_s (Ω)	R_p (Ω)	$\frac{\Delta\eta_{0.1\,msec}}{iA}$ (Ω)	$f(CD^{1/2}) \times 10^7$	$D \times 10^6$ (cm^2/sec)	$\eta_{5\,msec}$ (mv)	$\frac{\eta_{5\,msec}}{iA}$ (Ω)	i_o^a (A/cm^2)
224	0.8	21	1.6	-6.2	+2.0	0.06	0.01	- 5.1	-102	0.096
224	1.6	20	1.6	-4.2	+2.8	0.07	0.02	- 8.5	- 85	0.14
224	4.0	19	1.6	-3.0	0	0.06	0.02	-25.2	-101	0.17*
277	0.8	16	1.6	-5.4	+2.8	0.10	0.04	- 2.8	- 55	0.13
277	1.6	15	1.6	-2.3	+0.8	0.11	0.05	- 5.7	- 57	0.27*
277	4.0	14	1.6	-0.8	0	0.10	0.04	-16.1	- 66	0.60*
319	1.6	8	1.3	-1.7	0	0.13	0.07	- 5.1	- 51	0.39*
320	1.6	9	1.3	-2.2	0	0.13	0.07	- 5.2	- 53	0.31*
319	4.0	7	1.3	-0.7	+0.8	0.14	0.08	-12.3	- 50	0.77*
316	8.0	6	1.3	-0.3	0	0.12	0.06	-26.1	- 53	1.12*

a) The approximate i_o values calculated from eq. 13 are: trace 19, 0.22; trace 15, 0.30; trace 14, 0.94; trace 8, 0.46; trace 9, 0.35; trace 7, 1.10; and trace 6, 2.69 A/cm^2.

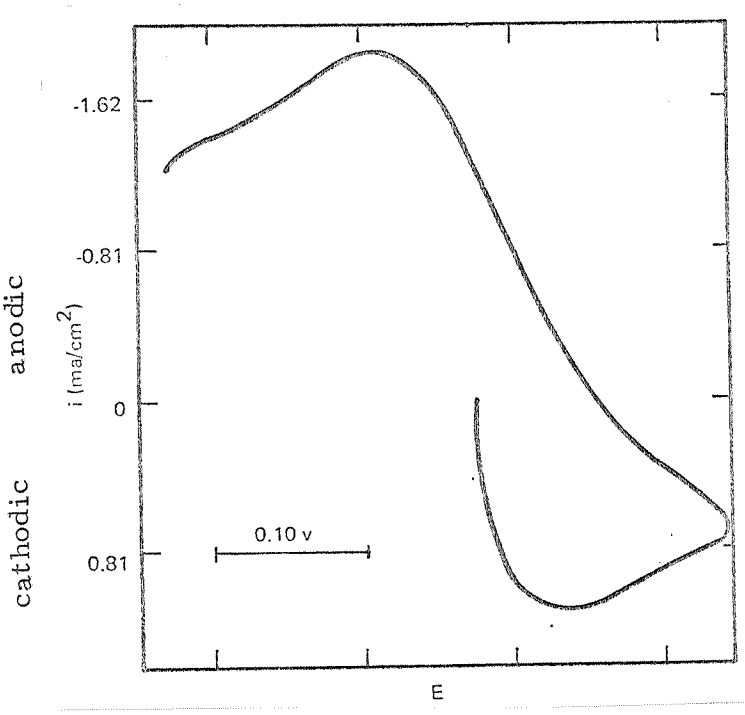

a) L.S.V.; T = 224°C; s = 207 mv/sec
E_{eq} = 0.920 v

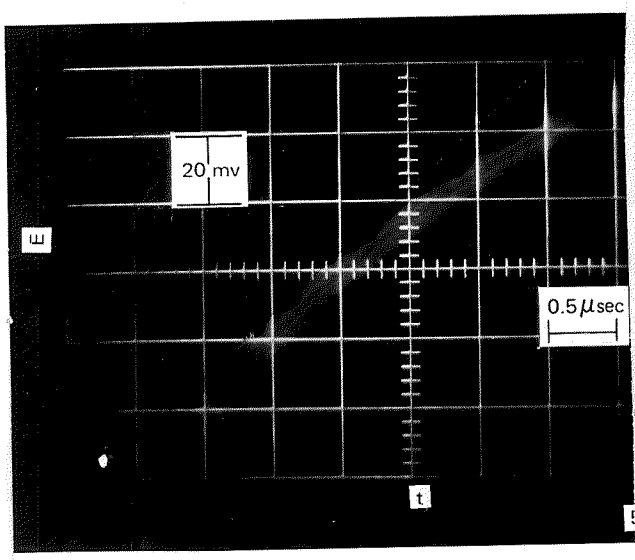

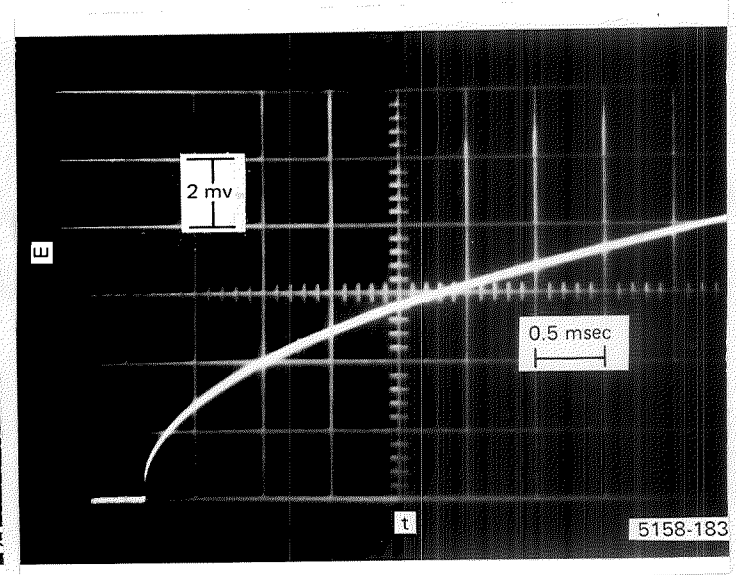

b) C.S.V.; Short Pulse
T = 224°C; i = 330 ma/cm^2
Trace #18

c) C.S.V.; Long Pulse
T = 224°C; i = 1.6 ma/cm^2
Trace #20

Fig. 15: Voltammetry of Pt/$CrCl_2$, $CrCl_3$ in $ZnCl_2$ Melts

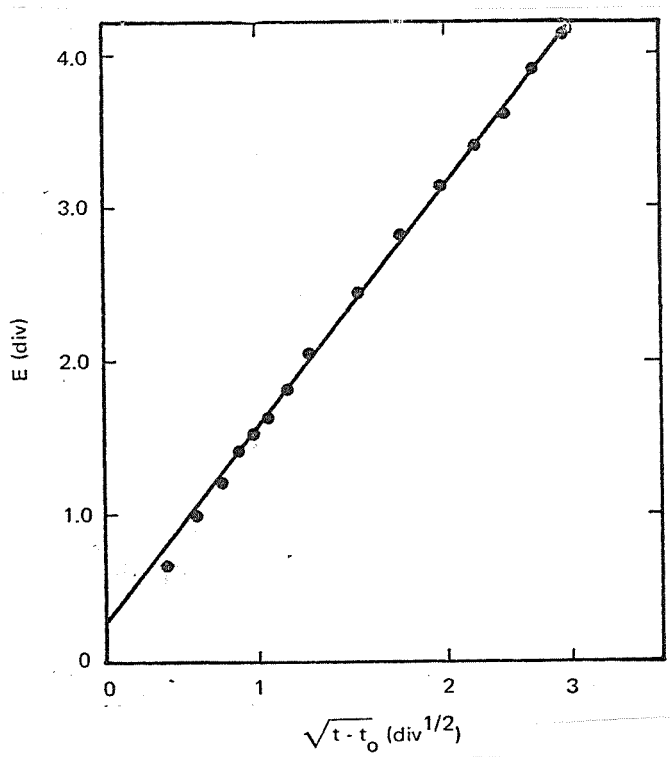

d) E vs $t^{1/2}$ Plot

Fig. 15: Voltammetry of Pt/$CrCl_2$, $CrCl_3$ in $ZnCl_2$ Melts

There appeared to be an increase in i_o with increasing i; this was the only system to exhibit this behavior. Values for $f(C_i D_i^{1/2})$ obtained from C.S.V. data were in considerably better agreement with those calculated from L.S.V. data in this redox case than in metal/metal ion cases. The very low values obtained by both methods suggest that the solubility of $CrCl_3$ is very low in the $ZnCl_2$ solvent. Due to this low solubility, both the total overpotential and the resistance corresponding to the total overpotential at 5 msec were very large and second only to the Ni/$NiCl_2$ couple. The exchange currents were satisfactory at all temperatures.

While this system appears to be quite reversible, the concentration polarization would be too severe if a soluble catholyte is required. However, the possibility of using W or Pt/$CrCl_3$(s), $CrCl_2$(s), in the melt should not be discounted.

(8) W/CuCl, $CuCl_2$ –

The voltammogram results are shown in Table 22 and in Fig. 16. This redox couple has an open circuit voltage between 1.30 and 1.43 v. A cyclic voltammogram of the melt is shown in Fig. 22a. (The zero potential is at the extreme right and becomes more positive (anodic) towards the left.) Starting from the open circuit potential and going cathodic, one has the reduction wave for Cu(II) → Cu(I) immediately and then commencing at about 0.3 v the plating out of copper, Cu(I) → Cu(0). Zinc reduction occurs at 0 v and on reversal a large anodic wave for the stripping of Cu and Zn is observed. The oxidation of Cu(I) to Cu(II) begins at about 1.3 v and chlorine evolution or tungsten anodization occurs at 1.8 v. Cyclic voltammograms of the redox couple at 226° and 320° are presented in Fig. 16b and c. The cathodic waves at all temperatures (except for the fastest sweep rate at 230 and 271°) initiated at infinite slope and the wave couple at the lower temperature appears well behaved. At 320°, however, the oxidation peak was not well-defined but merged with the anodic limiting wave for the melt. (Thus values of $E_{eq} - E_p$ instead of ΔE_p were taken for the cathodic wave at 320°.) This indicates that $CuCl_2$ is barely stable at 320°C. The cathodic peak voltage at 320° was constant with sweep rate; at 271° ΔE_p was constant for the first three sweeps, and at 230° ΔE_p was constant at only the two slowest sweep rates. The values of ΔE_p are about the same as those for the $CrCl_2$+$CrCl_3$ system. The cathodic i_p data are linear with $s^{1/2}$ indicating that the reduction step has no complications. The higher i_p, as well as $CD^{1/2}$ values, at 271° than at 320° may be due to loss of some $CuCl_2$ from decomposition. A repeated voltammogram after the system had remained at 320° for some time showed a decrease in the $CuCl_2$ concentration. The solubility of

TABLE 22

VOLTAMMETRY OF W/CuCl, $CuCl_2$ in $ZnCl_2$ SOLVENT

(#11; A = 0.060 cm^2; n = 1)

a) LINEAR SWEEP VOLTAMMETRY

Temp (°C)	E_{eq} (v)	$CD^{1/2} \times 10^7$ $\left(\frac{moles}{cm^2 sec^{1/2}}\right)$	s (mv/sec)	i_p/m (ma/cm^2)	$E_{eq} - E_p$ (mv)
230	1.43	0.72	23	2.3	110
			92	2.3	110
			207	2.3	125
			368	2.3	140
271	1.30	0.93	23	2.8	115
			92	2.9	115
			207	2.7	120
			368	2.9	130
320	1.40	0.74	23	2.2	45
			92	2.2	45
			207	2.1	45
			368	2.1	45

b) CURRENT STEP VOLTAMMETRY-SHORT PULSE

Temp (°C)	i (ma/cm^2)	trace	C_d ($\mu F/cm^2$)	R_s (Ω)
230	330	17	3.7	4.58
230	330	18	3.9	4.95
230	330	19	3.8	4.83
230	330	23	4.3	4.88
271	330	6	7.5	2.40
271	330	10	8.6	2.42
318	330	11	20.3	2.02
318	330	12	20.6	1.96
318	330	16	27.2	2.14

TABLE 22 (con't)

VOLTAMMETRY OF W/CuCl, $CuCl_2$ in $ZnCl_2$ SOLVENT

c) CURRENT STEP VOLTAMMETRY-LONG PULSE

Temp (°C)	i (ma/cm^2)	trace	R_s (Ω)	R_p (Ω)	$\frac{\Delta\eta_{0.1\,msec}}{iA}$ (Ω)	$f(C_i D_i^{1/2})$ x 10^7	D x 10^6 (cm^2/sec)	$\eta_{5\,msec}$ (mv)	$\frac{\eta_{5\,msec}}{iA}$ (Ω)	i_o (A/cm^2)
230	4.0	20	4.8	-2.2	0	0.37	0.55	- 4.6	-18.2	0.32
230	8.0	21	4.8	-2.4	0	0.33	0.44	- 9.3	-18.7	0.30
230	16.0	22	4.8	-1.7	0	0.31	0.39	-18.9	-18.9	0.41
271	1.6	9	2.4	-1.1	0	0.36	0.52	- 2.9	-29.1	0.60
271	4.0	8	2.4	+0.2	0	0.19	0.15	- 7.9	-31.7	WS-8.5*
271	8.0	7	2.4	+1.7	-1.2	0.17	0.12	-17.0	-34.0	WS(-4.7)
317	4.0	13	2.0	-0.20	0	0.42	0.70	- 3.9	-15.6	3.8*
318	8.0	14	2.0	-0.20	0	0.45	0.81	- 7.3	-14.7	3.3*
318	16.0	15	2.0	+0.80	-0.9	0.42	0.70	-16.7	-16.7	WS(-1.0)

a) The approximate i_o values, calculated from eq. 13 are: trace 8, -4.0; trace 13, 4.8; and trace 14, 4.2 A/cm^2.

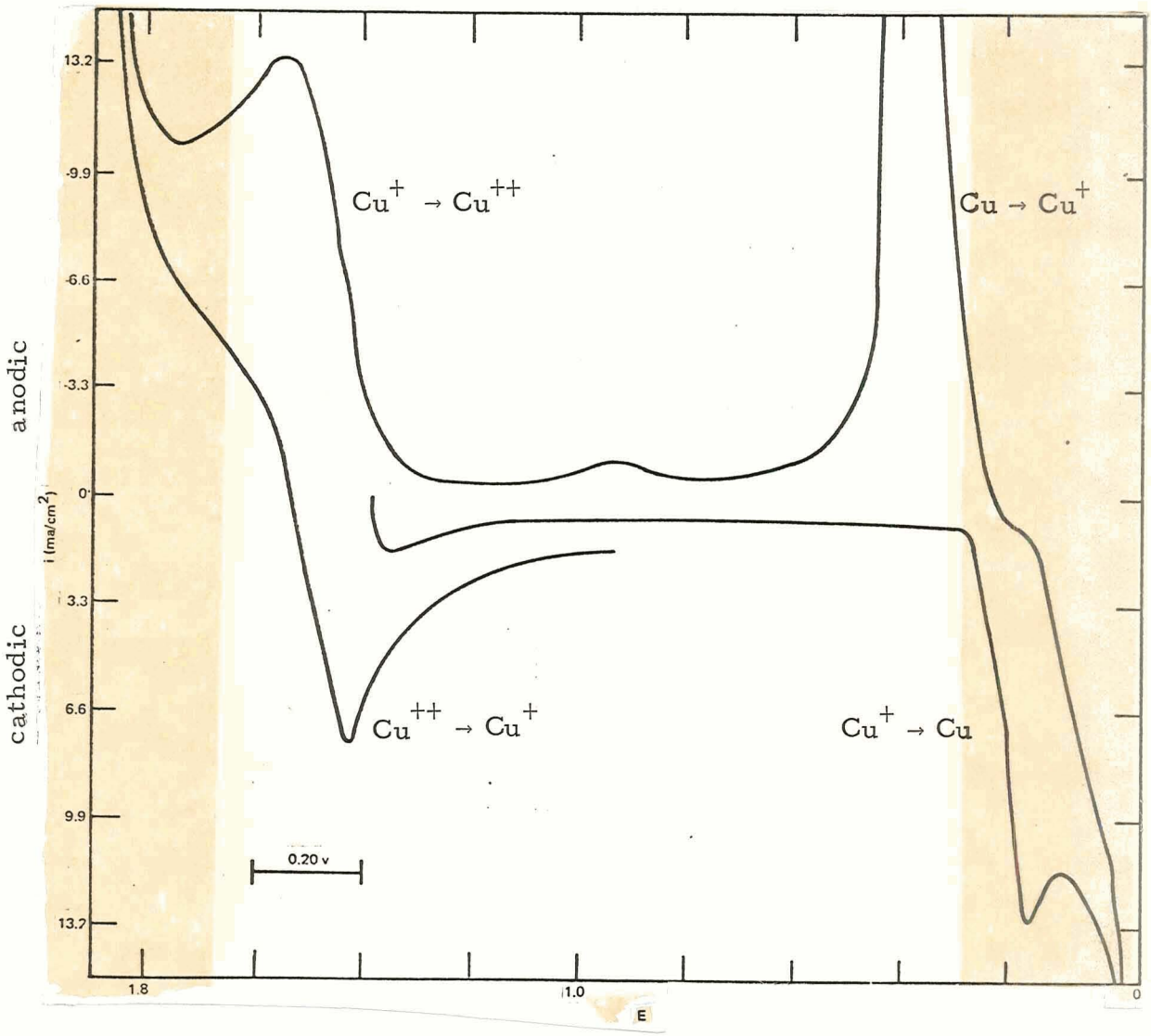

Fig. 16: Voltammetry of W/CuCl, $CuCl_2$ in $ZnCl_2$ Melt

a) L.S.V.; T = 230°C
s = 23 mv/sec

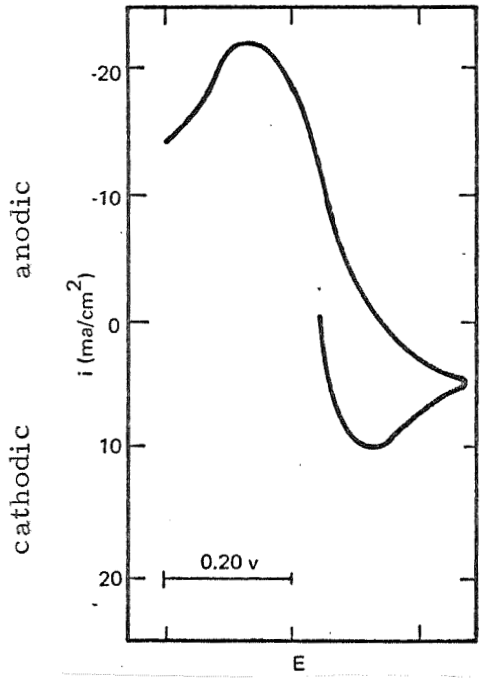

b) L.S.V.; T = 226°C; s = 92 mv/sec
E_{eq} = 0.143 v

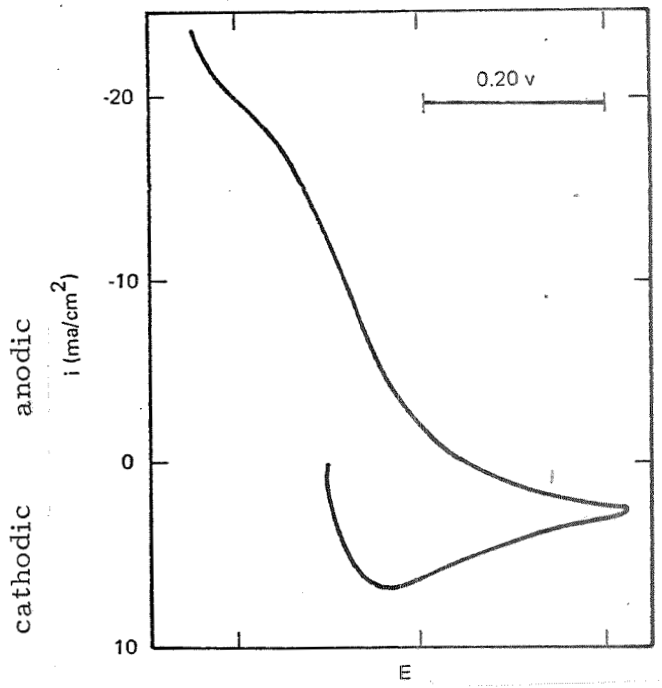

c) L.S.V.; T = 330°C; s = 23 mv/sec
E_{eq} = 0.140 v

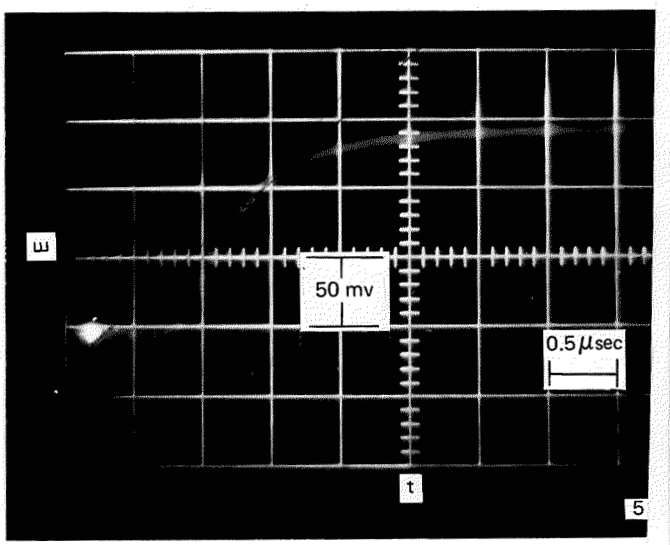

d) C.S.V.; Short Pulse
T = 230°C; i = 330 ma/cm^2
Trace #17

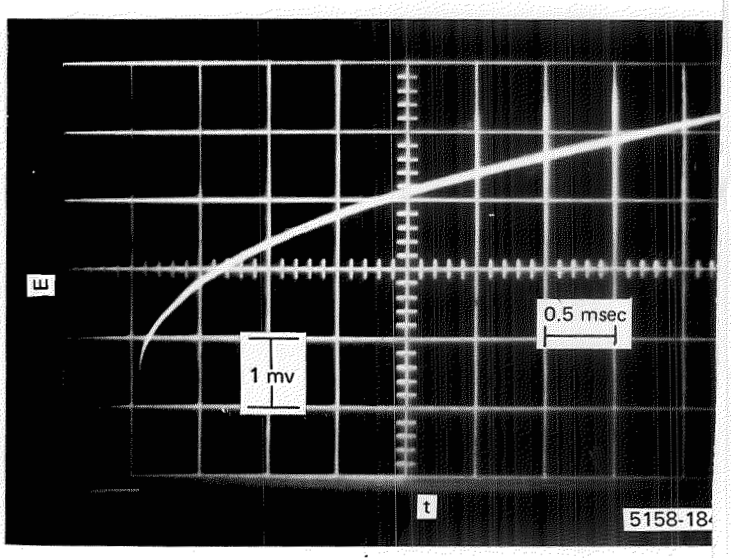

e) C.S.V.; Long Pulse
T = 230°C; i = 4.2 ma/cm^2
Trace #20

Fig. 16: Voltammetry of W/CuCl, $CuCl_2$ in $ZnCl_2$ Melt

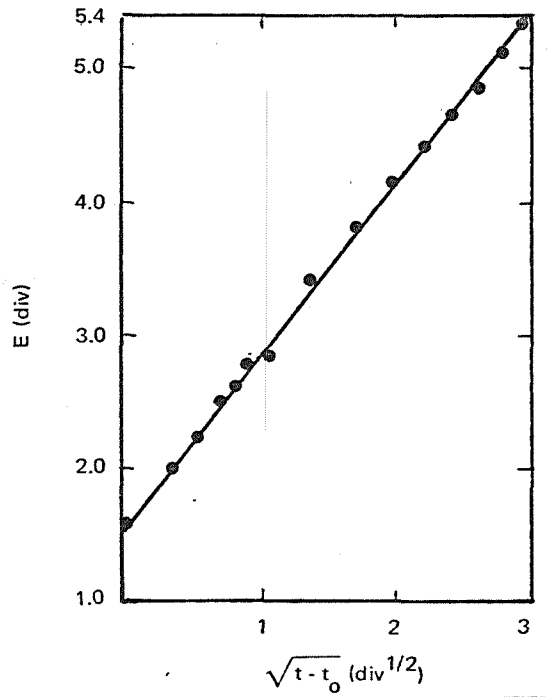

f) E vs $t^{1/2}$ Plot

Fig. 16: Voltammetry of W/CuCl, $CuCl_2$ in $ZnCl_2$ Melt

$CuCl_2$ is probably less than 0.1 M but from the $CD^{1/2}$ results $CuCl_2$ appears to be more soluble than either $CrCl_3$ or $FeCl_3$. From the ratio of i_p values for anodic and cathodic single sweeps the ratio of CuCl to $CuCl_2$ concentration in solution is about two.

A typical current-step voltammogram set is shown in Fig. 22d-f. The C_d values in this redox system were again low except at the highest temperature (318°C) where values of 20 $\mu F/cm^2$ were obtained. There was essentially no deviation from linearity in this couple. The agreement in the $f(C_i D_i^{1/2})$ obtained from C.S.V. was in fair agreement with $CD^{1/2}$ obtained from L.S.V. The exchange currents were quite high, although there were 3 traces where the i_o values were negative. The resistance due to the total overpotential at 5 msec was rather high, probably due to concentration

polarization resulting from the limited solubility.

Just as in the $Pt/CrCl_2$, $CrCl_3$ case, the $W/CuCl$, $CuCl_2$ couple is reversible but suffers from excessive concentration polarization due to the limited solubility of $CuCl_2$ in the melt. In addition, the excessive decomposition pressure of $CuCl_2$ at the highest temperature is a disadvantage for battery applications.

(9) $\underline{W/FeCl_2}$, $\underline{FeCl_3}$–

The voltammogram results are shown in Table 23 and in Fig. 17. Open circuit voltages of about 1.3 v were measured in this system. The reduction of divalent iron to the metal occurs at about 0.23 v. The cathodic waves start with infinite slope and appear to be reversible (Fig. 17a). The ΔE_p values at all three temperatures were constant with sweep rate. However, the ΔE_p values are much larger than the calculated values (Table 14). The i_p/m data showed an increase with sweep rate at 225° but appeared relatively constant at 275°C (except for the first sweep) and at 328°. The $CD^{1/2}$ data indicate that the $FeCl_3$ solubility is slightly greater than $CrCl_3$ in these $ZnCl_2$ melts. The solubility of $FeCl_2$ from i_p results appears to be about twice as great as $FeCl_3$.

A typical current-step voltammogram set is shown in Fig. 17b-d. Again rather low values were obtained for C_d which decreased with increasing temperature. There was slight positive deviation from linearity in most of the traces. The agreement in $f(C_iD_i^{1/2})$ obtained by C.S.V. agreed fairly well with $CD^{1/2}$ calculated from L.S.V. data. Since in this system the initial concentrations were not equal (i.e., $C_o \neq C_r$), calculations of D were not made. Many traces had overpotentials in excess of 5 mv, but plots of

TABLE 23

VOLTAMMETRY OF W/$FeCl_2$,$FeCl_3$ in $ZnCl_2$ SOLVENT

(#6; A = 0.090; n = 1)

a) LINEAR SWEEP VOLTAMMETRY

Temp (°C)	E_{eq} (v)	$CD^{1/2} \times 10^7$ $\left(\frac{moles}{cm^2 sec^{1/2}}\right)$	s (mv/sec)	i_p/m (ma/cm^2)	$E_{eq} - E_p$ (mv)
225	1.32	0.25	23	0.67	14
			92	0.78	15
			207	0.86	15
			368	0.93	16
275	1.30	0.31	23	0.78	15
			92	0.92	15
			207	0.98	15
			368	0.95	16
328	1.34	0.38	23	1.11	15
			92	1.16	15
			207	1.12	15
			368	1.11	16

b) CURRENT STEP VOLTAMMETRY-SHORT PULSE

Temp (°C)	i (ma/cm^2)	trace	C_d ($\mu F/cm^2$)	R_s (Ω)
231	220	1	10.8	1.50
231	220	2	8.7	1.50
230	170	6	8.3	1.40
230	170	7	8.5	1.40
230	220	8	8.7	1.52
274	220	9	4.5	1.47
274	220	10	5.2	1.52
273	220	15a	5.4	1.50
329	220	15b	3.7	1.98

TABLE 23 (cont'd)

VOLTAMMETRY OF $W/FeCl_2$, $FeCl_3$ in $ZnCl_2$ SOLVENT

c) GALVANOSTATIC-LONG PULSE

Temp (°C)	i (ma/cm^2)	trace	R_s (Ω)	R_p (Ω)	$\frac{\Delta\eta_{0.1\,msec}}{iA}$ (Ω)	f ($CD^{1/2}$) x 10^7	D^a	$\eta_{5\,msec}$ (mv)	$\frac{\eta_{5\,msec}}{iA}$ (Ω)	i_o (A/cm^2)
230	2.7	5	1.4	-9.1	-0.4	.17	—	—[b]	—[b]	0.047
230	5.5	4	1.4	-5.9	-2.4	.12	—	—[b]	—[b]	0.076
230	11.0	3	1.4	-8.3	-1.0	.15	—	-32.1	-32.1	0.055
274	2.7	14	1.5	-3.8	-0.9	.11	—	- 4.5	-17.8	0.14
274	5.5	13	1.5	-3.1	-1.4	.15	—	- 8.5	-17.1	0.17
274	11.0	11	1.5	-3.5	-1.0	.11	—	-15.7	-15.7	0.15
274	11.0	12	1.5	-3.2	-1.3	.16	—	-16.5	-16.5	0.16
328	2.7	18	2.0	-8.8	0	.30	—	- 6.2	-24.9	0.063
328	5.5	17	2.0	-9.4	0	.27	—	-12.2	-24.3	0.065
328	11.0	16	2.0	-7.5	-1.3	.25	—	-23.2	-23.2	0.10
328	11.0	19	2.0	-7.2	0	.29	—	-22.2	-22.2	0.076

a) $C_o \neq C_r$; therefore D's were not calculated.

b) Pulse was shorter than 5 msec.

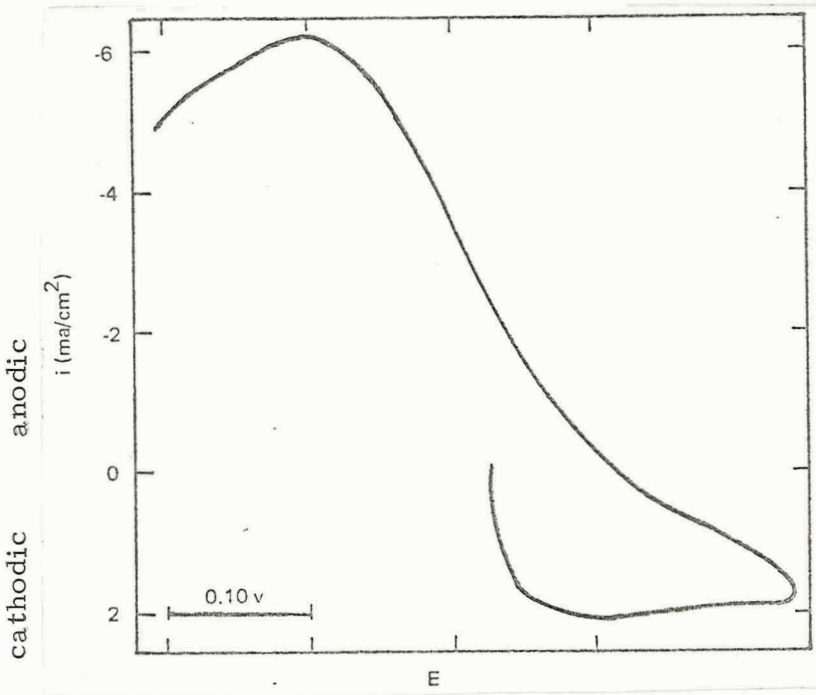

a) L.S.V.; T = 328°C; s = 92 mv/sec
E_{eq} = 1.34 v

122

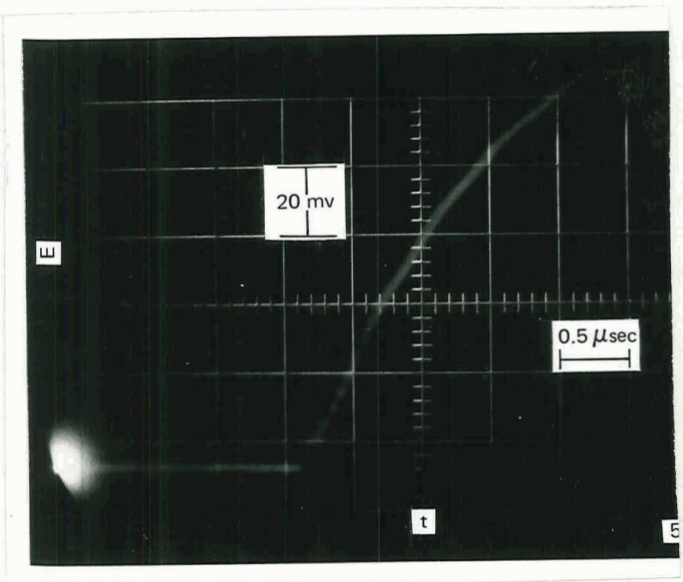

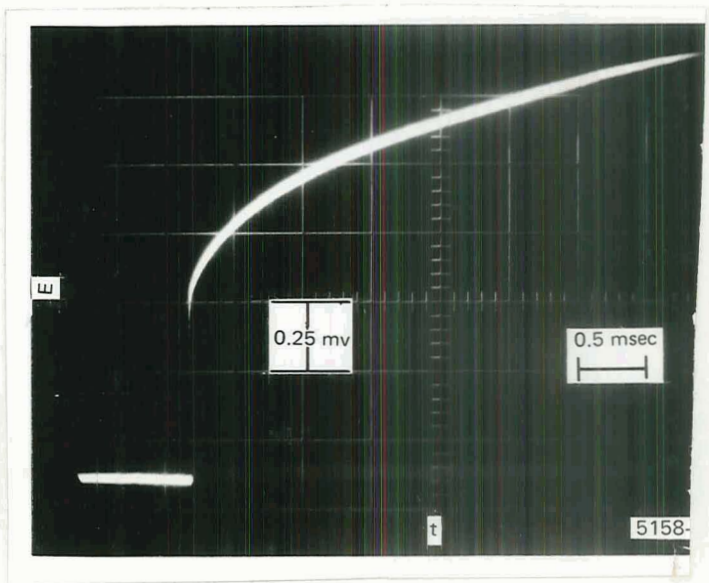

b) C.S.V.; Short Pulse
T = 329°C; i = 220 ma/cm^2
Trace #15 b

c) C.S.V.; Long Pulse
T = 328°C; i = 2.8 ma/cm^2
Trace #18

Fig. 17: Voltammograms of W/$FeCl_2$, $FeCl_3$ in $ZnCl_2$ Melts

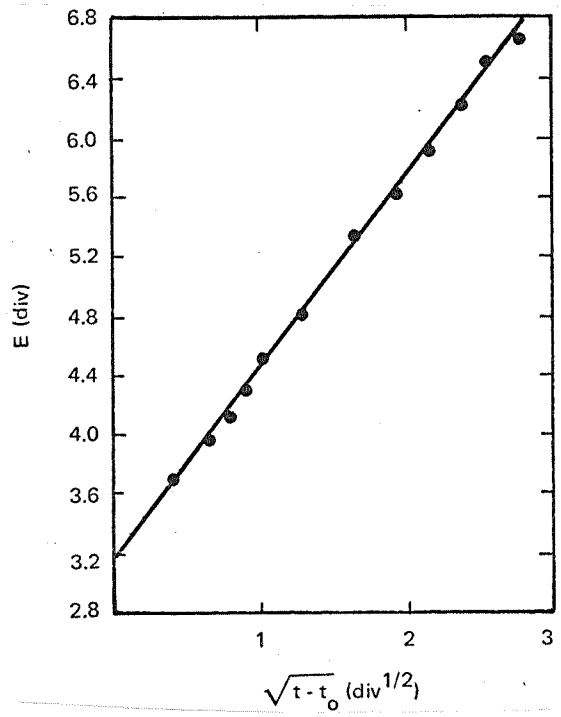

d) E vs $t^{1/2}$ Plot

Fig. 17 : Voltammograms of $W/FeCl_2$, $FeCl_3$ in $ZnCl_2$ Melts

E vs $\sqrt{t}$ were still linear. For example, in trace 19 where $\eta_{5\ msec}$ was -22 mv, the deviation from linearity was zero. The exchange current densities at 328° were less than those at 274°C. One possible reason for this is that some volatile $FeCl_3$ distilled away. However, $f(C_i D_i^{1/2})$, which is a measure of the concentration of the $FeCl_3$, increased rather than decreased. The resistance corresponding to the total overpotential was somewhat high due to concentration polarization.

While the exchange currents are barely satisfactory, the concentration polarization was excessive and the $FeCl_3$ volatility is a great disadvantage for battery applications.

(10) $\underline{Zn/ZnCl_2}$

The voltammetry results are shown in Table 24 and in Fig. 18. The open circuit voltages were zero at all temperatures as expected

since $Zn/ZnCl_2$- solvent is the reference. Due to the high concentration of electroactive species (60 mole %), cyclic voltammetry (Fig. 18a) yielded no peaks but resistance-limited plots up to current densities of 1 amp/cm^2, the saturation limit of the instrument. The slopes of these voltammograms were independent of sweep rate up to the fastest sweep rate applied, 200 mv/sec. Dendrites were present on the Zn electrode.

Two typical sets of cathodic current step voltammograms are shown in Fig. 18b-e. The first set (b and c) depicts the low temperature behavior while the second set shows the behavior at the highest temperatures. Due to the high concentration of electroactive species (2.38×10^{-2} mole/cm^3), the long pulses were virtually flat, indicating little concentration polarization. Considering the high concentration of Zn(II), one would think that the i_o values would have been considerably higher, especially at the two lower temperatures. One possible explanation is that the Zn(II) is complexed strongly in this system so that the concentration is actually very low. At higher temperatures the complexes become more dissociated resulting in higher exchange currents.

Attempts to generate meaningful short anodic pulses with the pulse generator used for cathodic pulses were not successful. A typical trace is shown in Fig. 18f. The occurrence of a peak is difficult to rationalize since short anodic pulses were expected to produce similar curves (apart from the polarity) as short cathodic pulses. Similar peaks were found with short anodic pulses for Zn and Al in the $AlCl_3$ melts. Since the differential input of the oscilloscope plug-in unit was employed in the anodic pulse, a small non-alignment in the two amplifiers of the plug-in could cause such behavior. However, a test with a resistor circuit did not show such a peak. The peak was only seen with high, anodic current pulses at short times; the long anodic pulses yielded normal appearing curves (Fig. 18g). The

calculated i_o values from the long pulses were the same as from the horizontal portion of the short pulse after the peak. Since R_s values could not be obtained for anodic pulses, to analyze the anodic long pulses values of R_s were taken from cathodic short pulses and were assumed to be equal to the anodic R_s.

At 222°C, i_o calculated from anodic and cathodic pulses were the same. At 270°C the cathodic i_o was somewhat greater than the anodic, while at 324°C the values were again the same, within experimental error.

Exchange current densities were also calculated from short pulse data. In the anodic traces, the flat portion at the end of the trace was assumed to be equal to $R_s + R_p$; R_s was taken from the cathodic pulses. As can be seen in Table 24, part c, good agreement was obtained between cathodic and anodic traces. Also, good agreement was obtained between short pulses (5 μsec) and long pulses (5 msec). The conclusion then is that charge transport is the only source of polarization and that adions are not important in this system.

The $Zn/ZnCl_2$ couple appears to be quite reversible. Dendrite formation, however, may prove to be a problem for battery application.

d) Voltammetry Results of $AlCl_3$-containing Melts

(1) $AlCl_3$-NaCl Solvent

A cyclic voltammogram run on the $AlCl_3$-NaCl solvent at 138°C with tungsten electrodes is presented in Fig. 19. The background current over a wide voltage span is less than 0.015 ma/cm^2, considerably less than in the $ZnCl_2$-solvent. Here an important contribution to the current is

TABLE 24

VOLTAMMETRY OF $Zn/ZnCl_2$ in $ZnCl_2$ SOLVENT

(#4; A = 0.060 cm^2; n = 2)

a) CURRENT STEP VOLTAMMETRY-SHORT PULSE (CATHODIC)

Temp (°C)	$i \times 10^3$ (A/cm^2)	trace	C_d ($\mu F/cm^2$)	R_s (Ω)
222	330	10	3.9	3.30
270	330	1	12.5	2.46
322	330	27	—	2.06

b) CURRENT STEP VOLTAMMETRY-LONG PULSE

Temp (°C)	Polarity	i (ma/cm^2)	trace	R_s [a] (Ω)	R_p (Ω)	i_o (A/cm^2)
222	cathodic	16	11	3.3	-3.4	0.10
222	cathodic	48	12	3.3	-3.6	0.10
223	anodic	- 8	15	-3.3	+3.1	0.11
223	anodic	-24	14	-3.3	+3.0	0.11
224	anodic	-48	13	-3.3	+3.0	0.11
224	anodic	-82	12	-3.3	+2.8	0.12
269	cathodic	8	2	2.5	-1.0	0.40
271	cathodic	24	3	2.5	-1.0	0.37
272	anodic	- 8	7	-2.5	+1.9	0.19
272	anodic	-24	6	-2.5	+1.7	0.22
272	anodic	-48	8	-2.5	+1.5	0.23
324	cathodic	41	23	2.1	-0.16	2.7
324	cathodic	82	24	2.1	-0.32	1.4
327	cathodic	243	25	2.1	-0.31	1.3
322	cathodic	330	26	2.1	-0.25	1.6
325	anodic	-41	22	-2.1	+0.22	1.9
325	anodic	-82	20	-2.1	+0.19	2.1
325	anodic	-82	21	-2.1	+0.18	1.8
325	anodic	-165	19	-2.1	+0.29	0.7

a) Anodic R_s assumed equal to cathodic R_s.

TABLE 24 (con't)

VOLTAMMETRY OF $Zn/ZnCl_2$ in $ZnCl_2$ SOLVENT				
c) EXCHANGE CURRENT DENSITIES FROM SHORT PULSES				
Temp (°C)	$i \times 10^3$ (A/cm^2)	Trace	Polarity	i_o (A/cm^2)
222	330	10	cathodic	0.11
224	330	17	anodic	0.12
270	330	1	cathodic	0.38
270	330	9	anodic	0.25
322	330	27	cathodic	2.4
325	330	18	anodic	3.0

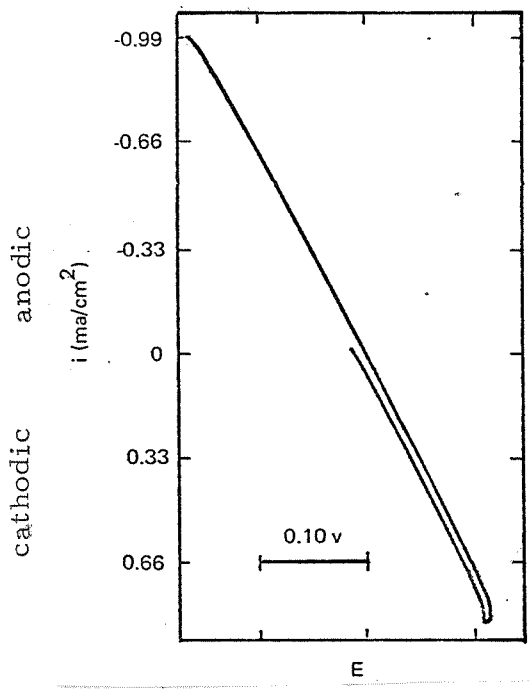

a) L.S.V.; T = 326°C; s = 92 mv/sec
E_{eq} = 0 v

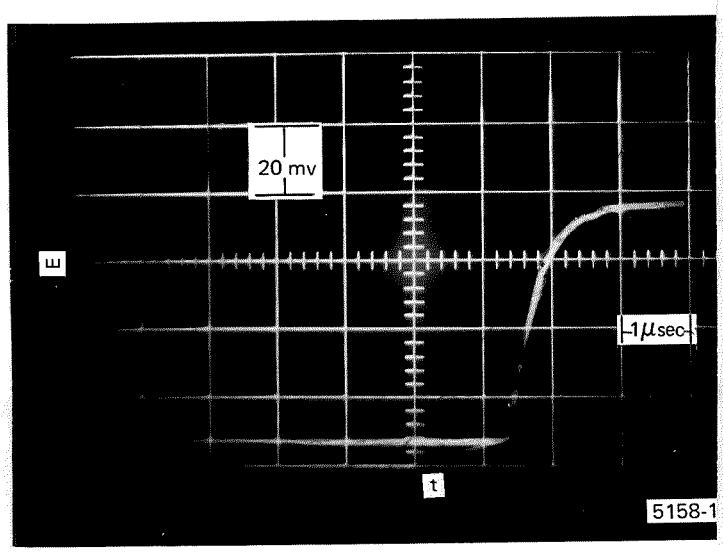

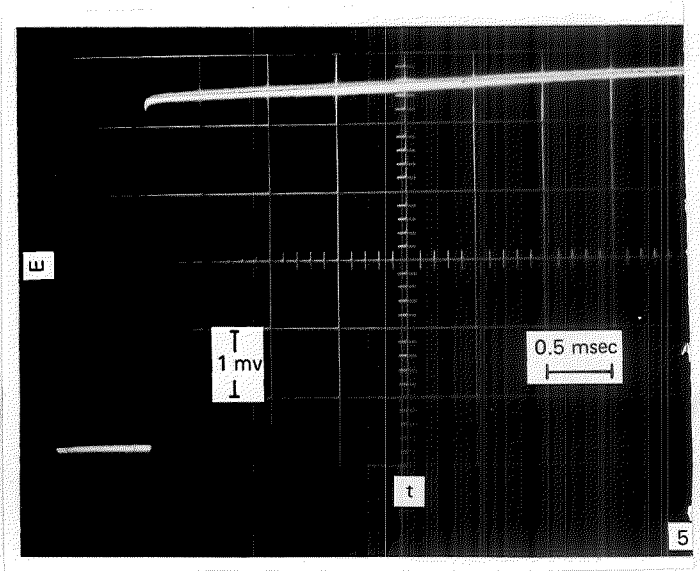

b) C.S.V.; Short Pulse
T = 269°C; i = 330 ma/cm^2
Trace #1

c) C.S.V.; Long Pulse
T = 271°C; i = 25 ma/cm^2
Trace #3

Fig. 18: Voltammetry of $Zn/ZnCl_2$ System

TOP
1129

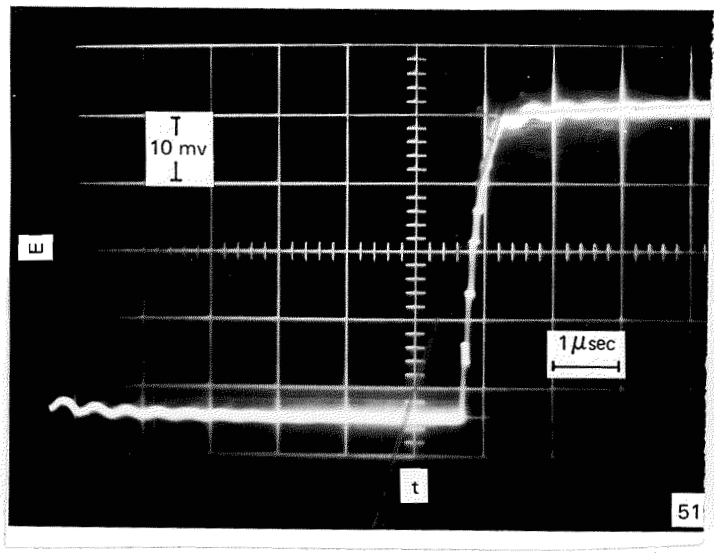

d) C.S.V.; Short Pulse
T = 322°C; i = 330 ma/cm^2
Trace #27

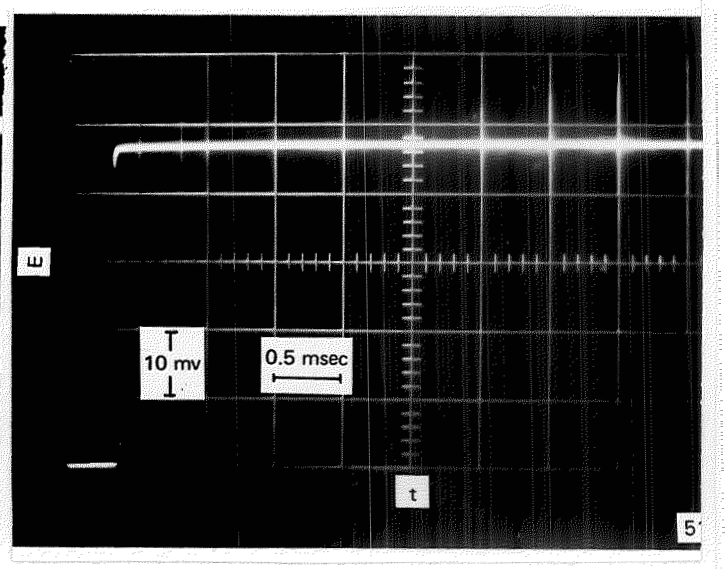

e) C.S.V.; Long Pulse
T = 322°C; i = 330 ma/cm^2
Trace #26

1129
Bottom

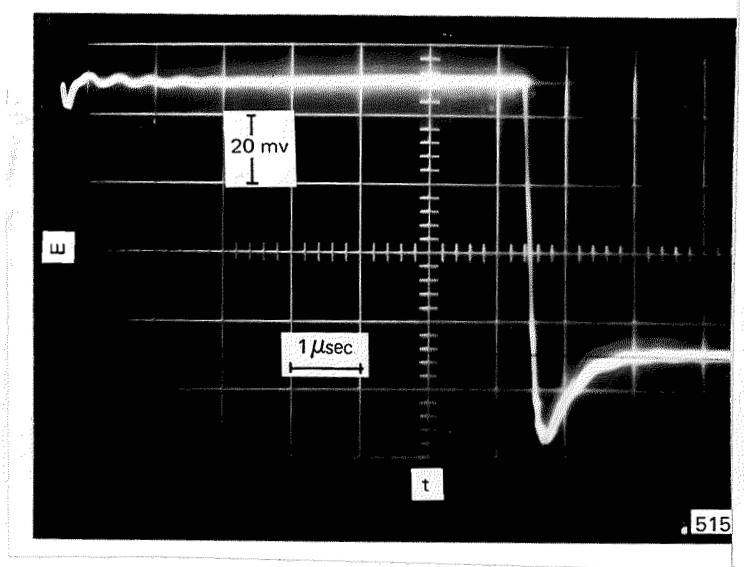

f) C.S.V.; Anodic Short Pulse
T = 270°C; i = 330 ma/cm^2
Trace #9

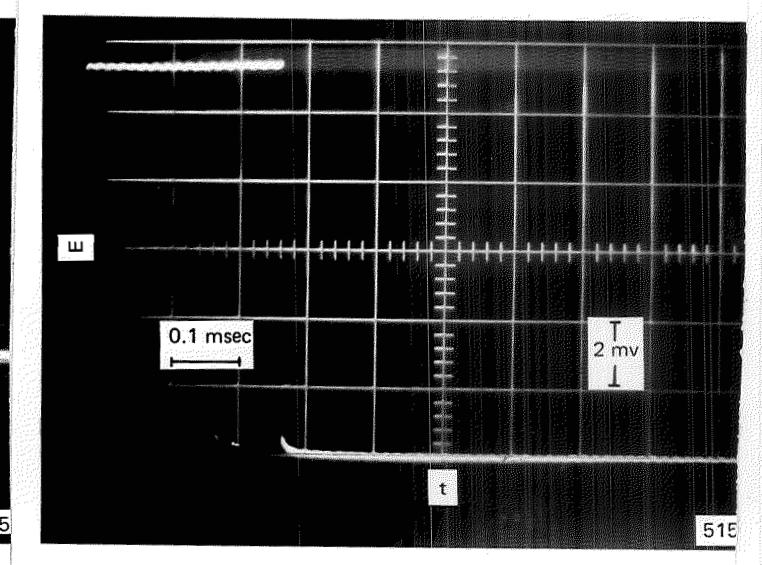

g) C.S.V.; Anodic Long Pulse
T = 325°C; i = 82 ma/cm^2
Trace #20

Fig. 18: Voltammetry of $Zn/ZnCl_2$ System

the charging of the double layer. However, there does appear to be some impurities present which reduce at about 0.8 v and 0.4 v but the peak current density from these is less than 0.17 ma/cm^2.

The working voltage range of this solvent with tungsten electrodes is about 2.35, 2.25, and 2.15 v at 135, 150 and 200°C. The cathodic and anodic limiting reactions are the reduction of Al(III) and anodization of tungsten or chlorine evolution, respectively.

(2) Ag/AgCl

The voltammetry results are shown in Table 25 and in Fig. 20. The rest potentials of this couple were 0.660, 0.646 and 0.640 v at 130, 152 and 196°C, respectively. These values may be compared with those of Anders and Plambeck,[28] who studied this couple in an $AlCl_3$ (66%)-NaCl (20%)-KCl (14%) melt. Their values, corrected to 0.1 M, were 0.614 v at 135° and 0.656 v at 150°C. The temperature coefficient of the Ag/AgCl emf in the ternary melt is much larger and of opposite sign that in $AlCl_3$-NaCl. However, it was shown in this study (Appendix I) that the freezing point of this ternary is 135° and not 70°C and so measurements made at 135°C are open to question. The waves, except at the slowest sweep rate, do not have an initial infinite slope and even at the slowest sweep depart rapidly from this infinite slope (Fig. 20a). In addition, the E_{eq}-E_p values are much larger than the theoretical ones and increase with sweep rate at all temperatures. The shift in E_p is greatest at the lowest temperature and decreases with increasing temperature. From these results the Ag/AgCl couple does not appear to be well-behaved, but it should be noted that the apparent current densities here were much higher than for other systems. The resulting polarization was not excessive for such high current densities. The i_p/m

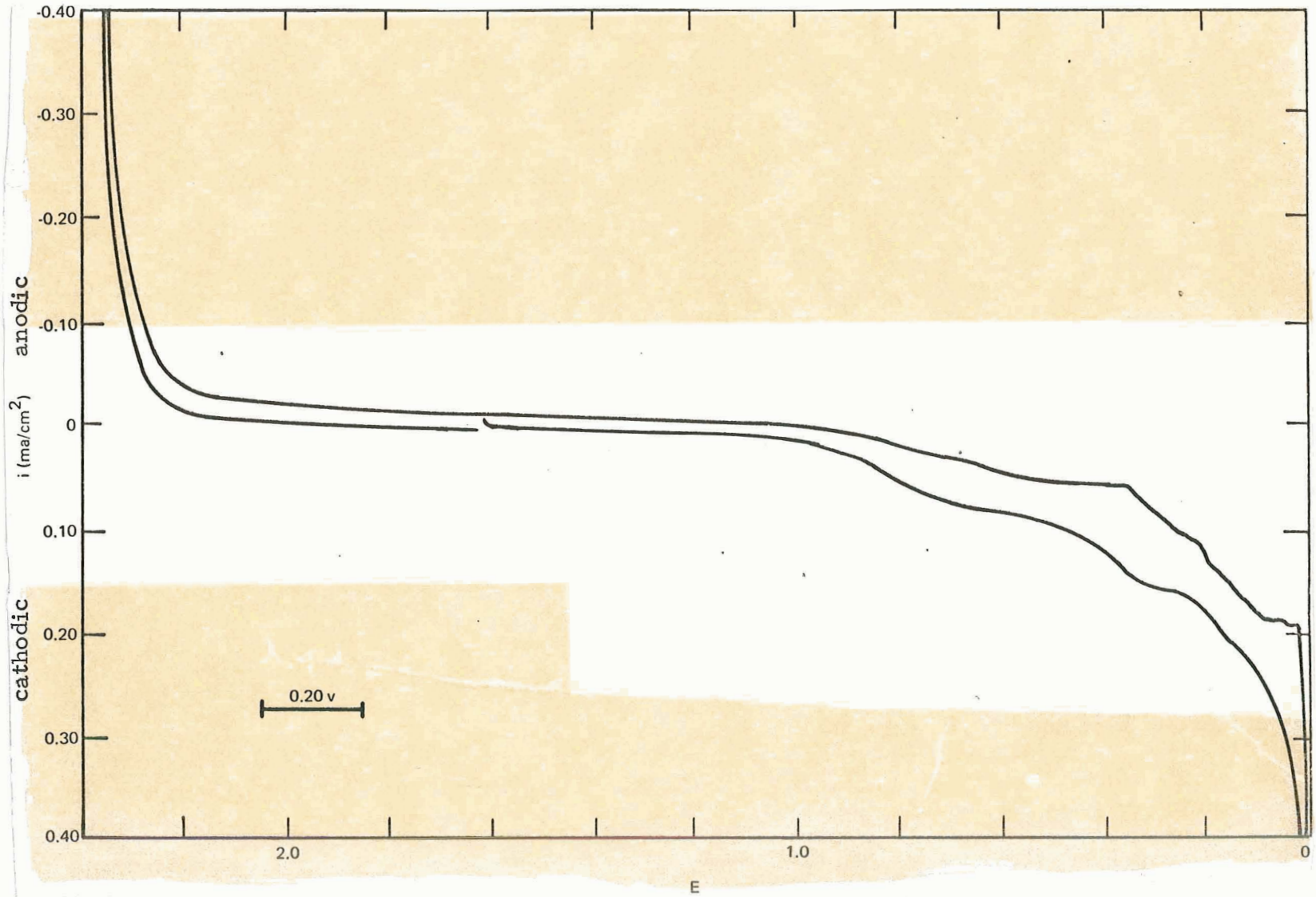

Fig. 19: Voltammetry Of $AlCl_3$-NaCl Solvent

T = 138°C; s = 23 mv/sec

W electrodes

TABLE 25

VOLTAMMETRY OF Ag/AgCl in $AlCl_3$ MELT
(No. 13; A = 0.061 cm^2; n = 1)

a) LINEAR SWEEP VOLTAMMETRY

Temp (°C)	E_{eq} (v)	$C D^{1/2} \times 10^7$ $\left(\frac{moles}{cm^2 sec^{1/2}}\right)$	s (mv/sec)	i_p/m (ma/cm^2)	$E_{eq} - E_p$ (mv)
130	0.666	19	23	76.7	45
			92	90.7	80
			207	93.0	110
			368	92.8	135
152	0.646	29	23	122	50
			92	135	75
			207	140	105
			368	142	125
196	0.640	(18)	23	74.2	55
			92	82.5	65
			207	84.7	75
			368	117	125

b) CURRENT STEP VOLTAMMETRY-SHORT PULSE

Temp (°C)	i (ma/cm^2)	trace	C_d ($\mu F/cm^2$)	R_s (Ω)
129	330	1	35	0.65
128	330	6	-	0.38
151	330	7	52	1.53
150	330	12	-	1.42
195	330	13	-	1.71
194	330	18	-	2.01
194	330	19	-	1.97

TABLE 25 (cont'd)

VOLTAMMETRY OF Ag/AgCl in $AlCl_3$ MELT

c) CURRENT STEP VOLTAMMETRY-LONG PULSE

Temp (°C)	i (ma/cm^2)	trace	R_s (Ω)	R_p (Ω)	$\frac{\Delta\eta_{0.1\ msec}}{iA}$ (Ω)	$CD^{1/2}$ x 10^7	D x 10^6 (cm^2/sec)	$\eta_{5\ msec}$ (mv)	$\frac{\eta_{5\ msec}}{iA}$ (Ω)	i_o (A/cm^2)
129	16	2	0.5	-2.8	+0.4	15.4	240	-3.1	-3.1	0.20
128	33	3	0.5	-2.6	+0.3	9.8	96	-6.0	-3.0	0.21
128	48	4	0.5	-2.3	+0.1	7.5	56	-8.7	-2.9	0.24
128	48	5	0.5	-2.0	+0.2	8.9	81	-9.0	-3.0	0.22
151	16	8	1.48	-0.74	+0.3	37.3	1400	-0.9	-0.9	0.77
150	33	9	1.48	-0.49	+0.3	14.7	215	-1.6	-0.8	1.13
150	48	10	1.48	-0.45	+0.1	14.3	205	-2.3	-0.8	1.29
150	66	11	1.48	-0.45	+0.2	19.2	370	-2.8	-0.7	1.29
195	16	14	1.90	-1.24	+0.3	25.0	625	-1.4	-1.4	0.51
194	48	15	1.90	-0.29	+0.1	18.8	350	-1.7	-0.6	2.16
194	82	16	1.90	-0.34	+0.1	29.0	850	-2.6	-0.5	1.87
194	165	17	1.90	-0.33	+0.1	23.6	560	-2.5	-0.3	1.95

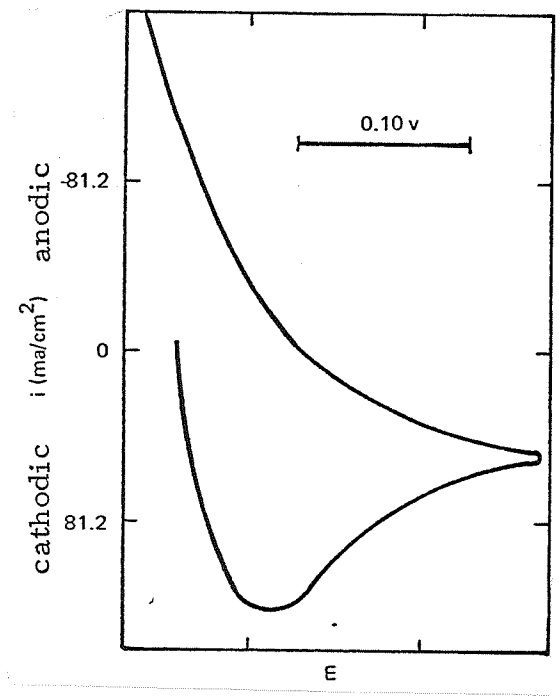

a) L.S.V.; T = 152°C; s = 23 mv/sec
E_{eq} = 0.646 v

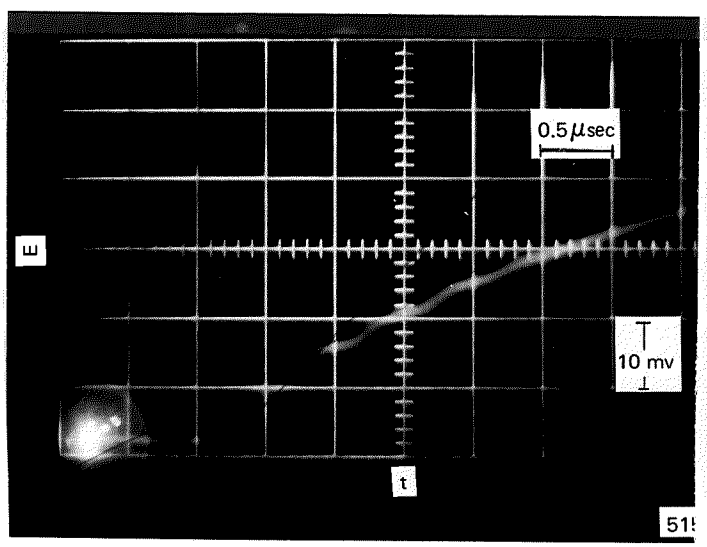

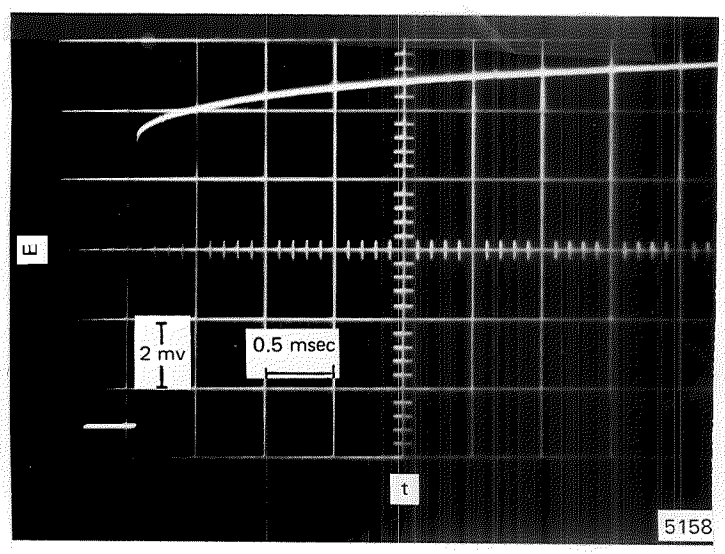

134

b) C.S.V.; Short Pulse
T = 129°C; i = 330 ma/cm^2
Trace #1

c) C.S.V.; Long Pulse
T = 128°C; i = 50 ma/cm^2
Trace #5

Fig. 20: Voltammetry of Ag/AgCl in $AlCl_3$ Melts

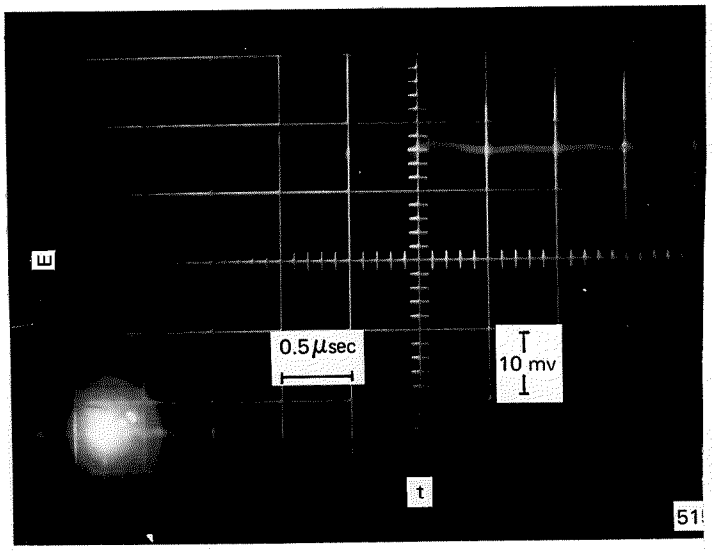

d) C.S.V.; Short Pulse
T = 194°C; i = 330 ma/cm^2

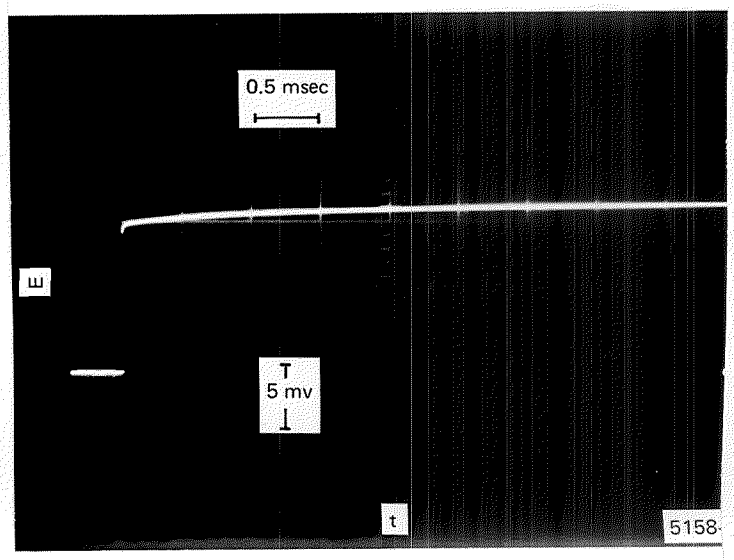

e) C.S.V.; Long Pulse
T = 194°C; i = 75 ma/cm^2

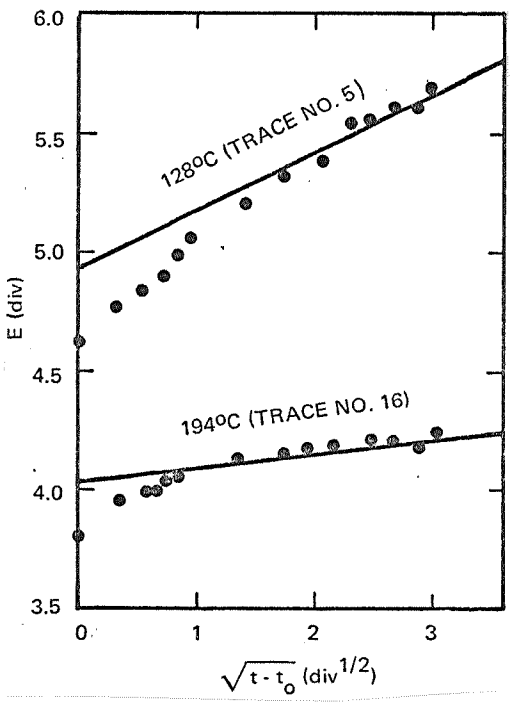

f) E vs $t^{1/2}$ Plot

Fig. 20: Voltammetry of Ag/AgCl in $AlCl_3$ Melts

values were, in general, relatively insensitive to sweep rate. The $CD^{1/2}$ values were considerably higher than one would expect with normal diffusion coefficients. Little dendrite formation and no electrode attack were evident.

Two typical current-step voltammograms are shown in Fig. 20b-e. The first two are at the lowest temperature (129°C) while the last two are at the highest temperature. Almost all the short pulses were of the pure resistor type. Due to the predominance of resistor-like curves not many values of C_d could be calculated. However, the two C_d values that were calculated were found to be considerably larger than usual. The $CD^{1/2}$ values were in good agreement with those obtained by L. S. V. In both cases they were very large, in fact the largest encountered in this study. These values lead to very high values of the diffusion coefficient. All the E vs $t^{1/2}$ type curves exhibited negative deviations from linearity. However, the deviation is not very large since $\Delta\eta_{0.1\,msec}/iA$ did not exceed 0.4 Ω. The effect appears large in the figures because the large values of $CD^{1/2}$ permitted the ordinant to be expanded with the result that the deviation is accentuated. The resistance corresponding to the total overpotential at 5 msec was small. The exchange current densities were about 0.2 A/cm^2 at 130°C and about 2 A/cm^2 at 195°C.

Based on the C. S. V. results the Ag/AgCl couple has high exchange currents and is thus quite reversible, in contrast to the L. S. V. results which indicate in a qualitative manner that this couple does polarize. However, since the C. S. V. method is more quantitative, it will be assumed that the C. S. V. results are more correct with respect to reversibility.

On this basis the Ag/AgCl electrode appears to offer considerable promise, especially in view of the fact that little dendrite formation

was evident. The high solubility suggested in Table 13 precludes much concentration polarization. Thus this couple has potential use in a battery utilizing the $AlCl_3$-containing solvent.

(3) Cu/CuCl

The voltammetry results are shown in Table 26 and in Fig. 21. The open circuit potentials were 0.639, 0.613 and 0.595 v at 122, 146 and 190°C. At 135° an interpolated emf of 0.626 v may be compared to a reported value,[28] corrected to 0.1 M of 0.608 v in a ternary $AlCl_3$ melt. As with the silver system the potential in the binary melt is higher at 135°C. All the linear sweep voltammograms at 122 and 146° show an inflection in the wave shortly after onset of current (Fig. 21 a) similar to the $Ni/NiCl_2$ in $ZnCl_2$ system. At 190°, however, this inflection has disappeared (Fig. 21 b). In spite of this behavior the E_p values, though large at the lowest temperature, are relatively constant with sweep rate at the lowest two temperatures but vary strongly at the highest temperature. The i_p/m values were constant at the lower temperatures but increased with sweep rate at 190°. These results imply that the Cu/CuCl couple becomes a poorer one as the temperature increases. The i_p and $CD^{1/2}$ data show an abrupt increase at 190° with the latter value being similar to those for Ag/AgCl. This may indicate that not all the CuCl had dissolved at the lower temperatures. No dendrites were evident on the electrodes.

Two sets of typical current-step voltammograms are shown in Fig. 21 c-f. The first pair (c-d) were taken at the lowest temperature (122°C) while the last pair were taken at the highest temperature (186°C). The C_d values were nearer to what one would call normal, especially at the two higher temperatures. The $CD^{1/2}$ values obtained by C.S.V. were substantially different from those obtained by L.S.V. In both measurements there

TABLE 26

VOLTAMMETRY OF Cu/CuCl in $AlCl_3$ MELT
(No. 9 ; A = 0.061 cm^2; n = 1)

a) LINEAR SWEEP VOLTAMMETRY

Temp. (°C)	E_{eq} (v)	$CD^{1/2} \times 10^7$ $\left(\frac{moles}{cm^2 sec^{1/2}}\right)$	s (mv/sec)	i_p/m (ma/cm^2)	$E_{eq} - E_p$ (mv)
122	0.639	2.7	23	12.6	70
			92	12.7	70
			207	13.1	72
			368	13.1	79
146	0.613	3.3	23	16.6	63
			92	15.6	68
			207	15.3	68
			368	15.4	83
190	0.595	(27)	23	88.8	50
			92	115	70
			207	125	110
			368	133	145

b) CURRENT STEP VOLTAMMETRY-SHORT PULSE

Temp (°C)	i (ma/cm^2)	trace	C_d ($\mu F/cm^2$)	R_s (Ω)
122	330	1	14	2.05
122	330	2	12	2.15
117	330	7	10	2.36
146	330	8	26	1.90
142	330	13	24	0.91
188	330	14	29	1.05
186	330	18	37	0.60
186	330	19	41	0.68

TABLE 26 (cont'd)

VOLTAMMETRY OF Cu/CuCl in $AlCl_3$ MELT

c) CURRENT STEP VOLTAMMETRY-LONG PULSE

Temp (°C)	i (ma/cm^2)	trace	R_s (Ω)	R_p (Ω)	$\frac{\Delta\eta_{0.1\ msec}}{iA}$ (Ω)	$CD^{1/2}$ x 10^7	D x 10^6 (cm^2/sec)	$\eta_{5\ msec}$ (mv)	$\frac{\eta_{5\ msec}}{iA}$ (Ω)	i_o (A/cm^2)
118	8	5	2.2	+2.1	0	0.19	0.04	-10.1	-20.1	ws -.37
122	16	3	2.2	-0.8	0	0.34	0.12	-13.4	-13.4	0.66
122	16	4	2.2	-0.4	-	0.29	0.08	-a	-a	1.18
118	24	6	2.2	+0.7	-	0.18	0.03	-a	-a	ws -.77
143	8	11	1.4	+4.8	-1.2	0.15	0.02	-12.7	-25.4	ws -.12
143	8	12	1.4	+4.0	-2.4	0.16	0.03	-12.0	-23.9	ws -.14
143	16	10	1.4	-3.7	+4.5	0.26	0.07	-21.0	-21.0	0.15
146	24	9	1.4	-9.1	-0.4	0.52	0.27	-25.8	-17.1	0.06
186	16	15	0.8	-1.7	+0.6	11.9	140	-2.1	- 2.1	0.36
186	33	16	0.8	-1.3	+0.2	7.8	61	-3.9	- 1.9	0.48
186	49	17	0.8	-1.2	+0.2	8.5	72	-5.4	- 1.8	0.50

a) Pulse lasted 2 msec instead of 5 msec.

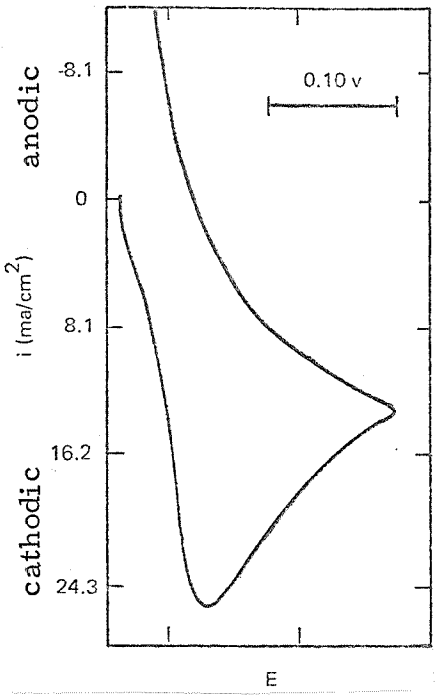

a) L.S.V.; T = 122°C; s = 92 mv/sec
E_{eq} = 0.639 v

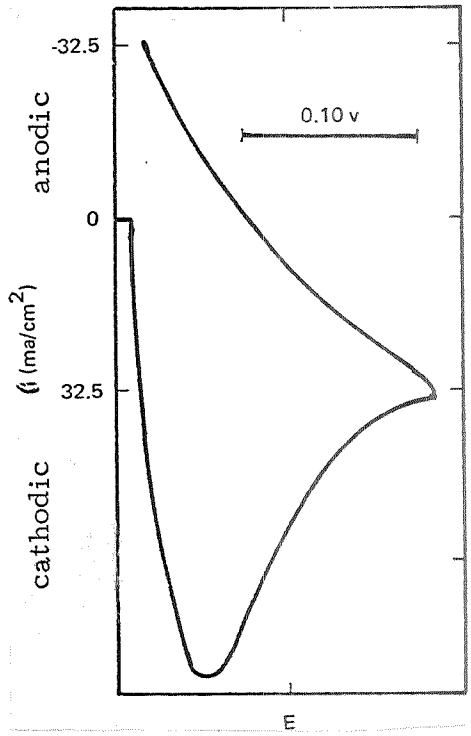

b) L.S.V.; T = 190°C; s = 23 mv/sec
E_{eq} = 0.595 v

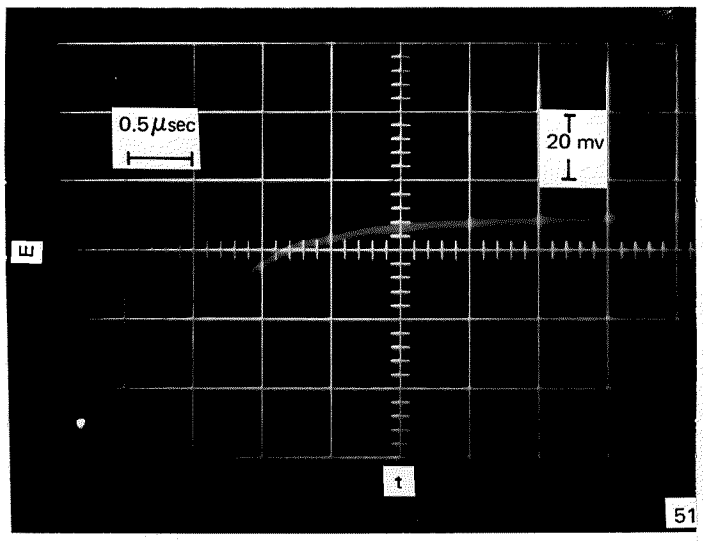

c) C.S.V.; Short Pulse
T = 122°C; i = 330 ma/cm^2
Trace #1

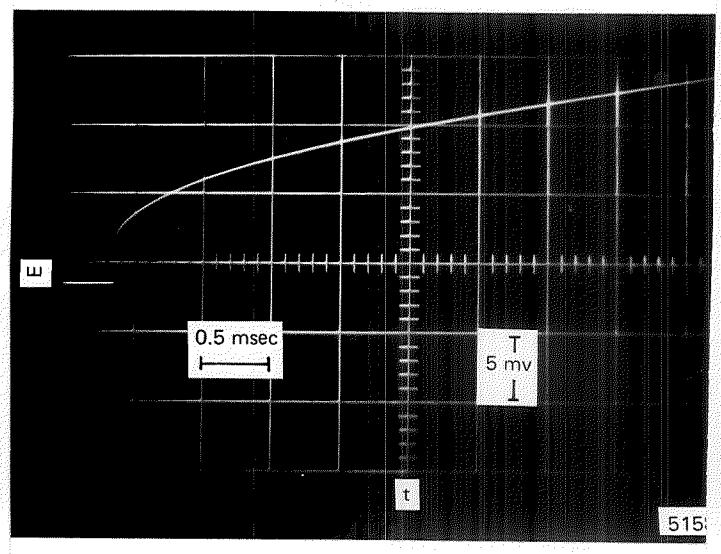

d) C.S.V.; Long Pulse
T = 122°C; i = 17 ma/cm^2
Trace #3

Fig. 21: Voltammetry of Cu/CuCl in $AlCl_3$ Melts

140

141

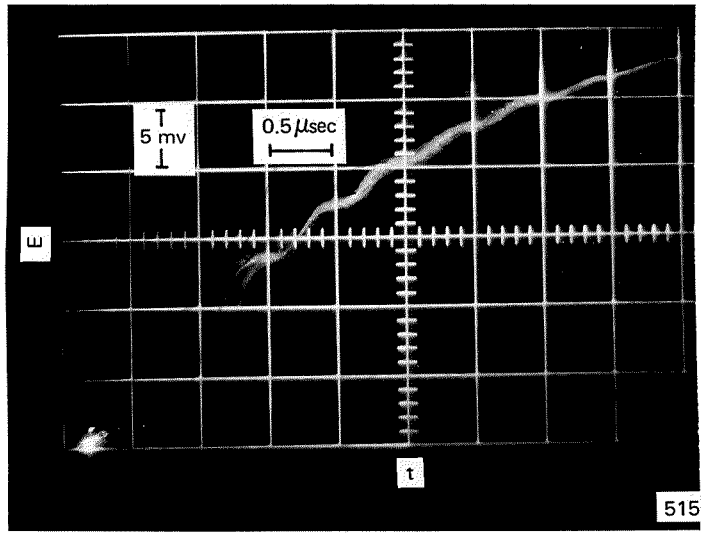

e) C.S.V.; Short Pulse
T = 186°C; i = 330 ma/cm^2
Trace #19

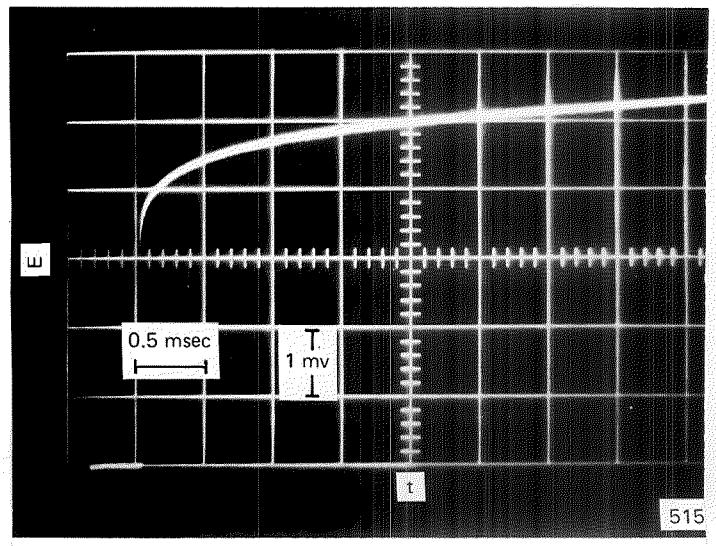

f) C.S.V.; Long Pulse
T = 186°C; i = 33 ma/cm^2
Trace #16

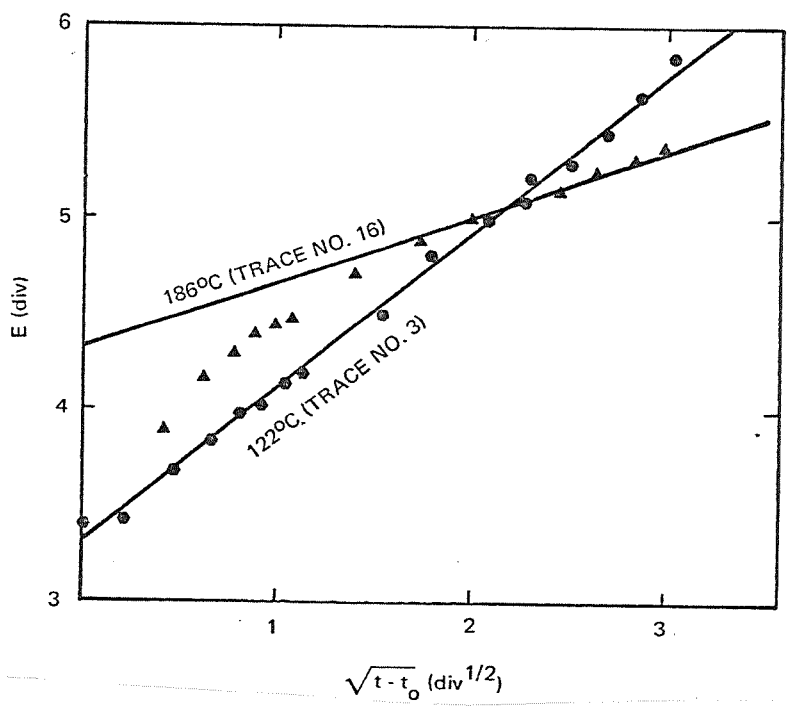

g) E vs $t^{1/2}$ Plot

Fig. 21: Voltammetry of Cu/CuCl in $AlCl_3$ Melts

appeared to be a marked increase in $CD^{1/2}$ at the highest temperature. In contrast to the $ZnCl_2$-solvent case no apparent dependency of D on i was obvious. While it appeared as if there were considerable negative deviation (e.g., trace 16, Fig. g), again this is a result of the expanded voltage scale because of the large value of $CD^{1/2}$, just as in the case of Ag/AgCl in the $AlCl_3$-containing solvent. Many of the traces at the two lowest temperatures had values over 5 mv after 5 msec, indicating that the applied current was too high. In contrast to the case of Cu/CuCl in the $ZnCl_2$-containing solvent, where no negative exchange currents were obtained, four such values were obtained in this system. The scatter in i_o for the two lowest temperatures was considerably greater than usual.

On the basis of the C.S.V. tests, Cu/CuCl is a reversible couple and, in agreement with the L.S.V. results, the reversibility appears to be the best at the lowest temperature. The high solubility of CuCl in the $AlCl_3$ melt plus the lack of dendrites suggest that this couple offers promise for batteries utilizing the $AlCl_3$-containing solvent.

(4) <u>Ni/$NiCl_2$</u>

The voltammetry results are shown in Table 27 and in Fig. 22. The potentials for this system ranged from 0.840 v at 129° to 0.852 v at 197°C. These values may be compared to 0.80 v arrived at from a decomposition potential measurement[29] for a one mole % solution in $AlCl_3$ (66%)-NaCl (20%)-KCl (14%) at 156°. The voltammetry waves start with infinite slope but quickly show a pronounced shoulder (Fig. 22a) at all temperatures and sweep rates. It appears that the electrode reaction slows up drastically and then continues after some overvoltage has been reached. This shoulder is larger than that for nickel in the $ZnCl_2$ melt and similarly, as in the latter

TABLE 27

VOLTAMMETRY OF $Ni/NiCl_2$ in $AlCl_3$ MELT
(No. 7; A = 0.061 cm^2; n = 2)

a) LINEAR SWEEP VOLTAMMETRY

Temp (°C)	E_{eq} (v)	$CD^{1/2} \times 10^7$ $\left(\frac{moles}{cm^2\ sec^{1/2}}\right)$	s (mv/sec)	i_p/m (ma/cm^2)	$E_{eq} - E_p$ (mv)
129	0.840	0.45	23	3.5	90
			92	3.1	100
			207	2.8	105
			368	2.8	105
150	0.847	0.65	23	4.2	95
			92	4.4	95
			207	4.3	100
			368	4.4	100
197	0.852	1.4	23	8.9	70
			92	9.5	70
			207	9.8	78
			368	8.5	100

b) CURRENT STEP VOLTAMMETRY-SHORT PULSE

Temp (°C)	i (ma/cm^2)	trace	C_d ($\mu F/cm^2$)	R_s (Ω)
128	330	2	17	2.24
147	330	5	18	2.33
147	330	6	24	2.20
193	330	10	-	1.98
197	330	14	-	2.01

TABLE 27 (cont'd)

VOLTAMMETRY OF $Ni/NiCl_2$ in $AlCl_3$ MELT

c) CURRENT STEP VOLTAMMETRY-LONG PULSE

Temp (°C)	i (ma/cm^2)	trace	R_s (Ω)	R_p (Ω)	$\frac{\Delta\eta_{0.1\,msec}}{iA}$ (Ω)	$CD^{1/2}$ x 10^7	D x 10^6 (cm^2/sec)	$\eta_{5\,msec}$ (mv)	$\frac{\eta_{5\,msec}}{iA}$ (Ω)	i_o (A/cm^2)
128	16	3	2.3	+0.4	-0.9	0.07	0.005	-14.3	-14.3	ws -.62
128	16	4a	2.3	+1.0	-3.0	0.06	0.004	-15.1	-15.1	ws -.08
128	16	4b	2.3	+1.6	0	0.02	0.0004	- 4.6	- 4.6	ws -.17*
193	4	13	2.0	+1.1	0	0.05	0.003	- 5.6	-22.3	ws -.11
196	8	12	2.0	+0.2	-1.4	0.05	0.003	-11.7	-23.4	ws -.07
197	16	11	2.0	+4.9	-2.6	0.05	0.003	-32.9	-23.1	ws -.07

* Approximate equation for i_o yielded -0.12 A/cm^2

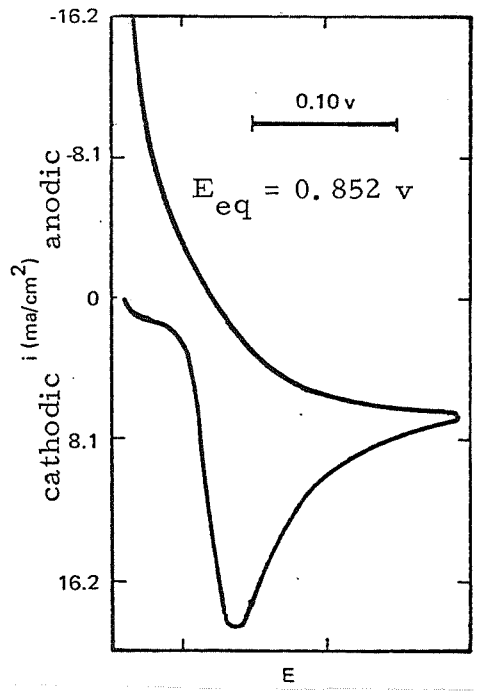

a) L.S.V.; T = 197°C; s = 92 mv/sec

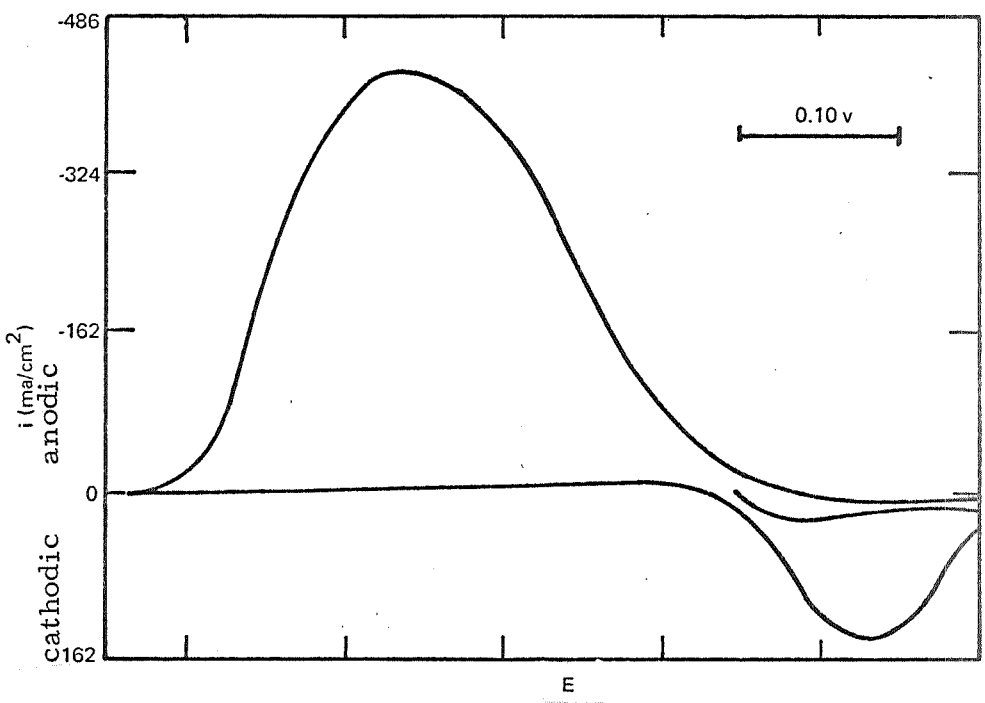

b)* L.S.V.; T = 198°C; s = 23 mv/sec

E_{eq} = 0.852 v

*Film Formation was observed during the anodic sweep

Fig. 22. Voltammetry of $Ni/NiCl_2$ in $AlCl_3$ Melts

146 TOP

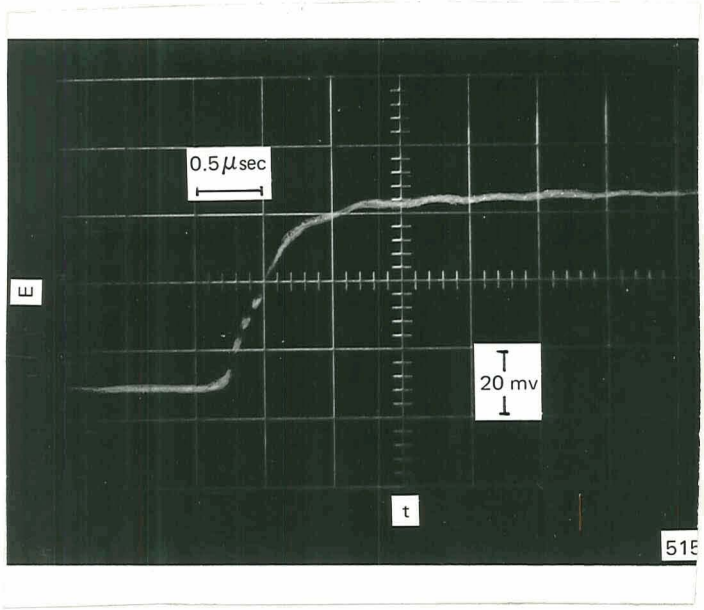

c) C.S.V.; Short Pulse
T = 128°C; i = 330 ma/cm^2
Trace #2

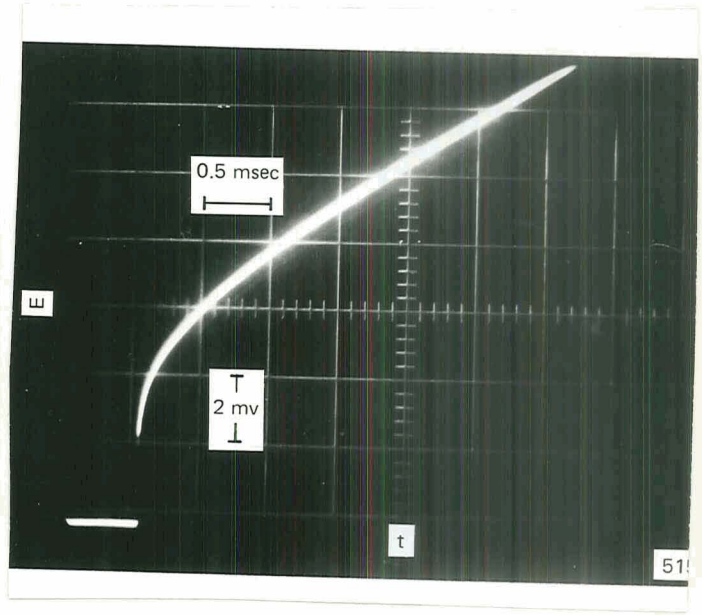

d) C.S.V.; Long Pulse
T = 128°C; i = 16 ma/cm^2
Trace #3

146 Bottom

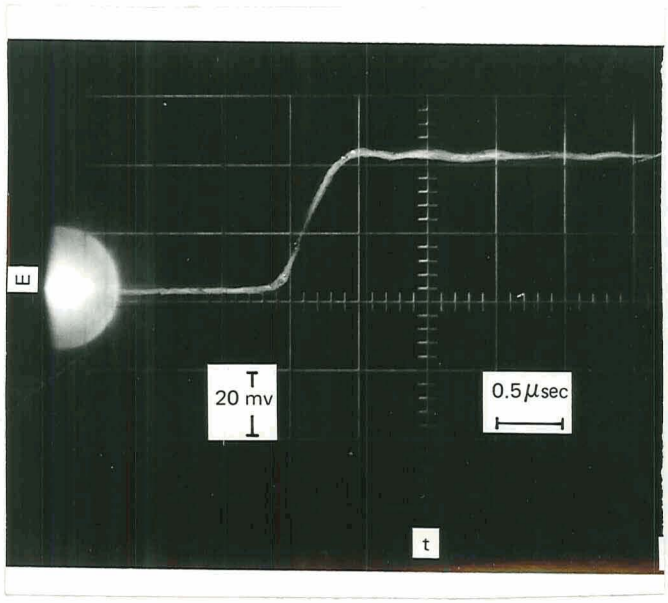

e) C.S.V.; Short Pulse
T = 193°C; i = 330 ma/cm^2
Trace #10

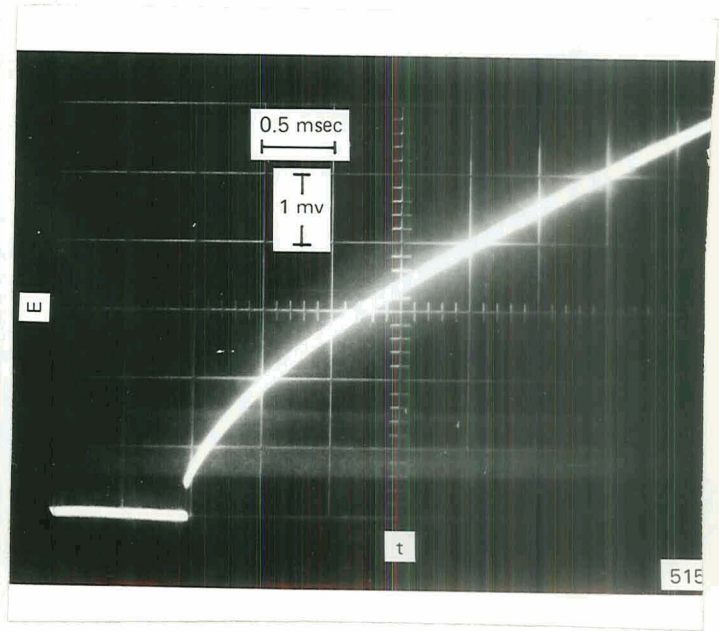

f) C.S.V.; Long Pulse
T = 193°C; i = 4.1 ma/cm^2
Trace #13

Fig. 22: Voltammetry of $Ni/NiCl_2$ in $AlCl_3$ Melts

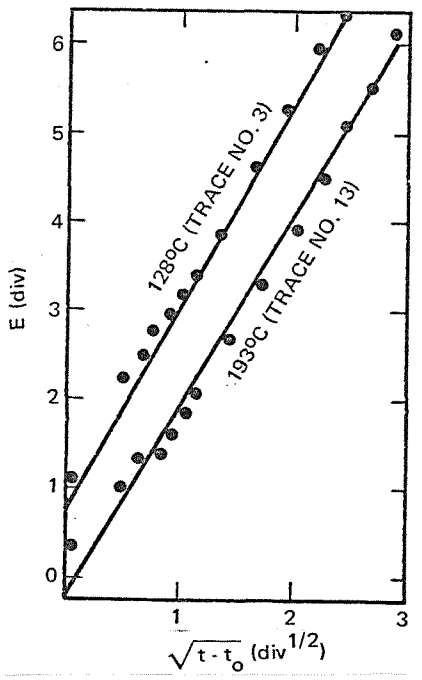

g) E vs $t^{1/2}$ Plot

Fig. 22: Voltammetry of $Ni/NiCl_2$ in $AlCl_3$ Melts

system, increases with increasing temperature. The $E_{eq} - E_p$ values are quite large for a 2-electron reaction but are reasonably constant except for the fastest sweep at 197° and the slowest sweep at 129°. The i_p/m results are also constant except for the same two sweeps. The i_p/m and the $CD^{1/2}$ values show that the solubility of $NiCl_2$ is less than 0.1 M but is much higher than in the $ZnCl_2$ melt. If an anodic sweep is made, a broad non-diffusion limited wave is formed indicating film formation. This film, presumably $NiCl_2$, can be reduced but the area under the cathodic wave is much less than that under the anodic wave (Fig. 22b). Thus it appears that most of the $NiCl_2$ film has been lost before it could be reduced. The voltammograms are very reproducible indicating that no buildup of film occurs on the electrode.

Typical current-step voltammograms are shown in Figs. c-g. Again the C_d values, when they could be calculated, were close to 20 $\mu F/cm^2$. Noise problems were severe on the day that this system was tested. The long pulse traces at 143°C could not be analyzed due to the noise.

Just as in the case with the $ZnCl_2$-containing melts, exchange current densities with the wrong sign were obtained and the $C D^{1/2}$ values calculated from C.S.V. data were considerably smaller than those from L.S.V. data. However, in both methods the $C D^{1/2}$ values in this system were, in general, considerably greater than for the $Ni/NiCl_2$ couple in the $ZnCl_2$ melt. Thus it is concluded that the solubility of $NiCl_2$ in the $AlCl_3$ solvent is considerably greater than in the $ZnCl_2$ solvent, although it appears that the solubility is still less than 0.1 M. The greater solubility of $NiCl_2$ in the $AlCl_3$ melts probably accounts for the considerably lower value of $\eta_{5\,msec}/I$. Again, just as in the $ZnCl_2$ case, no negative deviations were noted; however, the positive deviation was much less in the $AlCl_3$ case. The use of the exact equation 17 instead of 13 for calculating i_o was necessary only in trace 4b.

Since most of the $NiCl_2$ film is lost before it can be reduced, this precludes the use of $Ni/NiCl_2(s)$ electrodes for batteries.

(5) $\underline{Bi/BiCl_3}$

The voltammetry results are shown in Table 28 and in Fig. 23. Values of E_{eq} were 0.718 v at 126° and 0.695 v at 152°C. No measurements could be made at 200° due to a very high resistance arising in the cell. Voltages of 1.10 and 0.51 were found from a decomposition potential measurement[29] at 156° in a ternary $AlCl_3$ melt. The cathodic sweeps show a single peak but do not begin with a vertical rise (Fig. 23a). The $E_{eq}-E_p$ values at both temperatures vary with sweep rate and are large for a 3-electron reduction. In addition, the i_p/m data show a general decrease with increasing sweep rate at 152°. When an anodic sweep was made from 0 v, three anodic

peaks were observed. However, when an anodic sweep was made from the rest potential two peaks occurred and reversal after the second peak yielded two reduction waves (Fig. 23 b). If the reversal was made after the first anodic peak but before the second, only one cathodic wave appeared (Fig. 23c). This wave corresponded to the second cathodic wave (the more cathodic one) and also to the wave found when a cathodic sweep was begun from the rest potential. These results suggest that the species present in solution in equilibrium with bismuth metal is Bi(I) and not Bi(III). The presence of Bi(I) in $AlCl_3$-NaCl has been established,[30] the acid melt stabilizing the lower-valent species. Thus the first anodic peak may be ascribed to Bi(0) $\longrightarrow$ Bi(I) (which forms a film) and the second peak to Bi(I) $\longrightarrow$ Bi(III). On reversal the first reduction wave is the formation of Bi(I) from Bi(III) and the second the reduction of the monovalent species to the metal. Another possibility is that several different monovalent species (Bi^+, Bi_5^{+3}, Bi_8^{+2})[30,31] and not Bi(III) are involved. The small areas under the reduction waves as compared to the anodic waves are probably due to the loss of Bi(III) by reaction with the metal electrode. The formation of a film on the electrode is corroborated by the relatively large resistance (about 20 Ω) that increased with temperature. Other evidence that chemical reaction had occurred in this system is that the counter electrode, which had been equilibrated with the melt before the indicator electrode was immersed, showed attack; in addition, after the melt was dissolved in water a greyish, metallic-looking sludge remained. This sludge was probably formed from the decomposition of one or more lower-valent bismuth compounds.[32,33] The two decomposition voltages for Bi(III) found by Verdieck and Yntema[29] were also attributed by them to formation of a lower-valent species. It should be noted that since these investigators[29] used inert electrodes, Bi(III) was present in their solution initially. No evidence for a lower-valent Bi

TABLE 28

VOLTAMMETRY OF $Bi/BiCl_3$ in $AlCl_3$ SOLVENT

(No. 12; A = 0.049 cm^2; n = 3)

a) LINEAR SWEEP VOLTAMMETRY

Temp (°C)	E_{eq} (v)	$CD^{1/2} \times 10^7$ $\left(\frac{moles}{cm^2\ sec^{1/2}}\right)$	s (mv/sec)	i_p/m (ma/cm^2)	$E_{eq} - E_p$ (mv)
126	0.718	2.9	23	15.6	63
			92	15.7	88
			207	13.9	103
			368	14.0	123
152	0.695	(2.2)	23	12.6	50
			92	10.8	70
			207	10.1	85
			368	9.3	100

b) CURRENT STEP VOLTAMMETRY-SHORT PULSE

Temp (°C)	i (ma/cm^2)	trace	C_d ($\mu F/cm^2$)	R_s (Ω)
124	400	1	2.7	10.3
119	400	6	1.5	10.6
151	200	7	1.1	18.3
151	200	11	1.2	18.5

TABLE 28 (cont'd)

VOLTAMMETRY OF $Bi/BiCl_3$ in $AlCl_3$ SOLVENT

c) CURRENT STEP VOLTAMMETRY-LONG PULSE

Temp (C)	i (ma/cm^2)	trace	R_s (Ω)	R_p (Ω)	$\frac{\Delta\eta_{0.1\,msec}}{iA}$ (Ω)	$CD^{1/2} \times 10^7$	$D \times 10^6$ (cm^2/sec)	$\eta_{5\,msec}$ (mv)	$\frac{\eta_{5\,msec}}{iA}$ (Ω)	i_o (A/cm^2)
120	5.0	4	10.5	28.0	+10.6	0.08	0.006	- 8.0	-32.0	0.0078
124	10.0	2	10.5	26.1	+ 7.4	0.08	0.006	-16.7	-33.4	0.0083
120	10.0	5	10.5	28.5	+10.4	0.09	0.008	-17.5	-35.9	0.0077
124	20.0	3	10.5	23.0	+ 8.0	0.13	0.017	-27.6	-27.6	0.0095
151	2.0	9	18.4	18.8	+ 3.6	0.19	0.036	- 2.2	-22.0	0.012
151	5.0	8	18.4	15.5	+ 2.4	0.22	0.049	- 4.9	-18.2	0.015
151	10.0	10	18.4	20.5	+ 2.6	0.67	0.45	-10.6	-21.2	0.012

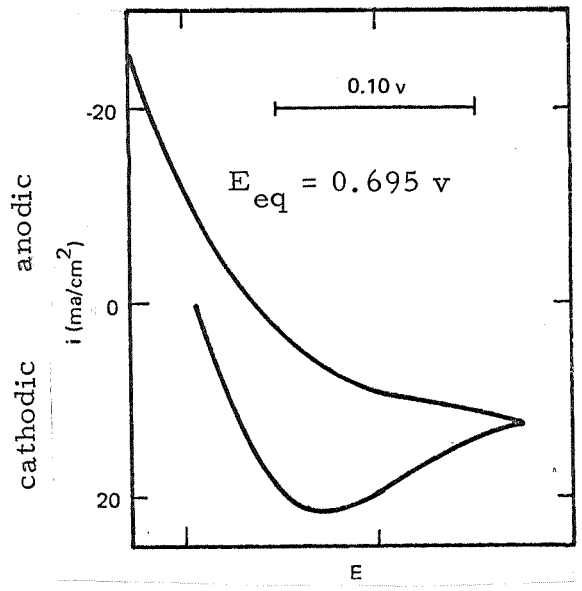

a) L.S.V.; T = 152°C; s = 92 mv/sec

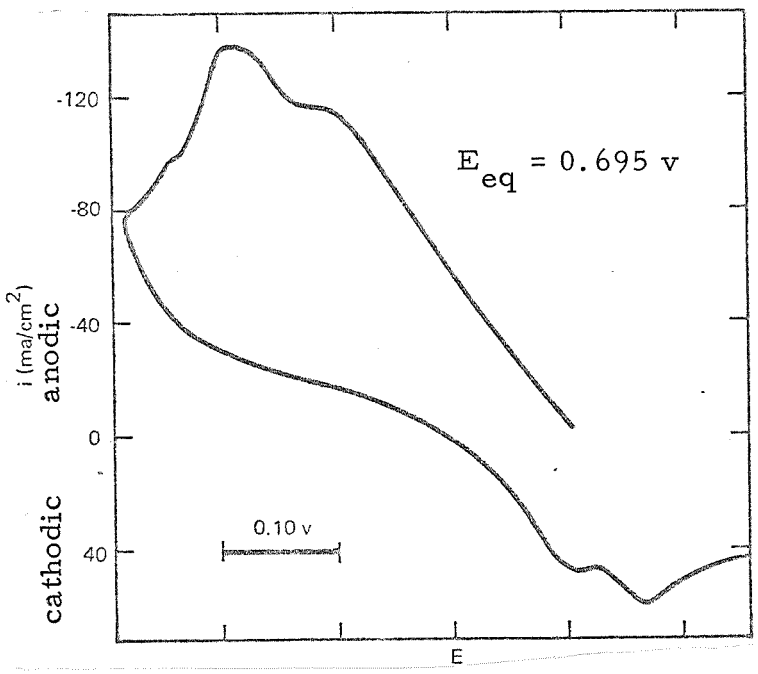

b)* L.S.V.; T = 152°C; s = 23 mv/sec

*Film formation was observed during the anodic sweep

Fig. 23. Voltammetry of $Bi/BiCl_3$ in $AlCl_3$ Melts

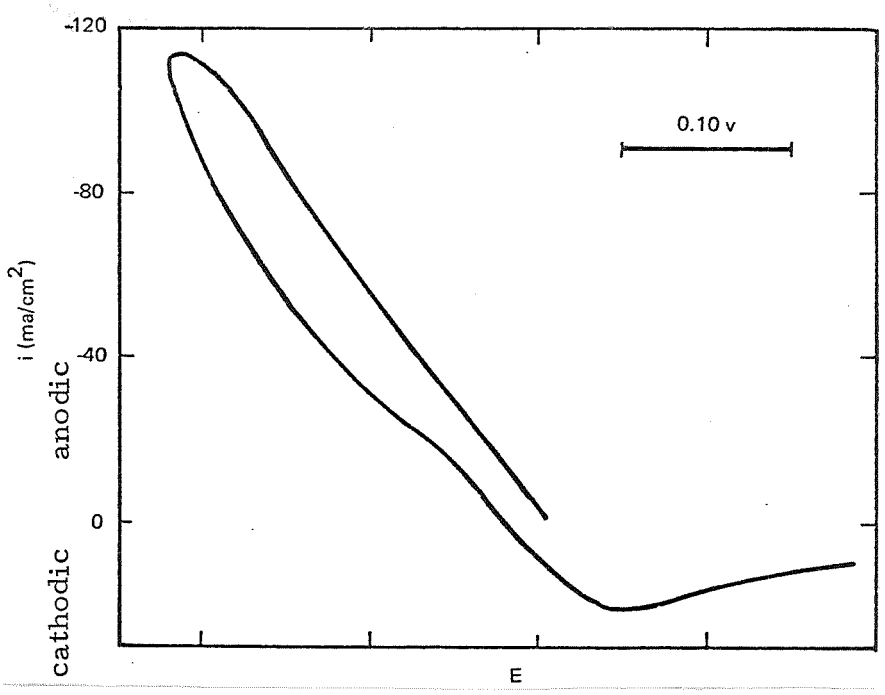

c) L.S.V.; T = 152°C; s = 23 mv/sec
E_{eq} = 0.695 v

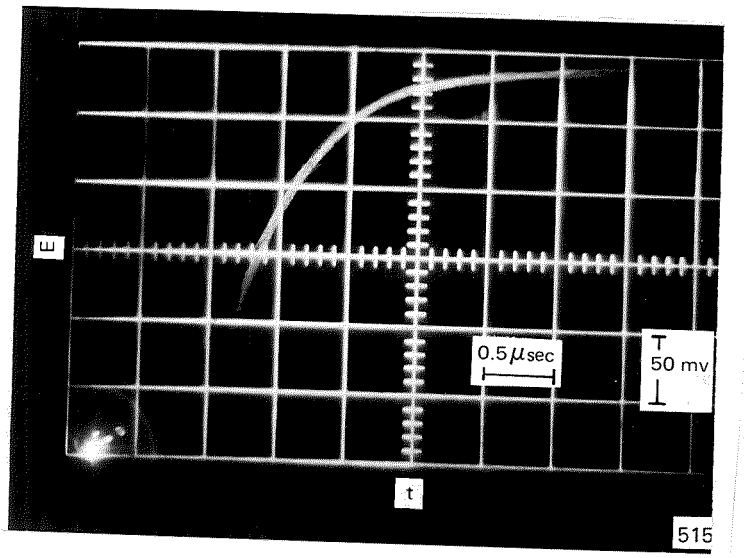

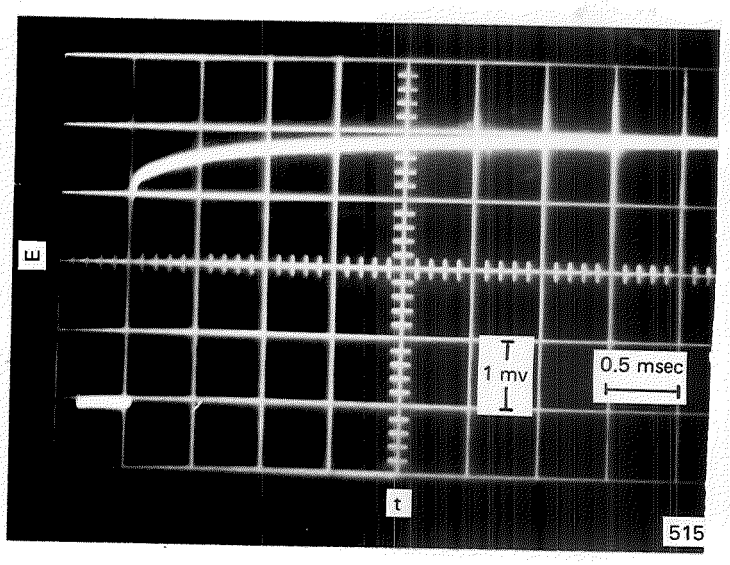

d) C.S.V.; Short Pulse
T = 151°C; i = 115 ma/cm^2
Trace #7

e) C.S.V.; Long Pulse
T = 151°C; i = 1.7 ma/cm^2
Trace #9

Fig. 23: Voltammetry of $Bi/BiCl_3$ in $AlCl_3$ Melts

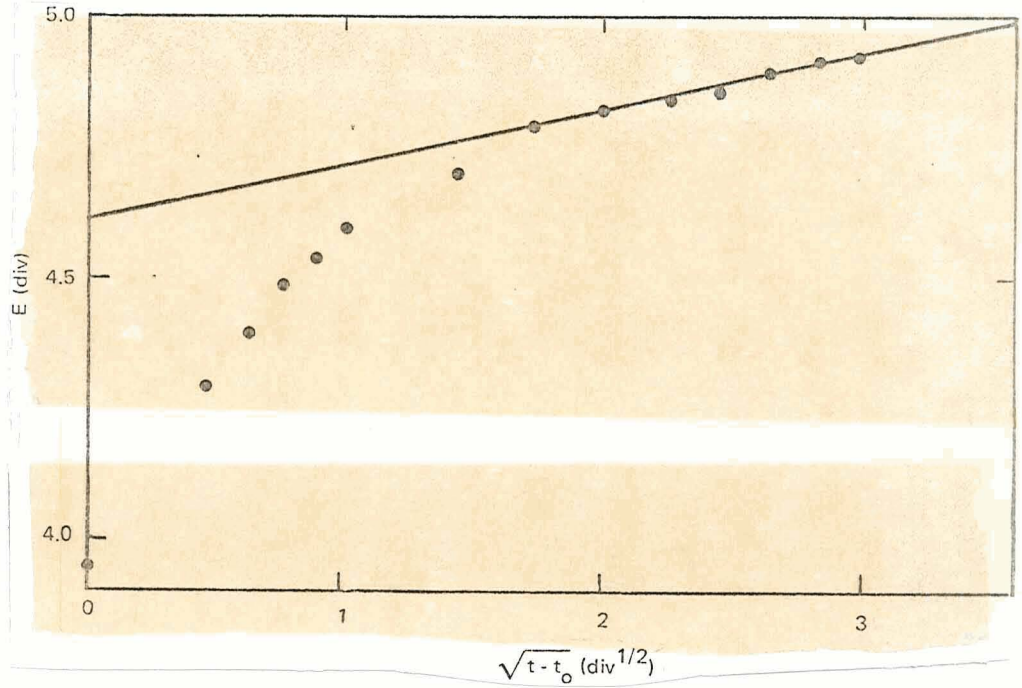

f) E vs $\sqrt{t}$ Plot

Fig. 23: Voltammetry of $Bi/BiCl_3$ in $AlCl_3$ Melts

species in the $ZnCl_2$ melts was found in the present study. However, no anodic sweeps to high current densities were performed in the $ZnCl_2$ melt except for the 15 wt % solution. The $CD^{1/2}$ values tabulated were calculated with n = 1 and indicate that the solute is fairly soluble in this system. However, since 0.1 M Bi(III) will yield 0.3 M Bi(I), the solutions studied may have been saturated.

Typical current-step voltammograms are shown in Fig. 23 d-e. In contrast to the $ZnCl_2$ case none of the short pulses had resistor-like appearances. However, the R_s values were again large and this probably was a reason for such low values of C_d, as in the $ZnCl_2$ case.

While the L.S.V. results suggest that n = 1 rather than 3, the values of $CD^{1/2}$ and i_o were calculated assuming an n of 3. If n is indeed 1, the values of $CD^{1/2}$ should be multiplied by 9 and D by 81/3 = 27. (The number 81 accounts for the change in n while the number 3 takes into consideration the change in concentration from 0.1 M of $BiCl_3$ to 0.3 M of BiCl.)

The long pulse traces tended to be flat as if the $CD^{1/2}$ values were large. However, this flatness was due to the fact that because of the high values of R_s small currents were used to get the entire trace with 5 msec pulses.

Pronounced negative deviations were obtained from all the traces (see Fig. 23 f) and only the $Ni/NiCl_2$ couple in the $ZnCl_2$ melt had a more pronounced deviation (although of opposite sign). The more pronounced negative deviation of the bismuth couple in the $AlCl_3$ case than in the $ZnCl_2$ case may be due to the lower temperature of the former system. The values of i_o, which must be regarded as formal values due to the large negative deviations, were considerably smaller than in the $ZnCl_2$ solvent, even if the former case is multiplied by 3 (correction for n = 1 rather than 3). The higher value of $\eta_{5\,msec}/iA$ is due to the high charge transfer resistance or possibly to crystallization polarization rather than to concentration polarization.

The facts that the exchange current is so low and that the $BiCl_3$ reacts with Bi metal producing high resistance, makes this couple less desirable than many of the others for battery application.

(6) $\underline{Sb/SbCl_3}$ –

The voltammetry results are shown in Table 29 and in Fig. 24. The open circuit potentials for this system ranged from 0.975 v at 126° to 0.990 v at 190°C. The decomposition potential in a ternary melt was reported[29] to be 0.95 v at 156°. The L.S.V. voltammograms at 126° have a smaller shoulder shortly after the onset of current and resemble the Cu/CuCl waves in $AlCl_3$ (see Fig. 21 a). At the highest temperature the shoulder had disappeared but the wave does not rise vertically even at the slowest sweep (Fig. 24 a). The $E_{eq} - E_p$ values are large for a 3-electron

process and vary with sweep rate at all temperatures, the shift increasing with temperature. From these results the antimony couple must be classified as an irreversible one. The i_p/m values at the two lower temperatures are constant but at 190° there appears to be some variation. Unlike its behavior in the $ZnCl_2$ melt the antimony couple does not show a second peak during its reduction. An anodic sweep to high current densities did not yield an anodic peak but affected the electrode causing it to produce ripples and oscillations even on reversal. The $CD^{1/2}$ values are high except at the low temperature where probably not all of the salt had gone into solution.

Typical current-step voltammograms are shown in Fig. 24b-c. In contrast to the two Bi systems and the $Sb/SbCl_3$ couple in the $ZnCl_2$ solvent, the R_s values were closer to the normal low values. Negative deviations were observed suggesting an additional polarization mechanism. As with most other metal/metal ion electrodes, the $CD^{1/2}$ values calculated from C.S.V. data were considerably less than those obtained from L.S.V. data. The resistance corresponding to the total overpotential at 5 msec was quite high at the lowest temperature but decreased considerably at the highest temperature. The exchange current densities were quite small (0.02 - 0.06 A/cm^2).

TABLE 29

VOLTAMMETRY OF $Sb/SbCl_3$ in $AlCl_3$ SOLVENT

(No. 18; A = 0.049 cm^2; n = 3)

a) LINEAR SWEEP VOLTAMMETRY

Temp (°C)	E_{eq} (v)	$CD^{1/2} \times 10^7$ $\left(\frac{moles}{cm^2\ sec^{1/2}}\right)$	s (mv/sec)	i_p/m (ma/cm^2)	$E_{eq} - E_p$ (mv)
126	0.975	0.71	23	6.0	58
			92	6.0	70
			207	5.8	75
			368	5.8	85
157	0.980	6.8	23	56.0	60
			92	52.6	100
			207	55.1	135
			368	56.2	170
190	0.990	17	23	135	90
			92	132	160
			207	125	225
			368	128	300

b) CURRENT STEP VOLTAMMETRY-SHORT PULSE

Temp (°C)	i (ma/cm^2)	trace	C_d ($\mu F/cm^2$)	R_s (Ω)
125	400	1	3.7	2.75
125	400	2	3.6	2.69
124	400	6	8.3	2.05
124	400	7	7.9	1.55
157	400	8	5.5	3.61
157	400	12	4.6	2.84
154	400	13	5.6	3.13
190	400	14	7.8	2.61
188	400	18	5.4	2.52
188	400	19	6.4	2.49

TABLE 29 (cont'd)

VOLTAMMETRY OF $Sb/SbCl_3$ in $AlCl_3$ SOLVENT

c) CURRENT STEP VOLTAMMETRY-LONG PULSE

Temp (°C)	i (ma/cm^2)	trace	R_s (Ω)	R_p (Ω)	$\frac{\Delta\eta_{0.1\,msec}}{iA}$ (Ω)	$CD^{1/2} \times 10^7$	$D \times 10^6$ (cm^2/sec)	$\eta_{5\,msec}$ (mv)	$\frac{\eta_{5\,msec}}{iA}$ (Ω)	i_o (A/cm^2)
124	2.0	5	2.3	-10.5	+13.2	0.01	0.0001	- 6.1	-61	0.021
124	5.0	4	2.3	- 9.0	+ 4.4	0.01	0.0001	-15.3	-61	0.024
124	10.0	3	2.3	-22.3	+ 3.3	0.02	0.0004	-26.6	-53	0.010
155	5.0	10	3.2	- 6.1	+ 2.4	0.07	0.005	- 3.7	-15	0.040
157	10.0	9	3.2	- 5.8	+ 1.7	0.08	0.007	- 6.6	-13	0.038
154	20.0	11	3.2	- 6.5	+ 2.1	0.09	0.009	-13.1	-13	0.037
188	10.0	15	2.5	- 4.3	+ 1.4	0.25	0.061	- 3.5	-6.9	0.060
189	20.0	16	2.5	- 4.6	+ 1.2	0.31	0.098	- 6.8	-6.8	0.055
188	40.0	17	2.5	- 4.9	+ 1.3	0.43	0.19	-12.6	-6.3	0.054

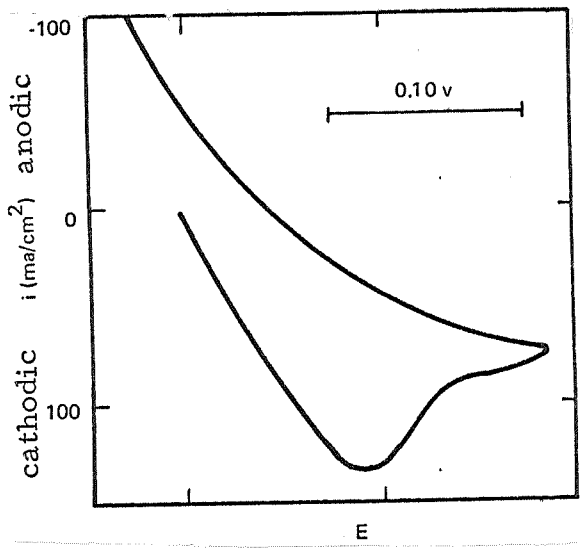

a) L.S.V.; T = 190°C; s = 23 mv/sec
E_{eq} = 0.990 v

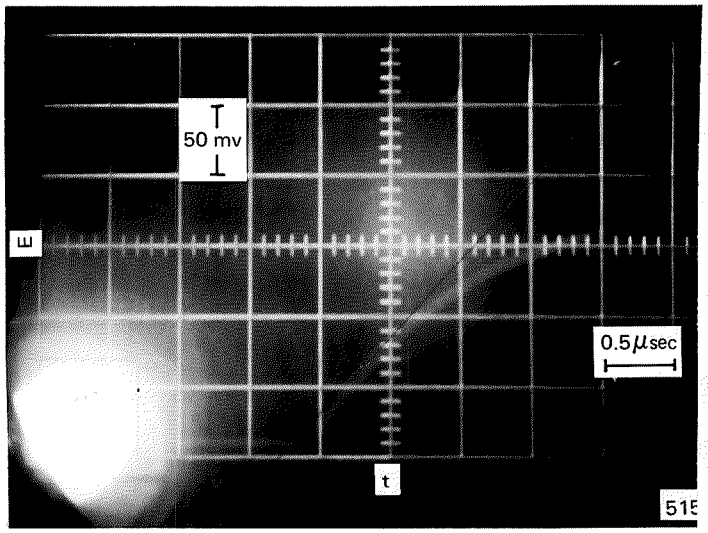

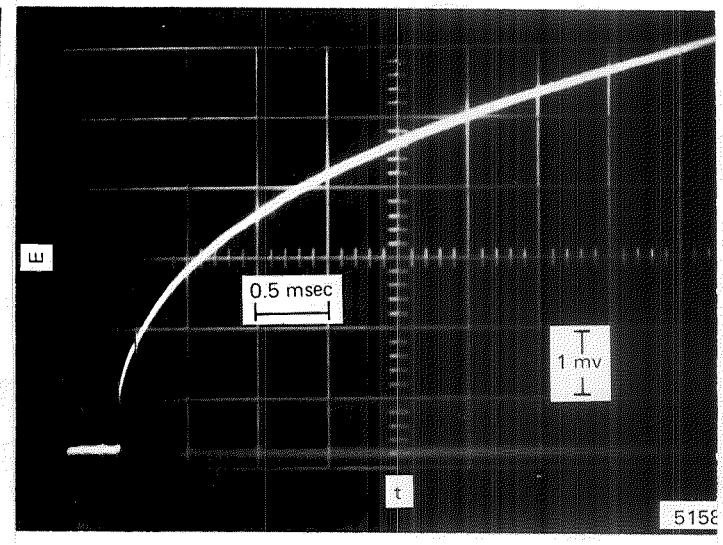

b) C.S.V.; Short Pulse
T = 125°C; i = 330 ma/cm^2
Trace #1

c) C.S.V.; Long Pulse
T = 124°C; i = 1.6 ma/cm^2
Trace #5

Fig. 24: Voltammetry of $Sb/SbCl_3$ in $AlCl_3$ Melts

159

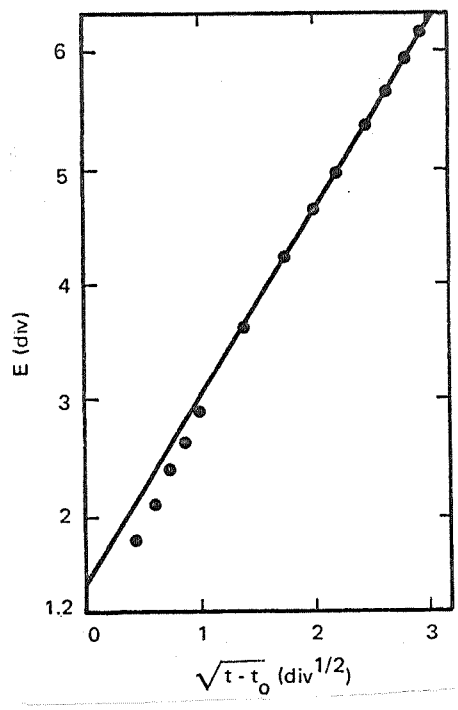

d) E vs $t^{1/2}$ Plot

Fig. 24: Voltammetry of $Sb/SbCl_3$ in $AlCl_3$ Melts

Based on the relatively low values of i_o, this couple is not considered desirable for high power battery applications.

(7) $\underline{W/CrCl_2, CrCl_3}$

The L.S.V. results are shown in Fig. 25. Potentials of about 1-1.5 v were measured at 208°C but these wandered around indicating an unpoised couple. The $CrCl_3$ is insoluble in this melt and no wave for the

reduction of Cr(III) in solution was obtained. A small cathodic wave, presumably for Cr(II) $\longrightarrow$ Cr(0), occurred at 0.17 v in agreement with a reported value.[29] The oxidation of Cr(II), which began at about 1.4 v, appeared to be diffusion limited and on reversal, a cathodic peak occured with a peak potential at about 0.95 v. This cathodic peak must be due to the reduction of a $CrCl_3$ (or a higher-valent chromium chloride) film formed on the electrode during the anodization sweep. On cycling at 208°, one can see that the reduction process consists of at least two steps (Fig. 25 a and b). Further, as the sweep rate is increased, the first step becomes more predominant. This suggests that the product A formed in the oxidation step reacts with the melt to yield B. The first cathodic peak (the smaller one at low sweep rates) is then due to the reduction of A and the second peak to the reduction of B. As the sweep rate is increased, less B is formed since A has less time to react. Similarly to the $Ni/NiCl_2$ couple in $ZnCl_2$, the $CrCl_2$, $CrCl_3$ couple cannot be employed as a soluble cathode but perhaps can be utilizable as a solid electrode. The areas under both peaks are comparable indicating that most of the oxidized material can be reduced. However, the ΔE_p is fairly large, 0.35 to 0.5 v.

Due to its insolubility, $CrCl_3$ cannot be utilized as a soluble cathode. It may be possible to use a $CrCl_3(s)$ electrode although its behavior is not as straightforward as the $NiCl_2(s)$ in the $ZnCl_2$ melt.

(8) <u>$W/CuCl, CuCl_2$</u>

The voltammetry results are shown in Table 30 and in Fig. 26. The rest potential for this system was 1.875 v $\pm$ 3 mv in the temperature range 125-196°C. A value of 1.866 v has been reported[28] for this couple at a concentration ratio of unity in a ternary $AlCl_3$ melt at 135°C.

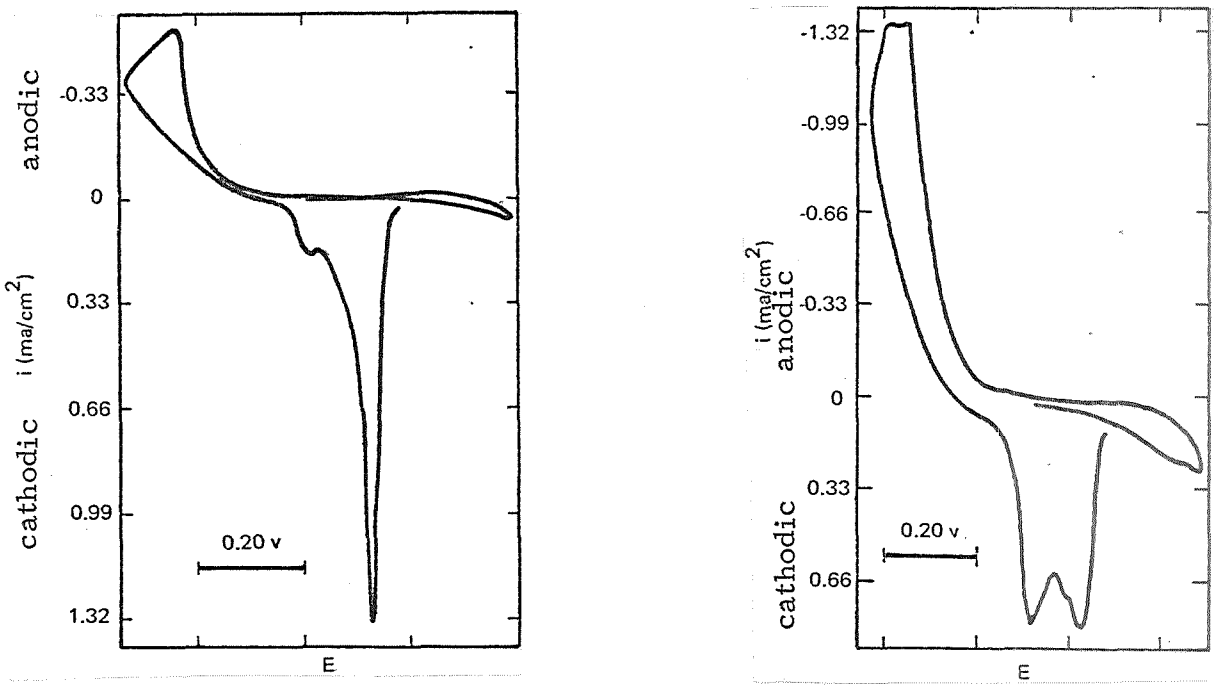

a) L.S.V.; T = 208°C; s = 23 mv/sec b) L.S.V.; T = 208°C; s = 368 mv/sec

Fig. 25: Voltammetry of W/$CrCl_2$, $CrCl_3$ in $AlCl_3$ Melts

In order to compare the reported value with that of this work, the former was adjusted to the concentration ratio of the latter. The concentration ratio in the present study (1.6) was calculated from the i_p values of single anodic and cathodic sweeps; the adjusted literature value was calculated to be 1.850 v. As in the other systems the potentials in the ternary melt at 135°C are lower than in the binary. A cyclic voltammogram of the melt at 139° is presented in Fig. 26 a. The reduction wave for Cu(II) is observed starting from the open circuit potential, 1.87 v. At 0.6 v the plating out of copper metal commences and then at about 0.25 v the reduction of Al(III). After reversal at 0 v, stripping peaks for Al and Cu appear and beginning at 1.7 v, the oxidation of Cu(I). The anodic limit is reached at about 2.4 v. All of the cyclic voltammograms for the couple began with an infinite slope and appeared normal (see Fig. 26 b). The ΔE_p values varied with sweep rate at 125° but were independent of s at 150 and 196°. However, the measured ΔE_p values were larger than

TABLE 30

VOLTAMMETRY OF W/CuCl, $CuCl_2$ in $AlCl_3$ SOLVENT

(No. 10; A = 0.090 cm^2; n = 1)

a) LINEAR SWEEP VOLTAMMETRY

Temp (°C)	E_{eq} (v)	$CD^{1/2} \times 10^7$ $\left(\frac{moles}{cm^2\ sec^{1/2}}\right)$	s (mv/sec)	i_p/m (ma/cm^2)	$E_{eq} - E_p$ (mv)
125	1.874	1.6	23	5.8	90
			92	5.8	95
			207	5.7	110
			368	5.7	120
150	1.872	1.6	23	5.6	110
			92	5.5	110
			207	5.4	120
			368	5.3	120
196	1.878	1.9	23	6.7	130
			92	6.5	130
			207	6.4	130
			368	6.3	135

b) CURRENT STEP VOLTAMMETRY-SHORT PULSE

Temp (°C)	i (ma/cm^2)	trace	C_d ($\mu F/cm^2$)	R_s (Ω)
123	220	8	4.0	2.55
120	220	12	3.9	2.45
152	220	6	16.8	1.82
150	220	7	17.0	1.78
168	220	1	9.2	1.99
195	220	13	16.4	2.14
195	220	14	17.8	2.24
187	220	19	-	2.45
187	220	20	-	2.47

TABLE 30 (cont'd)

VOLTAMMETRY OF W/CuCl, $CuCl_2$ in $AlCl_3$ SOLVENT

c) CURRENT STEP VOLTAMMETRY-LONG PULSE

Temp (°C)	i (ma/cm^2)	trace	R_s (Ω)	R_p (Ω)	$\frac{\Delta\eta_{0.1\,msec}}{iA}$ (Ω)	$f(C_i D_i^{1/2})$ x 10^7	D x 10^6 (cm^2/sec)	$\eta_{5\,msec}$ (mv)	$\frac{\eta_{5\,msec}}{iA}$ (Ω)	i_o (A/cm^2)
122	11.1	9	2.5	-2.4	+0.3	2.2	19	- 6.8	-6.8	0.15
122	22.2	10	2.5	-2.2	0	2.2	19	- 3.4	-6.7	0.17
120	33.3	11	2.5	-2.2	0	2.1	18	-20.4	-6.8	0.17
154	5.6	5	1.8	-2.7	+0.6	0.92	3.4	- 4.0	-7.9	0.16
164	11.1	2	2.0	-1.5	+0.2	0.87	3.0	- 5.3	-5.3	0.26
160	22.2	3	1.8	-1.4	+0.1	0.84	3.5	-10.5	-5.3	0.28
158	33.3	4	1.8	-1.6	0	0.83	2.8	-16.4	-5.5	0.25
189	11.1	18	2.3	-0.7	+0.4	3.9	60	- 3.5	-3.5	0.78
191	22.2	17	2.3	-1.3	+0.1	3.6	51	- 7.0	-3.5	1.39
190	33.3	15	2.3	-0.09	0	3.5	49	-10.3	-3.4	4.94
194	44.4	16	2.2	-0.25	0	3.5	49	-14.3	-3.8	1.73

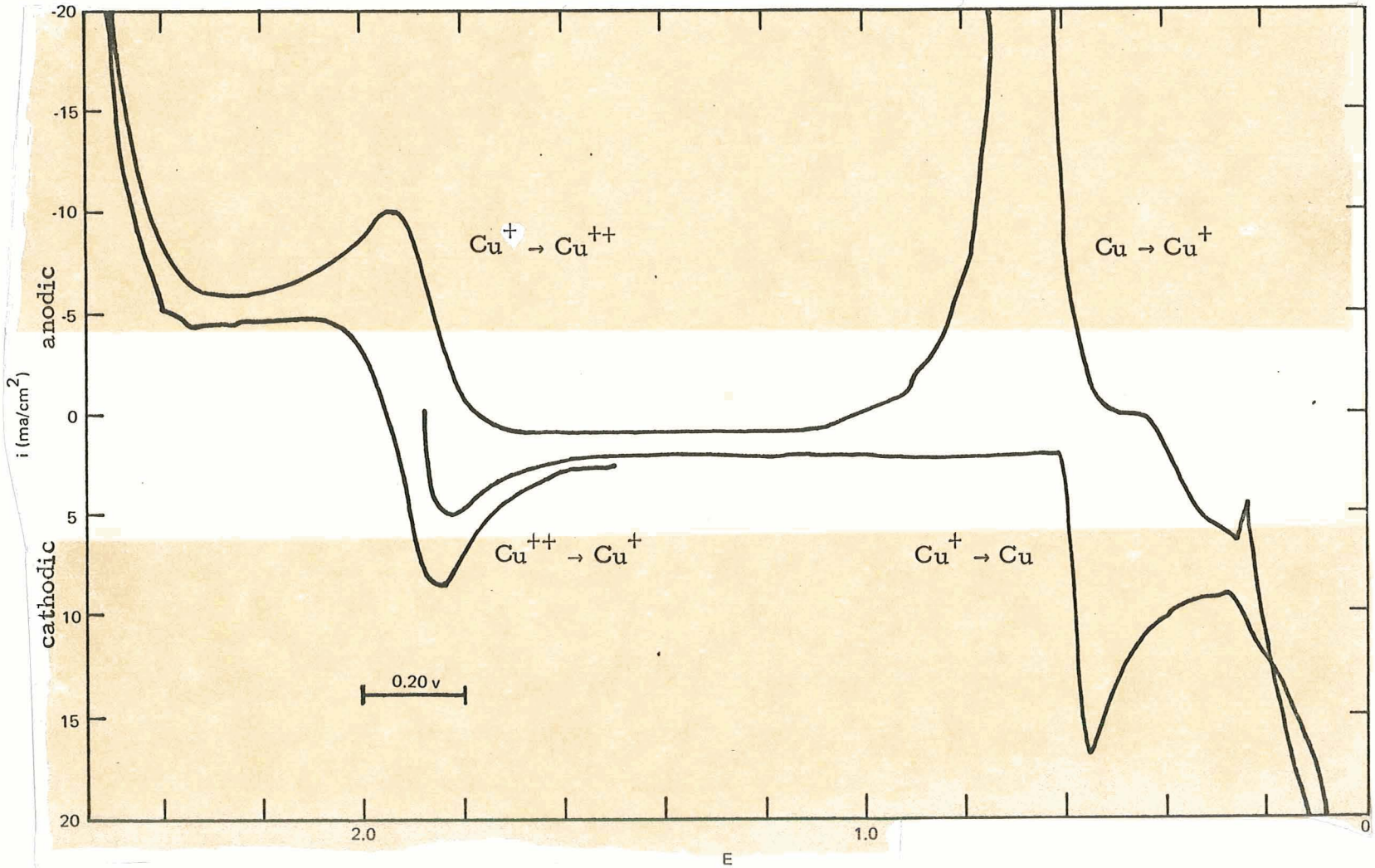

Fig. 26: Voltammetry of W/CuCl, $CuCl_2$ in $AlCl_3$ Melts

a) L.S.V.; T = 139°C; s = 23 mv/sec

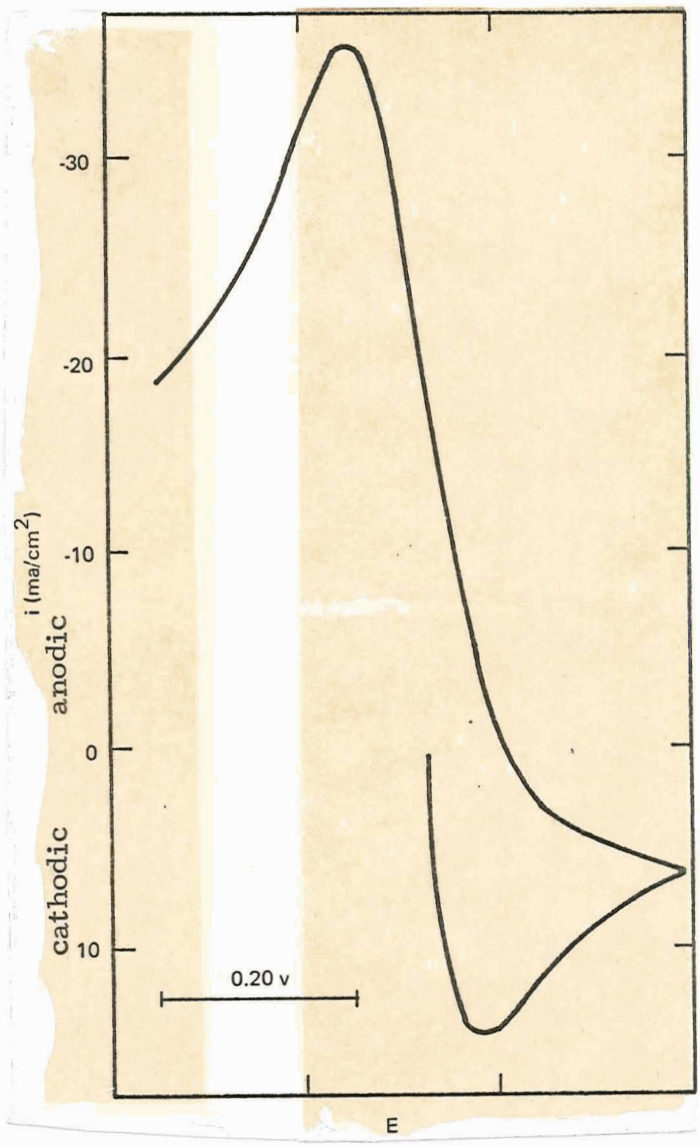

b) L.S.V.; T = 150°C; s = 207 mv/sec
E_{eq} = 1.872 v

Fig. 26: Voltammetry of W/CuCl, $CuCl_2$ in $AlCl_3$ Melts

Top 167

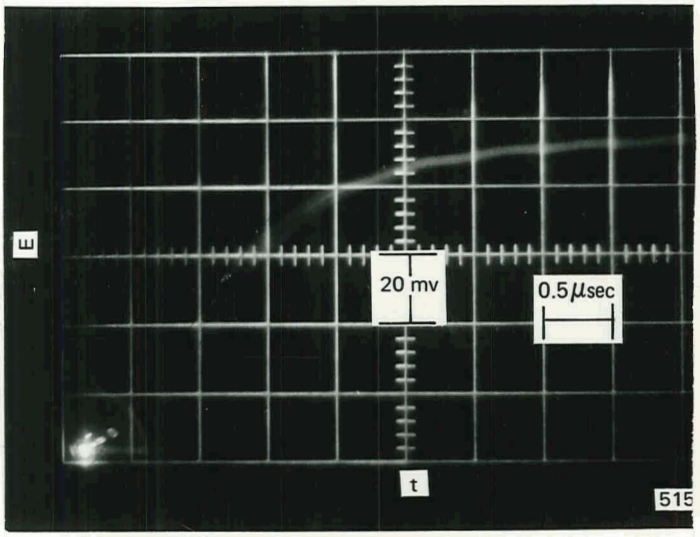

c) C.S.V.; Short Pulse
T = 123°C; i = 220 ma/cm^2
Trace #8

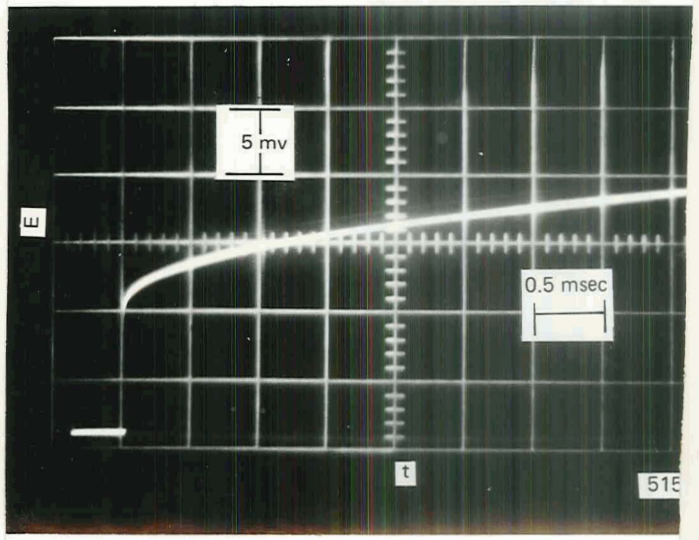

d) C.S.V.; Long Pulse
T = 122°C; i = 22 ma/cm^2
Trace #10

Bottom 167

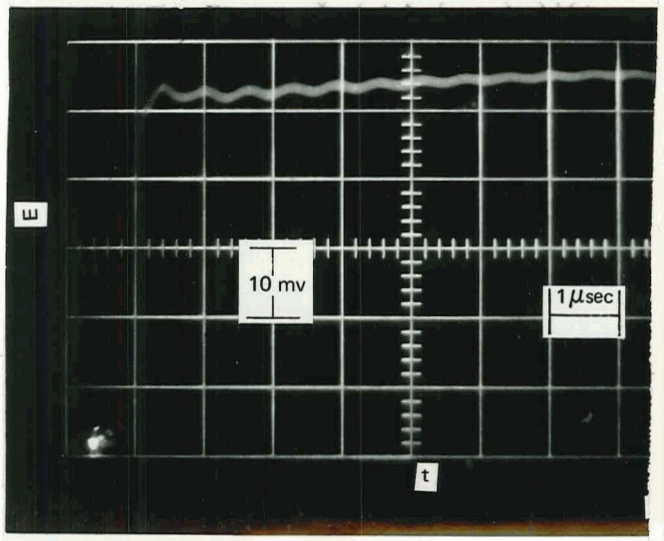

e) C.S.V.; Short Pulse
T = 187°C; i = 220 ma/cm^2
Trace #20

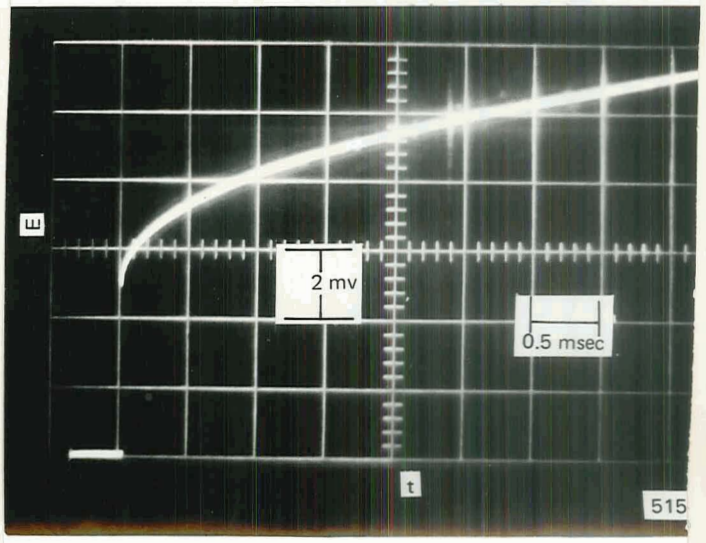

f) C.S.V.; Long Pulse
T = 191°C; i = 22 ma/cm^2
Trace #17

Fig. 26: Voltammetry of W/CuCl, $CuCl_2$ in $AlCl_3$ Melts

the calculated ones as was found for all the redox systems in this study. The i_p/m results were fairly constant although they appeared to decrease slightly with increasing sweep rate at 150 and 196°C. In contrast to the $ZnCl_2$ melt where the temperatures were higher, the $CuCl_2$ decomposed to a lesser extent and the i_p as well as the $CD^{1/2}$ values at 196° were larger than at the lower temperatures. The $CD^{1/2}$ results were about twice as large here as in the $ZnCl_2$ melt and the i_p ratio of 1.6 above suggests a solubility close to 0.06 M.

Two sets of C.S.V. traces are presented in Fig. 26 c-f. The first pair shows the low temperature behavior while the last pair depicts the high temperature behavior (the resistor-like appearance of the short pulse). However, two high temperature short-pulse traces (19 and 20) were not resistor-like. Deviations from linearity were small. The $f(C_iD_i^{1/2})$ values from C.S.V. data agreed quite well with the $CD^{1/2}$ values from L.S.V.

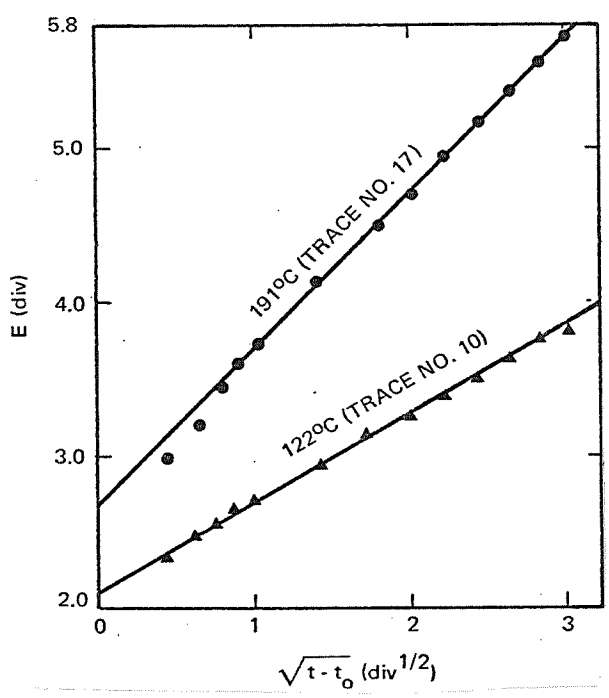

g) E vs $t^{1/2}$ Plot

Fig. 26: Voltammetry of W/CuCl, $CuCl_2$ in $AlCl_3$ Melts

results. The values of $(\eta/iA)_{5\,msec}$ are satisfactorily low. The exchange current densities, which ranged from 0.2 to 2.1 A/cm^2, are high. However, the possible limited solubility of $CuCl_2$ could present a problem. This couple is worthy of further testing for battery applications.

(9) $\underline{W/FeCl_2, FeCl_3}$ –

The voltammetry results are shown in Table 31 and in Fig. 27. The rest potentials, 1.974, 1.940 and 1.892 v at 128, 152 and 194°C, were the largest measured in any system. An L.S.V. of the melt at 129° is shown in Fig. 27a. The reduction wave for Fe(III) occurred at the open circuit voltage and the plating out of Fe began at 0.47 v or about 0.56 v anodic of Al(III) reduction in this cell. It appears that aluminum requires an overvoltage of about 0.1 v to plate out on iron. (The 0.47 v potential is in agreement with the value found from the decomposition potential[29] in a ternary $AlCl_3$ melt at 156°.) After the sweep is reversed, two stripping peaks, the more cathodic one for Al and the other for Fe were observed. The oxidation of Fe(II) to Fe(III) began at about 1.9 v and chlorine evolution or tungsten anodization occurred at about 2.4 v. The cathodic waves all looked reversible (see Fig. 27b) and the peak potentials were independent of sweep rate (except for the first sweep). Similarly, the i_p/m data, except for the first value, were also constant with sweep rate. The more constant E_p and i_p/m values for redox systems, in general, as compared to metal/metal ion couples may be due to no electrode changes from metal plating out in the redox systems. From the $CD^{1/2}$ results it appears that the solubility of $FeCl_3$ is about the same as $CuCl_2$ in $AlCl_3$-NaCl. From the i_p value of single sweeps the solubility of $FeCl_2$ is about twice that of $FeCl_3$.

TABLE 31

VOLTAMMETRY OF W/$FeCl_2$, $FeCl_3$ in $AlCl_3$ SOLVENT

(No. 14; A = 0.060 cm^2; n = 1)

a) LINEAR SWEEP VOLTAMMETRY

Temp (°C)	E_{eq} (v)	$CD^{1/2} \times 10^7$ $\left(\frac{moles}{cm^2\ sec^{1/2}}\right)$	s (mv/sec)	i_p/m (ma/cm^2)	$E_{eq} - E_p$ (mv)
128	1.974	1.0	23	5.8	85
			92	3.7	60
			207	3.4	60
			368	3.3	60
152	1.940	1.2	23	4.1	55
			92	4.4	55
			207	4.3	60
			368	4.2	60
194	1.892	2.0	23	6.8	70
			92	6.8	75
			207	6.8	70
			368	6.8	75

b) CURRENT STEP VOLTAMMETRY-SHORT PULSE

Temp °C	i (ma/cm^2)	trace	C_d ($\mu F/cm^2$)	R_s (Ω)
125	330	1	5.4	2.55
125	330	2	4.7	2.06
123	330	7	6.6	1.68
149	330	8	9.2	2.14
148	330	13	11.3	2.20
147	330	14	9.1	2.11
193	330	15	12.7	1.75

TABLE 31 (cont'd)

VOLTAMMETRY OF $W/FeCl_2$, $FeCl_3$ in $AlCl_3$ SOLVENT

c) CURRENT STEP VOLTAMMETRY-LONG PULSE

Temp (°C)	i (ma/cm^2)	trace	R_s (Ω)	R_p (Ω)	$\frac{\Delta\eta_{0.1}}{iA}$ (Ω)	$f(C_i D_i^{1/2})$ x 10^7	D x 10^6 (cm^2/sec)	$\eta_{5\,msec}$ (mv)	$\frac{\eta_{5\,msec}}{iA}$ (Ω)	i_o (A/cm^2)
125	4.0	5	2.1	-6.1	+0.8	0.39	0.60	- 4.2	-17.0	0.087
125	8.0	4	2.1	-6.4	+0.1	0.42	0.71	- 8.4	-16.7	0.083
125	16.0	3	2.1	-5.6	0	0.38	0.58	-16.6	-16.6	0.095
125	16.0	6	2.1	-5.4	0	0.38	0.58	-16.4	-16.4	0.11
148	8.0	11	2.2	-3.1	+0.4	0.52	1.1	- 3.9	- 7.9	0.18
148	16.0	9	2.2	-3.3	+0.5	0.55	1.2	-11.6	-11.6	0.17
149	16.0	10	2.2	-2.2	+0.2	0.50	1.0	-11.3	-11.3	0.26
148	24.0	12	2.2	-2.5	0	0.52	1.1	-17.3	-11.5	0.23
194	8.0	17	1.8	-2.1	+0.5	0.77	2.4	- 4.3	- 8.7	0.31
194	16.0	16	1.8	-1.6	+0.2	0.73	2.1	- 8.5	- 8.5	0.40

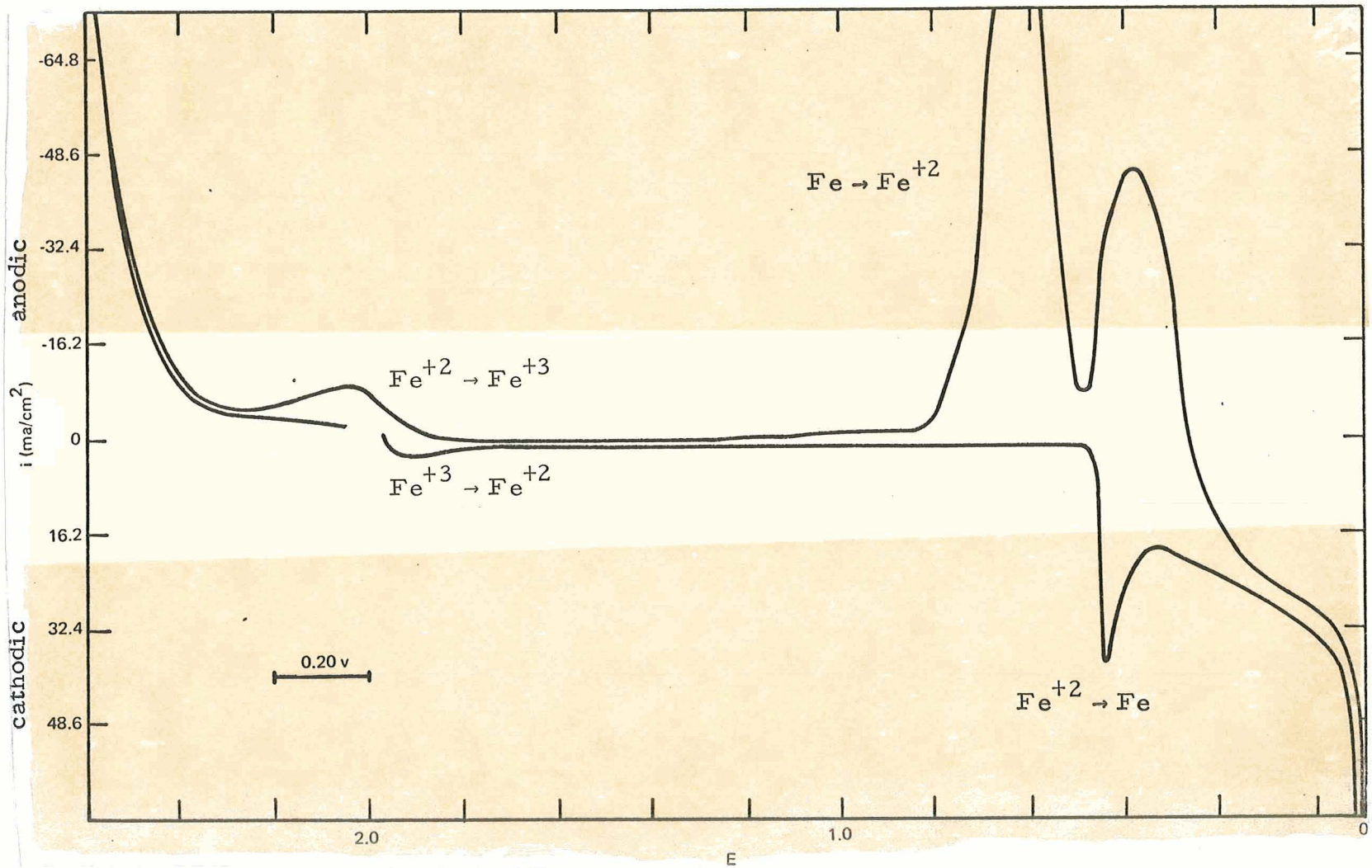

a) L.S.V.; T = 129 °C; s = 23 mv/sec

Fig. 27: Voltammetry of $W/FeCl_2$, $FeCl_3$ in $AlCl_3$ Melts

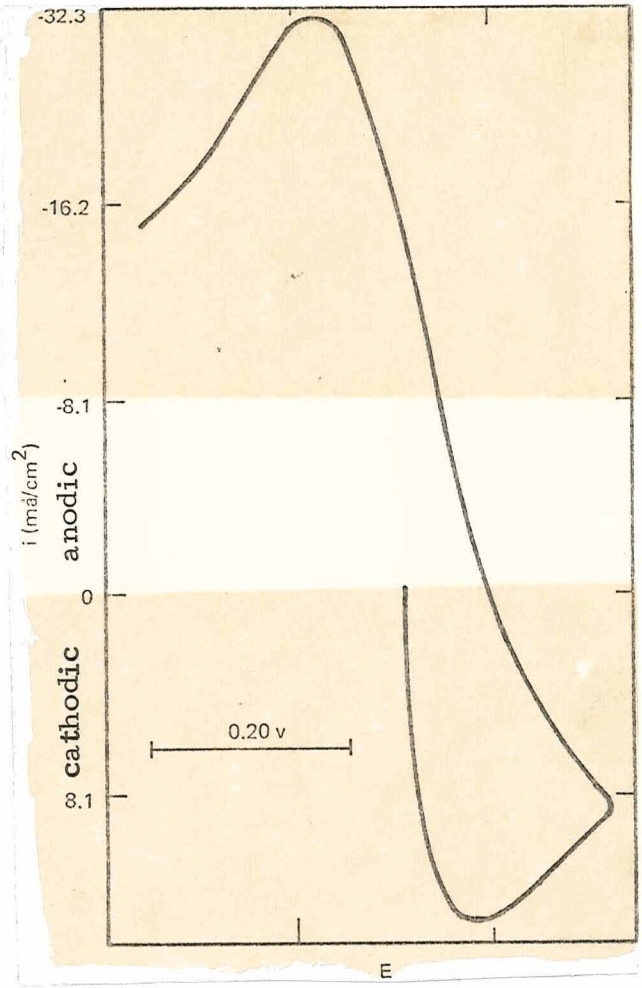

b) L.S.V.; T = 194°C; s = 92 mv/sec
E_{eq} = 1.892 v

Fig. 27: Voltammetry of W/$FeCl_2$, $FeCl_3$ in $AlCl_3$ Melts

174

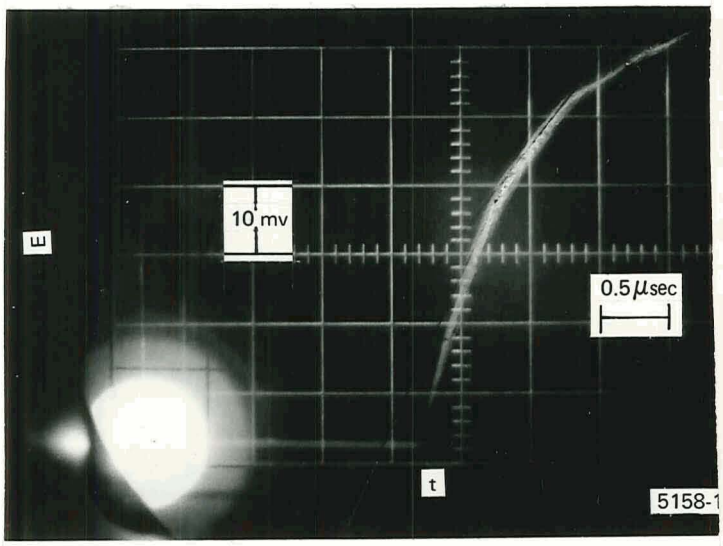

c) C.S.V.; Short Pulse
T = 193°C; i = 330 ma/cm^2
Trace #15

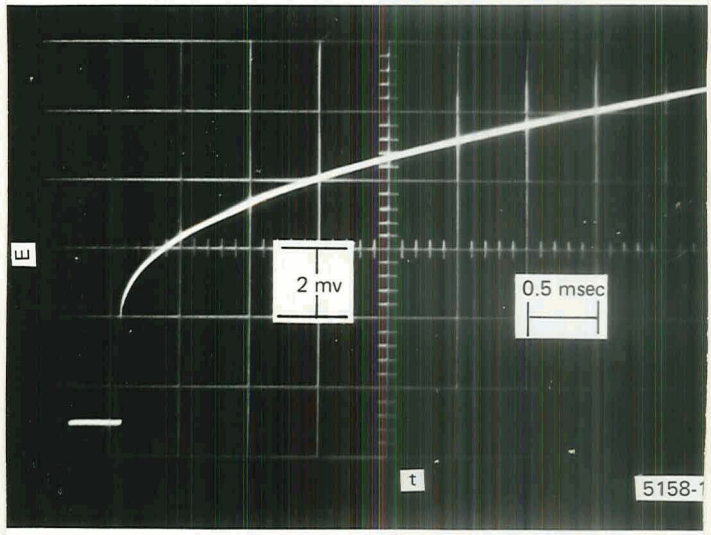

d) C.S.V.; Long Pulse
T = 194°C; i = 16 ma/cm^2
Trace #16

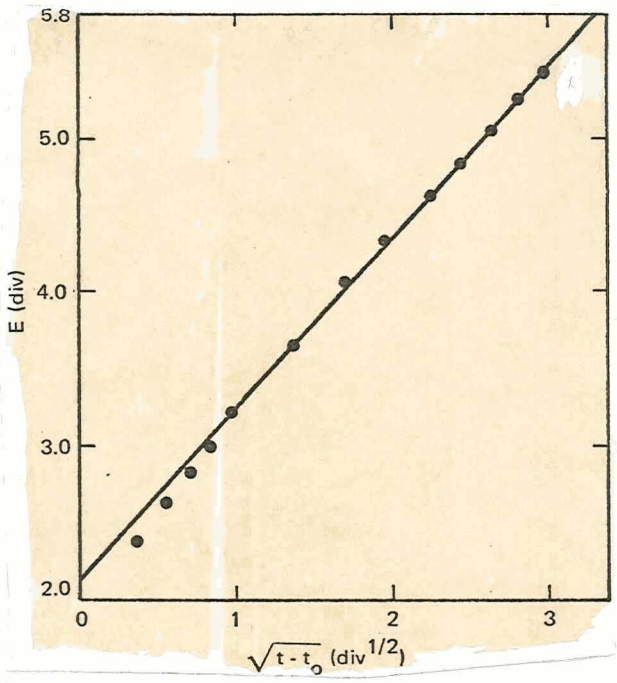

e) E vs $t^{1/2}$ Plot

Fig. 27: Voltammetry of W/$FeCl_2$, $FeCl_3$ in $AlCl_3$ Melts

A typical set of current-step voltammograms is shown in Fig. 27 c-e. No resistor-like short pulses were observed. As in the W/CuCl, $CuCl_2$ couple in $AlCl_3$, deviation from linearity was small. The resistance corresponding to the total overpotential at 5 msec was moderately high, especially at the lowest temperature and this may be due to concentration polarization resulting from limited solubility. The $f(C_iD_i^{1/2})$ values were a bit lower than the $CD^{1/2}$ values obtained from L.S.V. data. The exchange current densities are sufficiently high for battery applications. However, if a very soluble electrolyte is desired, this couple may not be suitable. Nevertheless, even with its limited solubility, this system warrants further testing for high power density battery applications.

(10) $\underline{Zn/ZnCl_2}$ –

The voltammetry results are shown in Table 32 and in Fig. 28. Open-circuit voltages of 0.194, 0.217 and 0.226 v were measured at 130, 156, and 207°C. The value at 156°C is in excellent agreement with 0.214 v, corrected for concentration from a reported value[34] of 0.254 v, in a ternary $AlCl_3$ melt. Unfortunately, no measurement was made at 135°C as in the other systems[28] so no further comparisons can be made. However, as with the Ag/AgCl couple the potentials at 150°C for the two couples measured in the ternary melt are in good agreement with those in the present study. In contrast, the potentials measured at 135°C in the ternary were all lower than those for the binary melt in this investigation. Further, for the only couple, Ag/AgCl, measured at both temperatures, the temperature coefficient of the emf in the ternary solvent was very large whereas in the binary it was small. These data plus the fact that 135°C is the freezing point of the solvent (Appendix I) suggest that composition changes might have been occurring in

the ternary solutions. The L.S.V. showed waves with infinite initial slope, especially at the slower sweeps and lower temperatures (Fig. 28a). The peak potentials at 130°C were constant up to the fastest sweep but at 156 and 207°C they shifted with sweep rate. The i_p/m values also varied somewhat with sweep. The $CD^{1/2}$ results indicated that the $ZnCl_2$ solubility is greater than 0.1 M. The $CD^{1/2}$ data yield a diffusion coefficient of 1×10^{-5} cm^2/sec at 156°C. This value is lower than 6.5×10^{-5} cm^2/sec calculated from a chronopotentiometric measurement.[34] No dendrites were found after the test.

The C.S.V. traces are shown in Fig. 28b-g. The first and second pairs of traces exhibit typical low and high temperature behavior when a cathodic current is applied. The third pair shows a low temperature and a high temperature anodic trace. The C_d values were, in general, considerably larger than usual, especially at the highest temperature. There appeared to be the least deviation from linearity at the lowest temperature. The $CD^{1/2}$ values calculated from C.S.V. results were somewhat lower than from L.S.V. data. The exchange current densities ranged from a relatively low 0.06 A/cm^2 at 128°C to about 0.4 A/cm^2 at 205°C. Measurements of the anodic exchange current densities with both long and short pulses yielded, in general, good agreement and were also in good agreement with the cathodic values. The i_o values were greater when $ZnCl_2$ was the solvent than when the salt was dissolved in the $AlCl_3$-containing solvent. Two reasons are that in the former case, the concentration of $ZnCl_2$ is much greater and the temperature is higher.

In view of the satisfactory i_o, the anticipated lack of concentration polarization due to the high solubility of $ZnCl_2$ in the $AlCl_3$

TABLE 32

VOLTAMMETRY OF $Zn/ZnCl_2$ in $AlCl_3$ SOLVENT

(No. 15; A = 0.060 cm^2; n = 2)

a) LINEAR SWEEP VOLTAMMETRY

Temp (°C)	E_{eq} (v)	$CD^{1/2} \times 10^7$ $\left(\frac{moles}{cm^2\ sec^{1/2}}\right)$	s (mv/sec)	i_p/m (ma/cm^2)	$E_{eq} - E_p$ (mv)
130	0.194	0.95	23	5.6	20
			92	6.6	20
			207	7.3	25
			368	5.9	50
156	0.217	3.5	23	18.7	22
			92	22.2	32
			207	23.8	45
			368	24.2	55
207	0.226	5.6	23	32.3	26
			92	35.1	33
			207	38.1	50
			368	34.8	75

b) CURRENT STEP VOLTAMMETRY-CATHODIC SHORT PULSE

Temp (°C)	i (ma/cm^2)	trace	C_d ($\mu F/cm^2$)	R_s (Ω)
129	330	1	26.2	1.06
129	330	2	27.3	1.17
128	330	6	26.2	1.16
127	330	12	28.2	1.05
157	330	17	10.8	2.30
157	330	18	8.9	2.20
206	330	26	41.4	2.57
204	330	30	41.9	2.66
202	330	35	27.2	2.58

TABLE 32 (cont'd)

VOLTAMMETRY OF $Zn/ZnCl_2$ in $AlCl_3$ SOLVENT

c) CURRENT STEP VOLTAMMETRY-CATHODIC LONG PULSE

Temp (°C)	i (ma/cm^2)	trace	R_s (Ω)	R_p (Ω)	$\frac{\Delta\eta_{0.1}}{iA}$ (Ω)	$CD^{1/2} \times 10^7$ (cm^2/sec)	$D \times 10^6$ (cm^2/sec)	$\eta_{5\,msec}$ (mv)	$\frac{\eta_{5\,msec}}{iA}$ (Ω)	i_o (A/cm^2)
127	8.0	4	1.11	-4.2	+0.1	0.34	0.12	-3.7	-7.4	0.065
127	16.0	3	1.11	-4.1	0	0.37	0.14	-7.2	-7.2	0.066
128	33.0	5	1.11	-5.3	+0.1	0.41	0.17	-15.9	-7.9	0.062
158	8.0	16	2.25	-2.2	+2.0	1.1	1.2	-1.5	-3.1	0.13
158	16.0	15	2.25	-2.1	+1.6	1.3	1.7	-2.9	-2.9	0.14
158	33.0	14	2.25	-2.2	+0.1	1.2	1.4	-6.2	-3.1	0.13
205	8.0	29	2.60	-1.4	+6.4	2.9	8.4	-0.9	-1.8	0.23
205	16.0	28	2.60	-0.72	+1.4	2.2	4.9	-1.3	-1.3	0.45
205	33.0	27	2.60	-0.53	+1.8	3.7	13.	-1.8	-0.9	0.61

TABLE 32 (cont'd)

VOLTAMMETRY OF $Zn/ZnCl_2$ in $AlCl_3$ SOLVENT

d) CURRENT STEP VOLTAMMETRY-ANODIC LONG AND SHORT PULSE

Temp (°C)	i (ma/cm^2)	trace	Time Scale (sec/div)	R_s (Ω)	R_p (Ω)	i_o (A/cm^2)
128	41	11	100	-1.1	5.4	0.064
127	165	10	100	-1.1	5.6	0.061
128	330	7	2	-1.1	5.2	0.061
128	330	8	2	-1.1	5.3	0.058
128	330	9	2	-1.1	5.6	0.061
157	41	22	5	-2.3	4.6	0.13
157	165	21	5	-2.3	4.2	0.15
157	330	19	2	-2.3	4.6	0.13
157	330	20	5	-2.3	4.2	0.15
157	330	25	5	-2.3	6.7	0.07
202	41	34	5	-2.6	3.6	0.34
203	165	33	5	-2.6	3.4	0.39
204	330	31	5	-2.6	3.4	0.42
204	330	32	5	-2.6	3.5	0.37

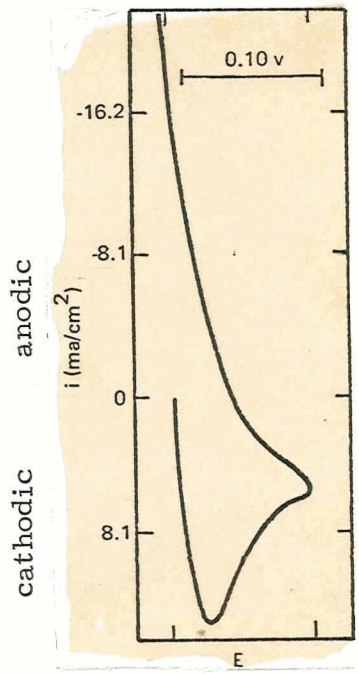

a) L.S.V.; T = 130°C; s = 92 mv/sec
E_{eq} = 0.194 v

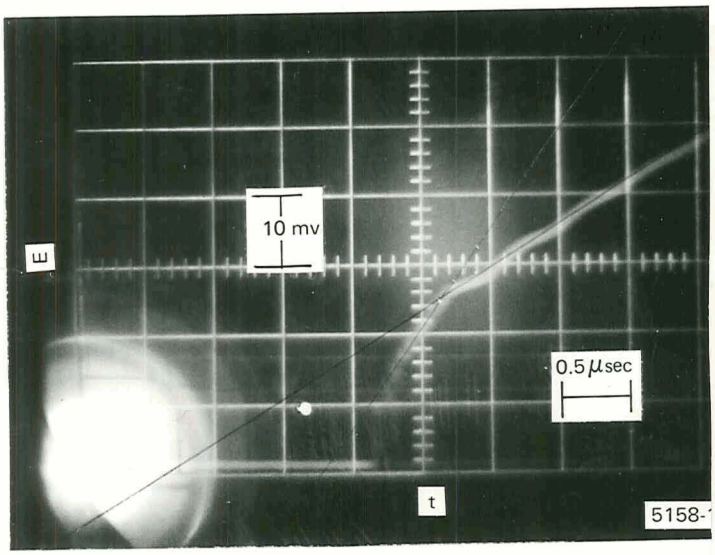

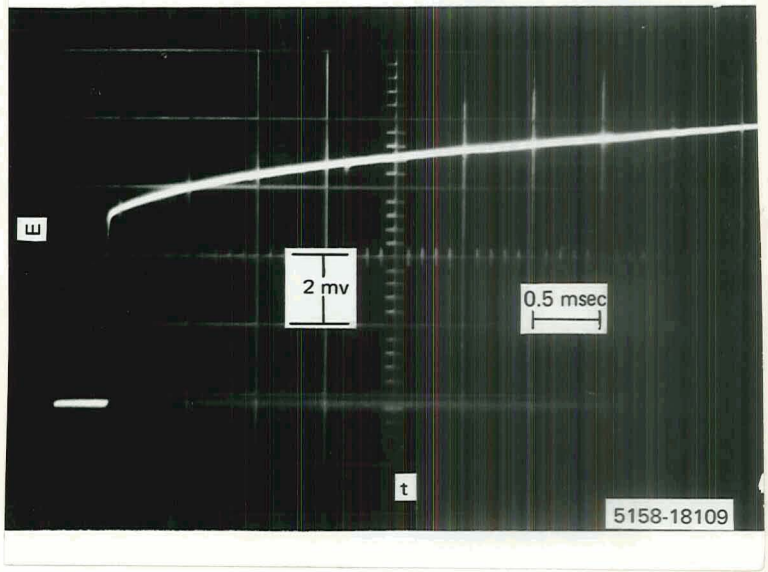

180

b) C.S.V.; Cathodic Short Pulse
T = 128°C; i = 330 ma/cm^2
Trace #6

c) C.S.V.; Cathodic Long Pulse
T = 127°C; i = 16 ma/cm^2
Trace #3

Fig. 28: Voltammetry of $Zn/ZnCl_2$ in $AlCl_3$ Melt

181 TOP

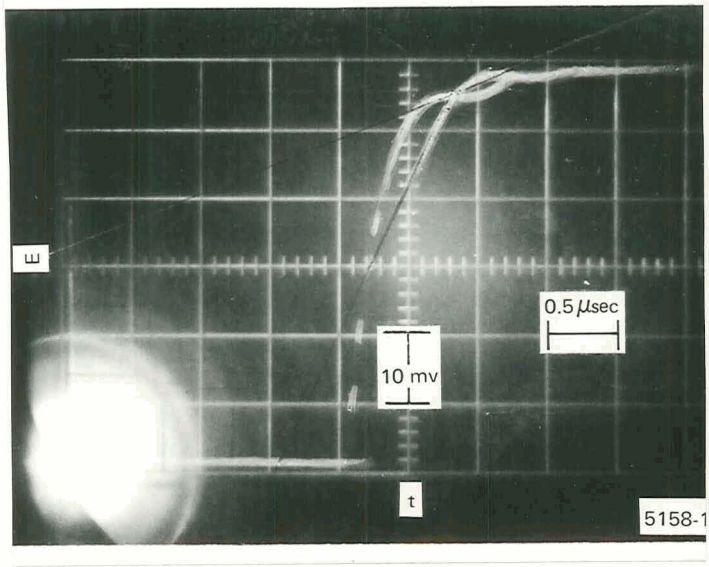

d) C.S.V.; Cathodic Short Pulse
T = 206°C; i = 330 ma/cm^2
Trace #26

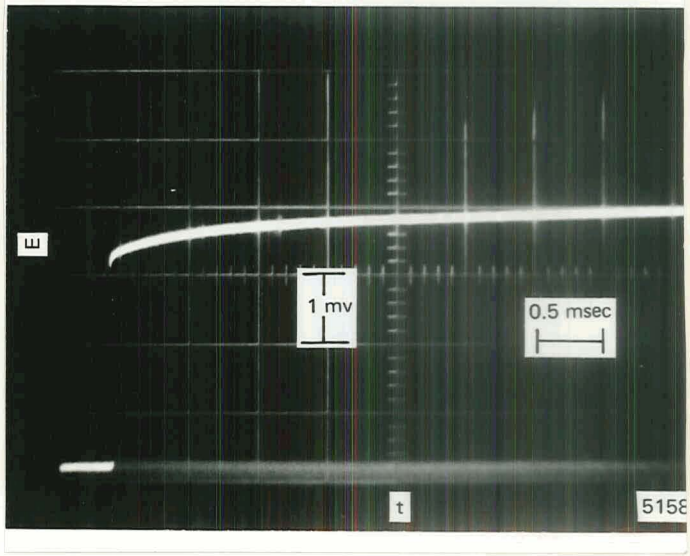

e) C.S.V.; Cathodic Long Pulse
T = 205°C; i = 16 ma/cm^2
Trace #28

181 Botta

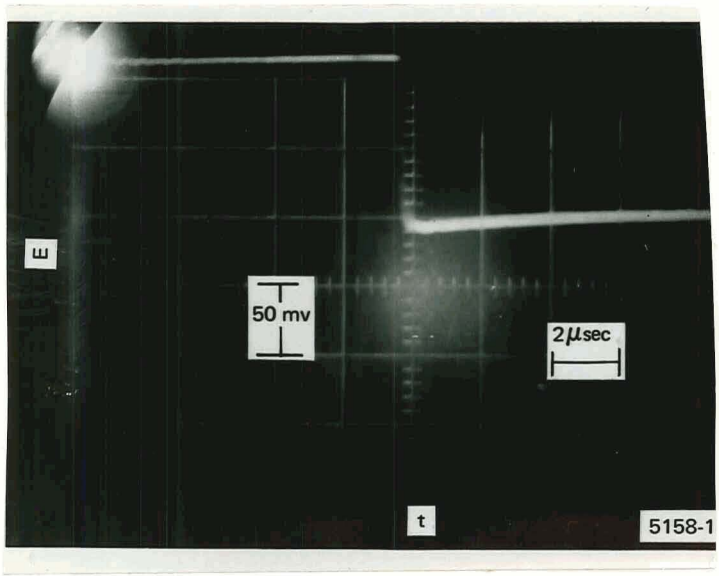

f) C.S.V.; Anodic Short Pulse
T = 128°C; i = 330 ma/cm^2
Trace #7

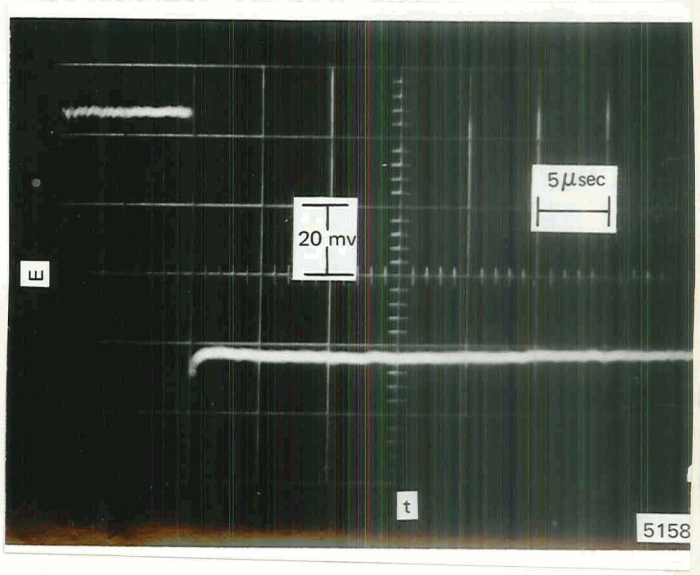

g) C.S.V.; Anodic Short Pulse
T = 203°C; i = 330 ma/cm^2
Trace #32

Fig. 28: Voltammetry of $Zn/ZnCl_2$ in $AlCl_3$ Melt

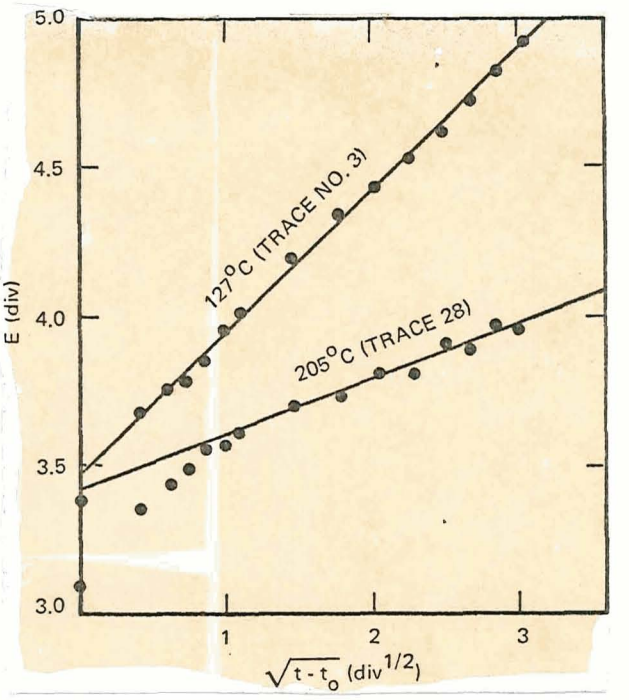

h) E vs $t^{1/2}$ Plot

Fig. 28: Voltammetry of $Zn/ZnCl_3$ in $AlCl_3$ Melt

solvent (as indicated in Table 13) and the absence of dendrite formation in this test, the $Zn/ZnCl_2$ couple has potential application for high-current drain batteries.

(11) $\underline{Al/AlCl_3}$ —

The voltammetry results are shown in Table 33 and in Fig. 29. The rest potentials were zero at all temperatures as expected. Although the $AlCl_3$ concentration was large, the L.S.V. yielded a limiting anodic current at 122°(Fig. 29 a) and 151°C. The limiting current occurred at much higher current densities at 151° (250 ma/cm^2) than at 122°C (110 ma/cm^2). Their occurrence may be due to the formation of a film of $AlCl_3$ on the electrode. At 195°C resistance-limited voltammograms with no peaks up to current densities of 1 amp/cm^2 were obtained (Fig. 29 b). The departures

from straight lines in the figure are probably due, at least in part, to saturation of the instrument. No dendrites were evident in the cell.

Typical current-step voltammograms are shown in Fig. 29 c-h. Due to the unusual results of this test, the measurements will be discussed for different temperature regimes.

At the lowest temperature 124°C, the C_d values were low ($\sim 5\ \mu F/cm^2$). The cathodic long pulse trace (Fig. 29 d) had a long tail and a continuous increase in voltage in spite of the fact that the $AlCl_3$ was the major component of the solvent. The deviations from linearity were very high in both the cathodic and anodic E vs $t^{1/2}$ plots (Fig. 29 i-j). In addition, the formal i_o's were very low ($< 0.01\ A/cm^2$). These results are in general accord with those of Del Duca[35] who found low exchange current densities and no steady state potential in times as long as 5 msec. The anodic i_o's both from long and short pulse data were somewhat lower than the cathodic values. These i_o's were among the lowest obtained in any system where C.S.V. measurements were carried out.

At 150°C, the long pulse traces were more normal (Fig. 29f). The deviation from linearity, given by $(\Delta\eta/iA)_{0.1\ msec}$, decreased markedly from about 8.5 Ω at 123°C to 0.1 Ω at 150°C. The exchange current density increased by an order of magnitude. It appears unlikely that a mere 25°C increase in temperature could result in such drastic changes. It would seem more probable that the condition of the electrode had been altered.

The plan was to repeat the lowest temperature measurements. However, after trace 17 was taken, a temperature excursion to over 220°C took place; the reason for the excursion is unknown. Values of R_s

TABLE 33

VOLTAMMETRY OF $Al/AlCl_3$ in $AlCl_3$ SOLVENT

(No. 16; A = 0.060 cm^2; n = 3)

a) CURRENT STEP VOLTAMMETRY-SHORT PULSE (CATHODIC)

Temp (°C)	i (ma/cm^2)	trace	C_d ($\mu F/cm^2$)	R_s (Ω)
124	330	1	5.8	2.24
124	330	2	4.4	2.09
124	330	3	5.2	2.57
151	330	14	19.0	2.48

b) CURRENT STEP VOLTAMMETRY-LONG PULSE

Temp (°C)	i (ma/cm^2)	Polarity	trace	R_s^* (Ω)	R_p (Ω)	$\frac{\Delta\eta_{0.1}}{iA}$ (Ω)	i_o (A/cm^2)
123	4.0	cathodic	6	2.3	-25.7	+9.9	0.0070
124	8.0	cathodic	5	2.3	-24.2	+9.2	0.0074
124	16.0	cathodic	4	2.3	-24.7	+9.5	0.0072
121	- 4.0	anodic	12	-2.3	+41.9	+6.0	0.0042
121	- 8.0	anodic	11	-2.3	+41.6	+9.0	0.0042
123	- 16.0	anodic	10	-2.3	+39.7	+8.4	0.0045
124	82	anodic	13	-2.3	-	-	0.0050*
122	165	anodic	9	-2.3	-	-	0.0023*
122	330	anodic	8	-2.3	-	-	0.0012*
151	16.0	cathodic	15	2.5	- 1.7	+0.2	0.12
150	33.0	cathodic	16	2.5	- 2.4	+0.1	0.080
150	49.0	cathodic	17	2.5	- 3.2	+0.1	0.061

* From short pulse data

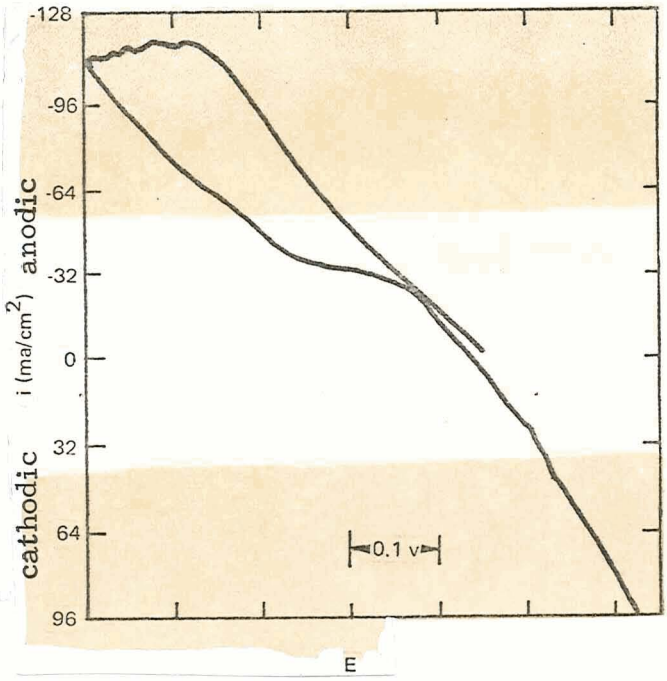

a) L.S.V.; T = 122°C; s = 23 mv/sec
E_{eq} = 0 v

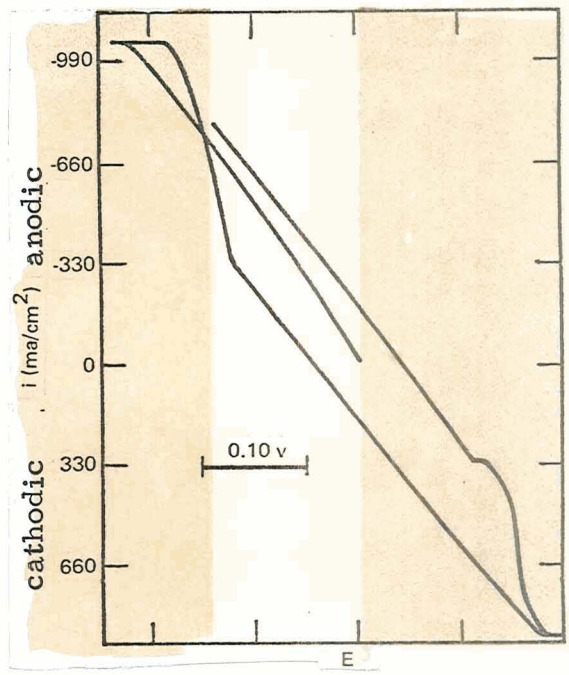

b) L.S.V.; T = 195°C; s = 23 mv/sec
E_{eq} = 0 v

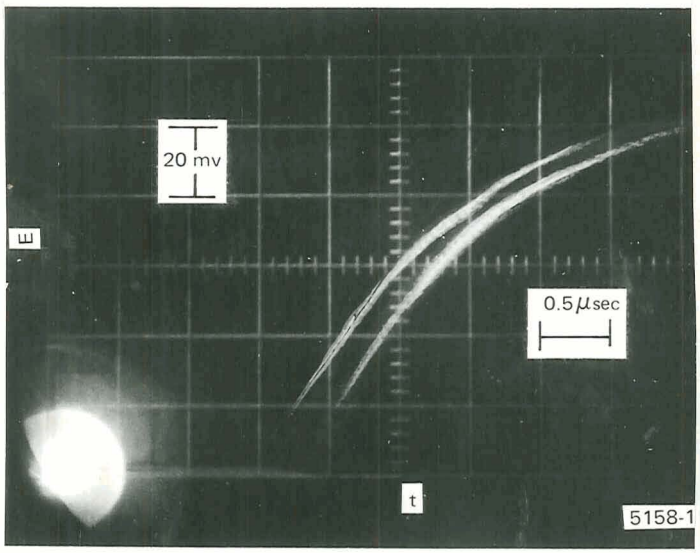

c) C.S.V.; Cathodic Short Pulse
T = 124°C; i = 330 ma/cm^2
Trace #1

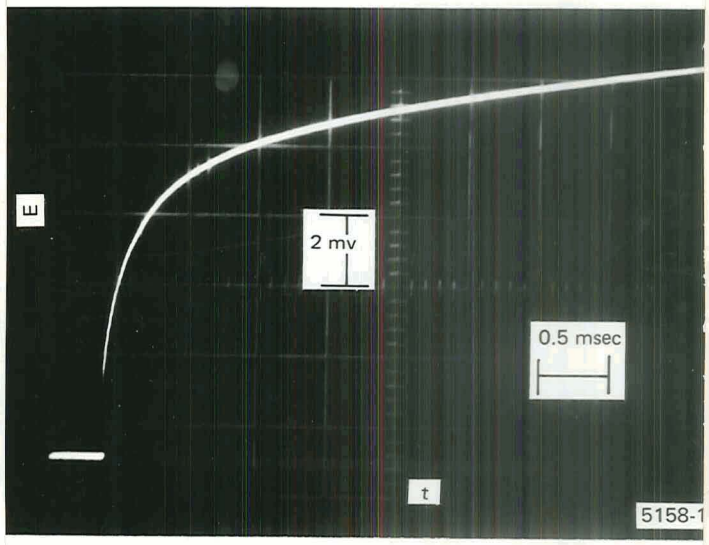

d) C.S.V.; Cathodic Long Pulse
T = 123°C; i = 4.1 ma/cm^2
Trace #6

Fig. 29: Voltammetry of $Al/AlCl_3$ System

Top 186

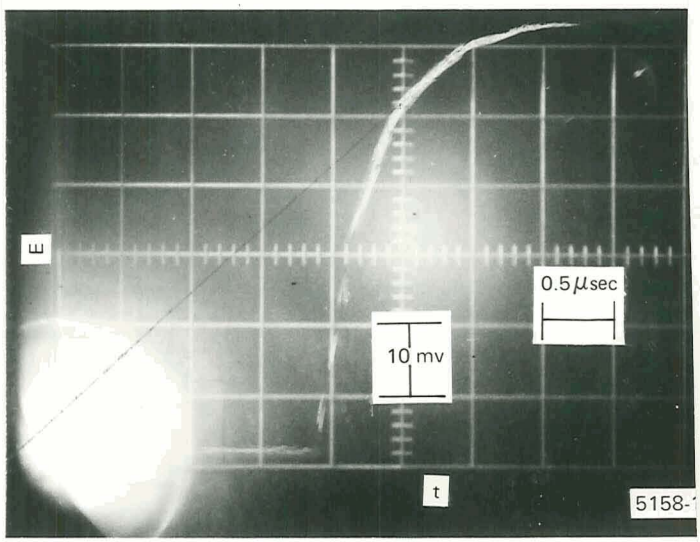

e) C.S.V.; Cathodic Short Pulse
T = 151°C; i = 330 ma/cm^2
Trace #14

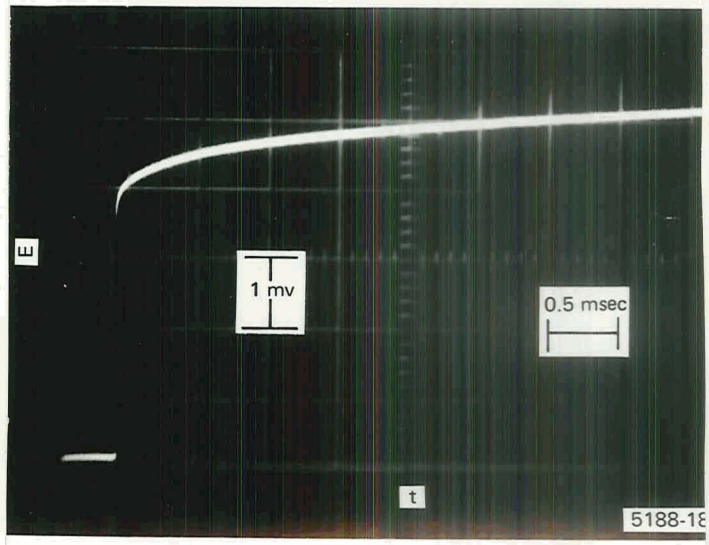

f) C.S.V.; Cathodic Long Pulse
T = 151°C; i = 16 ma/cm^2
Trace #15

186 Bottom

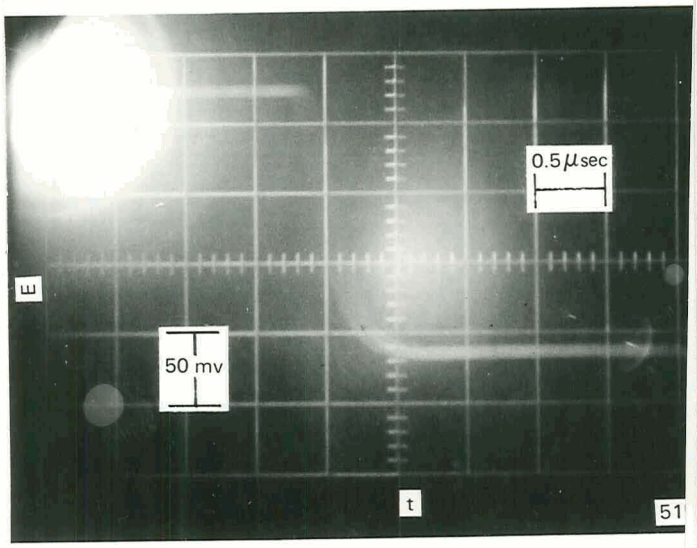

g) C.S.V.; Anodic Short Pulse
T = 121°C; i = 82 ma/cm^2
Trace #13

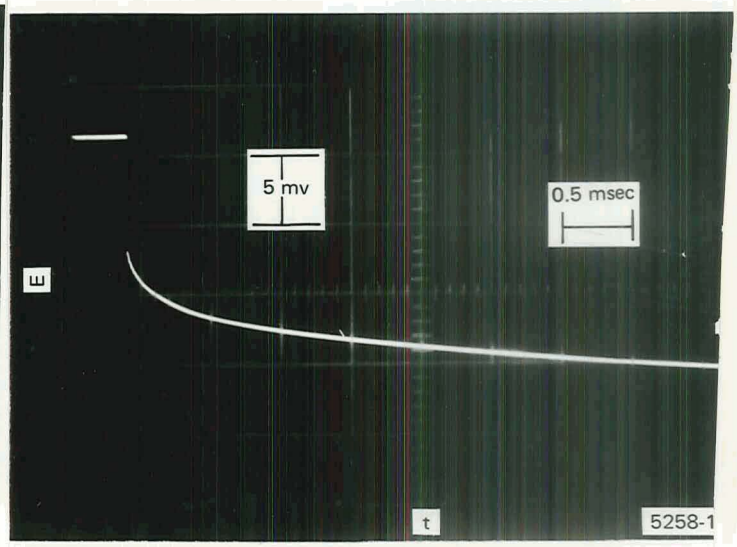

h) C.S.V.; Anodic Long Pulse
T = 121°C; i = 4.1 ma/cm^2
Trace #12

Fig. 29: Voltammetry of $Al/AlCl_3$ System

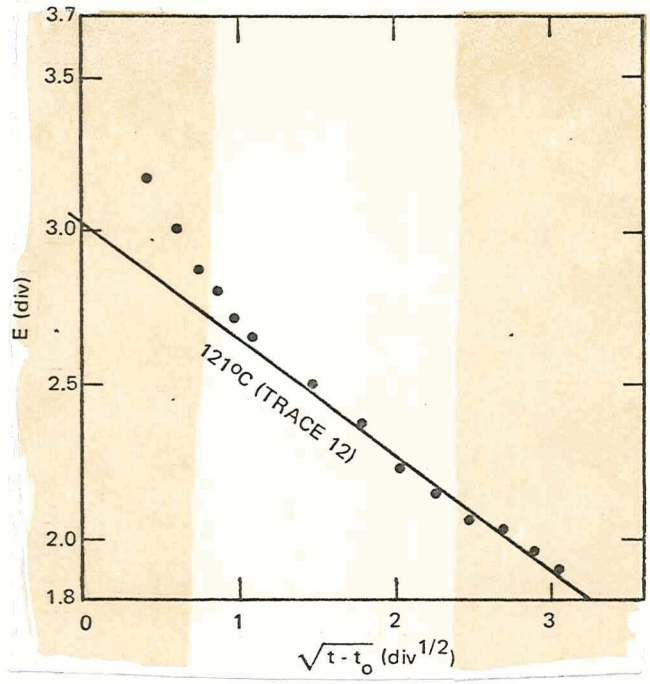

i) E vs $t^{1/2}$ Plot

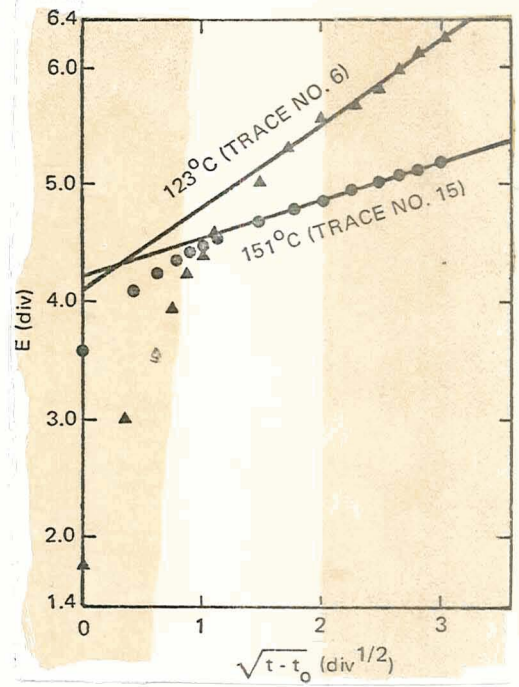

j) E vs $t^{1/2}$ Plot

Fig. 29: Voltammetry of $Al/AlCl_3$ System

varied from 4.8 to 9.6 Ω, suggesting that a film was formed and partially broken off. The cell behavior then became very erratic, precluding the measurement of meaningful high temperature data.

In view of the relatively low i_o values, the aluminum electrode does not appear to be as reversible as the Zn electrode and therefore will not yield batteries with as high power densities as Zn. However, as will be shown in a following section, the energy densities of batteries with Al electrodes will be considerably higher.

e) Voltammetry Results of Hydroxide-containing Melts

(1) NaOH-KOH Solvent

A cyclic voltammogram of an equimolar NaOH-KOH melt taken at 315°C with platinum electrodes is presented in Fig. 30. This system was made anhydrous by reacting the water with sodium metal. A cathodic

sweep from the open circuit voltage, A, yields the reduction wave for Na(I). All the voltages in the hydroxides are taken with respect to Na(I) reduction. When the voltage is reversed, B, peak C, presumably due to Na stripping, occurs and then peak D, which may be H_2 oxidation. Just prior to the limiting reaction

$$2\ OH^- - 2e \rightarrow H_2O + 1/2\ O_2$$

there appears to be two anodic peaks, E, which have been suggested to be oxide ion oxidation to peroxide[36] and superoxide.[37] Reversal at the anodic limit yields peaks F and G (reduction of O_2^- and/or $O_2^=$ formed by oxide oxidation)[37] and then a long wave, H, beginning at about 0.6 v; none of the three waves show cathodic current indicating that oxidation is occurring also. The wave, H, which also is present in these melts before sodium is added, is assumed to be due to the reduction of H_2O[36] formed in the OH^- limiting reaction above

$$H_2O + e \rightarrow OH^- + 1/2\ H_2$$

or

$$H_2O + 2e \rightarrow OH^- + H^-.$$

However, the hydride is not stable in the presence of OH^- and will react forming hydrogen and oxide ion

$$H^- + OH^- \rightarrow H_2 + O^=.$$

The lack of a distinct peak for the water reduction wave may be due to the reduction of hydrogen formed as a product at H. This may also be the cause of peak I.

An anodic sweep from the open circuit voltage, A, is also presented in the figure. Wave D is present, although smaller in amplitude, and the rest of the voltammogram is identical. The occurrence of D in the

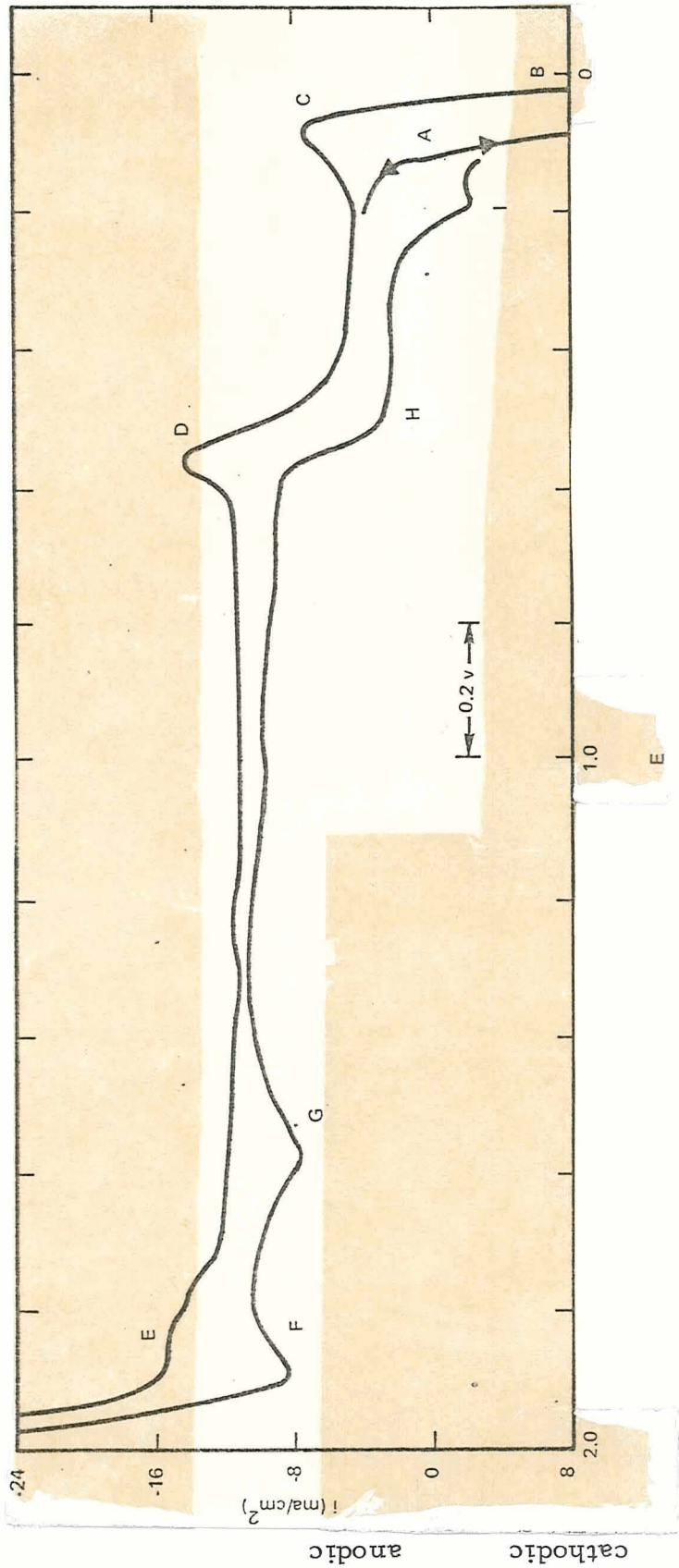

Fig. 30: Voltammetry of NaOH-KOH Solvent
T = 315°C; s = 46 mv/sec
Pt electrodes

anodic sweeps suggests that hydrogen is still being formed by the slow reaction of Na with the melt. Since current occurs at A immediately with cathodic or anodic sweeps, no background current was measured.

In a hydroxide melt containing some water the open circuit potential is usually about 0.7 to 0.8 v, anodic of the water reduction wave H. A cathodic sweep starting from zero current shows the reduction wave for water. The rest of the voltammogram is similar to that in Fig. 30, except that peak E is much smaller or gone completely. Since the open circuit potential in hydroxide melts containing water is anodic of peak D, this peak cannot appear unless a cathodic sweep for the reduction of water is run first. It was found that hydroxide melts that were not completely water-free showed reduction waves for many of the metal oxide systems studied below. These diffusion-limited waves indicated that the electrode metal ion was soluble in the incompletely dehydrated melt.

The working voltage span for anhydrous NaOH-KOH with platinum electrodes is about 2.0 v in the temperature range 200 to 300°C. The cathodic limit is set by Na(I) reduction and the anodic limit by hydroxide oxidation.

(2) $\underline{Ag/Ag_2O}$

In a hydroxide melt containing some water, a diffusion-limited cathodic wave was present after Ag was anodized. This indicates that Ag(I) has some solubility in the non-anhydrous melt. In the anhydrous melt open circuit voltages for Ag/Ag_2O (with Na_2O added in an attempt to increase the Ag_2O solubility by formation of an argenate ion[38]) were 1.63 to 1.82 v in the temperature range 200 to 300°C. Cathodic sweeps yielded waves but they were not diffusion-limited and did not start from the rest potential. This

result showed that little, if any, electroactive silver was in solution and the Ag/Ag_2O couple was not reversible. These observations indicated that the silver couple in anhydrous hydroxides would not be useful as a soluble cathode in batteries and precluded further voltammetric measurements on this system. The possible use of a solid Ag/Ag_2O cathode remains, however. A cyclic voltammogram (Fig. 5 A) and further discussion have been included in Appendix IV.

(3) Cu/Cu_2O

In NaOH-KOH with some water a cathodic diffusion-limited wave appeared after the Cu electrode was anodized. Thus Cu(I) is soluble in wet melts (see Fig. 6 A, b). In an anhydrous system rest potentials of about 0.8-0.9 v were measured at 200 to 300°C for Cu/Cu_2O with Na_2O added to help form CuO_2^{-3}.[39] Although cathodic and anodic sweeps both yielded small waves from the open circuit voltage, these waves were not well-defined, diffusion-limited ones in appearance. The small magnitude of the waves measured, indicating a low concentration of electroactive species in solution, and the uncertainty as to their origin, i.e. if they were due to a soluble copper entity, was evidence that the Cu/Cu_2O couple in this medium was not a satisfactory one for battery applications. The use of solid Cu/Cu_2O cathodes is not precluded, however. Two L.S.V. figures (6 A a and b) along with comments have been added to Appendix IV.

(4) Cu/CuO

The rest potential of Cu/CuO with Na_2O initially was 0.4 v at 300°C but it changed slowly with time approaching the values for the Cu/Cu_2O system. The results were similar to those for Cu/Cu_2O and suggest that the CuO is being reduced to Cu(I). A cyclic voltammogram (Fig. 7 A) and discussion are included in Appendix IV.

(5) Cd/CdO

In wet hydroxides a soluble Cd(II) was found as for the other metal ions above. Open circuit potentials of 0.70 to 0.60 v at 200 to 300°C were found for Cd/CdO with Na_2O added to the anhydrous melt. Small non-diffusion limited waves indicated that little soluble Cd(II) was in solution and the couple was not evaluated further. Voltammograms of the system may be found in Appendix IV (Fig. 8 A a and b).

(6) Be/BeO

An open circuit potential of about 0.1 v was observed at 300°C. The beryllium had reacted with any water originally present in the melt. Only a small anodic wave occurred indicating passivation of the electrode (presumably by a BeO film). This wave decreased in size with temperature and/or time. This passivation would preclude the use of beryllium anodes in hydroxide melts. A voltammogram and discussion have been included in Appendix IV (Fig. 9 A).

(7) Mg/MgO

Magnesium dissolves in the hydroxides yielding a bluish melt. This incompatibility negates the utilization of Mg anodes in molten hydroxides. A voltammogram taken before all the indicator had reacted is shown in Appendix IV (Fig. 10 A).

(8) Zn/ZnO

In the incompletely dehydrated hydroxide melt without added ZnO a cathodic sweep yielded a well defined diffusion-limited wave from the open-circuit potential, 0.62 v at 300°C. This wave suggests that the zinc electrodes had reacted with the melt to a small extent forming soluble

Zn(II). An anodic sweep produced a limiting wave (Zn oxidation) from the rest potential. The addition of Na to the melt shifted the rest potential to about 0.30 v and removed the soluble Zn(II). The addition of ZnO + Na_2O did not cause any obvious changes. On sweeps, small cathodic and anodic currents at the rest potential were obtained and these led into other larger waves (see Fig. 11 A-insert). The anodic limiting wave was still present but it now lies about 0.2 v anodic of the open circuit potential (Fig. 11 A). Thus, although Zn may be utilizable as an anode in molten hydroxides (if reaction with the melt is not excessive), it does not appear to show as reversible behavior in the anhydrous system as in melts where sodium (or Na_2O) has not been added.

(9) $\underline{Al/Al_2O_3}$ –

Aluminum showed no anodic current until voltages greater than 2.5 v were attained and even then the current was small. The fact that large voltages could be impressed on this electrode suggests that a large IR drop was present due to a resistant oxide film. (The presence of a high resistance in the cell was verified.) This film could be removed by cathodization (see Fig. 12 A) but it must reform immediately since no stripping wave of any size occurred. These results show that aluminum cannot be employed as anode material in this system.

E. Evaluation of Couples for Battery Application

In order to evaluate the systems of this study for their potential battery utilization, some pertinent data have been tabulated to afford ready comparisons. These data include the voltages and exchange current densities measured as well as another important quantitative parameter, the calculated energy densities for all the anode and cathode combinations. In addition to these values, some of the results of the linear sweep voltammetry measurements are also presented to afford a comparison between this technique and the current-step voltammetry. A discussion of the results follows each table. Since none of the couples in the anhydrous NaOH-KOH melts appeared particularly promising, they have been excluded from this section but will be treated briefly in a later section (Systems Recommended for Further Study). Next, the parameters considered in the evaluation and the rating system for each of these criteria are given. Then each system is rated in all the categories and the results are judged and reviewed. Finally, from this evaluation some of the more promising systems will be recommended for further study.

1. Summary of Results

The voltages of the various cathode couples vs a Zn anode in $ZnCl_2$-NaCl-KCl and vs Zn and Al anodes in $AlCl_3$-NaCl are given in Table 34. In those cases where the measured potentials were not at the temperature listed, they were obtained by interpolation. For the Bi/$BiCl_3$ couple the emf at 275° was extrapolated from the 220 and 250°C values. For the $CrCl_2$ + $CrCl_3$ redox couple in $AlCl_3$-NaCl no open circuit voltages could be measured; the values tabulated were the potentials midway between the anodic and cathodic peaks formed during the linear voltammetric sweeps.

TABLE 34

Voltages of Couples (0.1 M) vs Zn in

$ZnCl_2$-NaCl-KCl and vs Zn and Al in $AlCl_3$-NaCl

Couple	Voltage (v)								
	vs Zn[a]			vs Zn[b]			vs Al[b]		
	225°	275°	325°	120°	150°	200°	120°	150°	200°
Ag/AgCl	(0.355)[c]	(0.370)[c]	0.455	0.472	0.431	0.415	0.662	0.646	0.640
Cu/CuCl	—	0.395	(0.310)[c]	0.449	0.400	0.370	0.639	0.612	0.595
$Ni/NiCl_2$	0.573	0.543	0.545	0.648	0.632	0.627	0.838	0.847	0.852
$Bi/BiCl_3$	0.717	0.640[d]	—	0.530	0.480	—	0.720	0.695	—
$Sb/SbCl_3$	0.716	0.662	—	0.783	0.765	0.767	0.973	0.980	0.992
$W/CrCl_2$, $CrCl_3$	0.920	0.945	0.959	1.01[e]	1.03[e]	1.08[e]	1.20[e]	1.25[e]	1.30[e]
W/CuCl, $CuCl_2$	1.430	(1.30)[c]	1.400	1.684	1.657	1.653	1.874	1.872	1.878
$W/FeCl_2$, $FeCl_3$	1.320	(1.30)[c]	1.340	1.780	1.725	1.670	1.970	1.940	1.895

a) In $ZnCl_2$-NaCl-KCl

b) In $AlCl_3$-NaCl

c) Value questionable

d) Extrapolated value

e) Interpeak voltage

The added concentration of electrochemically active materials to the catholyte in all cases and to the anolyte in the redox systems and in $Zn/ZnCl_2$ in $AlCl_3$ was 0.1 M (assuming complete solution). A comparison of the data shows that all the voltages are larger in the $AlCl_3$ melts than in the $ZnCl_2$ with two exceptions, Ag/AgCl and $Bi/BiCl_3$. The Ag/AgCl emf's in $ZnCl_2$-NaCl-KCl at 222 and 270° are believed to be in error since other parameters in this system (i_p and $CD^{1/2}$) suggested that incomplete solution had occurred at these temperatures. Note also that the temperature coefficient for Ag/AgCl in $ZnCl_2$ is opposite to that in $AlCl_3$. Unfortunately, there was not enough time to recheck any of the cells. Since the Ag couple is expected to be lower in the electrochemical series than Cu/CuCl, a potential greater than 0.40 v would be estimated for Ag/AgCl at 275°. The Ag/AgCl values, as well as some others that appear to be questionable, have been set in parentheses. The lower voltages for $Bi/BiCl_3$ in the $ZnCl_2$ melt is probably due to the presence of different valence states of bismuth in this media and in $AlCl_3$. In $ZnCl_2$ it appears that Bi(III) exists whereas in $AlCl_3$ Bi(I) occurs. Otherwise, the data indicate that, as expected, Al is the more electronegative anode. For cathodes, the redox couples yield the largest voltages and these voltages can be made greater by increasing the concentration ratio of higher-to-lower-valent salt. In an actual battery the concentration of catholyte might be about ten times greater, if solubility is not limiting, and the voltages would then increase (e.g., an additional 0.084 v for n = 1 at 150°C and 0.108 v for n = 1 at 275°C). In spite of these potential increases in voltage, the potentials of some of the more soluble couples, Ag/AgCl and Cu/CuCl vs Zn or Al, are low.

The average exchange current densities determined from C.S.V. for the couples in $ZnCl_2$-NaCl-KCl and in $AlCl_3$- NaCl are listed in Table 35.

TABLE 35 A

Exchange Current Densities[a] of Couples in

$ZnCl_2$-NaCl-KCl and in $AlCl_3$-NaCl

Couple[b]	i_o (amp/cm^2)					
	$ZnCl_2$-NaCl-KCl			$AlCl_3$-NaCl		
	225°	275°	325°	120°	150°	200°
Ag/AgCl	0.18	1.1	1.2	0.2	1.1	1.6
Cu/CuCl	0.05	0.3	3.	0.9	0.1	0.4
Ni/$NiCl_2$	—	—	—	—	—	—
Bi/$BiCl_3$	0.11	0.16	—	0.008	0.013	—
Sb/$SbCl_3$	0.01	0.05	—	0.02	0.04	0.06
W/$CrCl_2$, $CrCl_3$	0.14	0.3	0.6	—	—	—
W/CuCl, $CuCl_2$	0.3	0.6	4.	0.17	0.2	2.
W/$FeCl_2$, $FeCl_3$	0.06	0.16	0.08	0.09	0.3	0.4
Zn/$ZnCl_2$[c]	0.11	0.3	2.	0.06	0.13	0.4
Al/$AlCl_3$	—	—	—	0.006	0.09	—

a) Determined from C.S.V.

b) Catholyte concentration = 0.1 M

c) $ZnCl_2$ concentration = 0.1 M in $AlCl_3$-NaCl

As can be seen the exchange current usually increases rapidly with temperature. It will also increase with concentration of the electroactive species (and with the concentration of active sites on the solid electrode). The values for Cu/CuCl in $AlCl_3$ were erratic and show a questionable non-linear change with temperature. The cathodes exhibiting the highest i_o values are Ag/AgCl in both solvents, W/CuCl, $CuCl_2$ in both solvents and Cu/CuCl in $ZnCl_2$ at the highest temperatures. At corresponding temperatures, i.e., 225° for $ZnCl_2$ melts and 200°C for $AlCl_3$, the exchange current density for every couple is appreciably greater in the $AlCl_3$ solution with one exception. The exception is the $Zn/ZnCl_2$ couple which has a hundred-fold larger concentration in the $ZnCl_2$ solvent than in the $AlCl_3$. The somewhat higher value of i_o for $Zn/ZnCl_2$ in the $ZnCl_2$ solvent suggests that the $ZnCl_2$ has a low activity in the latter solvent.

Values of the exchange current densities were also determined from the linear sweep voltammograms, wherever possible, with the aid of the relation

$$i_o = \left(\frac{RT}{nFA}\right)\left(\frac{dI}{dE}\right)_{E=E_{eq}}$$

and are presented in Table 35b. The slopes were corrected for R_s, the electrolyte resistance, to yield R_p, the charge transfer resistance. No values were obtained for the redox systems or for $Zn/ZnCl_2$ in $AlCl_3$-NaCl at the higher temperatures because of the relatively poor sensitivity of the data. Values for the $Ni/NiCl_2$ couple in both solvents were calculated only when anodic sweeps were available since all the cathodic waves exhibited shoulders initially. Most of the L.S.V. i_o data are lower but are in fair agreement with those from C.S.V. in Table 35a. The $Al/AlCl_3$ couple

TABLE 35B

Exchange Current Densities[a] of Couples in

$ZnCl_2$-NaCl-KCl and in $AlCl_3$-NaCl

Couple[b]	i_o (amp/cm^2)					
	$ZnCl_2$-NaCl-KCl			$AlCl_3$-NaCl		
	225°	275°	325°	120°	150°	200°
Ag/AgCl	0.05	> 0.3	> 0.6	0.1	0.3	0.5
Cu/CuCl	0.05	0.09	0.2	0.06	0.03	0.3
Ni/$NiCl_2$	0.01[d]	-	-	0.008[d]	0.02[d]	0.03[d]
Bi/$BiCl_3$	0.05	0.08	-	0.02	0.04[d]	-
Sb/$SbCl_3$	0.008	0.03	-	0.004	0.02	0.05
Zn/$ZnCl_2$[c]	0.2	0.3	0.5	0.06	-	-
Al/$AlCl_3$	-	-	-	0.006	0.02	0.2
				0.003[d]	0.01[d]	0.1[d]

a) Determined from L.S.V.; cathodic sweeps except where noted.

b) Catholyte concentration = 0.1 M

c) $ZnCl_2$ concentration = 0.1 M in $AlCl_3$-NaCl

d) From anodic sweep

appears to have different exchange currents for anodic and cathodic sweeps with the cathodic values being larger. This agrees with the one set of data obtained by C.S.V. at 124° and with the results of Del Duca in various $AlCl_3$-LiCl-KCl systems.[35] However, in a 50-50 mole % NaCl-$AlCl_3$ melt the anodic exchange currents were found to be larger.[35]

Another measure of the irreversibility (or the exchange current) of an electrode is the shift of the peak voltage with sweep rate in the linear sweep voltammograms. These values have been cast into a semi-quantitative parameter $(E_{p_j} - E_{p_1})/m$ and are presented in Table 36. $(E_{p_j} - E_{p_1})$ denotes the shift in peak voltage between sweep rates 1 and j, and as before $m = \sqrt{s_j/s_1} = j = 2$, 3 and 4. The data tabulated are the averages of the three values at each temperature. Thus those couples with low values in Table 36 show good reversibility whereas those with high numbers should be irreversible. Some of the values in the tabulation, e.g., those for Ag/AgCl and Cu/CuCl in $ZnCl_2$, are questionable and have been set in parentheses. The data for these two couples (see Tables 16a and 17a) are constant for the first three sweeps and then show a large change in E_p in going from the third to fourth sweep. If these two couples were truly irreversible, a gradual change in peak voltage with increasing sweep rate would be expected over the whole range studied. This abrupt increase in voltage in the case of two couples with apparently high exchange currents is probably due to the response time of the recorder being exceeded.

The extent of reversibility of an electrode as determined by its exchange current appeared to be in agreement, in general, with that indicated in Table 36 from the linear sweep voltammetry. However, several of the metal/metal ion couples (e.g., Ag/AgCl in $AlCl_3$, Cu/CuCl in $AlCl_3$ at

TABLE 36

Variation in Peak Voltage with Sweep Rate

Couple	$(E_{p_j} - E_{p_1}) / m$ [a] (mv)					
	$ZnCl_2$-NaCl-KCl			$AlCl_3$-NaCl		
	225°C	275°C	325°C	120°C	150°C	200°C
Ag/AgCl	(4)[b]	0	(2)[b]	32	26	14
Cu/CuCl	(5)[b]	1	1	1	5	27
$Ni/NiCl_2$	0	1	3	7	1	5
$Bi/BiCl_3$	25	6	—	21	18	—
$Sb/SbCl_3$	23	3	—	10	38	69
$W/CrCl_2$, $CrCl_3$	0	0	0	—	—	—
W/CuCl, $CuCl_2$	6	2	0	8	4	0
$W/FeCl_2$, $FeCl_3$	7	1	1	0	1	0
$Zn/ZnCl_2$	—	—	—	4	11	12

a) $E_{p_j} - E_{p_1} / m$ = average shift in peak voltage j from peak voltage 1 divided by square root of ratio of sweep voltage j to 1; j = m = 2, 3, 4

b) These values are questionable because they involve a sudden large change in E_p

190° and $Zn/ZnCl_2$ in $AlCl_3$ at 205°) which had high i_o values exhibited large shifts in peak voltage with sweep rate. However, the exchange current and L. S. V. measurements were taken in different time scales and this may account for the differences. The number of equivalents of current passed was much greater in the L. S. V. than in the C. S. V. sweeps. In the L. S. V. measurements about 30 monolayers of metal (assuming an atomic volume of 10-15 cc and uniform deposition) are deposited in our systems by the time the wave peak is reached; in the C. S. V. less than one monolayer is deposited. Thus if the rate-determining mechanism were migration of ions or atoms on the surface of the electrode before incorporation into the crystal lattice, it is reasonable that the kinetics at short times (and after few coulombs as in the C. S. V.) would be different than at longer times (and many coulombs) when a different surface is present. The shoulders or inflections near the initial part of the L. S. V. waves in the copper and nickel systems in both solvents may be extreme examples of this behavior. Thus the initial part of the wave commences with infinite slope, corresponding to the deposition of the first monolayer on active sites, where lower potentials are required, and then the subsequent deposition rate decreases. (For waves with shoulders, e. g., $Ni/NiCl_2$, the initial current change cannot be entirely capacitative or pseudo-capacitative since on reversal the current change would have to be twice as large. Further, such wave shapes would indicate an irreversible or poorly poised couple. This is not in agreement with the C.S.V. voltammetry results.) The larger shoulders in the $AlCl_3$ systems than in the $ZnCl_2$ for both couples may be a specific effect of the medium or may be the effect of temperature or both. The larger voltages required to plate out the metals are seen in virtually all of the metal/metal ion systems where

$E_{eq}-E_p$ values are greater than theory predicts. These larger potentials infer that the freshly deposited metal has a greater activity than the substrate.

Another discrepancy that arises between the L.S.V. and C.S.V. measurements is in the calculated values of $CD^{1/2}$ in some of the metal/ion systems. In both the $ZnCl_2$ and $AlCl_3$ melts poor agreement in $CD^{1/2}$ (difference greater than a factor of two) was found for the nickel, bismuth and antimony couples. The agreement was also observed to be poor for Cu/CuCl in $AlCl_3$ at the lower temperatures. (Although the average Cu/CuCl in $ZnCl_2$ solution data were in reasonable accord, the $CD^{1/2}$ values from C.S.V. varied with applied current indicating the couple does not behave in a simple manner.) However, all of these couples also showed other examples of poor and non-simple behavior. It is interesting that the redox systems, where no metal is deposited during the measurements, exhibited more reasonable behavior, with the possible exception of $FeCl_2$, $FeCl_3$ in $ZnCl_2$ at 225°C. However, these data appear consistent for a poorly reversible couple. These results suggest that with metal/metal ion electrodes another mechanism, e.g., crystallization polarization, plays an important role in the electrode kinetics. This effect probably accounts for at least some of the differences between the L.S.V. and C.S.V. results. In the redox systems, where no metal is electrodeposited, polarization produced by crystallization on solid metal surfaces would, of course, not take place. Thus for metal/metal ion studies the linear sweep voltammetric technique does not give definitive results as to electrode reversibility. However, for battery feasibility any source of polarization is important and so the longer time results of the L.S.V. are probably more meaningful than those of the C.S.V.

The theoretical energy densities for cells with Zn anodes in $ZnCl_2$-NaCl-KCl at a median temperature of 275°C and with Zn and Al anodes in $AlCl_3$-NaCl at a median temperature of 150°C are presented in Table 37. These data were calculated with the relation

$$E.D. \text{ (watt-hrs/lb)} = 12{,}180 \ nE/\Sigma(gm)_{react}$$

where $\Sigma(gm)_{react}$ denotes the sum of the stoichiometric atomic and molecular weights in grams of the reactants in the cell reaction. For values of E the measured voltages at 275 and 150° in Table 34 were employed with three changes in the $ZnCl_2$ systems: for Ag/AgCl E = 0.410 v, for CuCl, $CuCl_2$ E = 1.40 v, and for $FeCl_2$, $FeCl_3$ E = 1.32 v. These values were substituted for the measured ones because they appear to be more reasonable. The results indicate that the $AlCl_3$ systems are generally better than the $ZnCl_2$ and, as expected, the Al anode yields higher values than Zn. The best cathodes in all systems are the copper chloride and iron chloride redox couples along with $Ni/NiCl_2$ and $Sb/SbCl_3$ in the $AlCl_3$ melt. However, none of the cells have exceedingly high energy densities and those for the highly soluble cathodes, AgCl and CuCl, are among the lowest of any of the systems. It thus appears that the chief advantage of these systems for batteries would be their potentially high current drains, i.e. their potentially high power densities. Unfortunately, no appropriate data to check this aspect are available.

2. Criteria for Battery Evaluation

The criteria that will be considered in judging the systems for battery feasibility are the following: voltage, energy density, exchange current density, solubility of catholyte, volatility of solvent and/or catholyte, and a general category which will encompass such considerations as cost,

TABLE 37

Theoretical Energy Densities of Cells in

$ZnCl_2$-NaCl-KCl at 275°C and in $AlCl_3$-NaCl at 150°C

Cathode	E.D.[a] vs. Zn-$ZnCl_2$ (watt-hrs/lb)	E.D.[b] vs. Zn-$AlCl_3$ (watt-hrs/lb)	E.D.[c] vs. Al-$AlCl_3$ (watt-hrs/lb)
Ag/AgCl	28.0[d]	29.8	51.6
Cu/CuCl	36.5	37.0	69.3
Ni/$NiCl_2$	67.8	78.9	139.4
Bi/$BiCl_3$	57.4	21.1	33.3
Sb/$SbCl_3$	74.2	85.7	140.0
W/$CrCl_2$, $CrCl_3$	60.2	65.7	90.8
W/CuCl, $CuCl_2$	102.0[e]	120.5	159.0
W/$FeCl_2$, $FeCl_3$	82.4[f]	107.8	138.0

a) Zn anode in $ZnCl_2$-NaCl-KCl at 275°C

b) Zn anode in $AlCl_3$-NaCl at 150°C

c) Al anode in $AlCl_3$-NaCl at 150°C

d) Voltage of 0.410 used

e) Voltage of 1.40 used

f) Voltage of 1.32 used

thermodynamic stability and dendrite formation. The order taken for these parameters was not meant to denote their relative importance but does place first those categories where data are available. All the systems will be rated in each of the above categories in terms of A, B, C, etc. Thus in judging the voltage of the cells, we give an A rating to voltages above 1.5, B for $E \geq 0.9$ v, C for E 0.5 v, and D for $E < 0.5$ v. Large voltages not only yield batteries of greater energy and power densities but also minimize the effect of IR losses. For the energy densities, values greater than 135 watt-hrs/lb are rated A, $B \geq 90$, $C \geq 50$, and $D < 50$. For the exchange current densities the median values were considered with $A \geq 1$ amp/cm^2, $B \geq 0.3$, $C \geq 0.1$, $D \geq 0.02$, and $E < 0.02$. Couples with high exchange current densities are desirable for batteries because larger current drains can be accommodated and they should be more utilizable in secondary batteries due to their ready rechargeability. This rating system is obviously an arbitrary one but should serve to delineate the different cells into several distinct classes. In the remaining categories where no quantitative parameters are available the classification is divided into fewer grades. For solubility, those catholytes which can form 15 wt % solutions are rated A, those above or about 0.1 M are B, and those well below 0.1 M are C. Although this gives less weight to insoluble cathodes, it doesn't rule out completely the possibility of using a solid cathode in a battery. Those systems which have no volatile materials are A-rated; if a solvent component is volatile it is B and if a catholyte is volatile it is C or D depending on the temperature range. The volatility of a solvent component is a minor detriment since these systems would have to be hermetically sealed to protect them from moisture and oxygen. (To minimize distillation, care will have

to be taken to prevent cold spots in the system.) However, if a catholyte is volatile or decomposes (e.g., $CuCl_2$ - $CuCl + 1/2\ Cl_2$), the problem is more severe since vaporization can occur into the anode compartment causing a vapor short circuit. As for dendrite formation the disadvantage occurs when recharging is required (i.e., for secondary batteries) since it can give rise to separator penetration.

3. Results of Evaluation

The cells are rated in the above categories for the $ZnCl_2$ systems in Table 38a, for the $AlCl_3$ systems with Zn anodes in Table 38b and with Al anodes in Table 38c. The grades were based on the data listed in Tables 34, 35, and 37 as well as elsewhere in this report. The exchange current rating for the $Ni/NiCl_2$ couple was estimated from the results in Table 35b as well as from a comparison of the variation of the peak voltage with sweep rate for the systems in Table 36. The cathodic exchange current ratings are meaningful for battery evaluation if the cathode were the limiting electrode. This is not the case for many of the couples, especially in the $AlCl_3$ melts where both Zn and Al have low i_o values. However, this problem can be rectified in practice by increasing the area of the anode so that the exchange current for anode and cathode are approximately equal.

Giving equal weights to all the categories, one finds that the cells with the highest ratings are in order: W/CuCl, $CuCl_2$ vs Al in $AlCl_3$; $W/FeCl_2$, $FeCl_3$ vs Al in $AlCl_3$; and $W/CrCl_2$, $CrCl_3$ vs Zn in $ZnCl_2$. A common drawback for all three of these systems is the relatively low solubility, of the order of 0.1 M, of the higher-valent salt. This aspect may not be too serious since many excellent batteries today function with insoluble, or only slightly soluble, electroactive components, e.g., lead-acid,

TABLE 38 a

Evaluation of Cells with Zn Anodes in $ZnCl_2$-NaCl-KCl

Couple	Voltage[a]	Energy[b] Density	Exchange[c] Current	Catholyte[d] Solubility	Volatility[e]	Other[f]
Ag/AgCl	D	D	A	A	A	C
Cu/CuCl	D	D	B	A	A	B
$Ni/NiCl_2$	C	C	(C)[g]	C	A	B
$Bi/BiCl_3$	C	C	C	A-B	A	B
$Sb/SbCl_3$	C	C	D	A-B	D	B
$W/CrCl_2$, $CrCl_3$	B	C	B	B-C	A	B
W/CuCl, $CuCl_2$	B	B	B	B	A	D
$W/FeCl_2$, $FeCl_3$	B	C	C	B	D	B

TABLE 38 b

Evaluation of Cells with Zn Anodes in $AlCl_3$-NaCl

Couple	Voltage[a]	Energy[b] Density	Exchange[c] Current	Catholyte[d] Solubility	Volatility[e]	Other[f]
Ag/AgCl	D	D	A	A	B	C
Cu/CuCl	D	D	B	A	B	B
$Ni/NiCl_2$	C	C	(C)[g]	C	B	B
$Bi/BiCl_3$	C	D	E	B	B	C
$Sb/SbCl_3$	C	C	D	B	C	B
$W/CrCl_2$, $CrCl_3$	B	C	—	C	B	B
W/CuCl, $CuCl_2$	A	B	C	B	B	B-C
$W/FeCl_2$, $FeCl_3$	A	B	C	B	C	B

TABLE 38c

Evaluation of Cells with Al Anodes in $AlCl_3$-NaCl

Couple	Voltage[a]	Energy[b] Density	Exchange[c] Current	Catholyte[d] Solubility	Volatility[e]	Other[f]
Ag/AgCl	C	C	A	A	B	C
Cu/CuCl	C	C	B	A	B	B
$Ni/NiCl_2$	C	A	(C)[g]	C	B	B
$Bi/BiCl_3$	C	D	E	B	B	C
$Sb/SbCl_3$	B	A	D	B	C	B
$W/CrCl_2$, $CrCl_3$	B	B	—	B	B	B
W/CuCl, $CuCl_2$	A	A	C	B	B	B-C
$W/FeCl_2$, $FeCl_3$	A	A	C	B	B-C	B

a) Voltage rating: A $\geq$ 1.5 v; B $\geq$ 0.9 v; C $\geq$ 0.5 v; D < 0.5 v

b) Energy density: A $\geq$ 135 watt-hrs/lb; B $\geq$ 90; C $\geq$ 50; D < 50

c) Exchange current density: A $\geq$ 1 amp/cm^2; B $\geq$ 0.3; C $\geq$ 0.1; D $\geq$ 0.02; E < 0.02

d) Solubility: A $\geq$ 15 wt %; B $\geq$ 0.1 M; C < 0.1 M

e) Volatility: Non-volatile = A; solvent volatile ($AlCl_3$) = B; catholyte volatile = C in $AlCl_3$ melt and D in $ZnCl_2$ melt

f) Other: Zn anodes — dendrites; Ag — cost, dendrites; Bi in $AlCl_3$ — reaction with $BiCl_3$; $CuCl_2$ — decomposes at higher temperatures

g) Based on linear voltammetric sweep results — Tables 35b and 36.

Ni-Cd. Thus if the catholyte can dissolve at a fast enough rate to maintain a reasonable concentration at the cathode under load, adequate current drain may be effected. Another disadvantage for each of the first two systems is the volatility of $FeCl_3$ and instability of $CuCl_2$ at higher temperatures. Although the two catholytes are affected less in the $AlCl_3$ melt (since the temperatures are lower), direct reaction between the anode and the vapor may occur yielding an effective short circuit. If highly soluble catholytes are desired, the Ag/AgCl or Cu/CuCl vs Al in $AlCl_3$ appear to offer the most promise. The catholytes are stable, non-volatile and have good exchange current densities. The problems with these two couples are their low voltages and energy densities, together with the need for an effective membrane or barrier to separate the catholyte from the anode. The need for a suitable barrier, of course, is common to all cells where any catholyte or anolyte is present in solution. A final system which appears interesting is $Ni/NiCl_2$ vs Zn in $ZnCl_2$. Here a solid cathode would have to be employed but the separator problem would not be as important.

4. Systems Recommended for Further Study

The halide systems which appear to hold the most promise for battery feasibility are the (In)/CuCl, $CuCl_2$ vs Al and (In)/$FeCl_2$, $FeCl_3$ vs Al both in $AlCl_3$-NaCl, and (In)/$CrCl_2$, $CrCl_3$ vs Zn in $ZnCl_2$-NaCl-KCl. Here (In) represents an inert, preferably inexpensive, electrode such as graphite. Three additional systems that appear interesting are Ag/AgCl vs Al and Cu/CuCl vs Al both in $AlCl_3$-NaCl, and $Ni/NiCl_2$ vs Zn in $ZnCl_2$-NaCl-KCl. The silver and copper couples have highly soluble catholytes, in contrast to the redox electrodes, and should support high current drains. The Ni couple would have to be a solid cathode and thus may suffer under

heavy loads. However, its high coulombic efficiency, as determined by the approximately equal areas under the anodic and cathodic L.S.V. peaks, and other electrochemical behavior, as well as the need for a less stringent separator are arguments in its favor. These systems are reviewed below.

Finally, two hydroxide systems which should be investigated to some extent are Cu/Cu_2O vs Na and Cu/Cu(I) vs Zn. In the first cell the anode compartment or the whole system would be anhydrous whereas in the second the system would not be anhydrous. These aspects are treated in greater detail below also.

In all batteries the discharge behavior under various loads, the self-discharge rate and the fraction of theoretical capacity realized are among the most important practical parameters to be determined. Acceptable values of these parameters depend on the type of battery desired. Thus for batteries which are meant to deliver small currents or high current drains for short times only, the voltage under load should be reasonably constant with time. For short-life batteries the self-discharge rate can be higher than for long-life cells. To minimize self-discharge, efficient separators between the anode and cathode compartments must be employed. This problem is common to all batteries but is more important in molten salt cells where diffusion and corrosion are more severe.

For secondary batteries the charge-discharge characteristics must be examined. Here the problem of shorting due to dendrite formation becomes important; this is especially true in the case of zinc anodes. However, it is possible that if one stays below a certain critical charging overvoltage or current, dendrites do not form. If this is the case, the critical value would have to be determined for each cell configuration tested.

Another aspect that must be examined is the retention of capacity on cycling; this will almost certainly be dependent on the depth and rate of discharge. Finally, container sealing (air must be excluded) and corrosion difficulties and the ability of cells to withstand thermal cycling are other common problems of these molten salt batteries. All the above aspects are common to the cells to be discussed and will not be pursued further.

a) Redox Cells in $AlCl_3$ and $ZnCl_2$ Melts

The chief difficulty with these systems may be the relatively low solubility of the catholyte so that adequate currents cannot be sustained under load. Another disadvantage for the $CuCl_2$ and $FeCl_3$ cells is the possibility of a short circuit occurring by oxidizing agents attacking the anode via the vapor phase. This problem would become more severe at higher temperatures. To minimize concentration polarization, various electrode geometries, configurations and physical modes of construction of solid cathodes should be tested. For the vapor phase attack of the anode a partition with a small hole for pressure equalization can be employed as a hindrance.

b) Soluble Cathodes in $AlCl_3$-NaCl

With Ag/AgCl or Cu/CuCl cathodes there is no immediate problem of sustaining high current densities due to concentration polarization. Thus the cathodes involve a much simpler electrode geometry. Conversely, the barrier problem is more important in these cells. However, for utilization in a short-life cell these systems appear to be feasible with a minimum of effort.

c) $Ni/NiCl_2$ vs Zn in $ZnCl_2$ Melts

Cathodes of $NiCl_2$, which is much less soluble in $ZnCl_2$ than the redox couples, would have to be used in a solid electrode configuration.

There is no way in predicting a priori if this type of electrode could be made to polarize more or less than the solid redox couples discussed above.

d) Hydroxide Systems

Although various couples were examined in anhydrous NaOH-KOH and found to be disappointing, two alternatives might be worth pursuing. The first is the use of a sodium anode and a solid Cu/Cu_2O or Cu/Cu_2O, CuO cathode; the second is a non-anhydrous melt with a zinc anode and Cu/Cu_2O cathode. In the anhydrous media none of the catholytes in this study were sufficiently soluble to be utilizable. Further, the only anodic material tested that could be oxidized was zinc. However, it was found that sodium reacts very slowly with the anhydrous hydroxides and so may be utilized as an anode. The advantage of sodium over zinc is the higher voltage available, about 0.6 v. Since sodium is liquid at these temperatures, it would have to be contained in an inverted cup or trapped in a metal mesh. The cathode in this system could be solid copper/copper oxide. Copper oxide has some electronic conductivity which increases its potential feasibility as an electrode. The electrodes could be formed in situ by electrolysis of the hydroxide, preferably at 300°C, with a stainless steel mesh cathode and copper anode. The cyclic voltammetry results indicate that the copper oxide would be a more efficient electrode at the higher temperatures. If the sodium can be contained in its collector so that no self-discharge occurs, no barrier should be needed in this cell. The open circuit voltage of this combination is about 1.4 v.

Since the cyclic voltammetry measurements indicated that many of the metal oxides were soluble in incompletely dehydrated hydroxide

melts, the possibility of making a battery with wet hydroxide arises. The choice of oxide for the cathode would depend on its solubility and other properties. Silver oxide would yield the largest voltage but it decomposes at the temperatures of interest. Thus copper oxide appears to offer the best possibility. Cu(I) has been shown to be soluble and have reasonable electrochemical behavior in wet hydroxides.[39] Of course, a separator would be required in this cell to minimize self-discharge. The anode here could be zinc which was found to undergo oxidation in this medium. It would appear that zinc should react with water in these melts but this reaction may be limited. Further study is required to ascertain if this reaction does occur and to what extent. The open circuit voltage of this cell would be about 0.8 v. Of course, if an ideal membrane were available, it would be possible to have a wet cathodic melt and a dry anodic one. For short-life batteries such a cell might be feasible.

V. SUMMARY

Conductivity, freezing point and voltammetric measurements were made on the three melts, $ZnCl_2$(60%)-NaCl(20%)-KCl(20%), $AlCl_3$(61%)-NaCl(39%), and NaOH(50%)-KOH(50%), containing various catholytes and anolytes.

For the halide systems the voltammetry studies consisted of both linear sweep and current step measurements. The conductivity and voltammetry runs were carried out at about 225°, 275° and 325°C for the $ZnCl_2$ systems and at about 120°, 150° and 200°C for the $AlCl_3$. The cathodes studied in both melts were Ag/AgCl, Cu/CuCl, Ni/$NiCl_2$, Bi/$BiCl_3$, Sb/$SbCl_3$ and the redox couples $CrCl_2$+$CrCl_3$, CuCl+$CuCl_2$ and $FeCl_2$+$FeCl_3$. The anodes

were Zn in both chloride solvents and Al in the $AlCl_3$ melt. For the conductivity and freezing point studies 15 wt % of the catholyte and 5 wt % of the anolyte were added. In the voltammetry measurements the added catholyte and anolyte concentrations were 0.1M. The metals and salts used in these measurements contained no metal impurity greater than 100 ppm; the salts in most cases also contained no anionic impurity (including oxygen) greater than 100 ppm. To achieve these purity specifications many of the salts had to be synthesized from the metal; others were purified by treating them with ultrapure HCl or Cl_2.

Some equilibration experiments showed that $CuCl_2$ was incompatible with Cu in both the $ZnCl_2$ and $AlCl_3$ solvents, Al was incompatible with $ZnCl_2$, and Be and Mg reacted with both solvents. It was also found that $BiCl_3$ reacted with Bi in the $AlCl_3$ melt forming a lower-valent species Bi(I).

The reversibility of the electrodes in the halide melts, as determined from the linear sweep studies (measured by the initial slope as well as the constancy of the peak voltage with sweep rate), was in reasonable agreement, on the whole, with the exchange current density values calculated from the galvanostatic measurements. However, the linear sweep technique showed some obvious inconsistencies in some systems and these are believed to be due to an increase in the activity of the deposited metal.

At corresponding temperatures, 200° for the $AlCl_3$ melt and 225°C for the $ZnCl_2$, the exchange current densities for all the cathodes were greater in the $AlCl_3$ than in the $ZnCl_2$ solutions. The electrochemical series in both solvents were similar with the voltages consistently higher for each couple in

the $AlCl_3$ melt with two exceptions, Ag/AgCl and $Bi/BiCl_3$. Aluminum is the most electronegative metal and the redox couples, $CuCl+CuCl_2$ and $FeCl_2+FeCl_3$ are the most electropositive couples.

Energy densities were calculated from the measured voltages for all the electrode combinations studied at a median temperature of 275°C for the $ZnCl_2$ system and 150°C for the $AlCl_3$. The highest value was 159 watt- hrs/lb. for Al vs CuCl, $CuCl_2$ in $AlCl_3$.

All the electrode couple combinations were evaluated for battery feasibility on the basis of their voltage, energy density, exchange current density, catholyte solubility, volatility and other factors. From the ratings in all of these categories the best systems appear to be Al vs CuCl, $CuCl_2$ in $AlCl_3$-NaCl, Al vs $FeCl_2$, $FeCl_3$ in $AlCl_3$-NaCl, and Zn vs $CrCl_2$, $CrCl_3$ in $ZnCl_2$-NaCl-KCl. Other systems that have promising aspects are Al vs Ag/AgCl or Cu/CuCl in $AlCl_3$-NaCl and Zn vs $Ni/NiCl_2(s)$ in $ZnCl_2$-NaCl-KCl.

In the hydroxide systems conductivity, freezing point and linear sweep voltammetry studies were also carried out. The linear sweep voltammetry measurements were run on the equimolar melt with Ag/Ag_2O, Cu/Cu_2O, Cu/CuO and Cd/CdO cathodes and Be/BeO, Mg/MgO, Zn/ZnO and Al/Al_2O_3 anodes. In an attempt to increase the solubility of the cathodic oxides in the anhydrous melt, Na_2O was added. The conductivity and voltammetry runs were made at about 200, 250 and 300°C. The hydroxides were reagent grade and were dehydrated by heating under vacuum. The residual water was removed

by reacting it with sodium. The metal oxides were purified by heating them under oxygen or in the case of Cu_2O under vacuum.

The voltammetry results showed that none of the metal oxides were soluble to any extent in the anhydrous melt. However, oxide films on the cathodes could be reduced. The only anode tested that did not form a passivating film was zinc. These results preclude the use of soluble cathodes in the medium but the utilization of solid cathodes might be feasible.

VI. CONCLUSIONS

The results of this study yielded evidence that linear sweep voltammetry data did not agree with exchange current values for some metal/metal ion couples. It appears that the measurements taken at longer times with linear sweep voltammetry were affected by the electrode surface changing due to metal deposition.

As expected, the $Al/AlCl_3$ systems yielded the highest voltages and energy densities. However, these energy densities were not very large, less than 159 watt-hrs/lb, and so the chief use of such batteries would be for high power sources. The systems which rated most highly for battery feasibility were $Al/AlCl_3$ vs CuCl, $CuCl_2$; $Al/AlCl_3$ vs $FeCl_2$, $FeCl_3$ and $Zn/ZnCl_2$ vs $CrCl_2$, $CrCl_3$. Other interesting systems appear to be $Al/AlCl_3$ vs AgCl/Ag, $Al/AlCl_3$ vs CuCl/Cu and $Zn/ZnCl_2$ vs $Ni/NiCl_2$ (solid).

Since none of the metal oxides showed any reasonable solubility in anhydrous NaOH-KOH melts, batteries with this medium must involve solid cathodes. Anodes of zinc or sodium appear utilizable in these systems.

VII. REFERENCES

1. M. M. Nicholson, J. Am. Chem. Soc., 79, 7 (1957).
2. T. Berzins and P. Delahay, J. Am. Chem. Soc., 75, 555 (1953).
3. P. Delahay, New Instrumental Methods in Electrochemistry, Interscience Publishers, Inc., New York, 1954.
4. W. T. De Vries and E. Van Dalen, J. Electroanal. Chem., 10, 183 (1965).
5. R. S. Nicholson and I. Shain, Anal. Chem., 36, 706 (1964).
6. H. A. Laitnen, R. P. Tischer, and D. K. Roe, J. Electrochem. Soc., 107, 546 (1960).
7. A. D. Graves, G. J. Hills and D. Inman, in Advances in Electrochemistry and Electrochemical Engineering, Vol. 4, P. Delahay and C. W. Tobias Eds. Interscience, New York, 1966.
8. D. Inman, J. O'M. Bockris and E. Blomgren, J. Electroanal. Chem., 2, 506 (1961).
9. T. Berzins and P. Delahay, J. Am. Chem. Soc., 77, 6448 (1955).
10. K. J. Vetter, Electrochemical Kinetics, Academic Press, New York 1967 (Chapter II).
11. C. R. Boston, Oak Ridge National Laboratory, private communication.
12. Inorganic Synthesis, L. F. Audrieth, ed., vol. 3, p. 191, McGraw-Hill Book Co., Inc., New York, (1950).
13. Handbuch der Praparativen Anorganischer Chemi, G. Brauer, ed., p. 463, 1954.
14. F. G. Donnan and J. S. Thomas, J. Chem. Soc., 99, 1788 (1911).
15. L. Brewer and J. L. Margrave, J. Phys. Chem., 59, 421 (1955).

16. G. W. Heylmun, J. Gas. Chrom. 3, 82 (1965).

17. G. Lauer, "Part II. Development of Electrochemical Instrumentation," California Institute of Technology, 1967. Dissertation Abstracts 27, 4268-B (1967).

18. G. Lauer, H. Schlein and R. A. Osteryoung, Anal. Chem. 35, 1789 (1963).

19. C. E. Wicks and F. E. Block, "Thermodynamic Properties of 65 Elements - Their Oxides, Halides, Carbides, and Nitrides," Bulletin 605, Bureau of Mines, U. S. Government Printing Office, Washington, D. C., 1963.

20. M. A. Klochko and M. M. Godneva, Zh. Neorg. Khim. 4, 2136 (1959).

21. I. N. Nikonova, S. P. Pavlenko and A. G. Bergman, Bull. acad. sci. U.R.S.S., Classe sci. chim. 1941, 391.

22. V. A. Plotnikov and U. I. Shvartsman, Mem. Inst. Chem. Acad. Sci. Ukrain. S.S.R. 3, 387 (1936); see Landolt-Bornstein, vol. 2, Part 3, Auflage 6, p. 218 (1956).

23. H. W. Otto and R. P. Seward, J. Chem. Eng. Data 9, 507 (1964).

24. F. R. Duke and R. A. Fleming, J. Electrochem. Soc. 104, 251 (1957).

25. C. R. Boston. J. Chem. Eng. Data 11, 262 (1965).

26. T. B. Reddy, J. Electrochem. Soc. 113, 117 (1966).

27. D. Inman, J. O'M. Bockris and E. Blomgren, J. Electroanal. Chem. 2, 506 (1961).

28. U. Anders and J. A. Plambeck, Can. J. Chem. 47, 3055 (1969).

29. R. G. Verdieck and L. F. Yntema, J. Phys. Chem. 48, 268 (1944).

30. N. J. Bjerrum, C. R. Boston, and G. P. Smith, Inorg. Chem. 6, 1162 (1967).

31. N. J. Bjerrum and G. P. Smith, Inorg. Chem. 6, 1968 (1967).

32. A. Hershaft and J. D. Corbett, Inorg. Chem. 2, 979 (1963).

33. J. D. Corbett, Inorg. Nucl. Chem. Letters, 3, 173 (1967).

34. D. A. Hames and J. A. Plambeck, Can. J. Chem. 46, 1727 (1968).

35. B. S. Del Duca, "Electrochemical Behavior of The Aluminum Electrode in Molten Salt Electrolytes," NASA TN D 5503, October, 1969.

36. J. Goret, Bull. Soc. Chim. Fr., 1074 (1964).

37. J. Goret, Bull. Soc. Chim. Fr., 67 (1966).

38. J. Goret and B. Tremillon, Electrochim. Acta, 12, 1065 (1967).

39. A. Eluard and B. Tremillon, J. Electroanal. Chem., 18, 277 (1968).

Appendix I

Characterization of the $AlCl_3$ (66%)-NaCl (20%)-KCl (14%) Mixture

The $AlCl_3$-NaCl-KCl mixture with the above composition has been reported to be a eutectic mixture with a melting point of 70°C.[1] However, when cooling curves were taken on this system as part of the screening program, a thermal halt occurred at 135°C and a large halt occurred at 90°C; no 70° thermal halt was obtained. When the sample was visually inspected at 125°C, a great deal of precipitate was observed. Therefore the original references on this system were examined. It was found that only one investigator,[1] reported a thermal halt at 70°C. On the other hand, three other investigators[2-4] found eutectic halts at 83, 88, and 89°C.

Midorikawa[2] suggested that the results of Wasilewski et al.,[1] were in error due to supercooling of the melt. It is thus concluded that the 70° halt ascribed by Wasilewski does not exist and that a system with the alleged ternary eutectic composition forms solids at 135°C. For this reason the composition of the $AlCl_3$-containing solvent was changed to the better known eutectic composition 61 mole % $AlCl_3$-39% NaCl, which has a melting point of 108°C.

References

1. L. Wasilewski, A. Kaczorowski, and M. Dynkin, Przemsyl Chem., 18, 608 (1937); C.A. 29, 5728 (1935).
2. R. Midorikawa, J. Electrochem. Soc., Japan, 23, 127 (1955).
3. W. Fischer and A. Simon, Z. anorg. allgem. Chem., 306, 1 (1960).
4. V. A. Plotnikov and U. I. Shvartsman, Mem. Inst. Chem. Acad. Ukrain, 3, 387 (1936); C.A. 31, 6093 (1937).

Appendix II

Theoretical Considerations of Synthetic Circuits

A. Theoretical Equation Taking Into Consideration the Rise Time of the Pulse Generator

The simplest circuit which can represent the combined faradaic and non-faradaic response of an electrode at very short times is

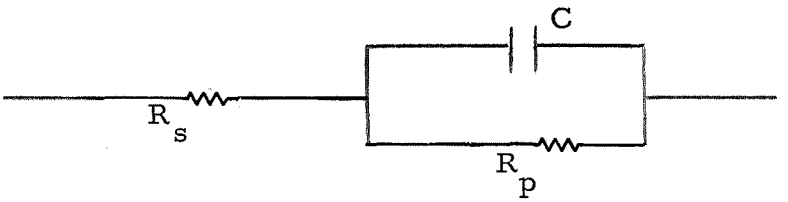

where R_s is the electrolyte resistance, C is the double-layer capacitance, and R_p is the charge transfer resistance given by

$$R_p = \frac{RT}{nFI_o} \tag{1A}$$

Here RT/nF has its usual significance and I_o is the exchange current. The diffusion process is not considered in this treatment. The current through the parallel elements must sum to I(t), the applied current, i.e.,

$$I(t) = C \frac{d}{dt} E_p(t) + \frac{E_p(t)}{R_p} \tag{2A}$$

where E_p is the potential across R_p. This linear differential equation has the solution

$$E_p(t) = \frac{1}{C} \exp\left\{\frac{-t}{R_p C}\right\} \int_o^t I(\lambda) \exp\left\{\frac{\lambda}{R_p C}\right\} d\lambda \tag{3A}$$

In addition

$$E(t) = I(t) R_s + E_p(t) \tag{4A}$$

Substituting Eq. (3A) into Eq. (4A) yields

$$E(t) = I(t) R_s + \frac{1}{C} \exp\left\{\frac{-t}{R_p C}\right\} \int_o^t I(\lambda) \exp\left\{\frac{\lambda}{R_p C}\right\} d\lambda \tag{5A}$$

The current pulse in this study appears to have the form

$$I(t) = \begin{cases} 0, & t < 0 \\ I\left[1 - \exp\left\{\frac{-t}{\tau}\right\}\right], & t > 0 \end{cases} \tag{6A}$$

where τ is a constant and is a characteristic of the pulse generator and I is the current at infinite time. When Eq. (6A) is substituted into Eq. (5A) and the integration performed,

$$E(t) = I\left[R_s + R_p\right] - I\left[R_s - \frac{\tau R_p}{R_p C - \tau}\right] \exp\left\{\frac{-t}{\tau}\right\}$$

$$- \left[\frac{I R_p^2 C}{R_p C - \tau}\right] \exp\left\{\frac{-t}{R_p C}\right\} \qquad (7A)$$

For very small τ so that $\exp\left\{\frac{-t}{\tau}\right\} \approx 0$, Eq. (7A) becomes

$$E(t) = I\left[R_s + R_p\right] - \left[\frac{I R_p^2 C}{R_p C - \tau}\right] \exp\left\{\frac{-t}{R_p C}\right\} \quad . \qquad (8A)$$

For times short enough so that the linearization

$$\exp\left\{\frac{-t}{R_p C}\right\} \approx 1 - \frac{t}{R_p C} \qquad (9A)$$

is valid, Eq. (8A) reduces to

$$E(t) = IR_s + It/C \quad . \qquad (10A)$$

Under these conditions the E vs t curve is linear. The value of R_s can be obtained from the intercept of the E vs t curve at zero time and the value of C is obtained from the slope of the curve

$$C = \frac{I}{dE/dt} \quad . \qquad (11A)$$

To summarize then, the condition for Eq. (10A) to apply is

$$\tau \ll t \ll R_p C \qquad (12A)$$

B. Determination of τ and the Rise Time

The value of τ for a pulse generator can be determined by analyzing the potential-time curve through a simple resistive circuit. The voltage E(t) is given by

$$E(t) = E_\infty\left[1 - \exp\left\{\frac{-t}{\tau}\right\}\right] \qquad (13A)$$

where E_∞ is the limiting potential at infinite time. Solving for exp $\{-t/\tau\}$

$$\log\left(1 - \frac{E}{E_\infty}\right) = - \frac{t}{2.303\,\tau} \quad . \tag{14A}$$

Thus by plotting the function log $(1 - E/E_\infty)$ vs t one can obtain the value of τ from the slope.

The value of τ for the pulse generator used in this work was determined by passing a current (I = 0.020 amp through a 5 ohm resistor for about 1.7 μ sec. It was found that at about 0.5 μ sec the current was essentially at its maximum. A plot of log $(1 - E/E_\infty)$ vs t yielded a straight line, the slope of which corresponded to a value of 0.138 μ sec for τ. If one defines the rise time as the time in which the voltage rises from 10% to 90% of the maximum voltage, the rise time is calculated to be 0.30 μ sec.

C. The Effect of R_s on the Apparent Capacitance

If one differentiates Eq.(7A) with respect to t and denotes dE/dt by I/C^*, where C^* is the apparent capacitance measured at time t, from the slope of the E vs t plot, one obtains

$$\frac{1}{C^*} = \left[\frac{R_s}{\tau} - \frac{1}{C - \tau/R_p}\right] \exp\left\{\frac{-t}{\tau}\right\} + \left(\frac{1}{C - \tau/R_p}\right) \exp\left\{\frac{-t}{R_p C}\right\} \quad . \tag{15A}$$

Values of C^* were calculated for various values of R_s for the following case: $R_p = 2\Omega$ (equivalent to $i_o = 0.416$ amp/cm^2), $C = 10^{-6}$ F (or 20×10^{-6} F/cm^2), $\tau = 1.38 \times 10^{-7}$ sec and $t = 5 \times 10^{-7}$ sec. These values were converted to C_d^* (which is equal to $C^*/0.05$ cm^2) because those were the reported capacitance data. Values of C_d^* as a function of R_s are depicted in Fig. 1A where it can be seen that R_s has a marked effect on C_d^*, especially when R_s is large.

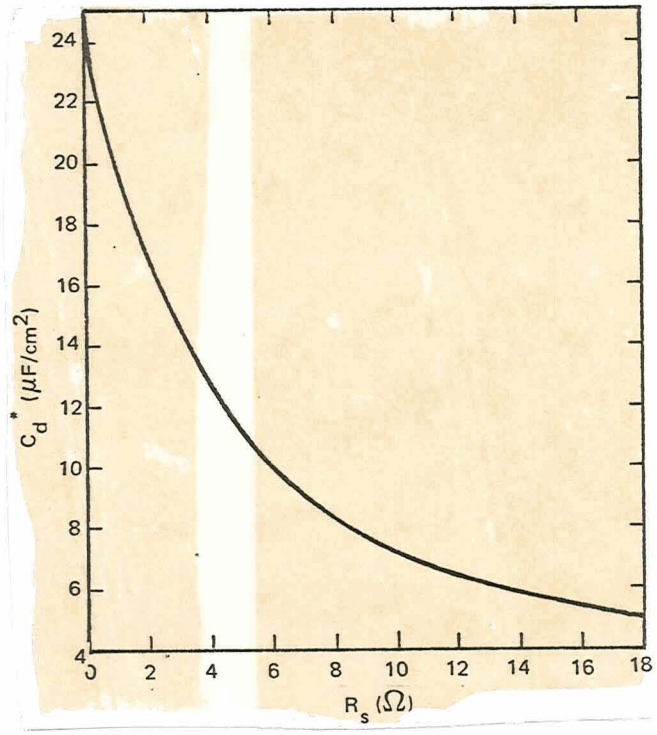

Fig. 1 A. Effect of Cell Resistance on Apparent Capacitance

D. Theoretical E vs t Curves for Different Exchange Currents and Rise Times

As shown in Eq. (9A), one of the conditions for obtaining accurate values of C from the slope of the E vs t curve (Eq. (11A)) is that the time t at which the slope is measured must be much smaller than $R_p C$. The second condition is that t must be considerably larger than τ. To show this more clearly, E vs t plots of Eq. (7A) have been prepared for six cases. For these calculations R_p was obtained from Eq. (1) using these values: R = 8.31 joules $mole^{-1}$ deg^{-1}, T = 500°K, n = 1 equiv/mole and F = 10^5 coulombs/equiv. In addition, R_s, I and C were taken to be 2 ohms, 0.02 amps and 10^{-6} F, respectively. The area of the electrode was taken to be 0.05 cm^2 so that a C of 10^{-6} F corresponds to a value of 20 $\mu F/cm^2$. In the first four cases, the rise time for the current generator was 0.30 μ sec and the experimental value of $\tau = 1.38 \times 10^{-7}$ sec was used. In the last two cases a rise time of 1.83 μ sec (τ assumed to be 8.28×10^{-7} sec) was taken.

The conditions of the six cases are shown in Table 1 A.

TABLE 1 A

SIX CASES FOR THEORETICAL E vs t PLOTS

Case	Rise Time (μ sec)	τ (μ sec)	R_p (ohm)	i_o (amp/cm^2)
1	0.30	0.138	0.10	8.32
2	0.30	0.138	1.00	0.832
3	0.30	0.138	2.00	0.416
4	0.30	0.138	10.00	0.0832
5	1.83	0.828	1.00	0.832
6	1.83	0.828	10.00	0.0832

The exchange current densities i_o were calculated from Eq. (1A), taking into consideration the area of the electrode (0.05 cm^2). The plots (Eq. 7A) are presented in Figs 2A-4A. Along with these are given (in dashed lines) plots of Eq. (10A), the slope of which gives accurate values of C. Thus only that portion of the solid curves parallel to the dashed curve

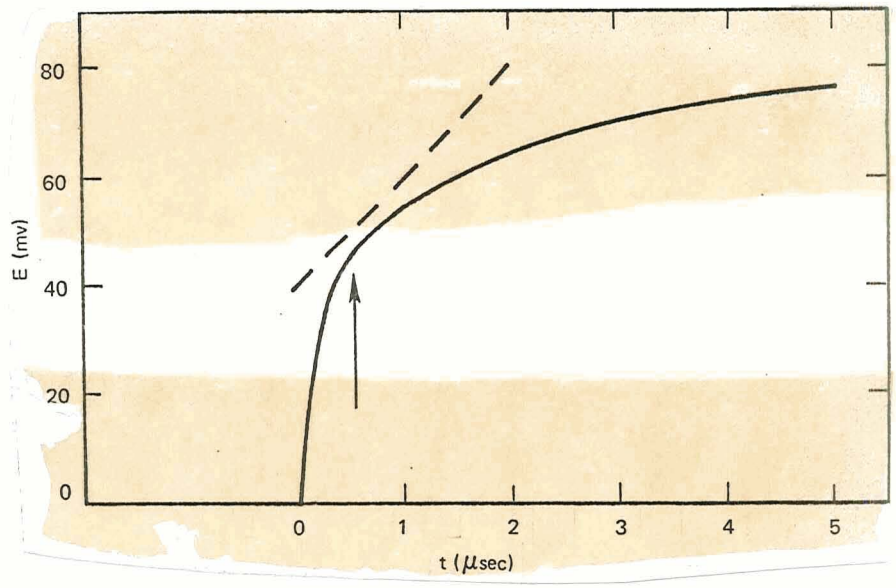

a) $R_p = 2.0\ \Omega$; $i_o = 0.416$ amp/cm^2

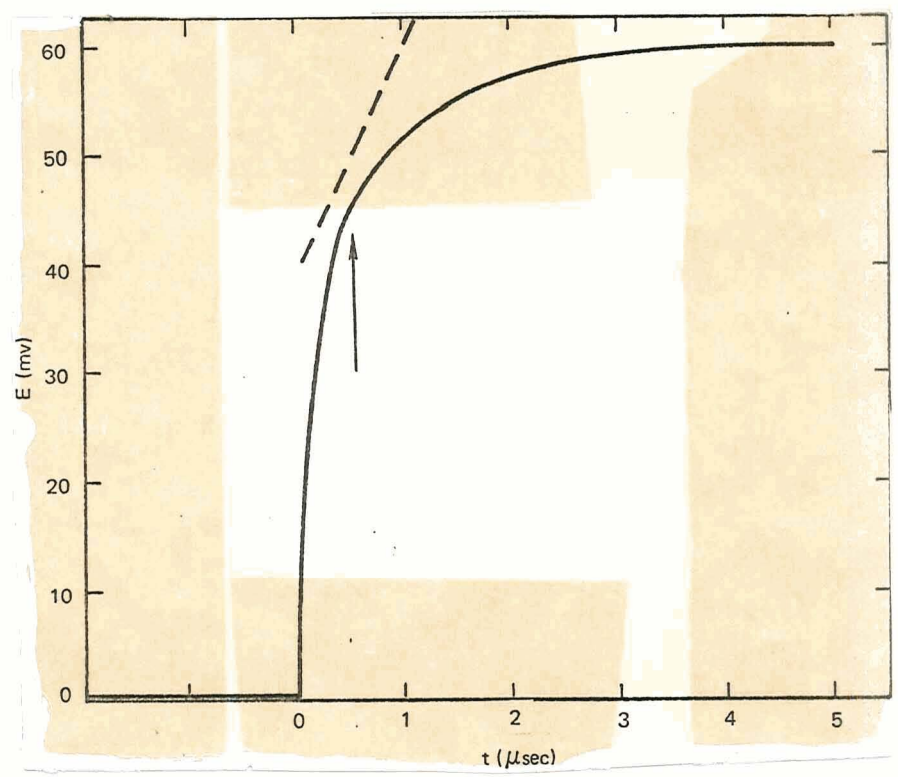

b) $R_p = 1.0\ \Omega$; $i_o = 0.832$ amp/cm^2

Fig. 2A: Theoretical E vs t Plots (Rise Time = 0.30 μsec)

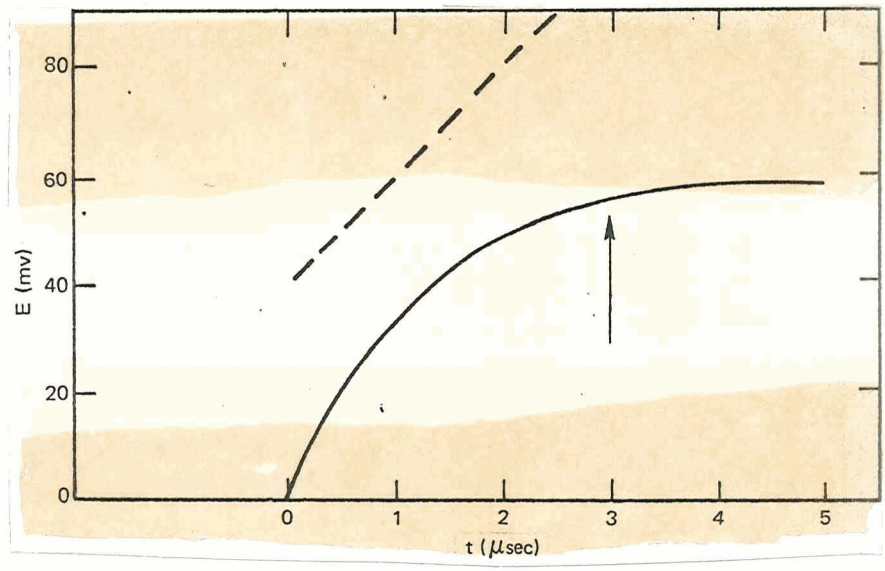

a) $R_p = 1.0\ \Omega$; $i_o = 0.832$ amp/cm^2

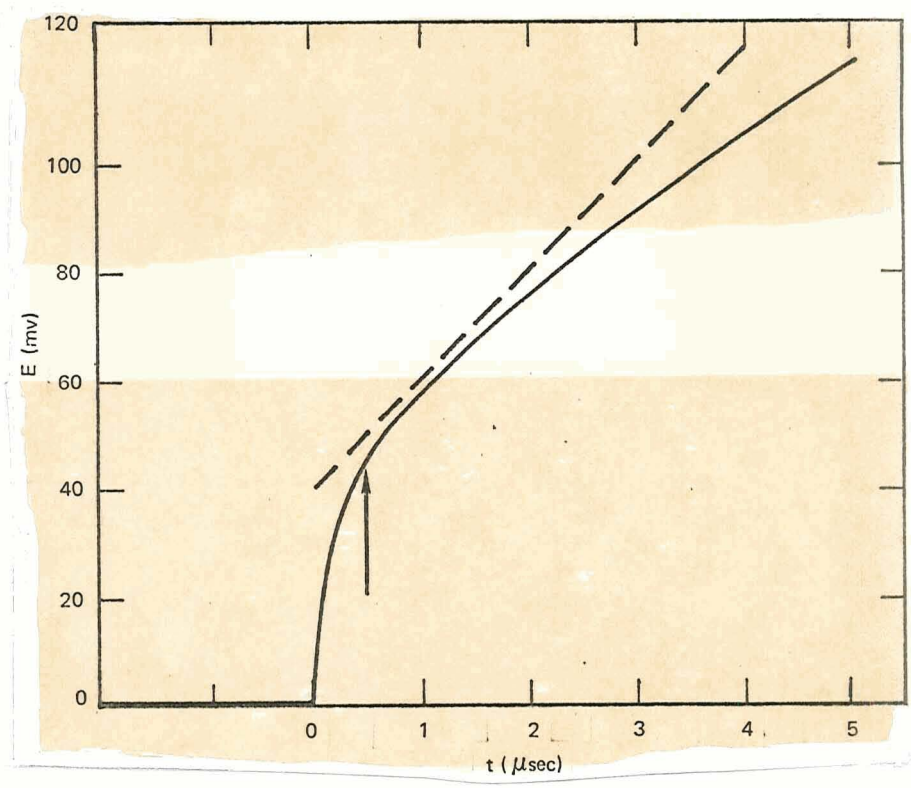

b) $R_p = 10.0\ \Omega$; $i_o = 0.0832$ amp/cm^2

Fig. 3 A: Theoretical E vs t Plots (Rise Time = 0.30 μsec)

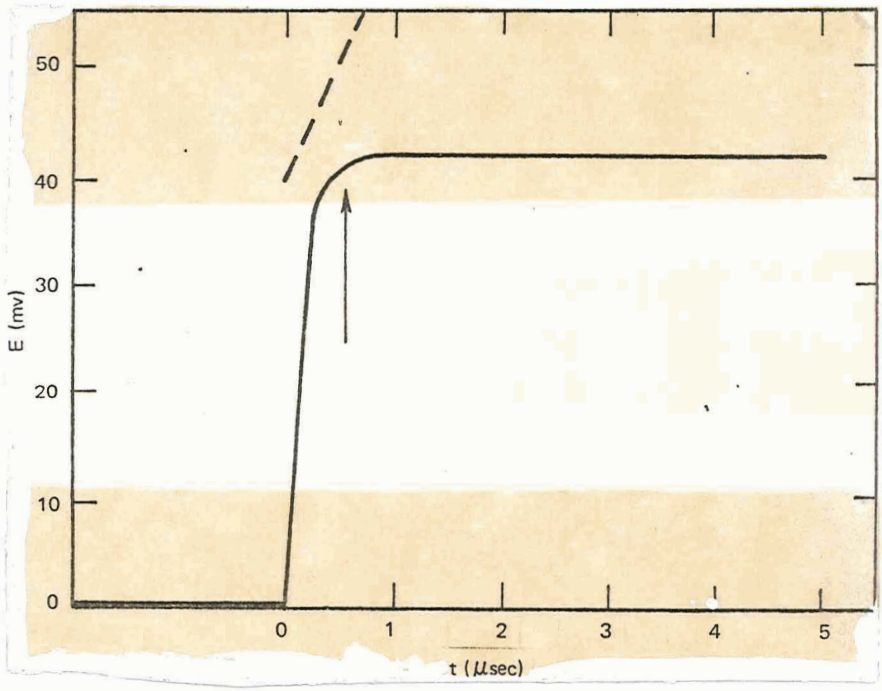

a) $R_p = 0.1\ \Omega$; $i_o = 8.32$ amp/cm^2

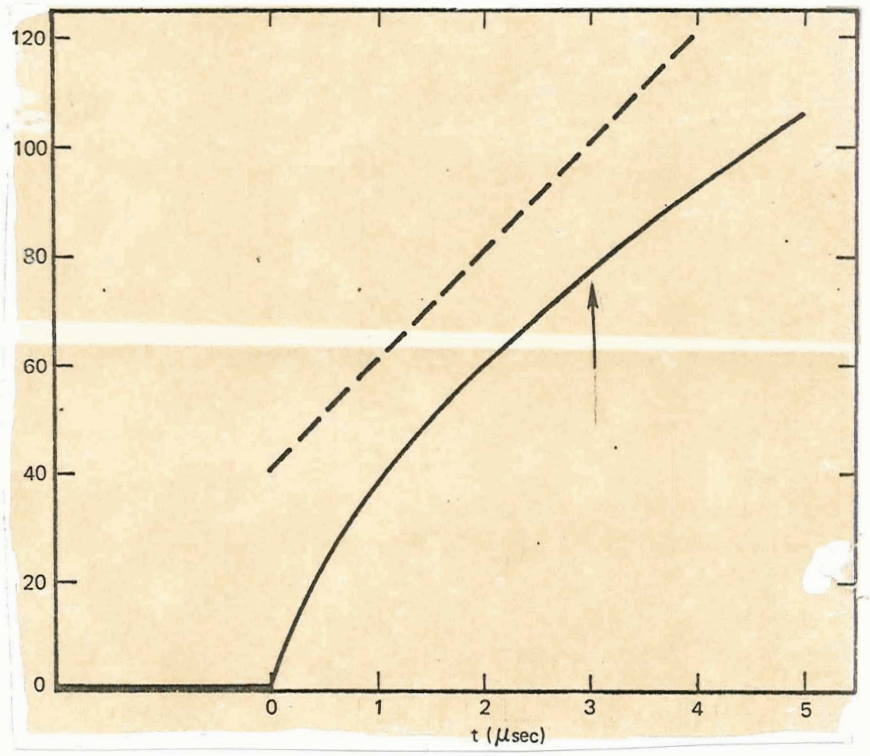

b) $R_p = 10.0\ \Omega$; $i_o = 0.0832$ amp/cm^2

Fig. 4A: Theoretical E vs t Plots (Rise Time = 1.83 μsec)

yields an accurate value of C. An arrow in the figure points to the intersection of the curve with the time at which C_d and R_s would be taken. It can be seen that with systems of high exchange current, especially above 1 amp/cm^2, the portion of the solid plots parallel to the dashed plots is negligible when the rise time is 0.3 μ sec (Fig. 2A). Thus at high exchange currents (1 amp/cm^2 and above) accurate values of C cannot be obtained when the rise time of the pulse generator is as long as 0.3 μ sec. When the rise time is longer (1.8 μ sec) the portion of the solid curve parallel to the dashed plot is longer, but in some cases the slope must be taken at an arbitrary value (lower half of Fig. 4A).

Appendix III

Analysis of Oscilloscope Traces

Instead of plotting η vs $t^{1/2}$ in terms of mv and seconds, which would have necessitated computing the values of η and t for each point on that curve, it was elected to plot the quantities directly from the oscilloscope trace in terms of divisions - i. e., E' vs $(t' - t_o')^{1/2}$ where E' is the number of divisions (in the ordinant) of the voltage-time trace and $t' - t_o'$ are the number of divisions (in the abscissa) after the pulse is initiated. Thus equations in terms of these divisional quantities with appropriate conversion factors were used. It was then decided to use this approach to compute R_s and C_d from short pulse data. Thus all equations are given in terms of E' and $t' - t_o'$ (in divisions or cm) rather than E and t. It should be noted that while the axes of the oscilloscope traces in Section IV-D are labelled E and t, they should, strictly speaking, be labelled E' and $t' - t_o'$, respectively. In the plots where it appears that E is plotted vs $(t - t_o)^{1/2}$, these quantities should be primed also.

A. Short Pulse Traces

1. Determination of Electrolyte Resistance

The short-pulse traces of about 4 μ sec were taken to obtain the electrolyte resistance, R_s, and the double layer capacitance, C_d. Since passing a current through a resistor yielded a constant voltage in about 0.5 μ sec (see page A-4), R_s and C_d values were calculated from the short-pulse traces at 0.5 μ sec. The following expression was used to calculate R_s

$$R_s = \frac{\left(E'_{0.5\ \mu sec} - E'_0\right)}{I} \quad k_1 \quad , \qquad (16A)$$

where $E'_{0.5\ \mu sec}$ and E'_0 are the number of divisions of the voltage-time curve at 0.5 sec after and just before the pulse was applied, respectively, k_1 is the number of volts/div and I is the applied steady state current (amps).

2. Determination of Double Layer Capacitance

From Eq. (6), C_d for a cathodic pulse is

$$C_d = \frac{-i}{(dE/dt)_{t = 0}} \quad .$$

The minus sign arises from the sign convention. However, due to the rise-time of the instrument, C_d was measured at 0.5 μ sec. Therefore, C_d is given by

$$C_d = \frac{-i}{(dE/dt)_{t = 5 \times 10^{-7}}} \quad . \tag{17A}$$

Since $E = -k_1 E'$ and $t = k_2(t' - t_o')$ where k_2 is the number of seconds/div and t' and t_o' are the number of divisions in the abscissa where the slope is taken and where the pulse is initiated, respectively, then

$$dE/dt = \frac{-k_1}{k_2} \frac{dE'}{dt'}$$

and

$$C_d = \frac{k_2 i}{k_1 (dE'/dt')_{t = 5 \times 10^{-7}}} \quad . \tag{18A}$$

B. Long Pulse Traces - Redox Systems

1. Calculation of $f(C_i D_i^{1/2})$

From Eq. (9), the function $f(C_i D_i^{1/2})$ is given by

$$f(C_i D_i^{1/2}) = \frac{C_o D_o^{1/2}}{1 + \frac{C_o D_o^{1/2}}{C_r D_r^{1/2}}} = \frac{-2RTi}{\pi^{1/2} n^2 F^2 (dE/dt^{1/2})} \quad .$$

Since

$$\frac{dE}{d\sqrt{t}} = -\frac{k_1}{k_2^{1/2}} \frac{dE'}{d(t' - t_o')^{1/2}} \quad ,$$

$$f(C_i D_i^{1/2}) = \frac{9.42 \times 10^{-10}\ Tik_2^{1/2}}{k_1 n^2\ dE'/d(t' - t_o')^{1/2}} \tag{19A}$$

2. Calculation of D_o

If $C_o = C_r = 10^{-4}$ moles/cm^3 and $D_o = D_r$, then

$$D_o = \frac{3.55 \times 10^{-10}\, T^2 i^2 k_2}{k_1^2\, n^4 \left[dE'/d(t' - t_o')^{1/2} \right]^2} \quad . \tag{20A}$$

3. Calculation of Extrapolated Overpotential, η_o

The overpotential, η, for a cathodic pulse is given by

$$\eta = E + iAR_s \tag{21A}$$

In the portion of the curve where E is proportional to $t^{1/2}$

$$E + IR_s = k_3 \sqrt{t - t_o} + \eta_o$$

where η_o is the intercept at $t = t_o$ and k_3 is a proportionality factor. Since

$$E = -k_1 E' + k_1 E_o', \; t = k_2 t' \text{ and } t_o = k_2 t_o' \quad ,$$

$$E' = E_o' + \frac{iAR_s}{k_1} - \frac{k_3 \sqrt{k_2}}{k_1} \sqrt{t' - t_o'} + \frac{\eta_o}{k_1} \tag{22A}$$

The intercept, E'_{int}, is thus given by

$$E'_{int} = E_o' + \frac{iAR_s}{k_1} - \frac{\eta_o}{k_1}$$

Thus

$$\eta_o = k_1 (E_o' - E'_{int}) + iAR_s \quad . \tag{23A}$$

4. Calculation of Exchange Current Density

Since

$$\frac{1}{C_o D_o^{1/2}} + \frac{1}{C_r D_r^{1/2}} = \frac{1}{f(C_i D_i^{1/2})} \quad ,$$

Eq. (11) can be written

$$i_o = \frac{\frac{-RTi}{nF\eta_o}}{1 - \frac{R^2T^2C_d i}{n^3F^3\eta_o f^2(C_i D_i^{1/2})}} \quad . \tag{24A}$$

Thus, by using Eqs. (23A), (18A) and (19A), i_o can be obtained. If, as in most cases of this work, the second term in the denominator is negligible because of the high concentration of dissolved solute, then

$$i_o = \frac{-RTi}{nF\eta_o} \tag{25A}$$

and only Eq. (23A) is needed.

5. Calculation of R_p

The charge transfer resistance, R_p, for a cathodic pulse is given by

$$R_p = -\frac{RT}{nFI_o} = \frac{-RT}{nFi_oA} \quad . \tag{26A}$$

From Eq. (24A)

$$\frac{-RT}{nFi_o} = \left[1 - \frac{R^2T^2C_d i}{n^3F^3\eta_o f^2(C_i D_i^{1/2})}\right]\frac{\eta_o}{2} \quad . \tag{27A}$$

Therefore substituting Eq. (27A) into (26A) yields

$$R_p = \left[1 - \frac{R^2T^2C_d i}{n^3F^3\eta_o f^2(C_i D_i^{1/2})}\right]\frac{\eta_o}{iA} \quad . \tag{28A}$$

If $f^2(C_i D_i^{1/2})$ is large

$$R_p = \frac{\eta_o}{iA} \quad . \tag{29A}$$

6. Calculation of $(\Delta\eta/iA)_{t = 0.1\ msec}$

An important parameter which should give an indication as to whether the overpotential is due only to charge transfer and diffusion polarization is

$$(\Delta\eta/I)_{t = 0.1\,msec}$$

where

$$\Delta\eta = \eta_{curve} - \eta_{linear} \quad . \tag{30A}$$

Here η_{curve} and η_{linear} are the overpotentials of the actual and linear η vs $(t - t_o)^{1/2}$ plots, respectively. As discussed on page 21, 0.1 msec was selected, because in most of the systems investigated in this study, the double layer charging should be completed by then. Substituting Eqs. (21A) and (22A) into (30A) yields

$$(\Delta\eta/iA)_{0.1\ msec} = k_1(E'_{linear} - E'_{curve})/iA \quad . \tag{31A}$$

7. Calculation of $\eta_{5\ msec}$ —

It was of interest to know the total overpotential at the end of the long pulse (usually about 5 msec). Using Eqs. (21A), (22A) and (23A) yields

$$\eta_{5\ msec} = \eta_o + k_1\,(E'_{int} - E'_{5\ msec}) \quad . \tag{32A}$$

Dividing Eq. (32A) by iA resulted in an equation which gave a measure of the effective resistance at 5 msec.

C. Long Pulse Traces - Metal/Metal Ion Systems

In this case $f(C_iD_i^{1/2}) = C_oD_o^{1/2}$ instead of

$$\frac{C_oD_o^{1/2}}{1 + \dfrac{C_oD_o^{1/2}}{C_rD_r^{1/2}}} \quad .$$

Therefore Eqs. (19A), (20A), (24A) and (28A) become

$$C_o D_o^{1/2} = \frac{9.42 \times 10^{-10} T i k_2^{1/2}}{k_1 n^2 \left[dE'/d(t' - t_o')^{1/2} \right]} \tag{33A}$$

$$D_o = \frac{8.87 \times 10^{-11} T^2 i k_2}{k_1^2 n^4 \left[dE'/d(t' - t_o')^{1/2} \right]} \tag{34A}$$

$$i_o = \frac{\dfrac{-RTi}{nF\eta_o}}{1 - \dfrac{R^2 T^2 C_d i}{n^3 F^3 \eta_o C_o D_o^{1/2}}} \tag{35A}$$

$$R_p = \left[1 - \frac{R^2 T^2 C_d i}{n^3 F^3 \eta_o C_o D_o^{1/2}} \right] \frac{\eta_o}{iA} \quad . \tag{36A}$$

The remaining equations [(21A), (23A), (25A), (29A), (31A) and (32A)] are unchanged.

Appendix IV

Cyclic Voltammograms in Molten NaOH-KOH Systems

A. Ag/Ag_2O

Since Ag_2O is not very stable at elevated temperatures, measurements were run at 200°C first. A voltammogram of the hydroxide melt at 208°C with Ag_2O and Na_2O is given in Fig. 5A. A cathodic sweep did not yield a well-defined, diffusion-limited wave from the rest potential A as was found in most of the chloride melts. Thus, no measurements with varying sweep rate were made. Two waves, B and C, with the first peaking about 0.3 v from the open circuit potential were observed. The reduction wave for Na(I) appeared at about O v and on reversal the Na stripping wave was evident. Two anodic waves, C' and B', which resulted from oxidation of the products formed at C and B, and another large wave, E, present even before the addition of Ag_2O or Na_2O, occurred before the limiting reaction, F. Reversal at F yielded a wave at about 2.4 v and another, E', due to a product formed at E. If an anodic sweep is made from A, a small peak D occurs and runs into the large one E. In the absence of Na_2O, waves B, C, B' and C' were diminished in magnitude. The insert in Fig. 5A depicts the anodic and cathodic sweeps from the open circuit voltage A.

In the NaOH-KOH melt without Ag_2O or Na_2O but containing some H_2O, the rest potential was about 0.9 v and waves B, C, B' and C' were absent. Waves E and F were present and they must be due to the anodization of silver

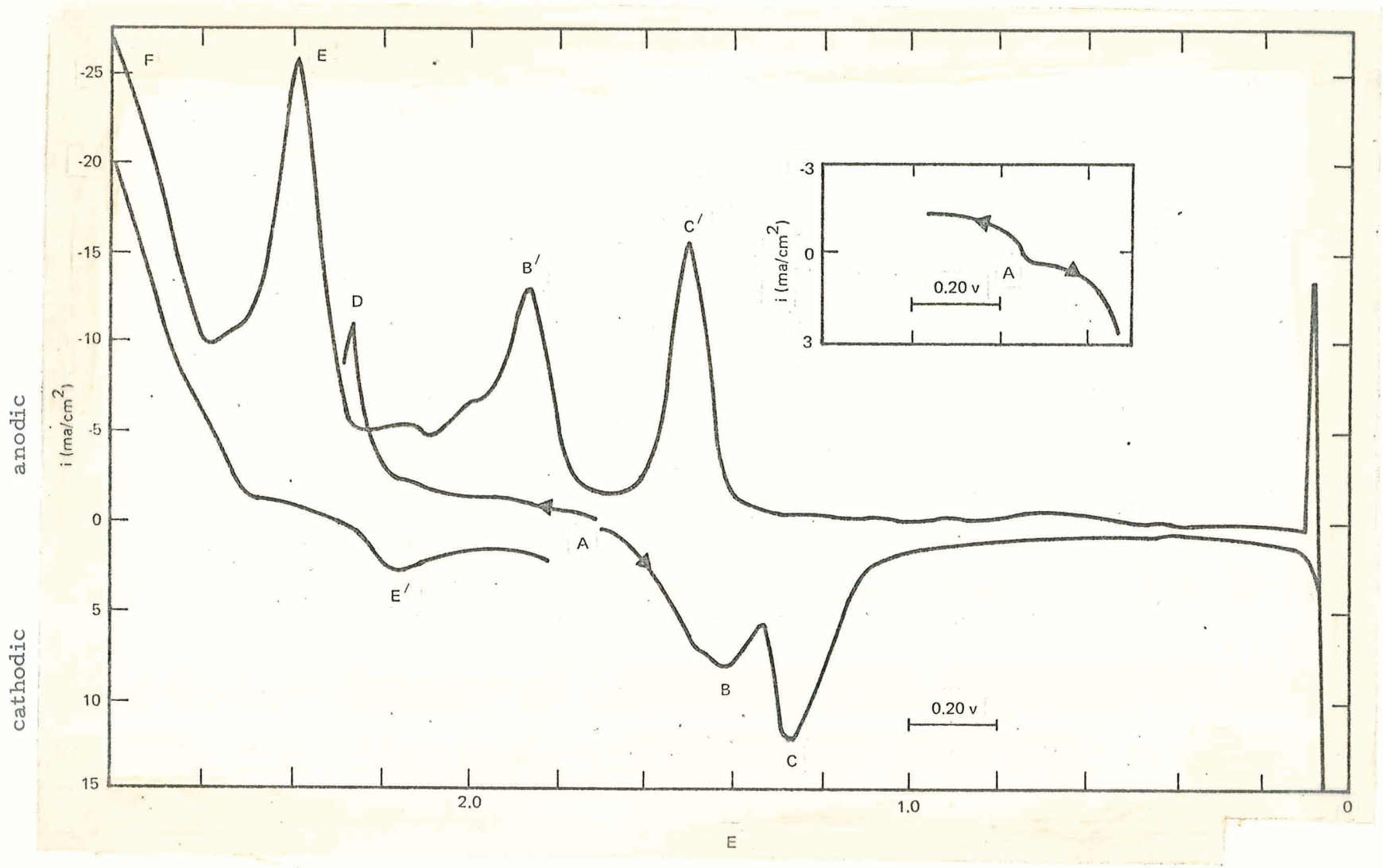

Fig. 5A. L. S. V. of $Ag/Ag_2O + Na_2O$ in NaOH-KOH
$T = 208^{o}C$; s = 46 mv/sec

and oxidation of OH^-, respectively. Reversal after E produced a diffusion limited wave (corresponding to E') which ran into two other waves (not B and C). This diffusion-limited wave must be due to reduction of Ag(I) in solution. When sodium was added to this melt and voltammetric sweeps run again, the reduction waves for H_2O and for Ag(I) were absent. Instead of the Ag(I) wave after reversal at F, there were two reduction peaks, apparently corresponding to B and C. These peaks appeared to be due to films. Voltammograms at 250°C were similar to those at 200°C, except that all the waves were larger and the peaks B, C, B' and C' were further apart. Again all these waves seem to be due to films. At 300°C the waves B, C, B' and C' were much smaller and B had split into two peaks. In addition, a third reduction peak anodic of B was present.

A summary of the above results follows. Peak E is due to the oxidation of Ag to form Ag_2O, higher oxides and/or a soluble species. Peak E' is the reduction of the soluble species. The concentration of this soluble species, presumably Ag(I), is increased by the presence of water. Peaks B and C appear to be reductions of oxide films. Several solid oxides of silver are known (Ag_2O, AgO, Ag_2O_3) but all except Ag_2O are very unstable at these temperatures. The entities AgO^- and $Ag_2O_3^=$ have been postulated by Goret and Tremillon[38] in these systems. In fact, they attribute a wave corresponding to peak C' to the reaction

$$Ag + AgO^- - e \rightarrow Ag_2O$$

This reaction cannot occur in this system since the wave C' is cathodic and not anodic of the open circuit potential. On the other hand, wave B' is anodic of A.

However, if B and C were produced by the reactions

$$Ag_2O + e \longrightarrow AgO^- + Ag$$

and

$$3Ag_2O + 2e \longrightarrow Ag_2O_3^= + 4Ag$$

and waves C' and B' by the reverse reactions, then B' and C' should be diffusion-limited. This does not appear to be the case. Similar arguments pertain if B and C represent reduction of silver oxides to the metal and soluble oxide entities ($O^=$, $O_2^=$, O_2^-) and B' and C' the oxidation of the oxide ions. Thus, in anhydrous hydroxide melts Ag/Ag_2O is not a reversible couple and no soluble species is apparent.

B. <u>Cu/Cu_2O</u>

A cyclic voltammogram of an anhydrous NaOH-KOH melt taken at 247° with copper electrodes is shown in Fig. 6Aa. Going anodic from the open circuit potential A, one observes three peaks B, C and D, commencing at 1.6, 1.9 and 2.1 v, before the limiting wave E for OH^- oxidation. On reversal at the anodic limit, several peaks, C', B', F and G, due to the reduction of the oxide films formed on anodization of copper appeared. These results are in agreement with those of Eluard and Tremillon[39] who postulate the oxides formed to be Cu_2O, CuO and Cu_2O_3. The reduction peaks for the oxides were smaller in area than the oxidation (formation) peaks and varied in potential from sweep to sweep. Peak C' is due to the reduction of the oxide formed at C and B' to that formed at B. At 300°C the peaks were larger and an additional anodic peak occurred near C'. Further, the double peak at B' had separated. At 200°C the results were similar to that in the figure except that the peaks had decreased in height and broadened out.

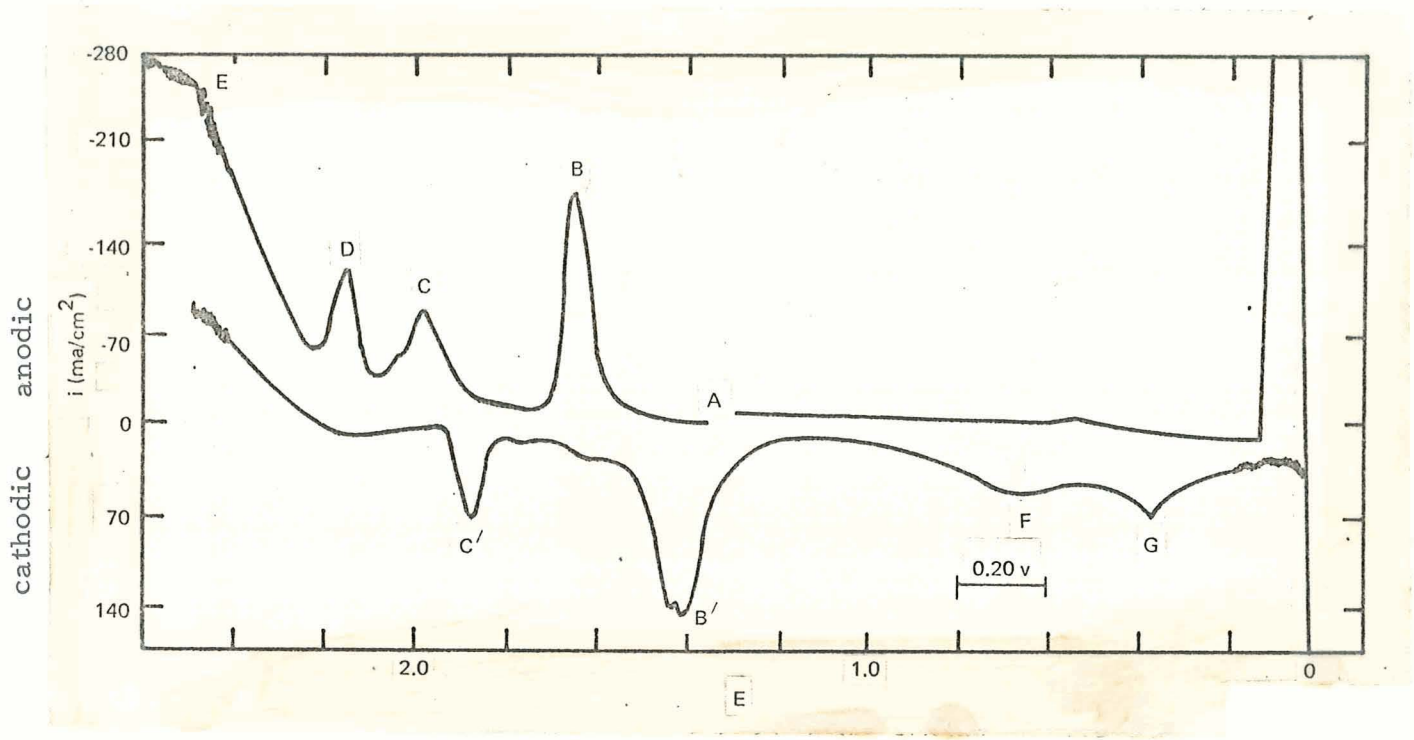

Fig. 6Aa. L.S.V. of Cu/Cu_2O in NaOH-KOH
T = 247°C; s = 46 mv/sec

Addition of Cu_2O and Na_2O resulted in an open circuit voltage around 0.8 v (see Fig. 6Ab). Cathodic sweeps from the open circuit potential A yielded a wave A which ran into another B just before sodium reduction C. The first cathodic wave may be due to the reaction

$$CuO_2^{-3} + e \longrightarrow Cu + 2O^{=}$$

which Eluard and Tremillon[39] reported for oxide-containing hydroxide melts. Since no distinct peak currents could be obtained for this wave, no sweeps were made at varying sweep rates. The reaction for the second wave B is unknown at present. When the scan was reversed after B, two peaks B' and D occurred before copper oxidation at E. B' was found to be due to oxidation of the product formed at B. Reversal at E produces a small reduction wave for soluble Cu(I), presumably formed to a small extent at E, and a large peak D' for the reduction of the product formed at D and E. If one sweeps anodic from the open circuit potential, a wave is present at A and then D and E appear. The anodic wave at A is probably due to the reverse reaction given above for CuO_2^{-3} formation. The melt had a greenish-yellow color.

C. <u>Cu/CuO</u>

A cyclic voltammogram of a hydroxide melt at 306°C with CuO and Na_2O added is presented in Fig. 7A. Cathodic sweeps from the rest potential A yielded a small wave which ran into Na(I) reduction B. On reversal, there appeared the Na stripping wave B', a broad wave C, which may correspond to B' in Fig. 6Ab, and copper oxidation peaks D (Cu_2O) and E (CuO). Reversal at F, the anodic limit,

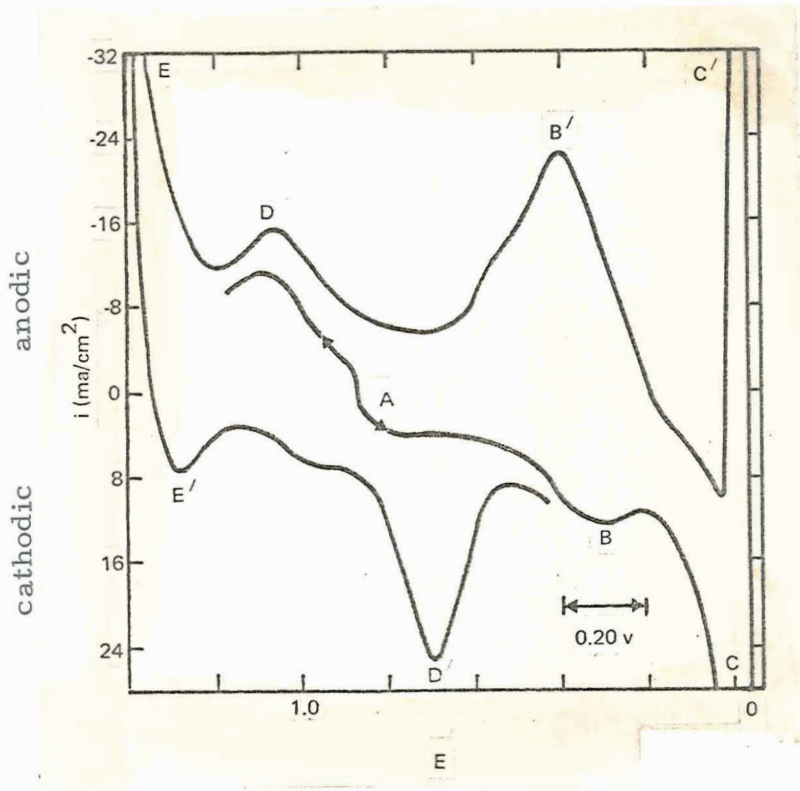

Fig. 6Ab. L. S. V. of $Cu/Cu_2O + Na_2O$ in NaOH-KOH

$T = 248^oC$; s = 46 mv/sec

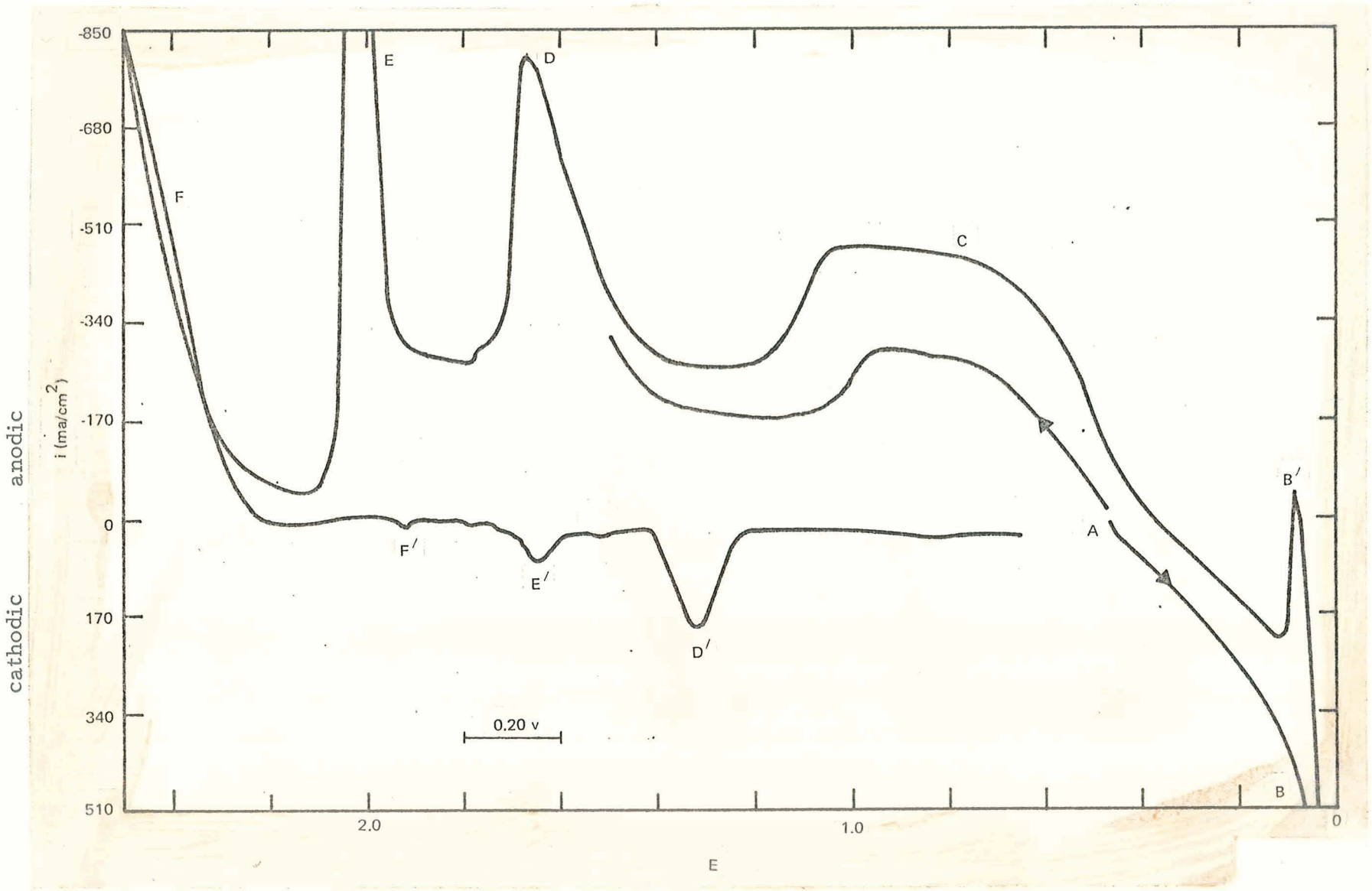

Fig. 7A. L. S. V. of Cu/CuO + Na_2O in NaOH-KOH
T = 306°C; s = 46 mv/sec

produced peaks F', E' and D' corresponding to reduction of the oxide films formed at F, E and D. On standing, the open circuit voltage drifted anodic and the voltammograms resembled that in Fig. 6Ab.

D. Cd/CdO

A linear sweep voltammogram of an NaOH-KOH melt at 255°C with CdO and Na_2O is shown in Fig. 8Aa. Immediately before the Na(I) reduction and stripping waves, C and C', there was another wave pair B and B' of unknown origin. Anodic sweeps yielded a prewave D and the large Cd oxidation wave E at 1.2v. After reversal at E, reduction wave D', due to the product of D and E, and peaks F and G from products of E appeared.

On a more sensitive current scale at 298°C (Fig. 8Ab) a cathodic peak B, commencing from the rest potential A, and a second reduction peak C were evident. (C' represents the oxidation of the film formed in the reduction step C.) Anodic waves D and E also occurred from A. Similar results were found at the lower temperatures. Insufficient evidence precludes speculation as to the species involved.

E. Be/BeO

An L.S.V. of Be in molten NaOH-KOH at 300°C is given in Fig. 9A. Two small oxidation waves C and D can be seen after the reduction step at B. This reduction current is probably due to BeO and not Na(I) since no stripping peak is evident at B'. There were no cathodic waves other than that for BeO reduction. If one cycled between the open circuit potential A and a point between

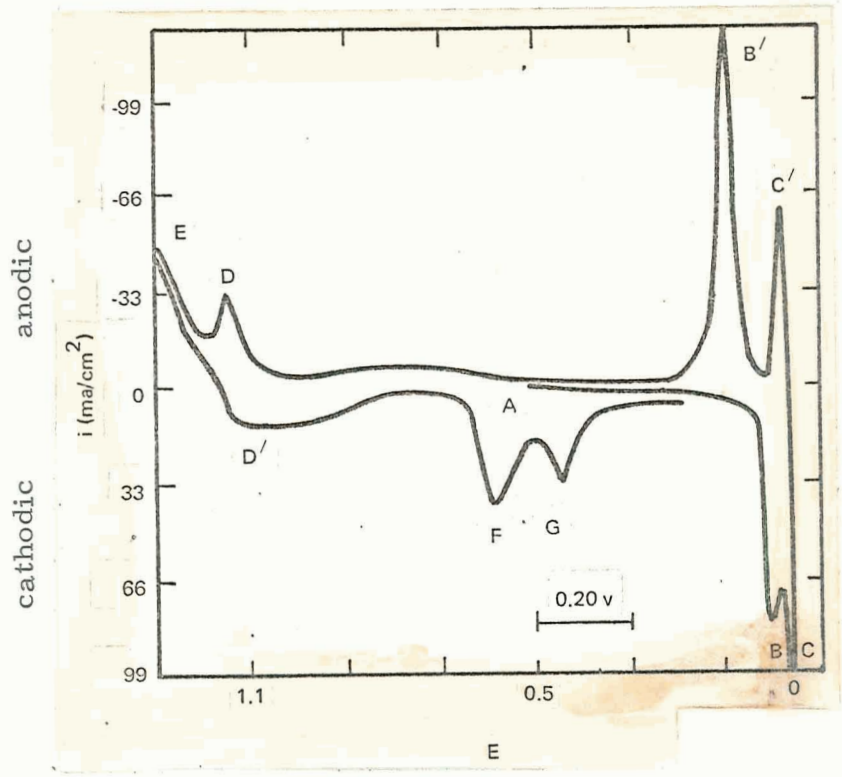

a) L. S. V. T = 255°C; s = 46 mv/sec

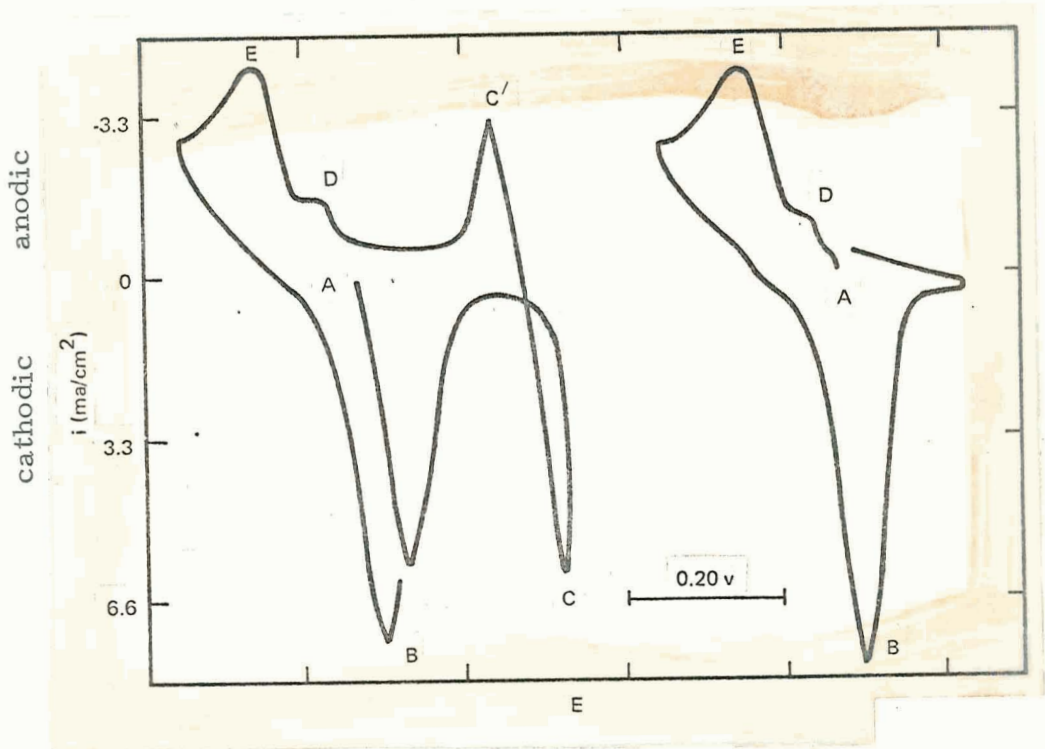

b) L. S. V. T = 298°C; s = 46 mv/sec

Fig. 8A. Voltammetry of Cd/CdO + Na_2O in NaOH-KOH Melts

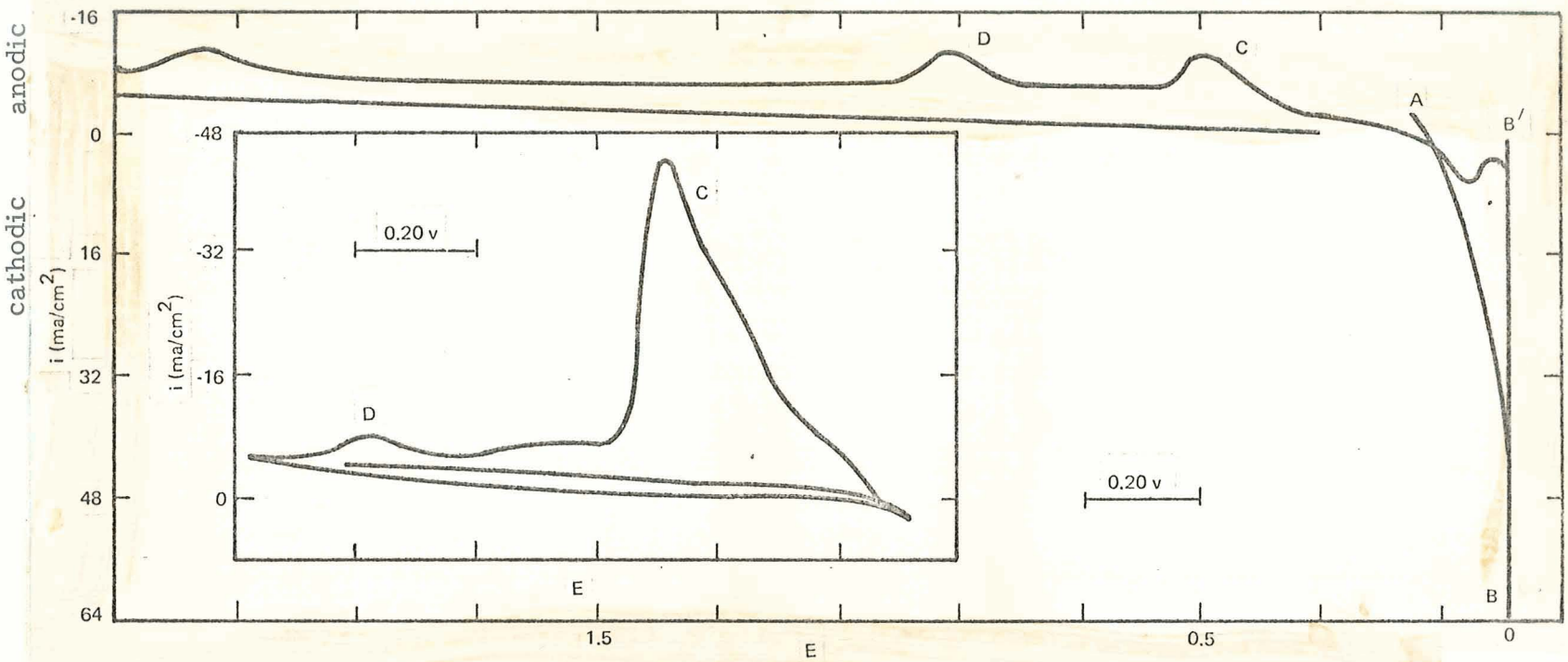

Fig. 9A. L. S. V. of Be in NaOH-KOH
T = 300°C; s = 46 mv/sec

C and D, wave C increased (see insert). If the scan was extended to or past D, wave C decreased or disappeared. Thus, if the Be is not made too anodic, there appears to be some reaction occurring which increases the oxidizability of the metal. The resistance between the electrodes increased with time and the peaks at C and D decreased and disappeared at the lower temperatures. When the cell was reheated to 300°, the peaks did not reappear. The resistance had become quite high, about 1000 ohms, and the electrodes were encrusted with a white cake which had crept up above the surface of the melt.

F. Mg/MgO

A cyclic voltammogram of an NaOH-KOH melt at 203°C with Mg electrodes is presented in Fig. 10A. The erratic tracing is probably due to the reaction occurring between the electrode and the melt. Note that after the cathodic scan B was reversed, the current was even more cathodic C. Only a small anodic current was present at D indicating that the electrode was passivated.

G. Zn/ZnO

A cyclic voltammogram of an NaOH-KOH melt containing ZnO and Na_2O at 290°C is given in Fig. 11A. Cathodic sweeps from the open circuit voltage A showed a wave which ran into a large one B, presumably Na(I) reduction. However, no Na stripping was apparent and no anodic wave appeared until zinc oxidation C. The large wave C' was due to the reduction of the ZnO film formed at C. On a more sensitive current scale both cathodic and anodic waves could be observed starting from the open circuit potential A (see insert). Neither wave was well-defined and both appeared to be running into other waves. Similar results were obtained at the lower temperatures.

Fig. 10A. L.S.V. of Mg in NaOH-KOH
T = 203°C; s = 46 mv/sec

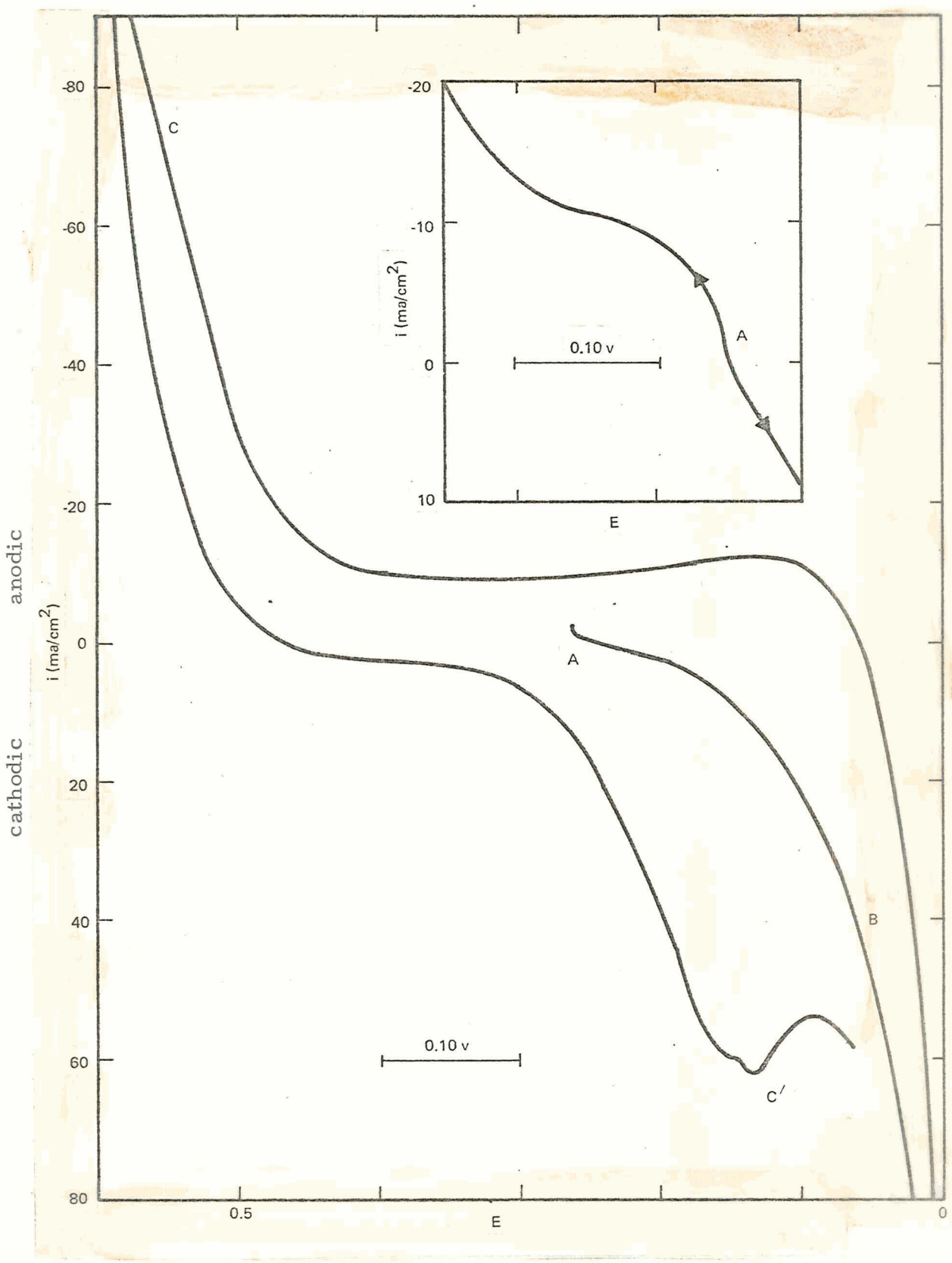

Fig. 11A. L. S. V. of Zn/ZnO + Na_2O in NaOH-KOH

T = 290°C; s = 46 mv/sec

H. $\underline{Al/Al_2O_3}$

An L. S. V. of Al in molten NaOH-KOH at 205°C is depicted in Fig. 12A. The cathodic current at D was probably due to Al_2O_3 reduction since, as with Be, no appreciable stripping peak appeared E. No anodic current occurred until high voltages, over 2.5 v, were impressed. The aluminum was highly passivated in this medium.

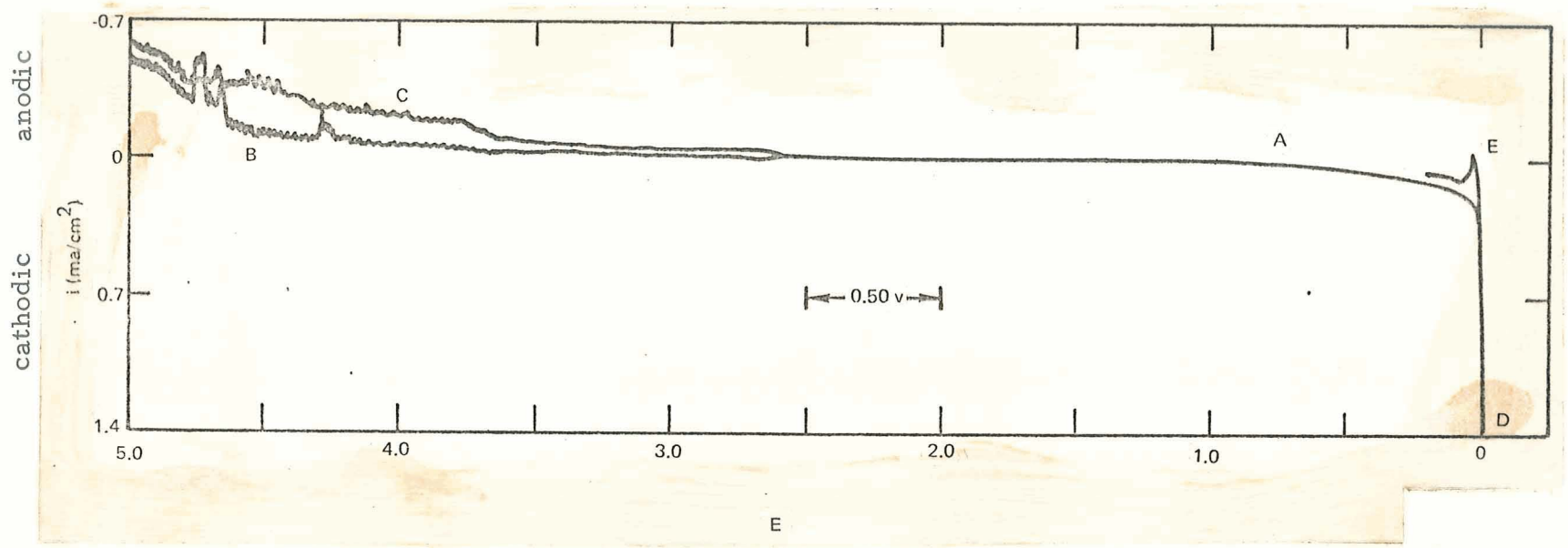

Fig. 12A. L. S. V. of Al in NaOH-KOH
T = 205°C; s = 46 mv/sec